NUREG/CR-1059
LA-8056-MS
Informal Report

TRAC-P1A Developmental Assessment

University of California

LOS ALAMOS SCIENTIFIC LABORATORY
Post Office Box 1663 Los Alamos, New Mexico 87545

This report was not edited by the Technical Information staff.

NUREG/CR-1059
LA-8056-MS
Informal Report
R-4

TRAC-P1A Developmental Assessment

Compiled and Edited by

J. C. Vigil
K. A. Williams

Contributors:

R. K. Fujita
J. S. Gilbert
W. L. Kirchner
J. K. Meier
J. J. Pyun
J. C. Vigil
G. J. Willcutt, Jr.
K. A. Williams

Energy Division
Los Alamos Scientific Laboratory
Los Alamos, New Mexico

Manuscript submitted: September 1979
Date published: October 1979

Prepared for
Office of Nuclear Regulatory Research
US Nuclear Regulatory Commission
Washington, DC 20555

NRC FIN No. A7016

UNITED STATES
DEPARTMENT OF ENERGY
CONTRACT W-7405-ENG. 36

CONTENTS

TABLES

FIGURES

FIGURES (cont)

FIGURES (cont)

FIGURES (cont)

FIGURES (cont)

FIGURES (cont)

TRAC-P1A DEVELOPMENTAL ASSESSMENT

Compiled and Edited by

J. C. Vigil

and

K. A. Williams

Contributors: R. K. Fujita, J. S. Gilbert, W. L. Kirchner, J. K. Meier, J. J. Pyun, J. C. Vigil, G. J. Willcutt, Jr., and K. A. Williams

ABSTRACT

The Transient Reactor Analysis Code (TRAC) is being developed at the Los Alamos Scientific Laboratory (LASL) to provide an advanced best-estimate predictive capability for the analysis of postulated accidents in light water reactors. TRAC-P1A provides this analysis capability for pressurized water reactors and for a wide variety of thermal-hydraulic experimental facilities. It features a three-dimensional treatment of the pressure vessel and associated internals; two-phase nonequilibrium hydrodynamics models; flow-regime-dependent constitutive equation treatment; reflood tracking capability for both bottom flood and falling film quench fronts; and consistent treatment of entire accident sequences including the generation of consistent initial conditions. Detailed descriptions of the thermal-hydraulic models, numerical solution methods, user information, and programming features are given in a separate report.

This report presents the results of initial developmental assessment calculations performed with TRAC-P1A prior to its public release. These calculations were performed with the same code version and include separate-effects experiments for the blowdown, refill, and reflood phases of a loss-of-coolant accident (LOCA); systems-effects experiments for the blowdown phase; and an integral-effects experiment for the blowdown/refill portion of a LOCA. Although the initial set of assessment calculations is not exhaustive, results obtained thus far are encouraging. Additional assessment of the code is in progress through predictions and analyses of other experiments.

I. INTRODUCTION

The Transient Reactor Analysis Code (TRAC) is an advanced best-estimate systems code for analyzing light water reactor accidents (LWRs). It is being developed at the Los Alamos Scientific Laboratory (LASL) under the sponsorship of the Reactor Safety Research Division of the U.S. Nuclear Regulatory Commission. TRAC-P1, completed in December 1977, was the first publicly released version and is described in Ref. 1. TRAC-P1 was designed primarily for the analysis of large-break loss-of-coolant accidents (LOCAs) in pressurized water reactors (PWRs). Because of its versatility, however, it can be applied directly to a wide variety of analyses ranging from blowdowns in simple pipes to integral LOCA tests in multiloop facilities. Models specifically required to treat boiling water reactors (BWRs) and other accident types, such as anticipated transients without scram (ATWS) and reactivity insertion accidents (RIAs), will be incorporated into future versions of the code. TRAC-P1A is an improved version of TRAC-P1 and is described in Ref. 2. While still treating the same class of problems, TRAC-P1A is more efficient, incorporates improved hydrodynamic and heat transfer models, and should be more easily implemented on various computers.

Developmental assessment of TRAC is the first stage of a two-stage assessment process. It is closely coupled to the code development activity and primarily involves posttest analyses of a wide variety of thermal-hydraulic experiments. The primary objective of developmental assessment is to define the limits of validity of the methods, models, and correlations in the developmental version of TRAC by comparing calculated results with experimental measurements. Other objectives include determination of code sensitivity to input data, model assumptions, and solution techniques; recommendation of standard calculational procedures for various classes of problems; and identification of code and model improvements or additional experiments needed for assessment of the advanced models in TRAC.

When the code developers determine that a particular code version meets the performance objectives, the code is released for external use and the second checkout stage begins. This is the independent assessment stage that involves pretest and posttest predictions of tests in designated facilities using the publicly released and documented version of TRAC. The primary

objective of this activity is to determine the predictive capability of TRAC when applied to new tests involving different scales and experimental configurations. Discrepancies between calculation and experiment are resolved by performing additional posttest analyses as required. Guidance for future code development and recommendations for future experiments are also provided by this activity.

Experimental tests selected for developmental assessment prior to release of TRAC-P1A and the more important thermal-hydraulic effects occurring during these tests are given in Table I. Note that the first five analyses use only the one-dimensional capability in TRAC whereas the remainder involve the multidimensional capability as well. Tests selected for developmental assessment include separate effects (tests involving basically only one component), synergistic or systems effects (several coupled components but only one LOCA phase) and integral effects (several components and more than one LOCA phase). These tests constitute a minimal set of assessment calculations which were performed with the same code, TRAC-P1A, prior to its public release. Calculations of other tests in these and other facilities are currently in progress to further assess the code. It is anticipated that further improvements will be identified as the result of this additional code testing.

Results of the initial developmental assessment calculations are presented in Sec. II. The following topics are included for each experiment:

1. Experiment description,
2. TRAC best-estimate model,
3. Comparison of calculation with experiment,
4. Any sensitivity or parameter studies performed,
5. Discussion of TRAC features assessed, and
6. Input data decks.

The description of the experiment includes its purpose, facility scale compared to a full-size PWR, components used in the experiment, and operating procedures. The best-estimate model description includes code modules, component noding, user options selected, calculational procedures, and modeling of important geometric features. If results are sensitive to particular input data, rationale for selection of best-estimate values is given. Comparisons

TABLE I

TRAC-P1A DEVELOPMENTAL ASSESSMENT ANALYSES

No.	Experiment	Thermal - Hydraulic Effects
1	Edwards Horizontal Pipe Blowdown (Standard Problem 1)	Separate effects, one-dimensional critical flow, phase change, slip, wall friction
2	CISE Unheated Pipe Blowdown (Test 4)	Same as 1 plus pipe wall heat transfer, flow area changes, and gravitational effects
3	CISE Heated Pipe Blowdown (Test R)	Same as 2 plus critical heat flux (CHF)
4	Marviken Full-Scale Vessel Blowdown (Test 4)	Same as 1 plus full-scale effects
5	Semiscale 1-1/2 Loop Isothermal Blowdown (Test 1011, Standard Problem 2)	Synergistic and systems effects, one-dimensional flow, phase change, slip, wall friction, critical nozzle flow
6	Semiscale Mod-1 Heated Loop Blodown (Test S-02-8, Standard Problem 5)	Same as 5 plus 3-D vessel model with rod heat transfer including nucleate boiling, DNB, and post-DNB
7	Creare Countercurrent Flow Experiments	Separate effects, countercurrent flow, interfacial drag and heat transfer, condensation
8	FLECHT Forced Flooding Tests	Separate effects, reflood heat transfer, quench front propoagation, liquid entrainment and carryover
9	Nonnuclear LOFT Blowdown with Cold Leg Injection (Test L1-4, Standard Problem 7)	Integral effects during blowdown and refill, scale midway between Semiscale and full-scale PWR

with experiment include initial conditions if these were obtained by a steady-state calculation. Comparisons of transient results include as many of the reliable experimental measurements as is possible within the limitations of the TRAC input model.

Noding or other parametric studies that were performed to arrive at the best-estimate input model are discussed. If these studies involved analyses of other experiments, results of those analyses are also discussed. TRAC features tested by each problem are discussed including component models, physical or phenomenological models, separate and integral effects, dimensional and geometric effects, etc. Areas are identified where better models are needed and where better or more experimental data are required. Listings of the input data decks for both steady-state and transient calculations (best-estimate only) are provided. The input decks are discussed as needed to explain special noding, complicated input, subtle points, etc. Computer time required to run each problem is also given.

II. ASSESSMENT CALCULATIONS

A. Edwards Blowdown Experiment

1. Description of Experiment

The Edwards horizontal pipe blowdown experiment studied depressurization phenomena of initially nonflowing subcooled water.[3] The experimental apparatus consisted of a straight steel pipe 4.096 m in length and 0.073 m in internal diameter. The apparatus was designed for a maximum pressure of 17.24 MPa at temperatures up to 616.5 K. The discharge end of the horizontal pipe was sealed with a 0.0127 m thick glass disk.

The pipe was filled with demineralized water; a hydraulic pump and a control valve regulated the pressure in the system. Air in the pipe was evacuated with a vacuum pump before filling the pipe with water. Prior to rupturing the glass disk the pipe was isolated from the supply tank thus preventing the discharge of cold water into the pipe during blowdown. Pressure and temperature transducers were located at gage stations GS-1 to GS-7, see Fig. 1. Also provided at GS-2 and GS-5 were two diametrically opposed aluminum alloy disks for transient void fraction measurements using an

x-ray absorption system. The pipe was electrically heated using heaters formed to the curvature of the pipe and was insulated using asbestos insulation.

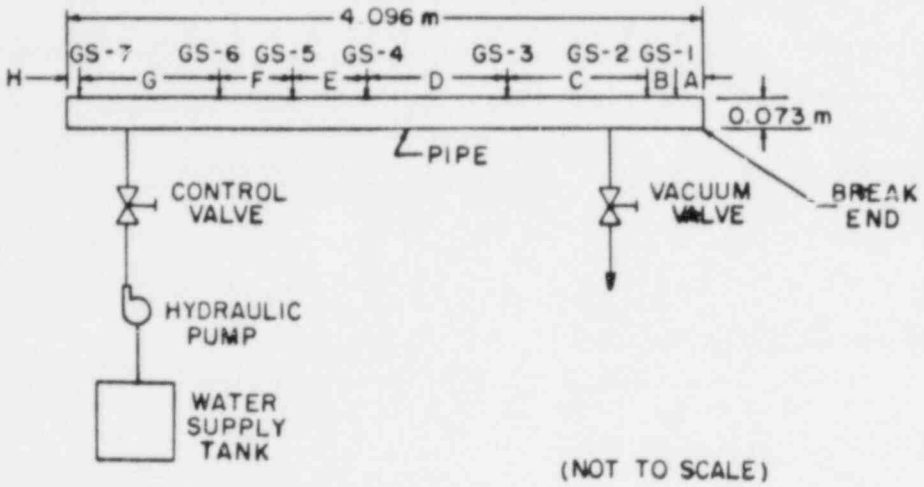

DIMENSION	m
A	0.168
B	0.158
C	0.835
D	0.911
E	0.555
F	0.555
G	0.835
H	0.079

Fig. 1. Schematic of Edwards horizontal pipe blowdown experiment (adapted from Ref. 3).

The operating procedure required that degassed water completely fill the pipe. The pipe was pressurized cold to approximately 25% above the initial depressurization test pressure of 7 MPa and checked for leaks. Next the pressure was reduced to 3.45 MPa and heating applied gradually for about 1.5 hours. During the heating of the water the system pressure was maintained at about 3.45 MPa above the saturation pressure to prevent flashing of the liquid. The temperature variation along the pipe was limited by adjustment of the voltage control for each heater. The system was initially brought to an approximately uniform temperature of 515 K and a pressure of 7 MPa. With the isolating valve between the pipe and the storage tank closed, the glass disk was ruptured and the data was automatically recorded.

2. TRAC-P1A Best-Estimate Model

The experiment is a straight horizontal pipe except for an abrupt area change at the exit. It is modeled with the one-dimensional components given in the component schematic in Fig. 2. The model consists of three different types of components coupled in series. The two pipe components are subdivided into 46 fluid cells. The noding given in Fig. 3 was determined by performing a noding sensitivity study. Based on a parametric study discussed in Sec. 4, the annular flow friction factor correlation option (NFF=4) was used. An additive loss coefficient (FRIC = 1.436) was determined for the exit flow cell. This accounts for form losses at the break due to two-dimensional effects which cannot be treated with the one-dimensional model.

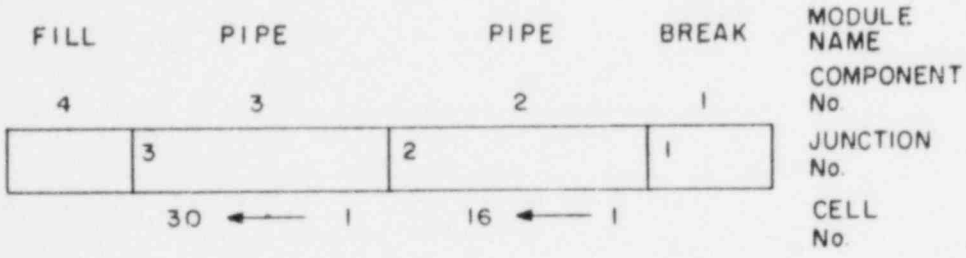

Fig. 2. TRAC model schematic of Edwards blowdown experiment.

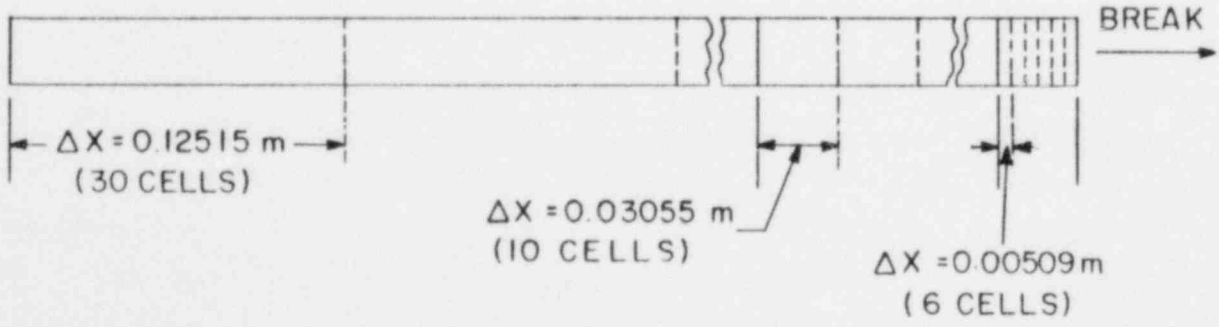

Fig. 3. TRAC noding of Edwards blowdown experiment.

Given initial conditions of uniform pressure, approximately uniform temperature and zero flow velocity, no steady-state calculations were required. Because the temperature distribution along the pipe may have varied as much as 9 K, an adjusted temperature distribution was used as suggested by Garner in Ref. 4.

3. Comparison of Best-Estimate Calculations with Experiment

The calculated pressure results for GS-1 through GS-7 (Figs. 4 through 10, respectively) are all similar in comparison to the experimental results. The following observations apply to all the pressure results. From 0.0 to 0.2 s the calculated pressures are within about 10% of the experimental values. During the midrange of the transient, 0.2 to 0.4 s, a faster rate of depressurization was predicted than observed. The maximum difference between calculation and experiment was 0.8 MPa at 0.25 s for GS-6. For the balance of the transient, 0.4 to 0.6 s, the calculated results were in good agreement with the experimental results. Experimental uncertainty information was not available; however, an uncertainty of ~0.3 MPa was suggested.[4]

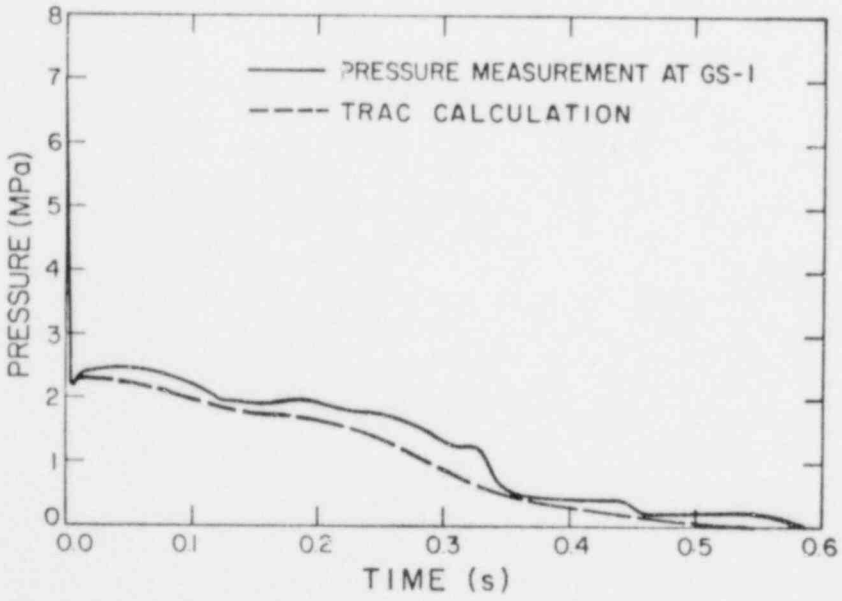

Fig. 4. Fluid pressure for Edwards blowdown experiment at location GS-1.

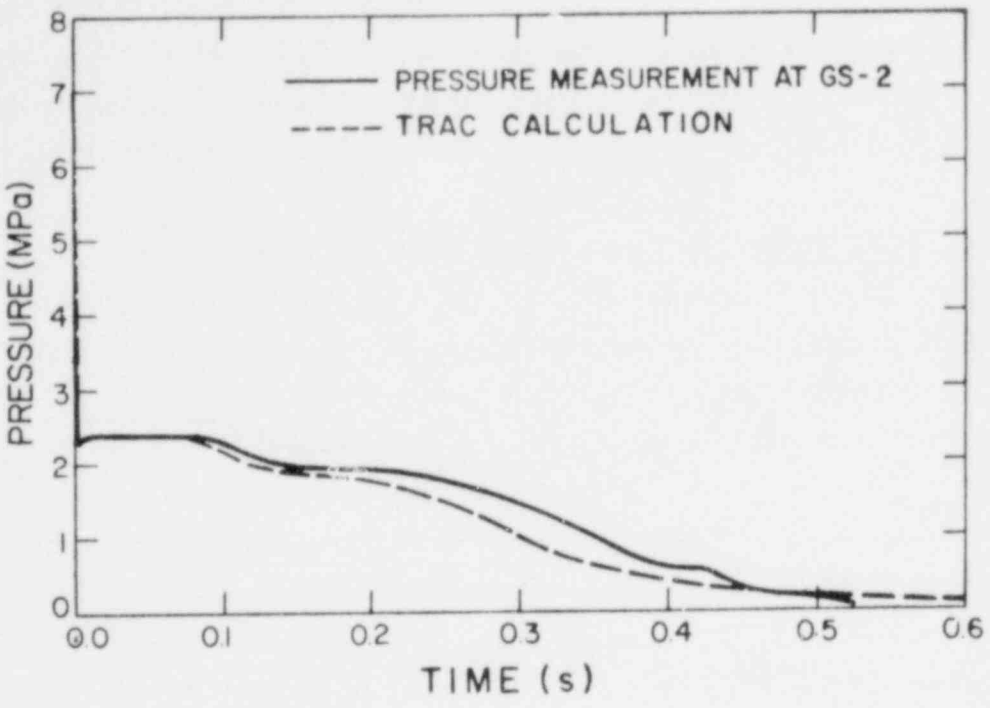

Fig. 5. Fluid pressure for Edwards blowdown experiment at location GS-2.

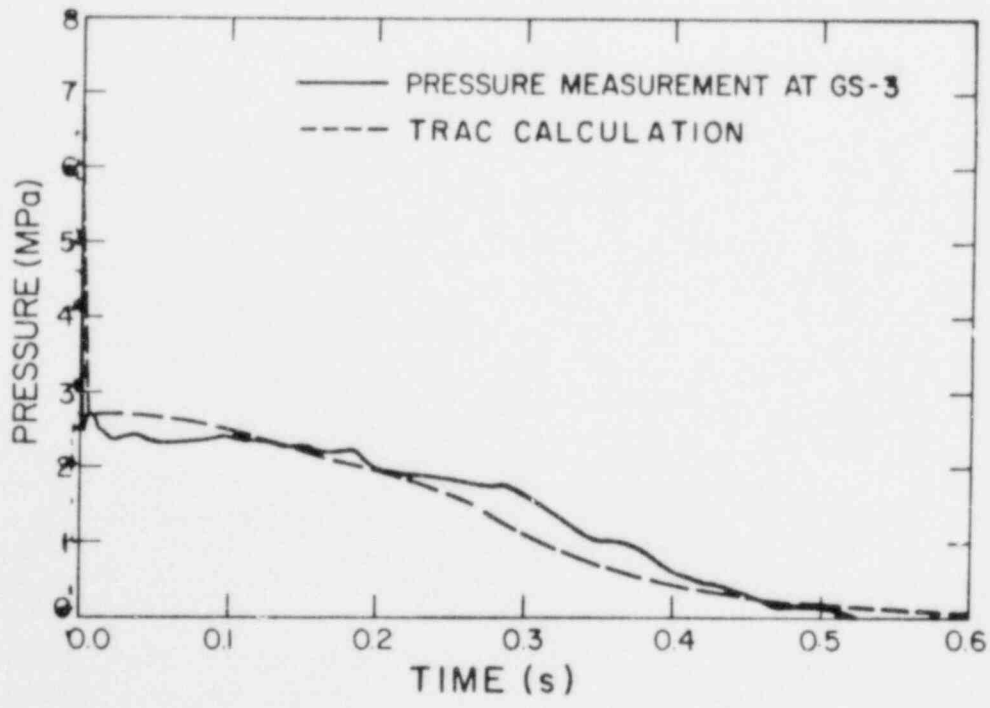

Fig. 6. Fluid pressure for Edwards blowdown experiment at location GS-3.

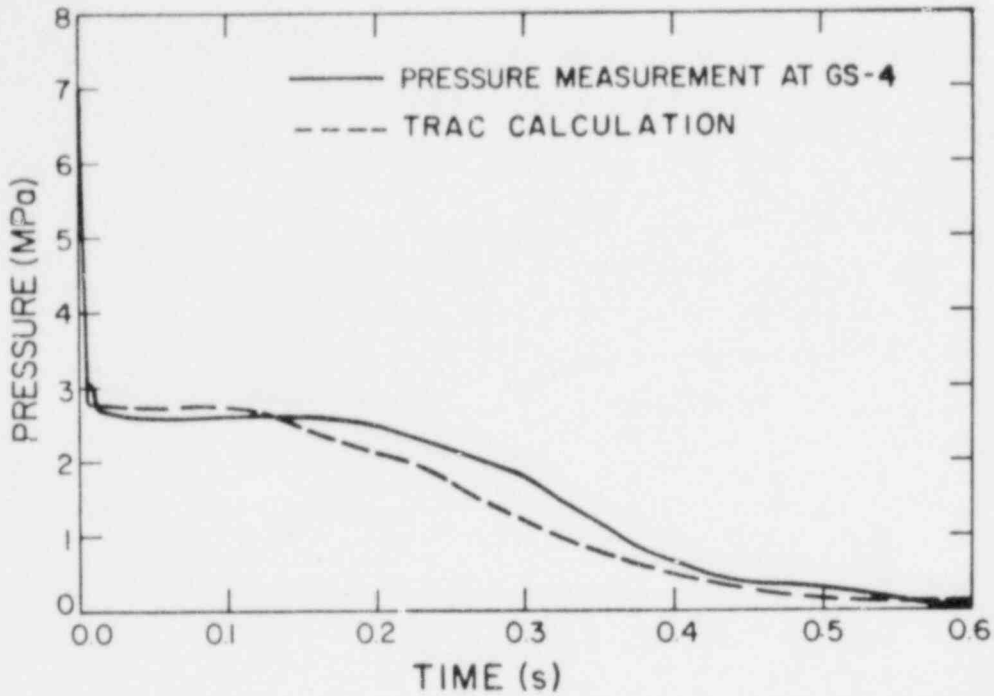

Fig. 7. Fluid pressure for Edwards blowdown experiment at location GS-4.

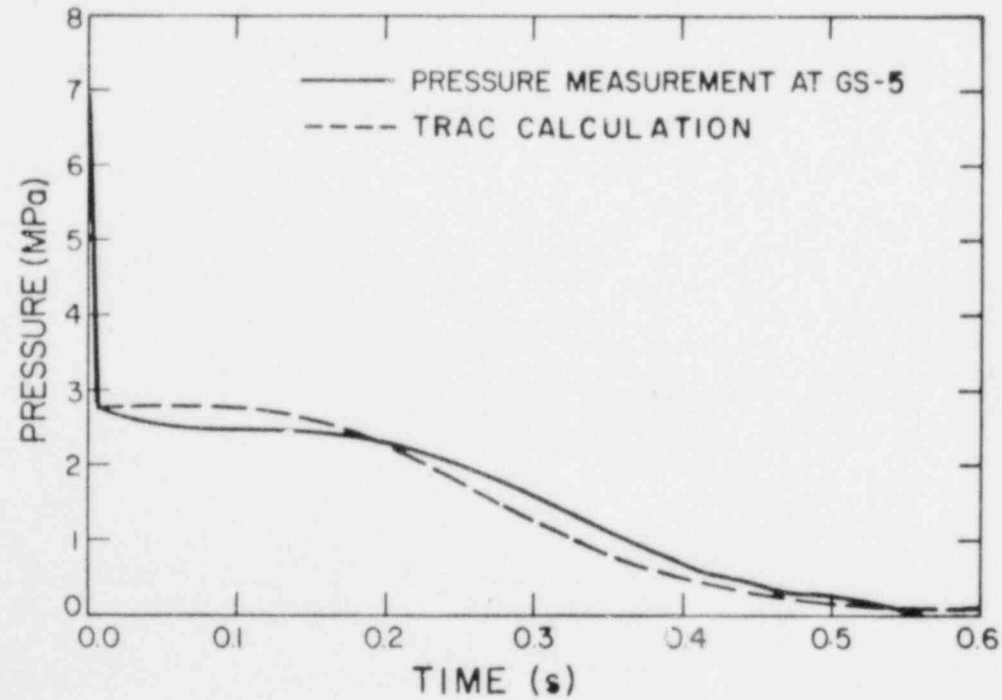

Fig. 8. Fluid pressure for Edwards blowdown experiment at location GS-5.

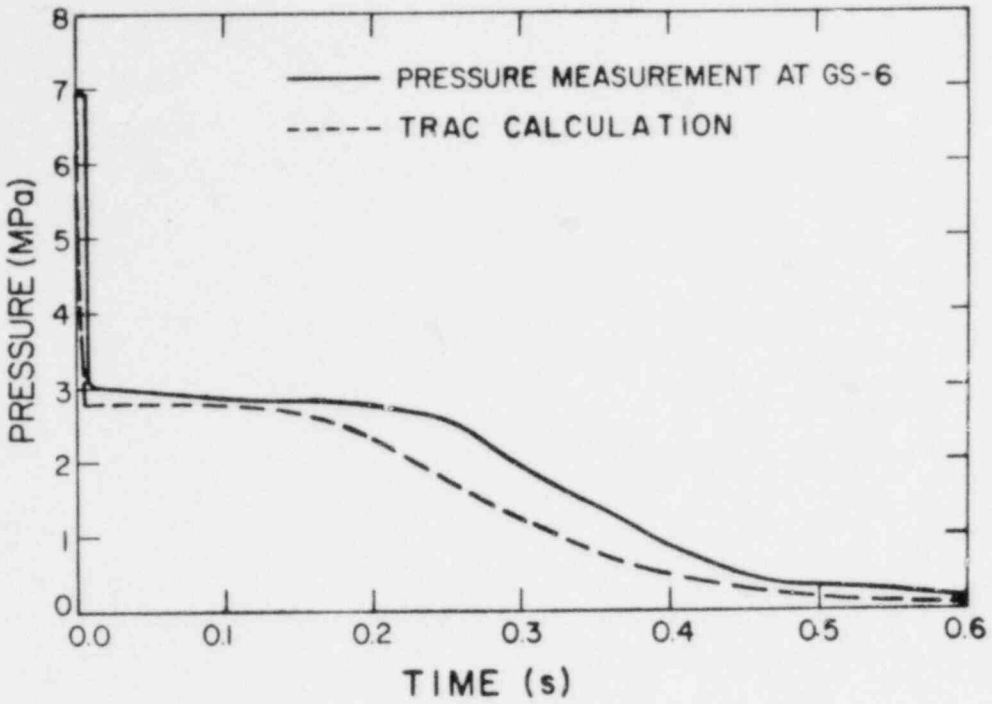

Fig. 9. Fluid pressure for Edwards blowdown experiment at location GS-6.

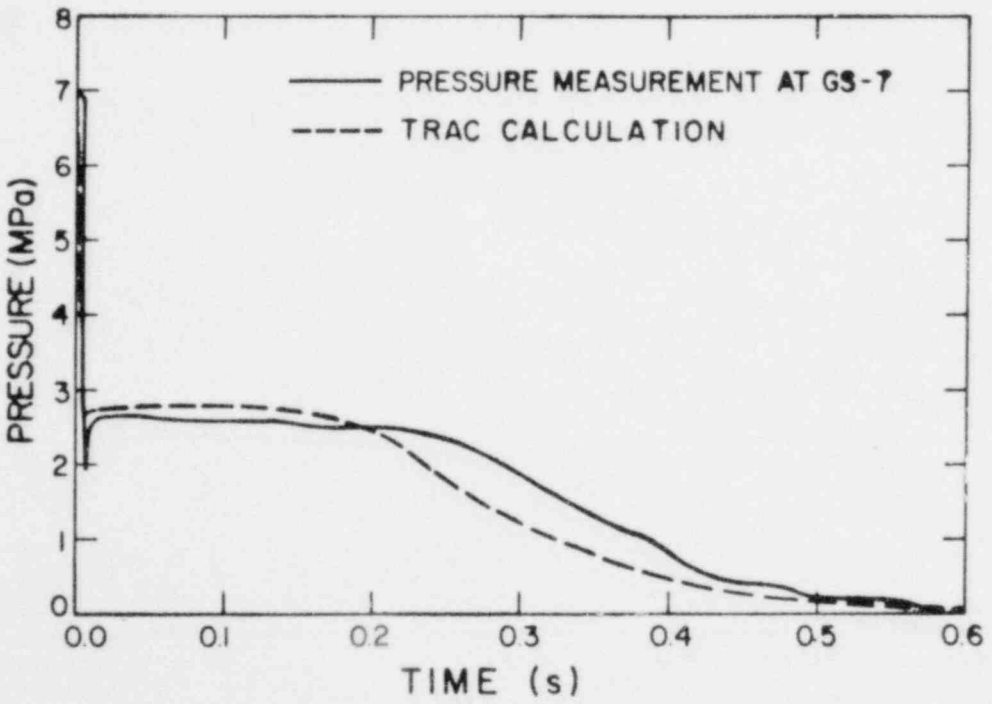

Fig. 10. Fluid pressure for Edwards blowdown experiment at location GS-7.

In Fig. 11 a comparison is made with the single available temperature measurement (GS-5). The plotted temperature is the liquid temperature. After 0.2 s the calculated saturation, liquid, and vapor temperatures are equal. The agreement with the measured temperature is excellent from 0.0 to 0.2 s and then the calculated results drop about 6% below the experimental results. The comparison in Fig. 12 between calculated and measured void fraction is fair from 0.0 to 0.3 s and good after 0.3 s. Note that the void fraction is greater than 90% after 0.3 s. The difficulty in measuring void fraction using the x-ray absorption technique partially explains the deviations between the calculated curve and the experimental results.

4. Parametric Studies

Because of the large pressure gradient near the break, the cell sizes were decreased along the pipe in the direction of the break. The selected cell length of 0.005 m at the break is 1/25 of the cell length at the fill end of the pipe. Parametric studies have shown that further refinement of the mesh near the break does not significantly affect the results. Results are not sensitive to the cell size profile away from the break.

Calculations were performed with five different friction factor correlation options (NFF = 1, 2, 3, 4, and 5). These results were generally bracketed by the annular flow friction factor (NFF=4) yielding maximum pressures and the CISE friction factor (NFF=3) yielding minimum pressures throughout the pipe. The pressures are sensitive to friction and the larger friction factor yields better results because the pipe was not smooth but rather was made up of six sections joined together by compression couplings.

When the glass disk was ruptured some of the glass was retained around the circumference of the disk support assembly reducing the discharge area by 10 to 15%. Flow areas of 60, 70, 85, 87 and 90% at the break were studied. To approximate the actual flow area (the vena contracta), the 60 and 70% flow areas were used. With these two cases the pressures were significantly increased. There was not sufficient experimental detail to justify selection of such small flow areas. For the 85, 87 and 90% flow area cases, only minor increases in pressure occurred with decreasing flow area. The nominal value of 87% was therefore selected.

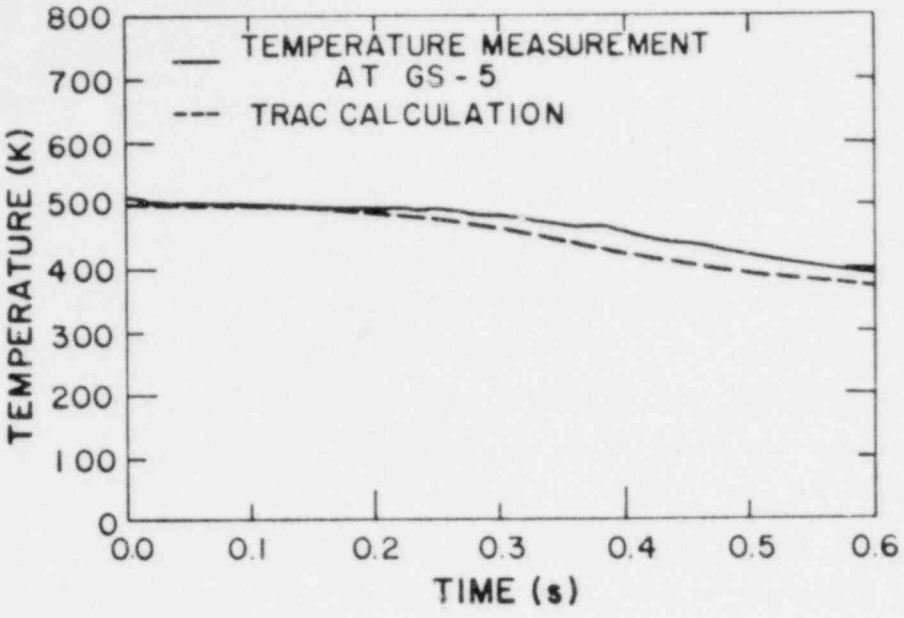

Fig. 11. Fluid temperature for Edwards blowdown experiment at location GS-5.

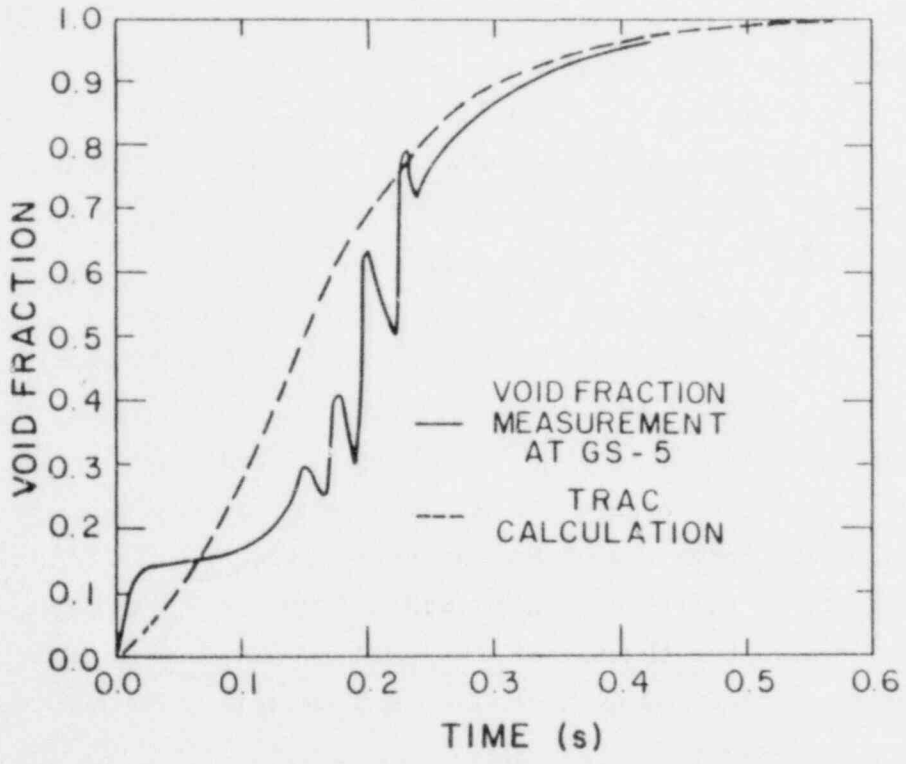

Fig. 12. Void fraction for Edwards blowdown experiment at location GS-5.

5. TRAC-P1A Features Tested

Some of the important thermal-hydraulic effects involved in this problem include one-dimensional critical flow, flashing, slip, wall friction, and break flow-area reduction. Code modules tested in this problem include PIPE, FILL, and BREAK. TRAC best-estimate calculations are in reasonable agreement with the available measurements. Mass flow rate and pipe wall temperature measurements were not made. In addition there are experimental uncertainties in the initial temperature distribution, rupture disk dynamics, and the effect of residual disk fragments on the flow field. Because of these factors, it is felt that code model improvements cannot be recommended based on the results for the Edwards experiment.

6. Input Data Deck

A listing of the input data deck is given in Fig. 13. The experimental facility is modeled with two PIPES, one FILL, and one BREAK module. The FILL module imposes a zero velocity boundary condition at the closed end of the pipe. The BREAK module imposes a fixed pressure (0.10 MPa) boundary condition at the broken end of the pipe. The fully implicit hydrodynamics option (IHYDRO=1) is used in the PIPE module adjacent to the break because of the high flow velocities occurring at the break. The other PIPE module uses the more efficient partially implicit hydrodynamics option (IHYDRO=0). An additive loss coefficient (FRIC=1.436) is supplied at the break junction. Linear interpolation was used to obtain initial temperatures at locations other than those given for the initial temperature distribution.[4]

The computer CPU time on a CDC 7600 was 24 s for the transient calculation.

B. Centro Informazoni Studi Esperienze (CISE) Blowdown Experiments

1. Description of Experiment

The CISE vertical pipe blowdown experiment studied depressurization and heat transfer phenomena of initially flowing subcooled water.[5] A schematic of the CISE blowdown loop test section is shown in Fig. 14. The loop consisted of feeder, heater, and riser sections with dimensions given in Table II and Fig. 15. The internal diameters of the loop tubing ranged from 0.01694 m for the feeder to 0.02618 m for the riser. The total length of the blowdown

```
                1
EDWARDS BLOWDOWN EXPERIMENT

                0                1                4                3
  1.000000E-03  1.000000E-03  1.000000E+00
               10               20               20
                1                2                3                4
FILL                             4                4
                3
  1.205000E-01  5.060000E-04                                        5.148000E+02
  6.996100E+06
PIPE                             2                2
               16                                1                2                6
                                 1


R 6   0.00509;7R 9     0.03055          0.0410E
R 6   0.214E-04R 9   1.284E-04      1.723E-04E
     0.0036560R16    0.004203E
       - 1.436R16          0.0E
F            0.0E
F       0.073152E
F              4E
F            0.0E
F            0.0E
F            0.0E
I14        498.3           497.8E
F     69.961E05E
PIPE                             3                3
               30                                2                3                6


R29      0.12515          0.1205E
R29     5.26E-04       5.060E-04E
F       0.004203E
F            0.0E
F            0.0E
F       0.073152E
F              4E
F            0.0E
F            0.0E
F            0.0E
I 5        497.8           505.5I 5        505.5           504.2E
I 5        504.2           505.5I 2        505.5           506.9E
I 5        506.9           504.2E
F     69.961E05E
BREAK                            1                1
                1
  5.291700E-03  0.214000E-04  1.000000E+00  3.731500E+02  1.013535E+05
         1.0E-5           0.1        15.1E-3
         1.0E-3         1.0E-4           1.0
         1.0E-5           0.1           0.6
           0.05          0.005           1.0
 -1.000000E+00
```

Fig. 13. Input deck for Edwards blowdown experiment.

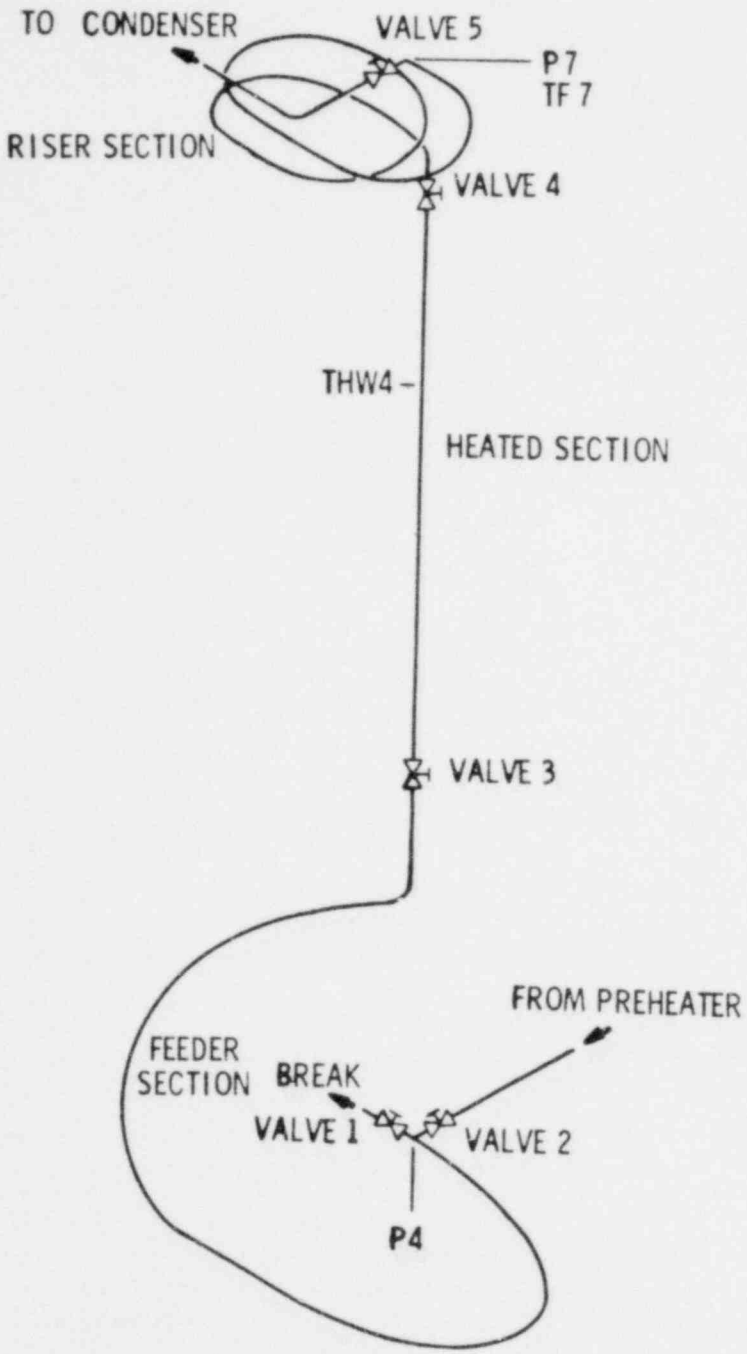

Fig. 14. CISE test section schematic (adapted from Ref. 6).

TABLE II

CISE TEST SECTION GEOMETRY TABULATION

Tube Section	Length (m)	Diameter (m)	Volume (ℓ)	Wall Thickness (m)	Elevation Change (m)
Feeder	9.848	0.01694	2.22	0.0015	3.600
Transition	0.072	0.01694	1.49	0.0015	4.222
Transition	0.042	0.02128		0.0020	
Heated	4.000	0.02128		0.0020	
Transition	0.108	0.02128		0.0020	
Riser	9.995	0.02618	5.38	0 0020	1.455

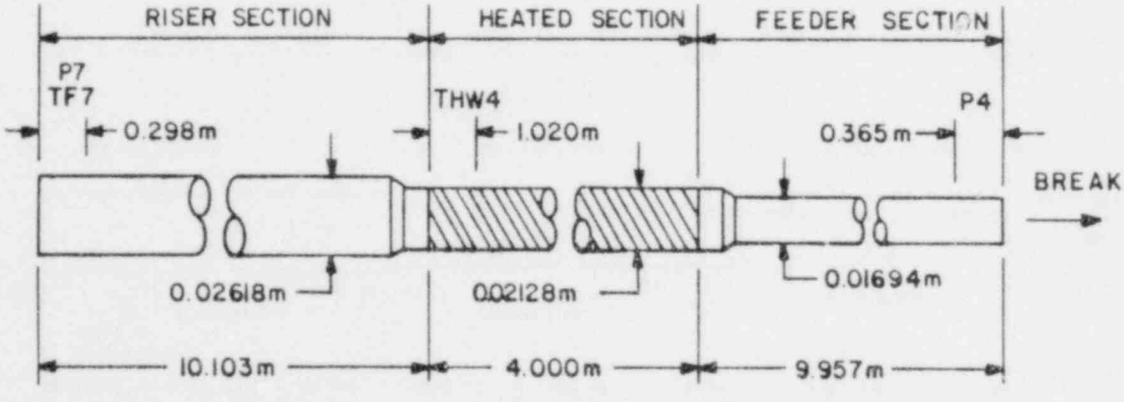

Fig. 15. CISE detailed test section geometry.

portion of the loop was 24.06 m. The heated section was vertical while the feeder and riser tubes were helically coiled with a radius of approximately 1 m resulting in elevation changes of 3.6 m and 1.455 m, respectively. For comparison some tests were run without heat addition in the heater section. All tubing was AISI 304 stainless steel with only the feeder and riser tubes insulated to reduce heat loss.

Four quick-closing valves (valves 2 through 5) and one quick-closing or quick-opening valve (valve 1) are used to isolate the test section from the loop during blowdown and to isolate the contents of the feeder, heated section, and riser. All valves are gas activated and close or open within 10 ms. These valves offer no additional resistance to flow while in the fully open position. A DC electrical current from a 300 kW controllable power supply provided uniform axial heat generation in the heated section tube wall. For the heated case analyzed here, 109.5 kW of electrical power was supplied to the heater section during blowdown.

Pressure and temperature transducers were located along the test section as indicated in Fig. 14. All transducers were connected to a digital data acquisition system while only selected transducers were connected to the analog strip chart recorders.

The operating procedure required that the experiment begin with subcooled water flowing under steady-state conditions through the test loop. At time zero the depressurization was initiated by closing valves 2 and 5 while simultaneously opening valve 1, the discharge valve. Thus, the test section was isolated from the remainder of the loop in less than 20 ms. The test section discharged to the atmosphere while energy input to the heater section was maintained at the initial rate. Pressure, fluid temperature and heater wall temperatures were continuously recorded. The mass inventory was determined at selected stages of the blowdown by simultaneous closing of valves 1, 3, and 4. This procedure isolated the contents of the feeder, heated section and riser, thus allowing the contents to be drained through a condenser and weighed. An experiment was terminated when the heated section wall temperature exceeded approximately 873 K.

2. TRAC Best-Estimate Model

The test section is composed of three tubes of different sizes connected by gradual area transitions. It is modeled with the one-dimensional TRAC-P1A

components given in the component schematic in Fig. 16. The model consists of three different types of components coupled in series. The noding given in Fig. 17 was determined from a noding sensitivity study. This resulted in the four pipe components being subdivided into 38 fluid cells. The annular flow friction factor correlation option (NFF=4) was selected based on the parametric study discussed in Sec. 4. Gravitiational effects and flow area changes are included in the modeling. In the heated test section case the critical heat flux option (ICHF=1) and the wall outer heat transfer coefficient (HOUTV=50) were used.

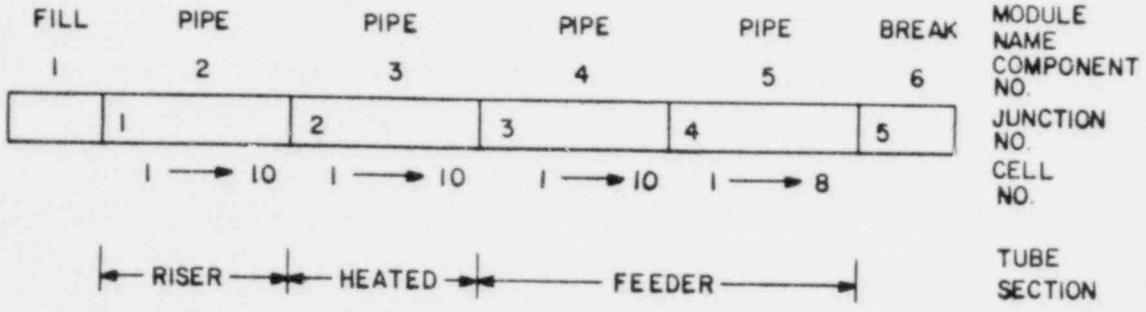

Fig. 16. TRAC model schematic of CISE blowdown experiments.

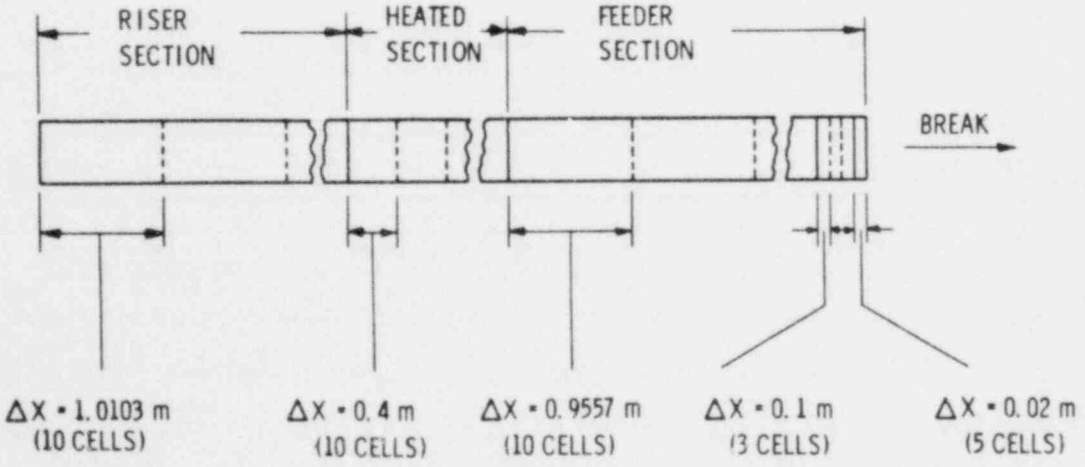

Fig. 17. Typical TRAC noding of CISE blowdown experiments.

Initial velocities, pressures, coolant temperatures, and wall temperatures were input to approximate the steady-state experimental conditions for both the heated and the unheated cases. In the heated test section case, five pipe wall nodes were used with a linear temperature drop of 20 K across the wall. In both the heated and the unheated cases the feeder and the riser pipe walls were modeled with two nodes using a flat initial temperature distribution across the pipe wall.

3. Comparison of Best-Estimate Calculations and Experiments

Calculated results for the heated and the unheated cases are compared with the experimental data from Refs. 6 and 7, respectively. The measurements selected for comparison are the following (see Fig. 14 for measurement locations):

P7 = fluid pressure near the closed end of test section,
T7 = fluid temperature near the closed end of test section,
P4 = fluid pressure near the break end of test section,
THW4 = pipe wall temperature in heater test section, and
MT = total test section water mass.

In Fig. 18 the fluid pressure comparison at P7 for the unheated case is reasonable but the calculated pressure somewhat exeeds the measured results. Similar results are obtained for the heated case (Fig. 19) except that there is better agreement during the initial part of the transient.

In Figs. 20 and 21 the calculated fluid pressure at P4 for the unheated and heated cases, respectively, are in good overall agreement with the experimental results. Discrepancies at very early times in the transient may be due to the assumption in the calculations of instantaneous opening of the blowdown valve. Actually this valve requires about 0.01 s to open completely.

The calculated and measured fluid temperatures at TF7 are shown in Figs. 22 and 23 for unheated and heated cases, respectively. Agreement is good throughout for the unheated case. In the heated case agreement is good for the first 1.5 s of transient. At 2 s the measured temperature dips sharply then recovers at 2.5 s. The reason for this dip is not known as there is no corresponding dip in the pressure and the fluid is at saturation conditions at this point in the transient.

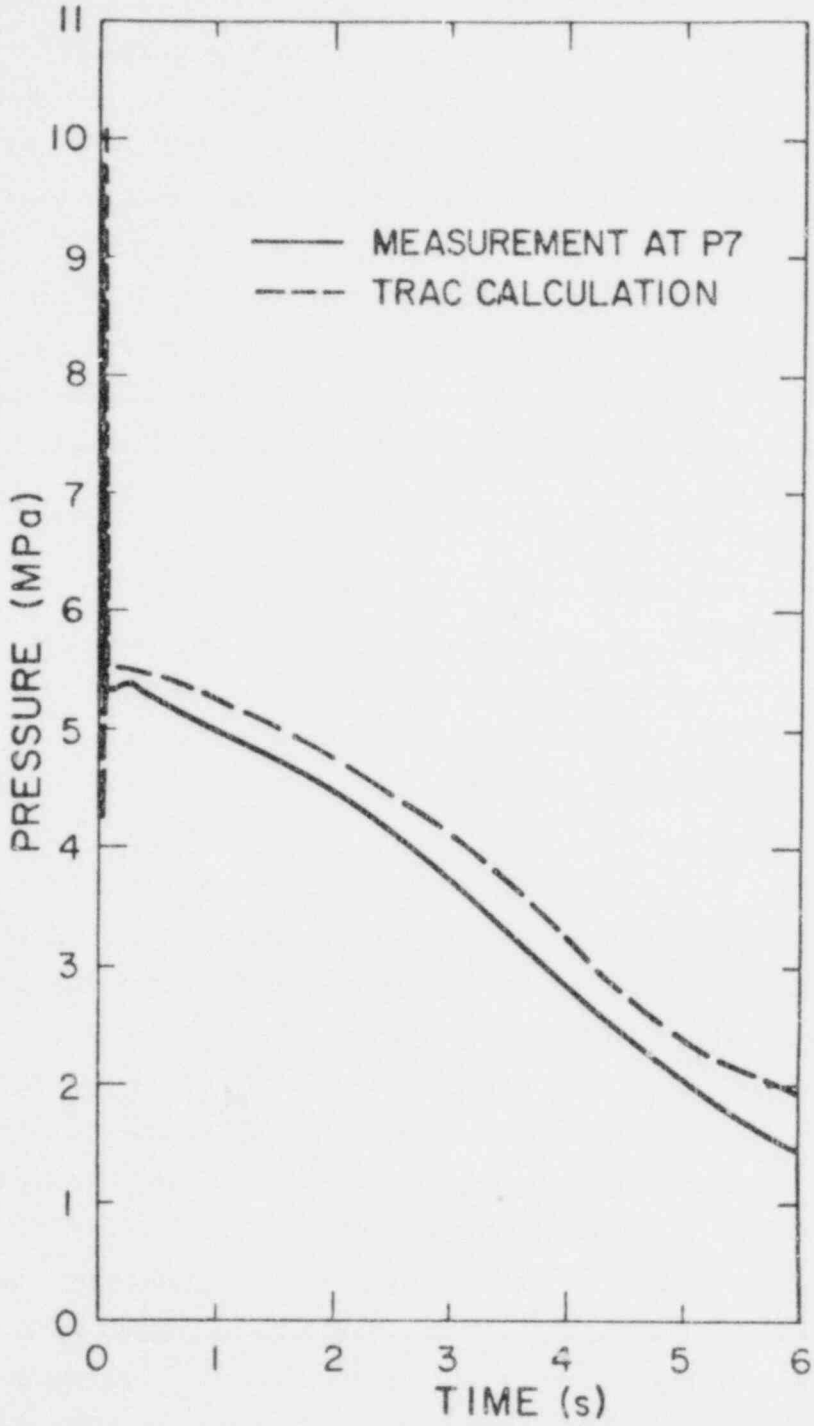

Fig. 18. Unheated CISE fluid pressure at measurement station P7.

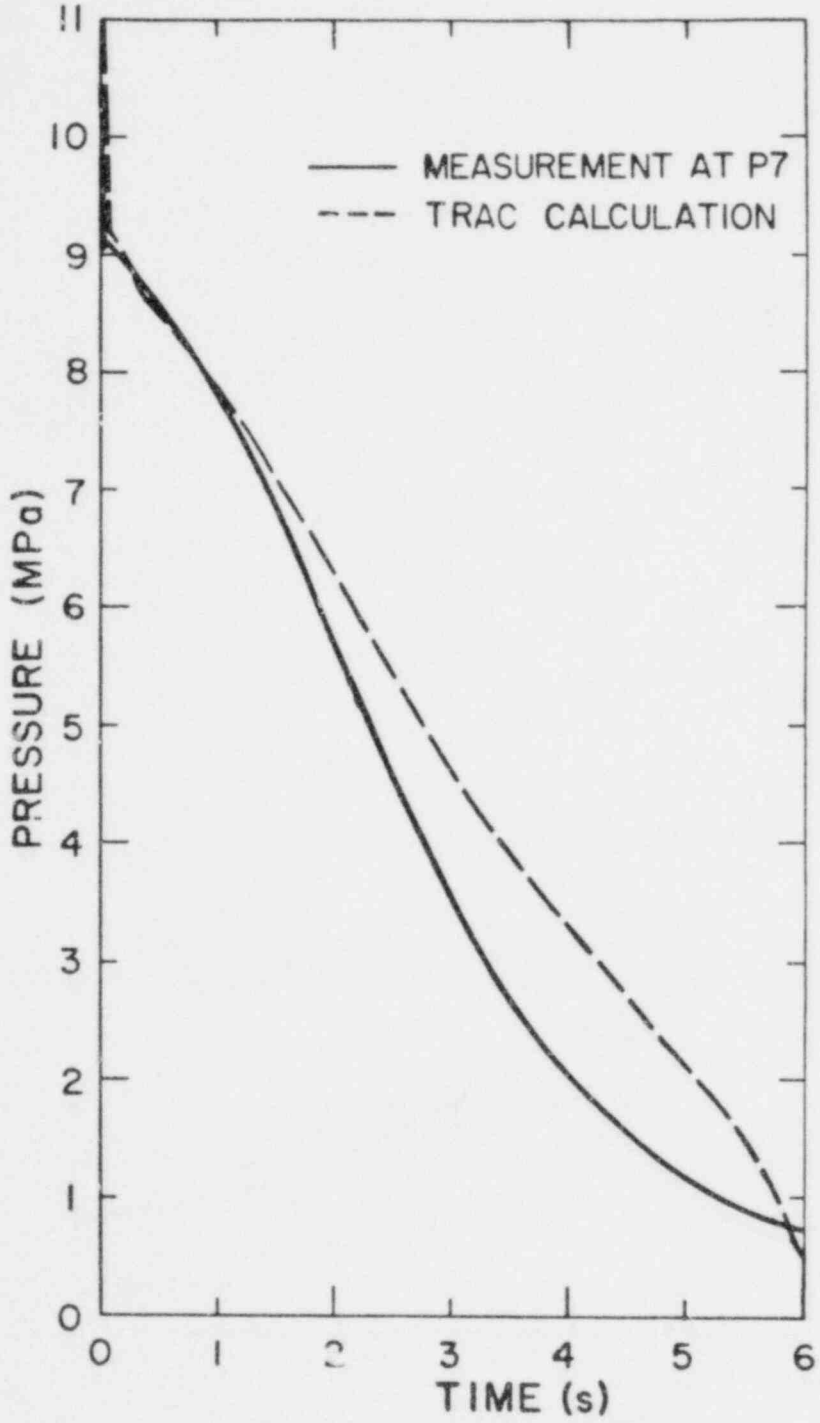

Fig. 19. Heated CISE fluid pressure at measurement station P7.

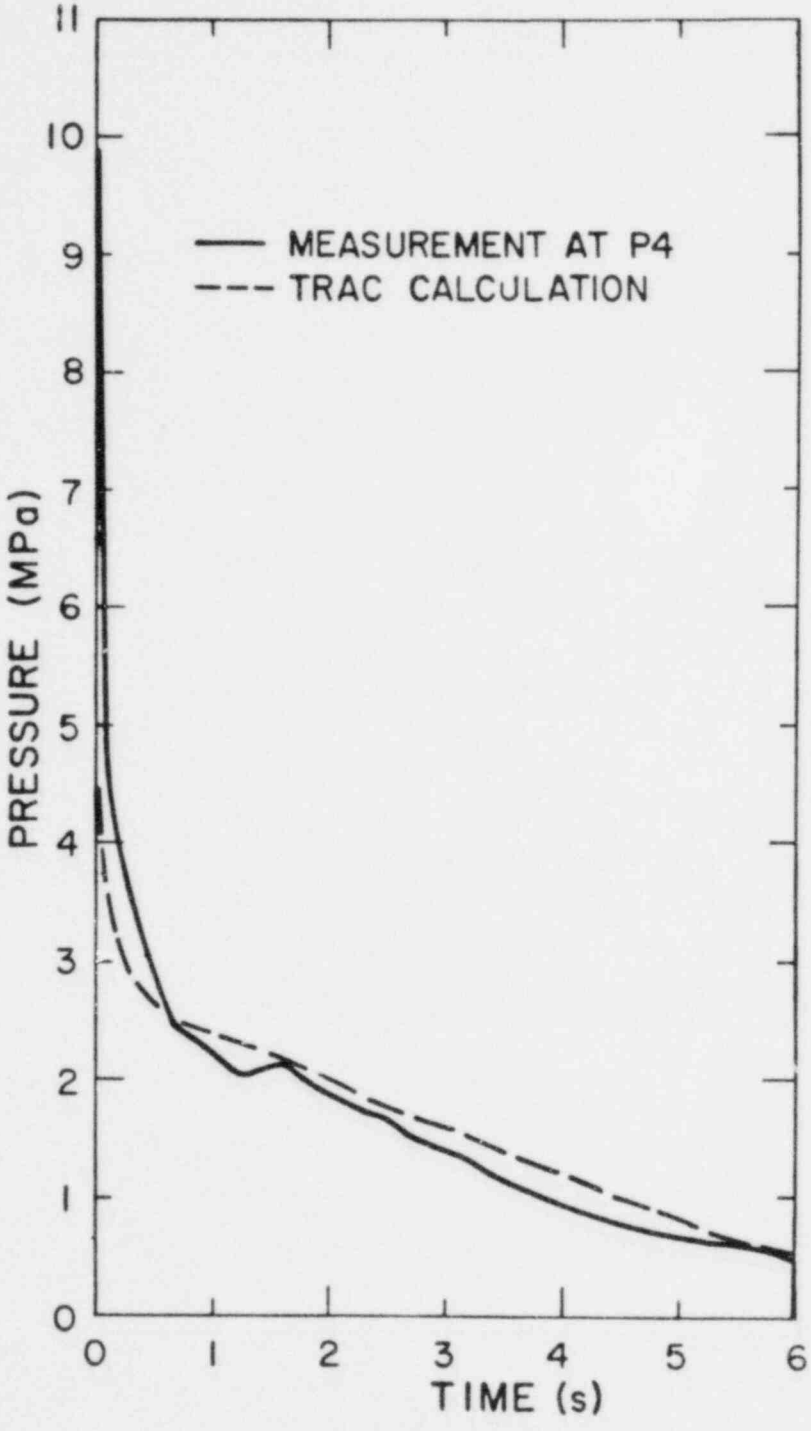

Fig. 20. Unheated CISE fluid pressure at measurement station P4.

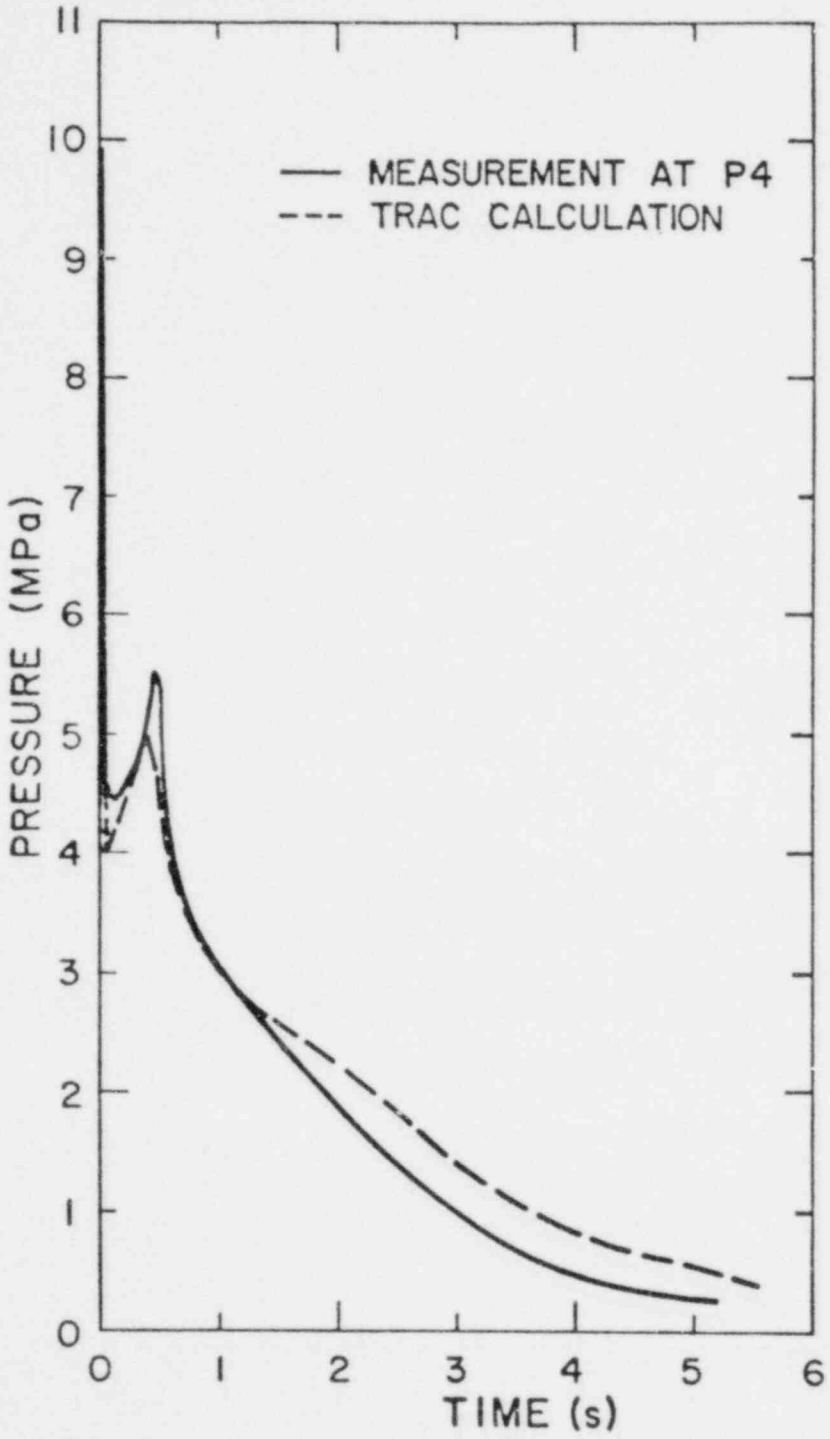

Fig. 21. Heated CISE fluid pressure at measurement station P4.

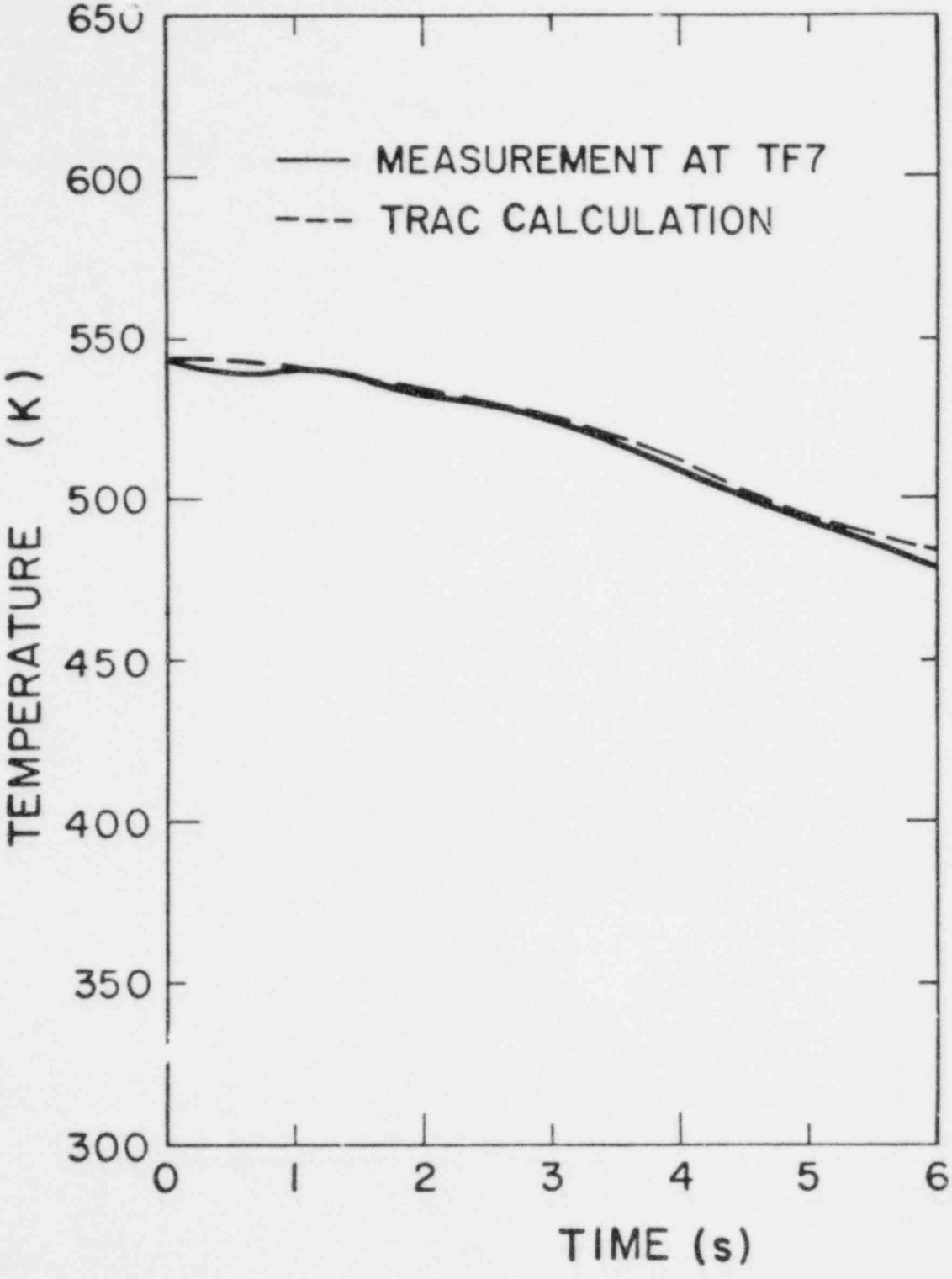

Fig. 22. Unheated CISE fluid temperature at measurement station TF7.

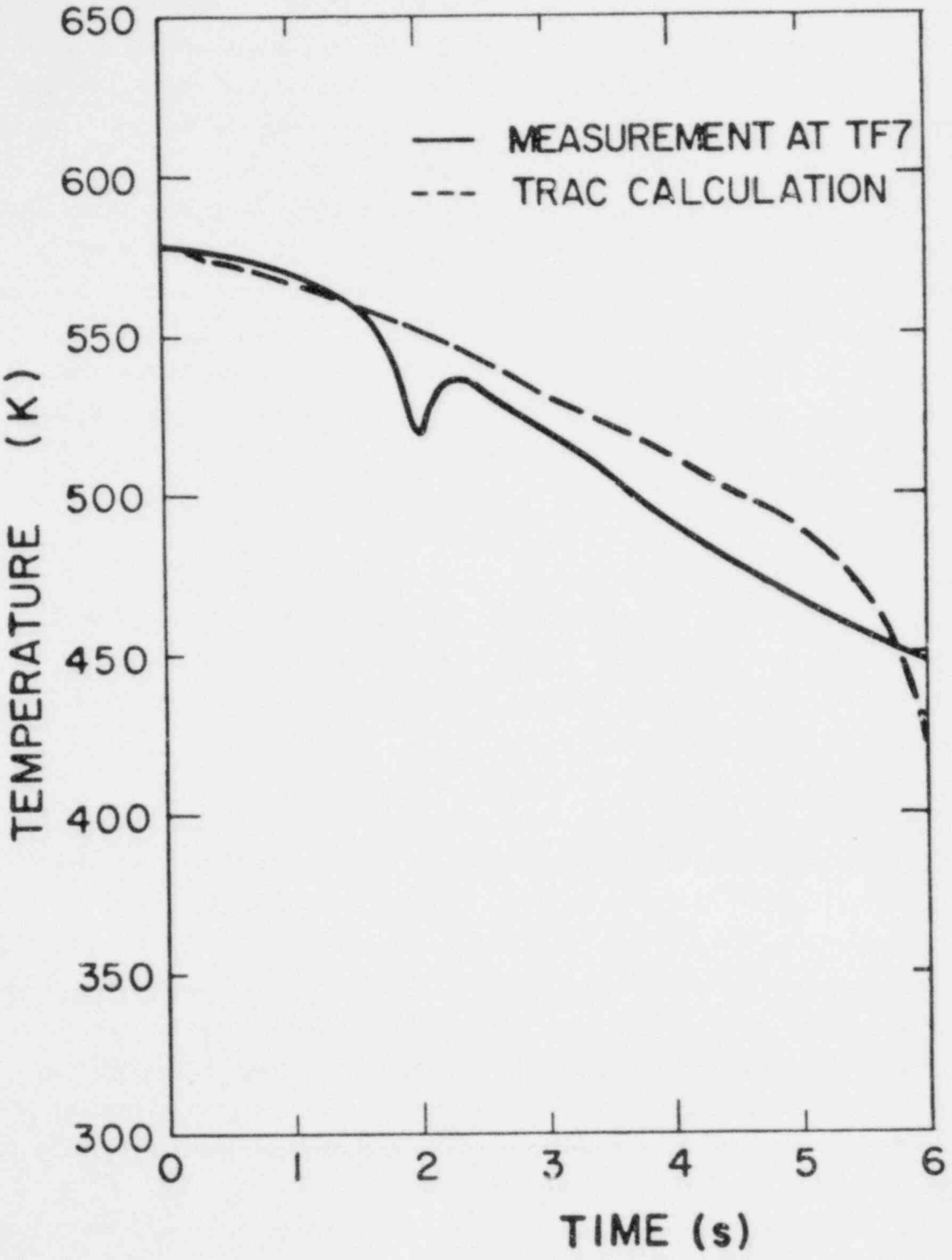

Fig. 23. Heated CISE fluid temperature at measurement station TF7.

The calculated and measured pipe wall temperatures near the top of the heater section and at the radial midpoint of the wall, THW4, are plotted in Figs. 24 and 25 for the unheated and heated cases, respectively. Agreement is good throughout the transient for the unheated case. For the heated case the calculated time to dryout is delayed 1 s beyond the measured time.

The total test section masses as a function of time for the unheated and heated cases are shown in Figs. 26 and 27, respectively. The agreement is good for the unheated case where measurements were available to 2 s only. For this case the calculated initial total test section mass was slightly below the experimental value. For the heated case the calculated mass deviates somewhat from the measurements after 1 s. Measured values are not available after 4 s in the heated case. Calculated and measured initial total test section masses agree more closely than in the unheated case and may be due to better matching of the initial fluid conditions.

Experimental uncertainty information was not provided; however, accuracy data for various transducers was given.[5] The pressure transducer accuracy for the range of 0 to 11 MPa with a 1 ms time constant was $\pm$ 0.150 MPa. Fluid temperature transducer in situ calibration showed that measured temperature accuracy was $\pm$2 K up to 543 K.

4. Parametric Studies

In the unheated case the parameters varied were the friction factor correlations, pipe-wall stored energy, and the fluid mesh spacing. Refinement of the fluid mesh spacing at the break and at the measurement station 0.365 m from the break had little effect on the results. The 38 fluid cells indicated in Fig. 17 represent the fluid mesh spacing used in both the unheated and the heated cases. The importance of heat transfer of energy stored in the pipe wall to the fluid was determined by performing calculations both with and without this effect included. Heat transfer of the stored energy significantly affected the results and was required for agreement between calculated and experimental results.

The 38-cell model with wall heat transfer was used to determine the effect of friction factor correlations for the unheated case. Calculated results were found to be sensitive to the friction factor correlation used. The annular correlation (NFF=4) gave the best agreement with experimental

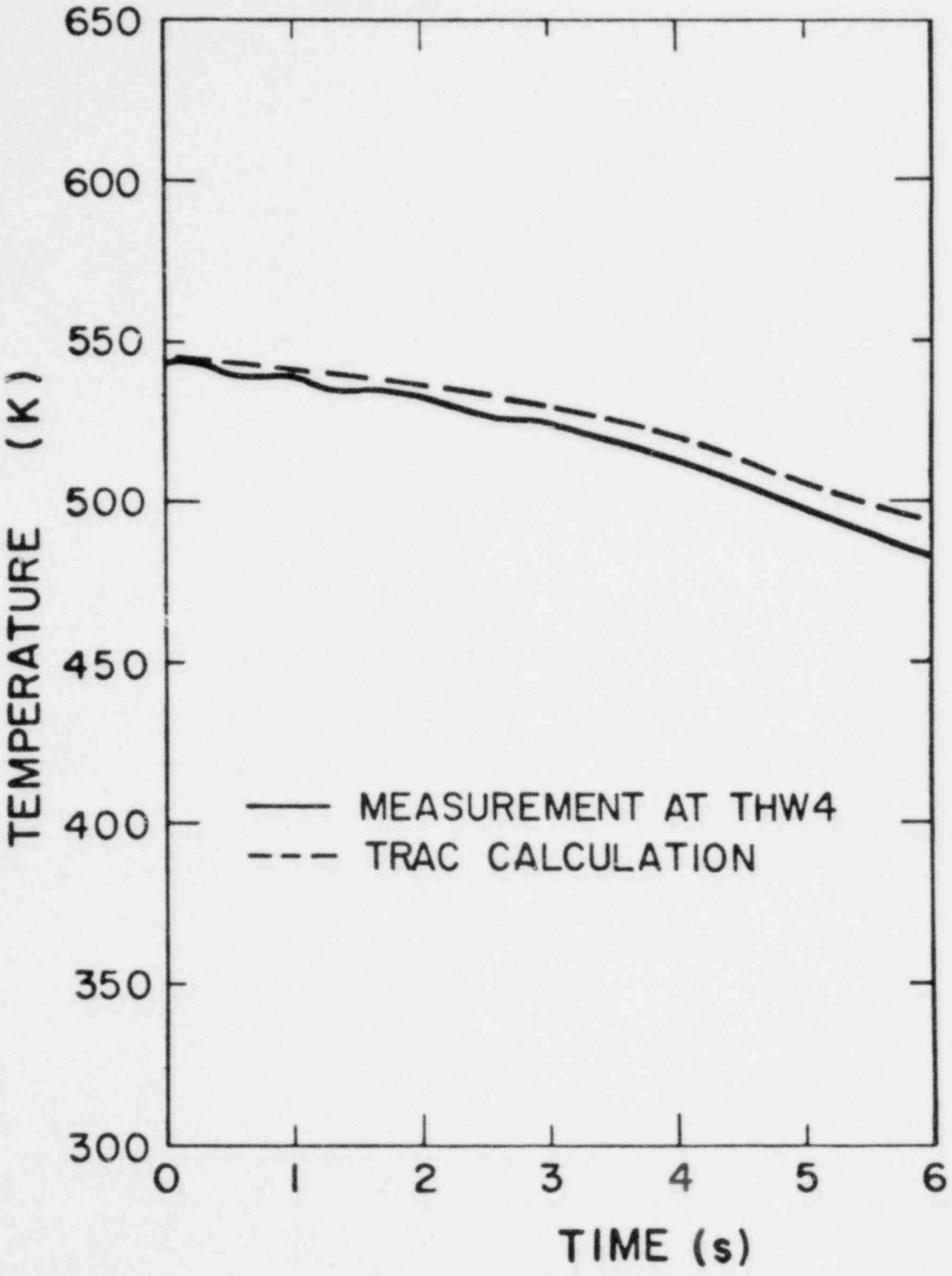

Fig. 24. Unheated CISE wall temperature at location THW4.

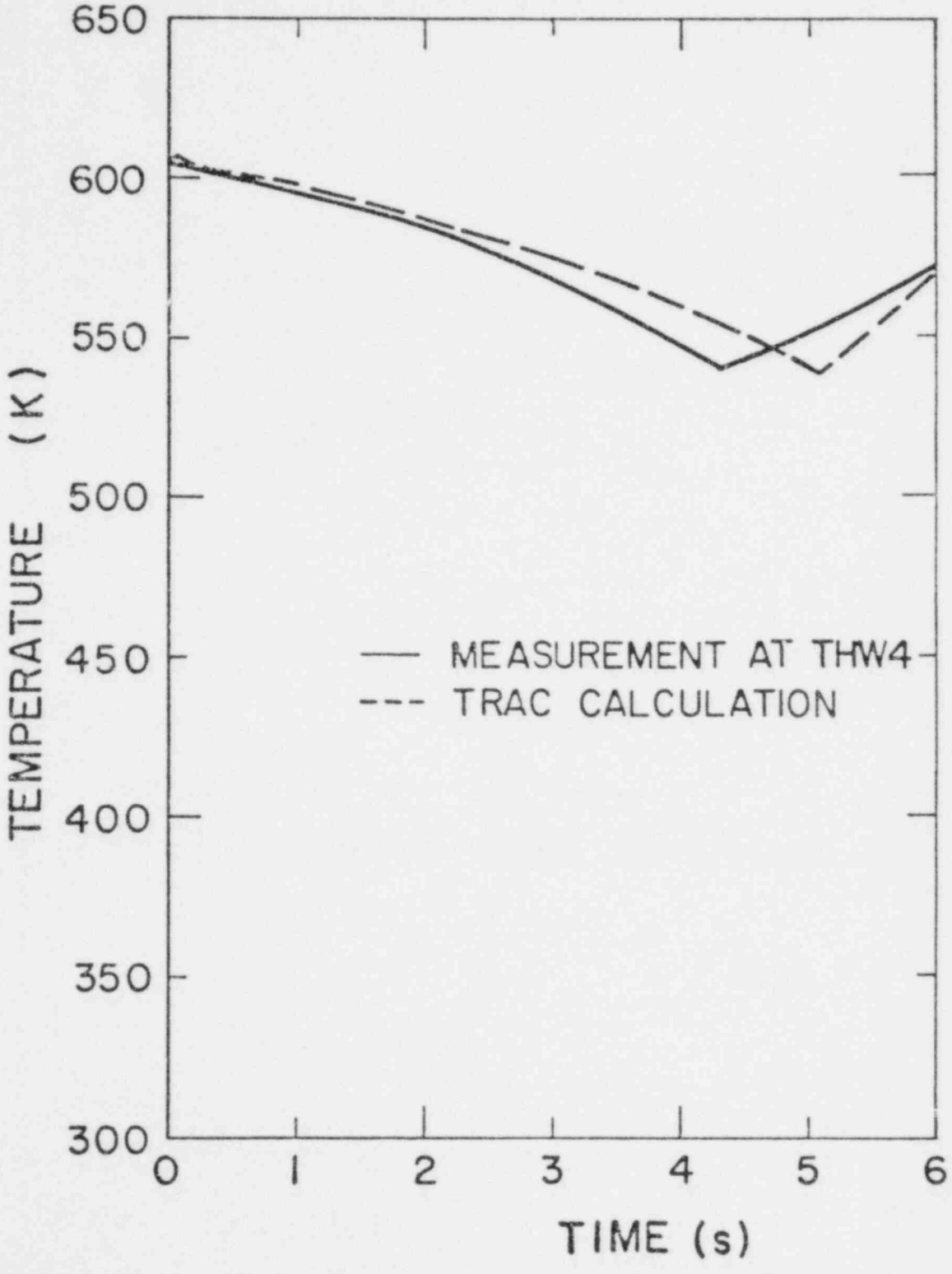

Fig. 25. Heated CISE wall temperature at location THW4.

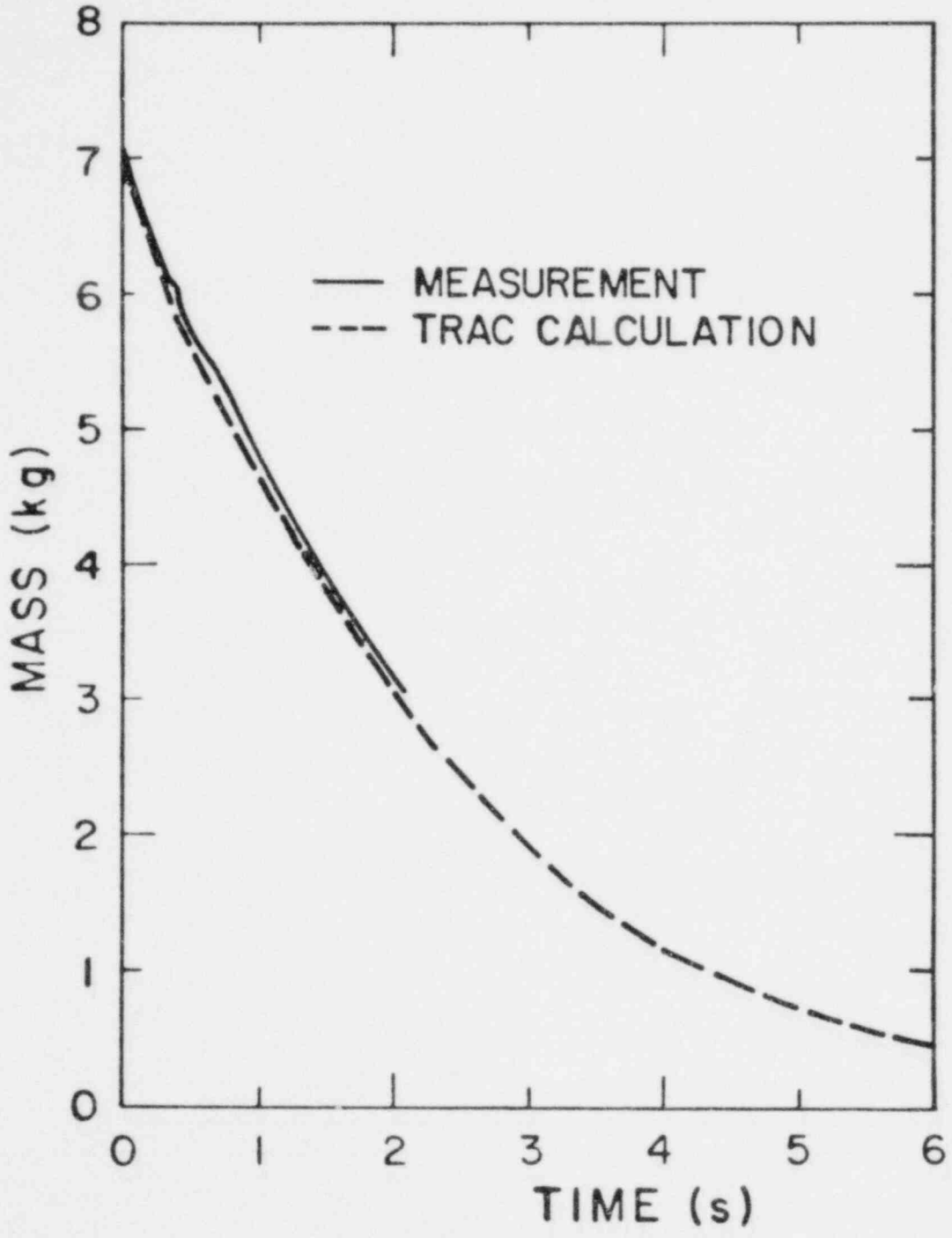

Fig. 26. Unheated CISE test section mass inventory.

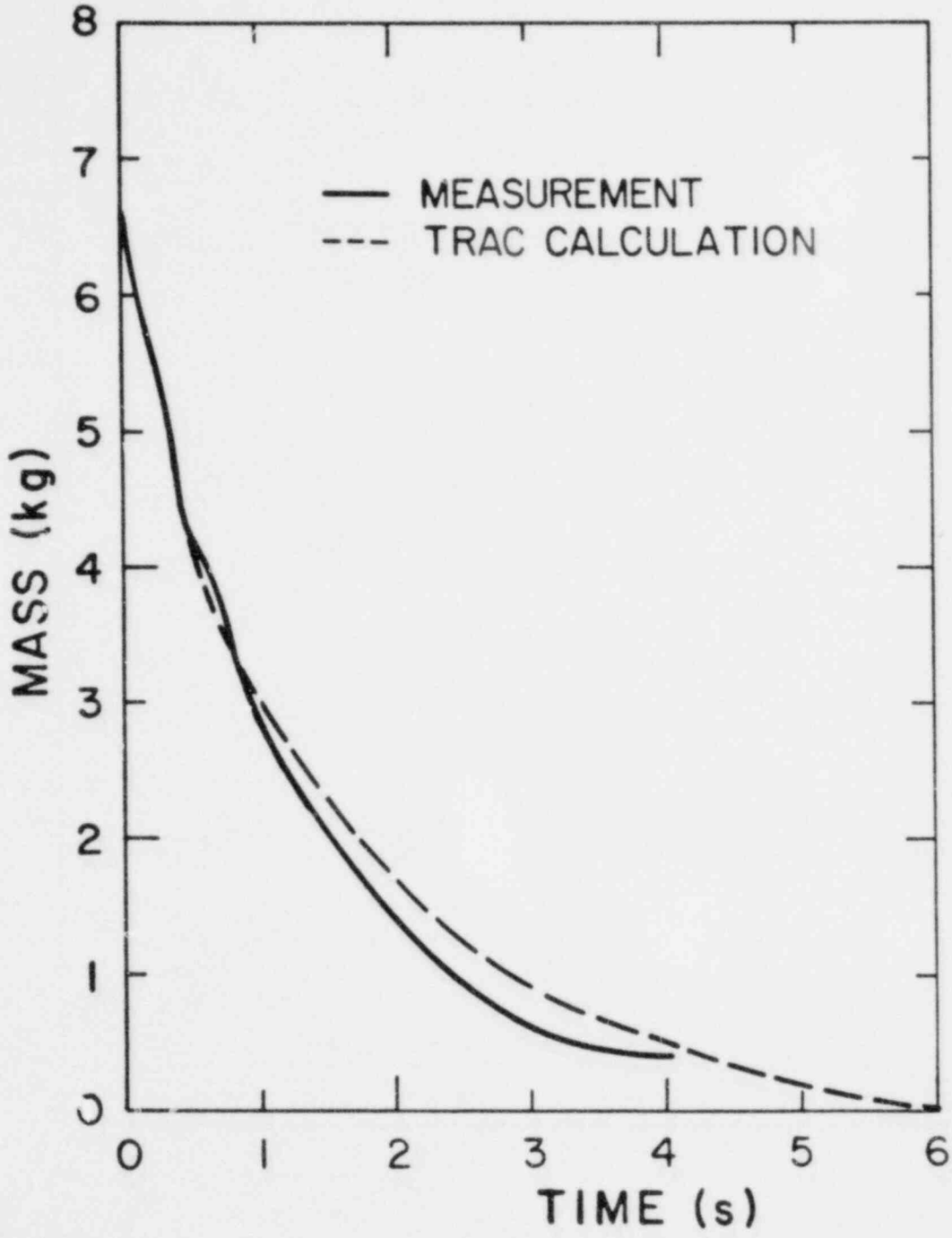

Fig. 27. Heated CISE test section mass inventory.

results. With the homogeneous correlation (NFF=1), the CISE correlation (NFF=3), and the Chisolm correlation (NFF=5) the system depressurizes too rapidly. For the Armand correlation (NFF=2) the system depressurizes too slowly.

The heated case parametric studies used the same friction factor correlation (NFF=4) and the same fluid mesh spacing determined for the unheated case. Parameters that were varied in the heated case included the number of radial heat transfer nodes and initial temperature distribution in the heater pipe wall, and the heat transfer coefficient at the outer surface of the heater pipe wall.

As in the unheated case, two radial nodes were used in the feeder and riser pipe walls. For the heated case with 109.5 kW of electrical power to the heater section, studies were performed with two, three, and five radial nodes in the heater wall. Calculated heater pipe wall temperatures are sensitive to the number of heat transfer nodes in the heater pipe wall. The best agreement with experimental data was obtained with five radial heat transfer nodes, but the use of only three nodes gave adequate results. Fluid pressure, temperature, and mass holdup are not sensitive to the number of wall nodes.

Flat initial radial temperature distributions were used in the feeder and riser pipe walls. Both flat and linear initial radial temperature distributions were used in the heater pipe wall. Calculated results were insensitive to the initial wall temperature distribution selected.

Calculations were performed for two different values for the heat transfer coefficient from the outer surface of the heater wall to the surrounding ambient air. The two values, 10 and 50 W/m^2K, correspond to minimum and maximum expected values. The 50 W/m^2K coefficient yields slightly better agreement with experimental results; however, the difference was not significant.

5. TRAC-PlA Features Tested

The CISE experiments involve the same thermal-hydraulic effects as the Edwards experiment (Sec. A) plus a few additional ones. These additional effects include wall heat sources, flow area changes (multisection pipes), and gravitational effects (nonhorizontal pipe sections). No new code modules are involved in the CISE experiments beyond those used in the Edwards experiment.

Because the CISE test section is longer and of smaller diameter than the pipe used in the Edwards experiment, the results are more sensitive to the wall friction factor correlation. The generally good agremeent obtained between calculation and experiment for the unheated case indicates that the annular friction factor correlation (NFF=4) is appropriate for this experiment. It would be desirable, however, if the friction factor selection were eliminated as a user input and replaced by the pipe roughness. The code would then select an appropriate friction factor correlation based on local flow conditions as is done with other constitutive relations.

The agreement between calculation and experiment for the heated test is not as good as that for the unheated test. It is possible that some of the discrepancy is due to the use of measured and assumed initial conditions that are inconsistent with a calculated steady-state solution. The heated test also provides a more stringent test of wall heat transfer effects during blowdown and the results indicate that further code testing is required in this area.

6. Input-Data Decks

Listings of the input data decks for the unheated and heated cases are given in Figs. 28 and 29, respectively. For both of these cases the CISE facility was represented by four PIPE modules located between a FILL module and a BREAK module. A zero velocity boundary condition was specified at the closed end of the riser section using the FILL module. The BREAK module imposes a fixed-pressure (0.1 MPa) boundary condition at a distance approximately one cell away from its adjacent PIPE module. The fully implicit hydrodynamics option (IHYDRO=1) is used in the PIPE module adjacent to the break because high flow velocities occur at this location. The other PIPE modules use the partially implicit numerical hydrodynamics option (IHYDRO=0). For the heated case the input for the PIPE module representing the heated test section uses several features not used by the other PIPE modules. One of these is specification of the heat transfer coefficient between the outer boundary of the pipe wall and the ambient air (HOUTV=50). Another is specification of a critical heat flux test (ICHF=1). Linear interpolation was used to obtain initial fluid cell temperatures and initial heater wall node temperatures.

The computer CPU time on a CDC 7600 was 75 s for the unheated transient calculation and 184 s for the heated transient calculation.

```
                1
CISE UNHEATED BLOWDOWN EXPERIMENT
                                0
                0               1                   6                   5
  1.000000E-03  1.000000E-03  1.000000E+00
               10              20                  20                   0
                1               2                   3                   4                   5
                6
FILL                            1                   1
                1
  1.010300E+00  5.364000E-04                                                    5.835000E+02
  9.820000E+06
PIPE                            2                   2
               10               2                   1                   2                   6
                0               0
  1.300000E-02  2.000000E-03                                                    3.000000E+02
  3.000000E+02
F    1.0103E+00E
F    5.3640E-04E
R1A 5.3093E-04R 1 3.4636E-04E
F    0.0000E+00E
R1A-1.4300E-01R 1-1.0000E+00E
R1A 2.6000E-02R 1 2.1000E-02E
F                4E
F                 E
F                 E
R1A-1.3200E+00R 1-1.9930E+00E
F    5.4400E+02E
I A 9.7800E+06     9.8000E+06E
F    5.4400E+02E
PIPE                            3                   3
               10               5                   2                   3                   6
                0               0
  1.050000E-02  2.000000E-03                    5.000000E+01  3.000000E+02
  3.000000E+02
F    4.2000E-01E
F    1.3854E-04E
R1A 3.4636E-04R 1 2.2698E-04E
F    0.0000E+00E
F   -1.0000E+00E
R1A 2.1000E-02R 1 1.7000E-02E
F                4E
F                 E
F                 E
R1A-1.9930E+00R 1-3.0410E+00E
F    5.4400E+02E
I A 9.8000E+06     9.8600E+06E
F    5.4400E+02E
PIPE                            4                   4
               10               2                   3                   4                   6
                0               0
  8.500000E-03  1.500000E-03                                                    3.000000E+02
  3.000000E+02
F    9.5570E-01E
F    2.1690E-04E
F    2.2698E-04E
F    0.0000E+00E
R 1-1.0000E+00R1A-3.6600E-01E
F    1.7000E-02E
F                4E
```

Fig. 28. Input deck for CISE unheated blowdown test.

```
F             E
F             E
F   -3,0410E+00E
F     5,4400E+02E
I A 9,8600E+06     9,9200E+06E
F     5,4400E+02E
PIPE                        5               5
              8             2               4               5              6
              0             1
  8,500000E-03  1,500000E-03                                  3,000000E+02
  3,000000E+02
R 3 1,0000E-01R 5 2,0000E-02E
R 3 2,2700E-05R 5 4,5400E-06E
F     2,2698E-04E
F     0,0000E+00E
R 1-3,6600E-01R 8 0,          E
F     1,7000E-02E
F             4E
F             E
F             E
R 1-3,0410E+00R 8 0,
F     5,4400E+02E
F     9,9200E+06E
F     5,4400E+02E
BREAK                       6               6
              5
  2,000000E-02  4,540000E-06  1,000000E+00  3,730000E+02  1,000000E+05
  1,000000E-05  1,000000E-01  1,000000E-01
  1,000000E-02  1,000000E-02  1,000000E+00
  1,000000E-05  5,000000E-03  5,000000E-01
  1,000000E-01  1,000000E-02  1,000000E+00
  1,000000E-05  1,000000E-02  6,000000E+00
  2,000000E-01  2,000000E-02  1,000000E+01
 -1,000000E+00
```

Fig. 28 (cont).

```
                1
CISE HEATED BLOWDOWN EXPERIMENT
                                0
                0               1                   6                   5
  1.000000E-03  1.000000E-03  1.000000E+00
               10              20                  20                   0
                1               2                   3                   4                   5
                6
FILL                            1                   1
                1
  1.010300E+00  5.364000E-04                                                        5.835000E+02
  9.820000E+06
PIPE                            2                   2
               10               2                   1                   2                   6
                0               0
  1.300000E-02  2.000000E-03                                                        3.000000E+02
  3.000000E+02
F    1.0103E+00E
F    5.3640E-04E
R1A 5.3093E-04R 1 3.4636E-04E
F            0.0E
R1A-1.4300E-01R 1-1.0000E+00E
R1A 2.6000E-02R 1 2.1000E-02E
F              4E
F               E
F               E
R1A-1.3000E+00R 1-1.9930E+00E
F    5.7900E+02E
I A 9.7800E+06    9.8000E+06E
F    5.7900E+02E
PIPE                            3                   3
               10               5                   2                   3                   6
                1               0
  1.250000E-02  2.000000E-03                  5.000000E+01  3.000000E+02
  3.000000E+02
F    4.0000E-01E
F    1.3854E-04E
R1A 3.4636E-04R 1 2.2698E-04E
F            0.0E
F   -1.0000E+00E
R1A 2.1000E-02R 1 1.7000E-02E
F              4E
F    1.8940E+08E
F               E
R1A-1.9930E+00R 1-3.0410E+00E
I A 5.7900E+02    5.4300E+02E
I A 9.8000E+06    9.8600E+06E
I A 5.9600E+02    6.1600E+02I 3 5.9500E+02    6.1500E+02I 3 5.9500E+02
    6.1500E+02I 3 5.9500E+02    6.1500E+02I 3 5.9500E+02    6.1500E+02
I A 5.9200E+02    6.1200E+02I 3 5.8700E+02    6.0700E+02I 3 5.8100E+02
    6.0100E+02I 3 5.7800E+02    5.9800E+02I 3 5.7500E+02    5.9500E+02
PIPE                            4                   4
               10               2                   3                   4                   6
                0               0
  8.500000E-03  1.500000E-03                                                        3.000000E+02
  3.000000E+02
F    9.5570E-01E
F    2.1690E-04E
F    2.2698E-04E
F            0.0E
```

Fig. 29. Input deck for CISE heated blowdown test.

```
R 1=1.0000E+00R10=3.6600E-01E
F   1.7000E-02E
F             4E
F              E
F              E
F  =3.0410E+00E
I A 5.4300E+02    5.4600E+02E
I A 9.8600E+06    9.9200E+06E
F   5.4400E+02E
PIPE                          5              5
                8             2              4              5              6
                0             1
  0.500000E-03  1.500000E-03                                  3.000000E+02
  3.000000E+02
R 3 1.0000E-01R 5 2.0000E-02E
R 3 2.2700E-05R 5 4.5400E-06E
F   2.2698E-04E
F            0.0E
R 1=3.6600E-01R 8 0.         E
F   1.7000E-02E
F             4E
F              E
F              E
R 1=3.0410E+00R 8 0.
    5.4460E+02    5.4200E+02    5.3970E+02    5.3800E+02    5.3450E+02
    5.2900E+02    5.2350E+02    5.1850E+02E
F   9.9200E+06E
F   5.4400E+02E
BREAK                         6              6
               5
  2.000000E-02  4.540000E-06  1.000000E+00  3.730000E+02  1.000000E+05
  1.000000E-05  1.000000E-05  1.000000E-05
  1.000000E-05  1.000000E-05  1.000000E+10
  1.000000E-05  1.000000E-04  1.000000E-02
  1.000000E-03  1.000000E-03  1.000000E+10
  1.000000E-04  1.000000E-04  1.000000E-01
  1.000000E-02  1.000000E-02  1.000000E+10
  5.000000E-04  5.000000E-04  5.000000E-01
  1.000000E-01  1.000000E-01  1.000000E+10
  5.000000E-04  1.000000E-02  6.000000E+00
  1.000000E-01  1.000000E-01  1.000000E+10
-1.000000E+00
```

Fig. 29. (cont).

C. Marviken Full-Scale Critical Flow Test 4

1. Description of Experiment

The Marviken full-scale critical flow tests[8] are designed to assess the ability of computer codes to predict large pressure vessel blowdowns. Four major components are included: a pressure vessel originally designed to be part of the Marviken nuclear power plant, a discharge pipe, a test nozzle with the minimum flow area in the system, and a rupture disk assembly. Figure 30 shows the vessel which still includes part of the core superstructure and moderator tank plus three gratings installed to eliminate vortex formation. Figure 31 shows the other components. All elevations in both figures are measured relative to the bottom of the vessel. For Test 4, the nozzle had a minimum diameter of 0.509 m with a length/diameter ratio of 3.

Before the test, deionized water partially filled the vessel and was heated by taking water from the bottom of the vessel out through an electric heater and adding it back into the steam dome at the top of the vessel. This procedure produced a rather complicated initial temperature distribution in the vessel. A saturated steam dome filled the vessel region above the initial water level and the water at the nozzle inlet had a substantial amount of subcooling (about 60 K). The test was initiated by release of the rupture disks and terminated after about 48 s by closing a ball valve in the discharge pipe.

2. TRAC Best-Estimate Model

The TRAC model of Marviken Test 4 includes four components. A zero velocity FILL models the vessel upper boundary; a semi-implicit PIPE models the vessel above the 2.6 m level including the maximum diameter region plus the top cupola; a fully implicit PIPE models the lower part of the vessel, discharge pipe, nozzle, and rupture disc assembly; and a BREAK component provides a pressure boundary condition at the rupture disk assembly lower boundary. Fifteen fluid cells were used in the semi-implicit pipe and 45 in the fully implicit pipe. Figure 32 shows the noding for the vessel and discharge pipe, and Fig. 33 shows the noding for the nozzle and rupture disk assembly. The cell lengths near the discharge end are 0.03 m.

Since the vessel includes some internal structure, the model diameter was reduced from the actual 5.220 m to 5.136 m to obtain the correct initial water

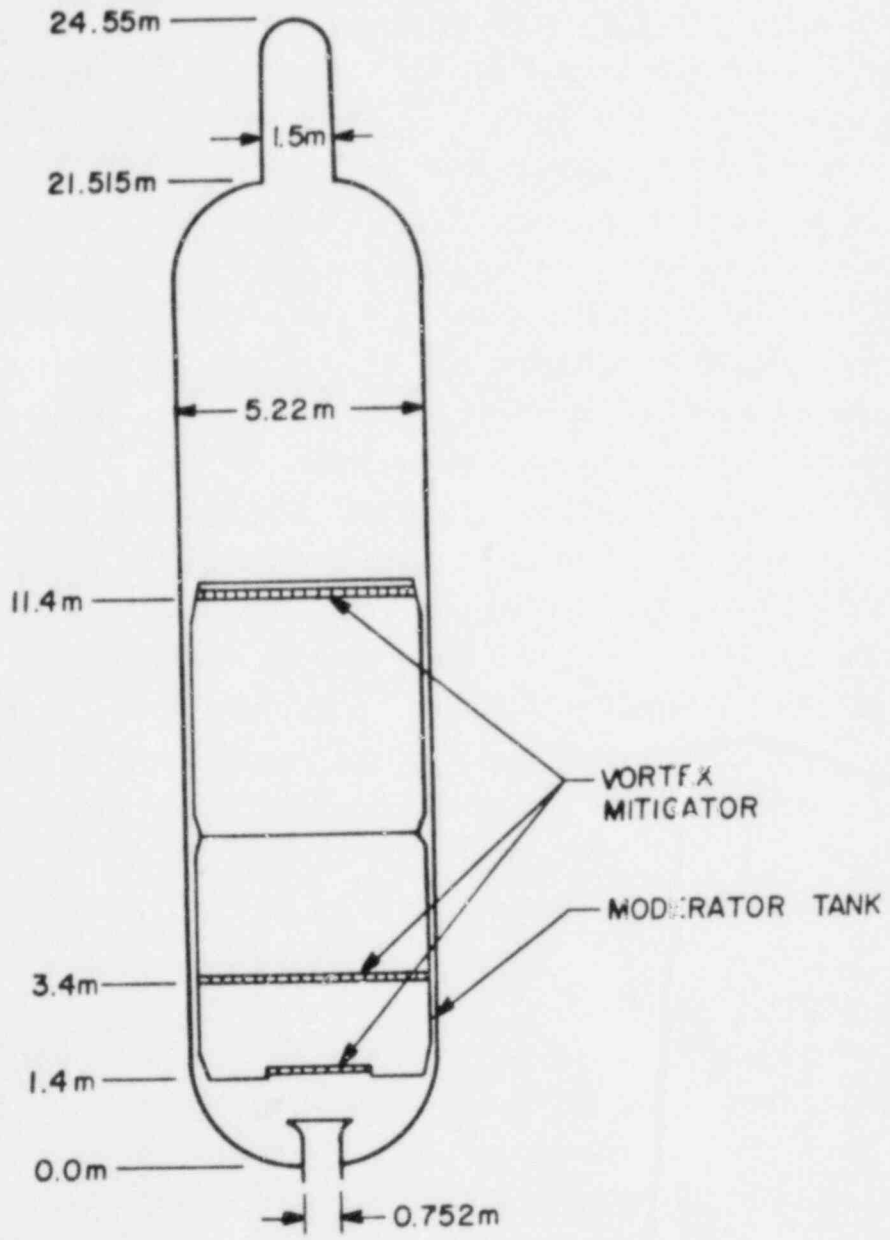

Fig. 30. Marviken pressure vessel schematic.

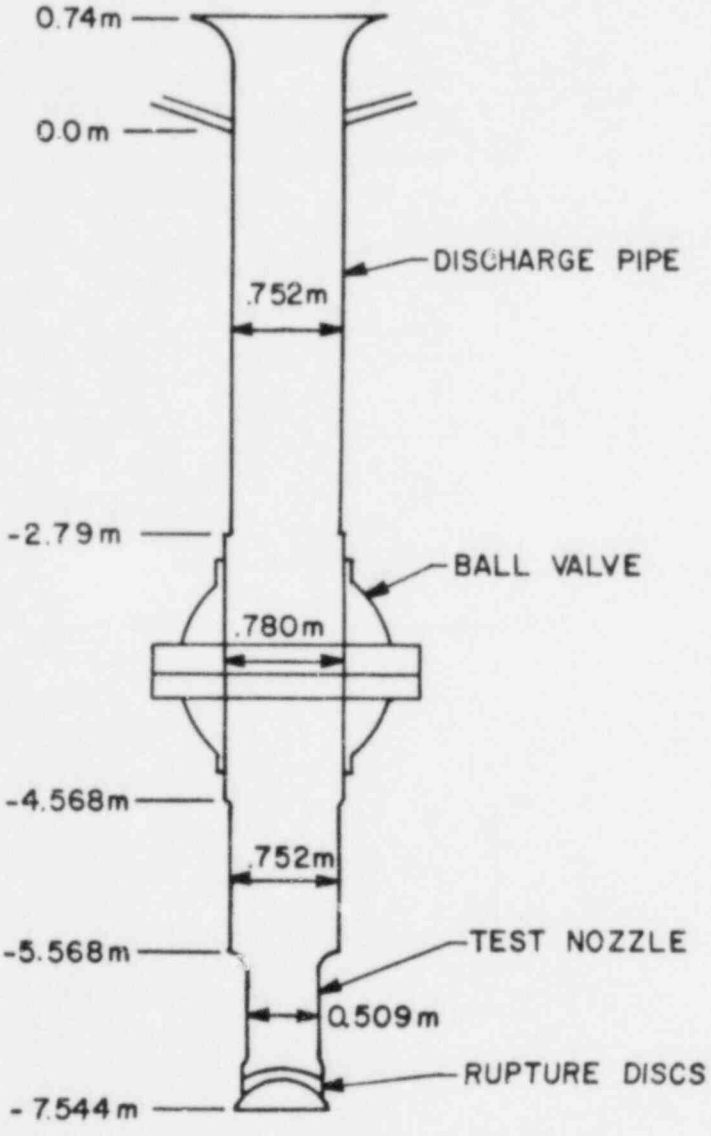

Fig. 31. Schematic of Marviken discharge pipe, test nozzle, and rupture disk assembly.

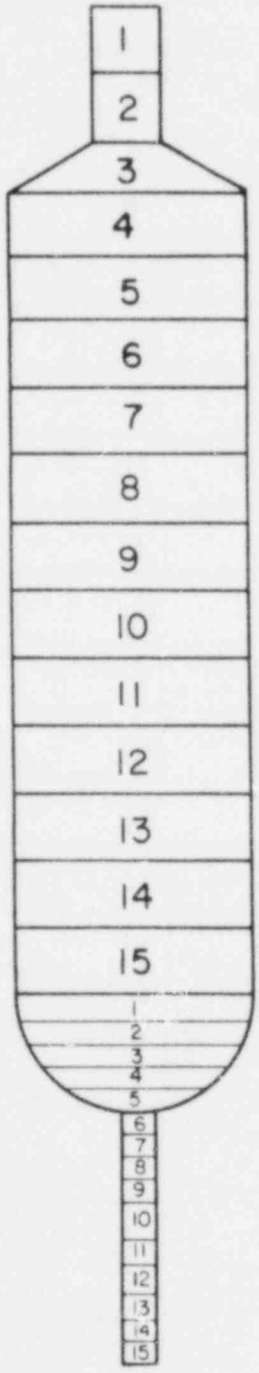

Fig. 32. TRAC noding for Marviken vessle and discharge pipe.

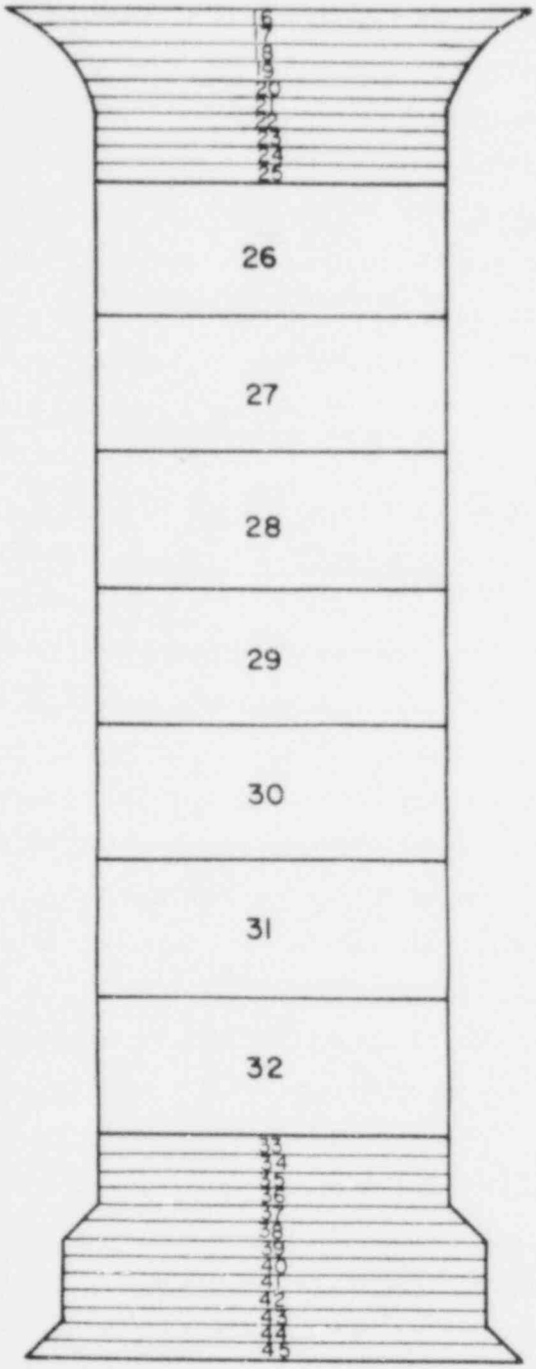

Fig. 33. TRAC noding for Marviken nozzle and rupture disk assembly.

mass and net available internal volume. The discharge pipe was modeled as starting at the vessel bottom and a loss coefficient was used to account for the fact that the inlet projects into the vessel. The annular flow friction factor correlation option (NFF=4) was specified based on comparison with results using the homogeneous flow friction factor.

3. Comparison of Best-Estimate Calculations with Experiment

TRAC results were compared with the Marviken blowdown flow rate and the pressures and temperatures at several locations. Figure 34 shows the TRAC mass flow rate compared with the flow rate derived from velocity (pitot-static) measurements. TRAC results agree very closely with the initial peak, somewhat underpredict the subcooled part of the blowdown, and agree very well with the saturated part of the blowdown (20-45 s).

Pressures near the vessel top, near the vessel bottom, and near the nozzle entrance are shown in Figs. 35, 36, and 37, respectively. The test report indicates a maximum error in pressure measurements of about 85 kPa.[8] For the vessel pressures, the TRAC results are very close to the experimental results after the first few seconds. During this early period, the data show a dip probably due to delayed nucleation in the deionized water which TRAC doesn't model. TRAC underpredicts the pressure near the nozzle entrance for the first 10 s and then is quite close to, but still below, the data for the remainder of the transient. This may be in part due to using too large a loss coefficient at the entrance to the discharge pipe.

Temperatures at three vessel locations and two discharge pipe locations were compared. The test report indicates a 2 K maximum error in temperature measurements.[8] However, there are also two-dimensional effects. For example, there are 11 thermocouples at the same axial location in the discharge pipe and the differences in their measurements range from about 2 K near the beginning and end of the transient to about 7.5 K at 10 s into the transient. These differences are probably caused by nonuniform flow due to the structures remaining in the vessel.

Figures 38 and 39 show the temperatures near the top and middle of the vessel with TRAC and data agreeing very closely except for the early dip in the data due to delayed nucleation. Figure 40 shows the temperature at the 5.97 m level in the vessel; the early temperature rise is due to the convection of initially hotter water from higher elevations. The more

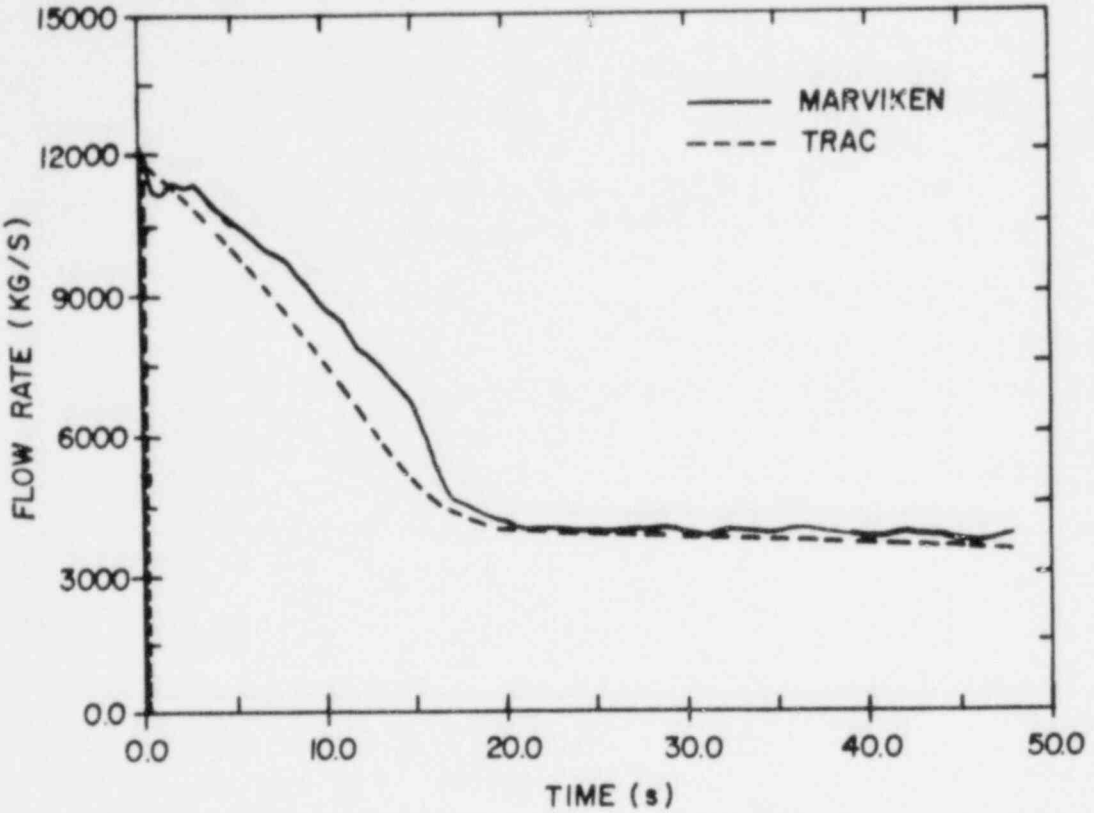

Fig. 34. Mass flow rate for Marviken blowdown experiment.

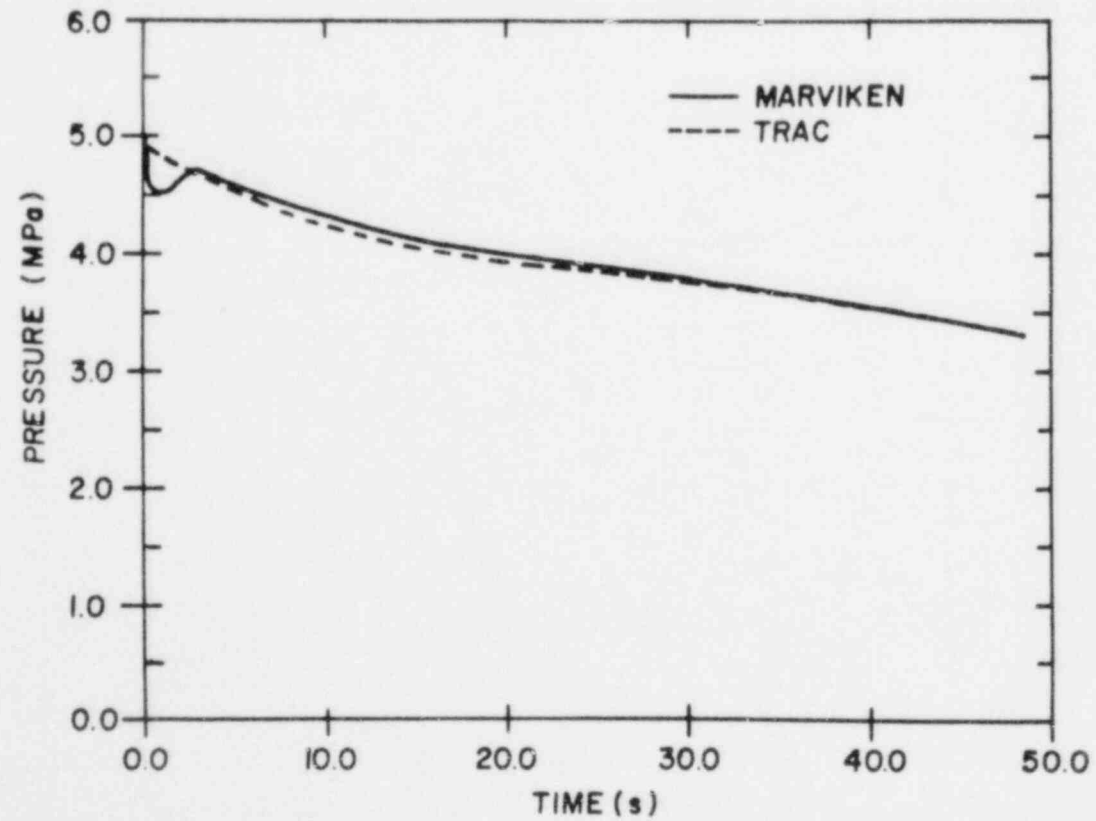

Fig. 35. Pressure near top of vessel (23.13 m) for Marviken blowdown experiment.

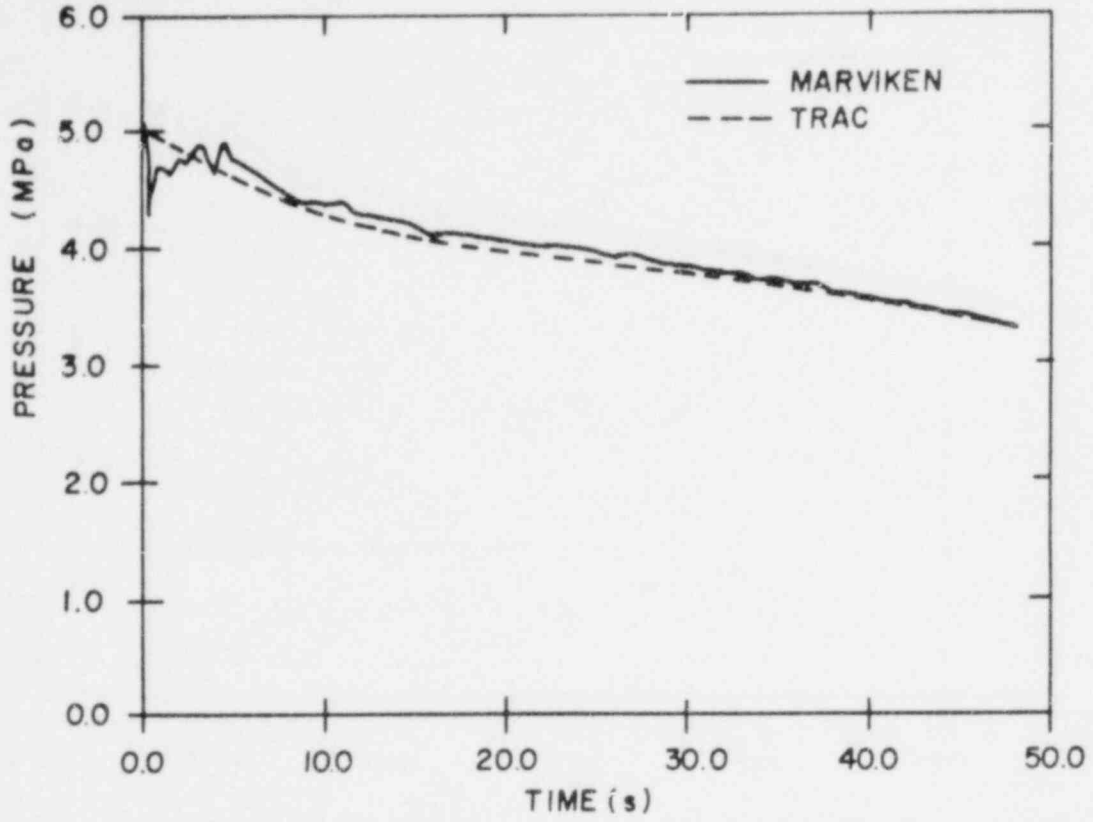

Fig. 36. Pressure near bottom of vessel (0.525 m) for Marviken blowdown experiment.

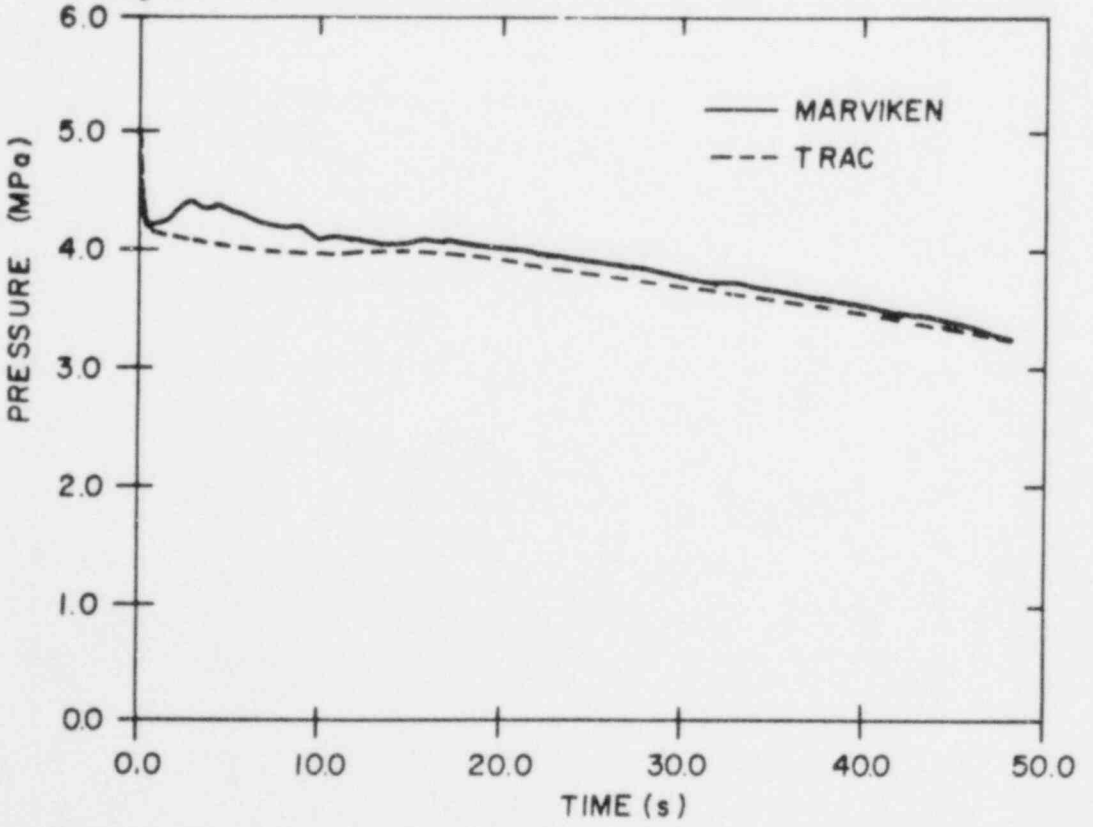

Fig. 37. Pressure near nozzle entrance (-4.868 m) for Marviken blowdown experiment.

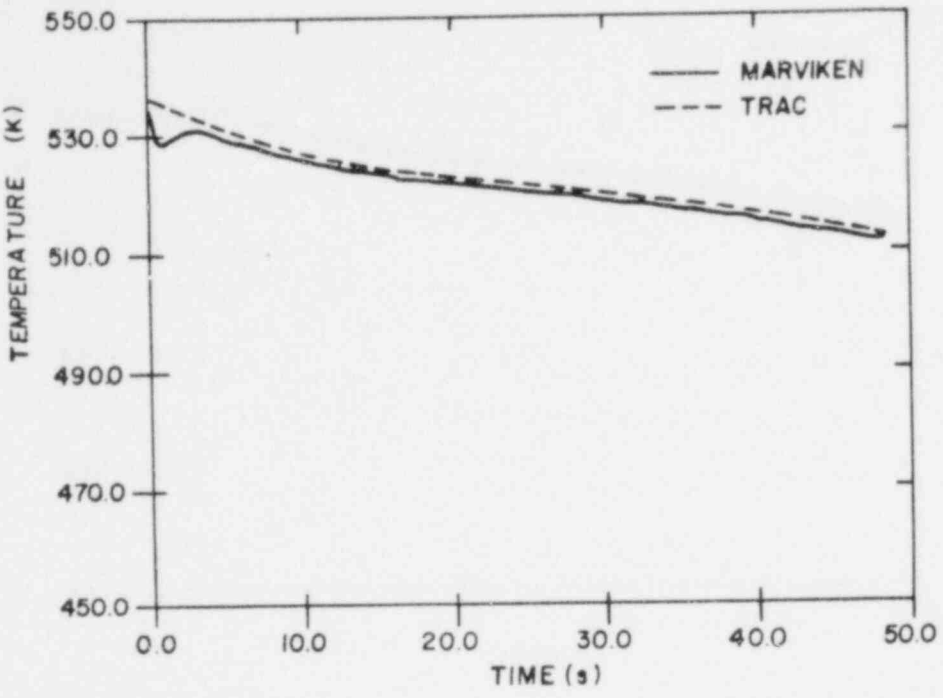

Fig. 38. Temperature near top of vessel (20.543 m) for Marviken blowdown experiment.

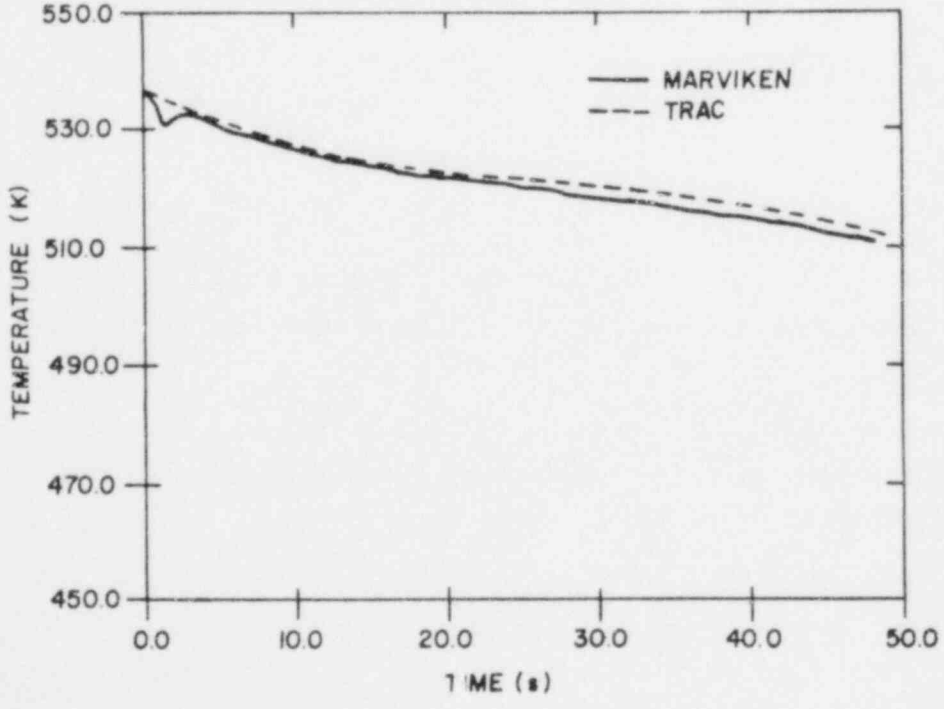

Fig. 39. Temperature near middle of vessel (10.836 m) for Marviken blowdown experiment.

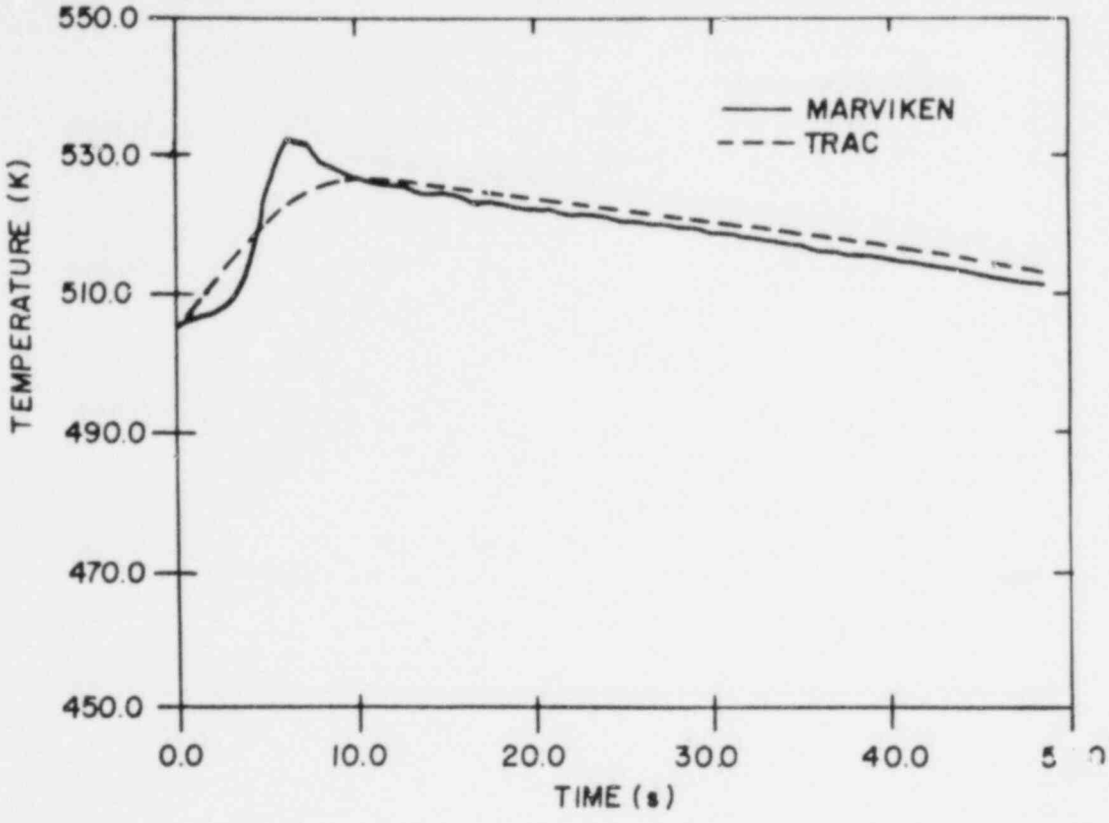

Fig. 40. Temperature at 5.97 m level in Marviken vessel.

pronounced early peak in the data may be due to nonuniform flow causing hotter fluid to move down through the center faster than the average flow at that elevation.

Figure 41 shows the temperature near the top of the discharge pipe. TRAC underpredicts the initial steep increase probably due to modeling the discharge pipe as joined flush with the vessel bottom. This causes cooler fluid to be pushed out of the vessel into the discharge pipe before the first steep ramp in the initial temperature profile arrives at this location. This ramp and also the second steep ramp may be accented in the test due to the nonuniform flow amplified by the vessel internal structure. Figure 42 compares the TRAC temperature with data near the nozzle inlet. Good agreement is obtained after the first few seconds.

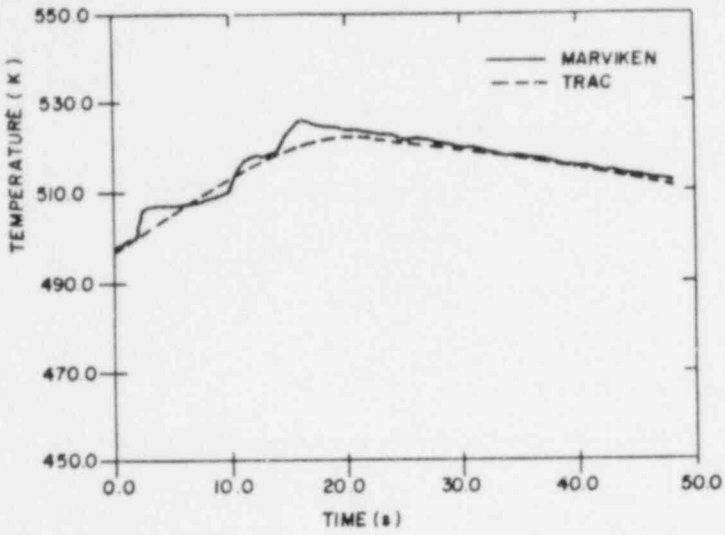

Fig. 41. Temperature near discharge pipe top (-0.63 m) for Marviken blowdown experiment.

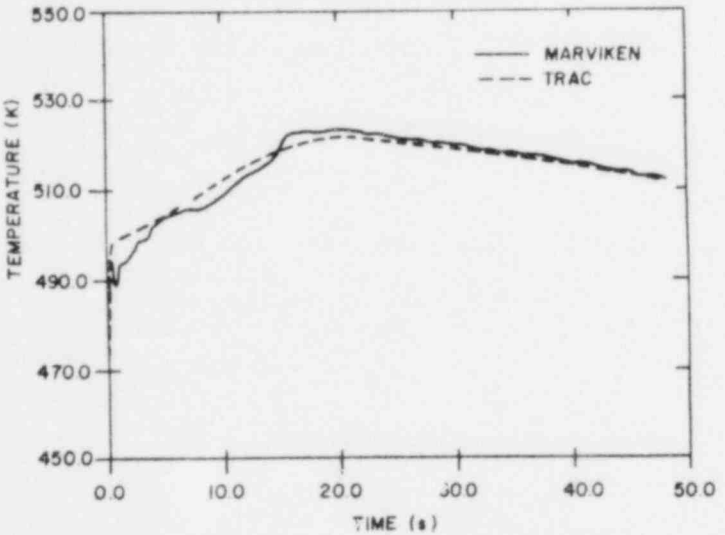

Fig. 42. Temperature near nozzle inlet (-5.543 m) for Marviken blowdown experiment.

4. Parametric or Sensitivity Studies

A 40 fluid-cell model was constructed with noding dimensions increased in all areas of the model. Flow rates differed by at most 10 percent from the 60-cell best-estimate model. The difference was largely due to the difficulty in accurately representing the steep initial temperature ramps in the vessel with the coarser noding. A model was also constructed that was identical to the best-estimate version except that the nozzle and rupture disc assembly noding was reduced from 30 cells to 14 cells. Virtually identical results were obtained indicating the best-estimate model was sufficiently detailed.

An additional calculation was performed with the best-estimate model but with the maximum allowable time step reduced from 50 ms to 20 ms. Only very small changes were observed in the results indicating the 50 ms limit was sufficiently small. Calculated results are sensitive to the initial non-uniform temperature distribution. Although this temperature distribution was specified by the experimentors, some averaging is necessary in describing the system with discretized fluid nodes.

5. TRAC Features Tested

The same code modules (PIPE, FILL, and BREAK) were used in the Marviken calculation as were used in the other blowdown calculations. In addition to most of the effects present in the Edwards and CISE experiments, the Marviken experiment includes full scale effects and large variations in flow areas. The good agreement between the calculated and measured results indicates that TRAC properly treats scale effects in one-dimensional critical-flow configurations. This calculation also identified the possible need for a delayed-nucleation model in TRAC.

6. Input Data Deck

The TRAC input data deck FOR Marviken Test 4 is shown in Fig. 43. The CPU time required to run the best-estimate model with a 50 ms time-step limit was 96 s for the 48 s transient.

D. Semiscale 1-1/2 Loop Isothermal Blowdown Test 1011

1. Description of Experiment

The Semiscale test series was designed to assess the ability of computer codes to predict the LOCA response of a scaled PWR reactor system. The volume scaling relationship between Semiscale and a large PWR is approximately 1:3000 and the test apparatus is designed with a system volume to break area ratio approximately equal to that of a large PWR.

The Semiscale isothermal test apparatus[9] in which Isothermal Test 1011 was conducted had both an intact loop with active components and a blowdown loop with simulated components. In this configuration, the operating loop represents three intact loops of a PWR and the blowdown loop represents the broken loop. An isometric view of the test apparatus is shown in Fig. 44.

```
                1
MARVIKEN II' TEST 4 DETAILED NODING

                0               1               4               3               0
             .001            .001            .01             .1
               30              80              80              0               0
                1               2               3               4
FILL                            1             128
                1               1               0               0
            1.550           2.7391             1.0             .0           535.6
          4940000.
PIPE                            2             128
              .5               0               1               2               1
                1               0
            2.610             .1              .0              .0            300.
             300.
            1.550           1.600        1.000R 2        1.400R10        1.500E
           2.7391          2.8274        9.511AR 2      29.0046R10      31.0764E
R 3        1.7671R13      20.7176E
F           .0000E
F          -1.0000E
R 3        1.5000R13       5.136E
F             4E
F           .0000E
R 5        1.0000R10        .0000E
F           .0000E
R10         536.2           523.          510.R 2         506.            501.
         4934000.R 3    4935000.R 2    4936000.        4949000.        4961000.
         4973000.       4985000.       4997000.        5009000.        5022000.
         5034000.       5046000.E
PIPE                            3             128
               45               0               2               3               1
                1               1
             .255             .1              .0              .0            300.
             300.
             .600R 8         .500            .790            .610            .600
             .568R 2         .500R10         .025R 7         .200R10         .025
             .022R 2         .028E
           12.1043         9.4300          7.7925          4.9886          1.5474
R 4         .2221           .3509           .2811           .2867           .2618
R 2         .2221          .010213         .008559         .007309         .006493
           .005834         .005300R 4      .005087R 7      .040696R 4      .005087
           .005561         .006552R 4      .007069         .005655         .008749
           .010522E
```

Fig. 43. Input data deck for Marviken blowdown experiment.

```
        20.7176          19.6349          18.0956          13.2025          7.0686
R A      .4441R 2         .4778R 3         .4441            .3739            .3117
         .2734            .2463            .2206R16         .2035            .2419
R A      .2827            .3432            .4094E
R S      .000             .752R40          .00PE
F       -1.0000E
        5.136            5.000            4.800            4.100            3.000
R A      .752R 2          .780R 3          .752             .690             .630
         .590             .560             .530R16          .589             .555
R 6      .600             .661             .722E
F           4E
F       .0000E
F       .0000E
F       .0000F
R S      490.             498.R 2          497.             496.             495.
         494.             492.             484.             479.             476.
R3       475.E
        5055000.         5060000.         5064000.         5068000.         5072000.
        5076000.         5081000.         5085000.         5089000.         5094000.
        5100000.         5105000.         5110000.         5115000.         5119000.
R P     5121000.R 4      5122000.R 4      5123000.         5124000.         5126000.
        5128000.         5129000.         5131000.         5133000.         5134000.
        5135000.R 4      5136000.R 5      5137000.R 3      5138000.E
HREAD                        4                128
                3                0                0                0
             .028          .010522             1.0            373.          101700.
          .00001             .05              5.0
              .1               .1             5.0
          .00001             .05              56.
             1.0               .1             10.
            -1.0
```

Fig. 43. (cont).

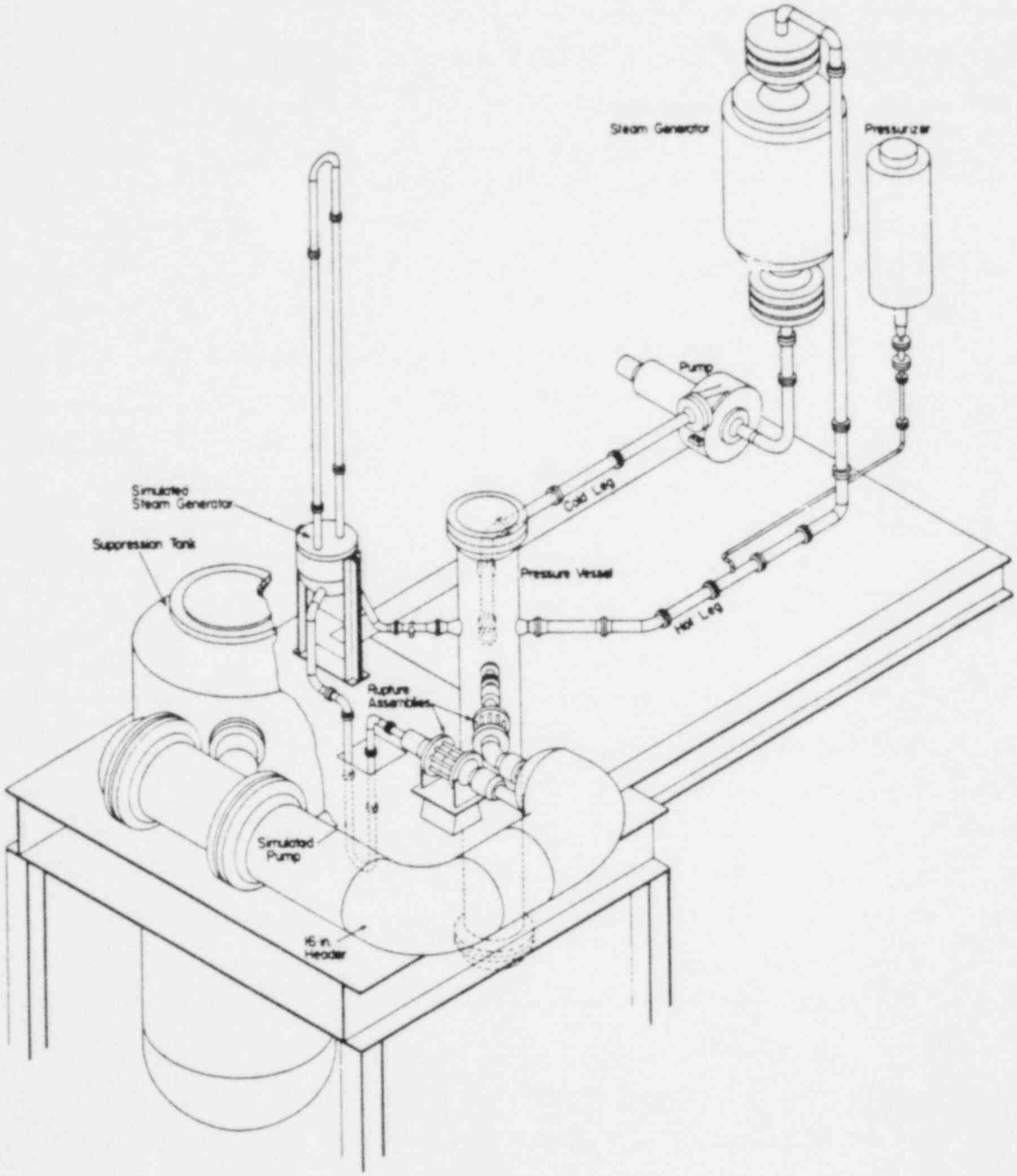

Fig. 44. Isometric of 1-1/2 loop Semiscale system (adapted from Ref. 9).

The pressure vessel contains nine electrically heated rods 1.68 m in length. For Test 1011, power to the heater rods was shut off prior to blowdown and the downcomer gap was 0.0429 m.

The operating (intact) loop of the apparatus contains a pressurizer, steam generator, and pump. The pressurizer is similar in design and function to a PWR pressurizer, the steam generator was passive (adiabatic) for Test 1011, and the pump is a centrifugal volute-type pump.

A simulated pump, simulated steam generator, two rupture assemblies, and two blowdown nozzles comprise the blowdown loop. The simulated pump and simulated steam generator are inactive and simulate the desired hydraulic resistance through the use of orifices. The full break area nozzles approximate the system volume to break area ratio of a full scale PWR. For Test 1011, however, the break area was reduced to 80% of the full size break. The nozzle used for this test has a throat diameter of 0.0149 m with an area of 1.746×10^{-4} m^2.

Prior to the test, the primary system is brought to its operating temperature by heat addition from the core and pressurizer heaters and by energy addition from the primary coolant pump. The system was brought to an approximately uniform temperature of 575 K with the upper plenum pressure at 1.57×10^7 Pa. The pressure and velocity distributions in the intact loop and vessel were determined by the loop flow rate, hydraulic resistance, and flow areas. Fluid in the blowdown loop was stagnant. The pump was operated at 84% of its rated speed prior to and after initiation of blowdown. Prior to blowdown initiation, the pressurizer liquid occupied 50% of the total pressurizer volume. The temperature of the fluid in the pressurizer surge line was not measured but was known to be cooler than that of the remainder of the system.

Blowdown is initiated by rupturing the two rupture disks. The calculation consists of predicting the system thermal and hydraulic response for 30 s following the blowdown initiation. Test 1011 is also referred to as RSR Standard Problem No. 2.

2. TRAC Best-Estimate Model

The TRAC model of the Semiscale system contains a variety of components interconnected in series and parallel branches. Although the system is complicated by area changes, orifices, and parallel branch connections, it was modeled entirely with one-dimensional components as shown in the noding diagram in Fig. 45. The system was modeled using the 16 components shown and

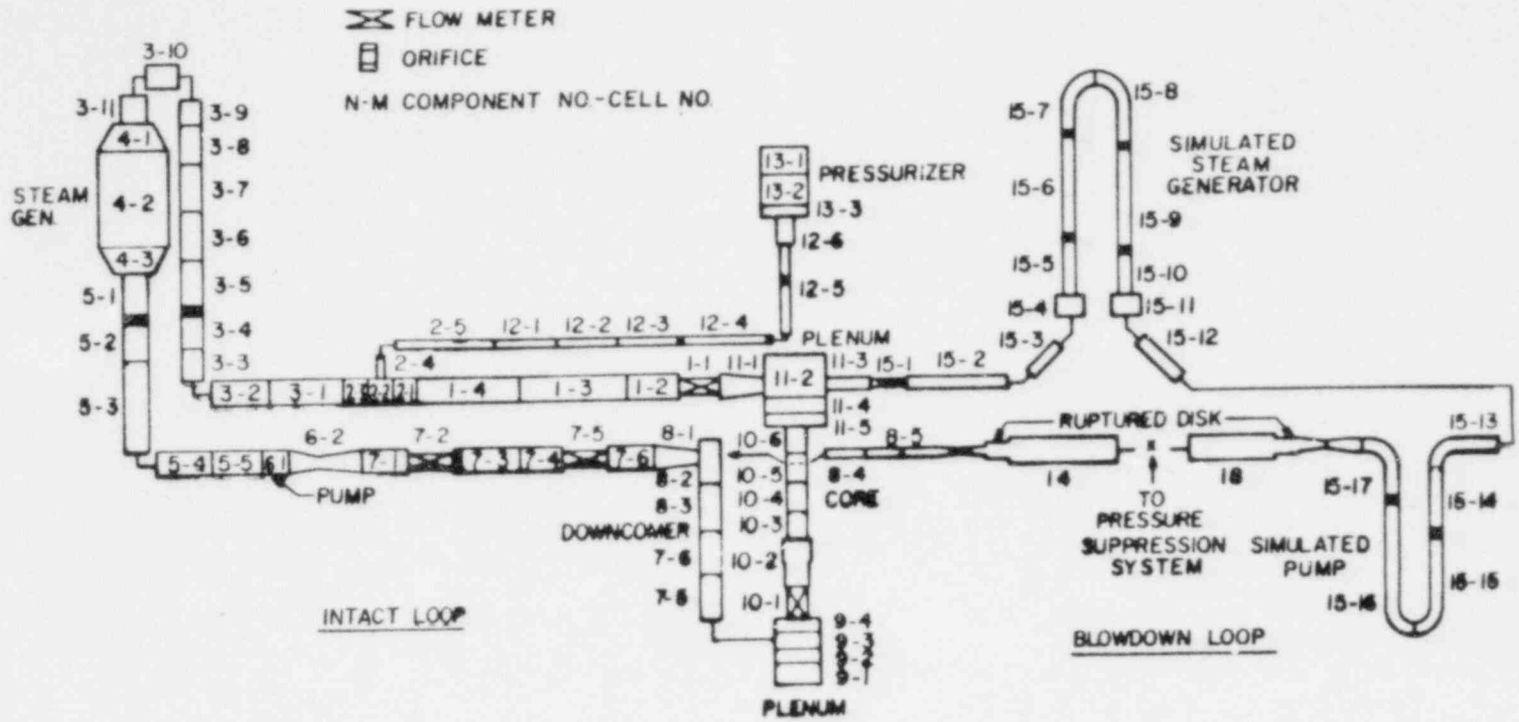

Fig. 45. TRAC noding and component schematic for Semiscale isothermal experiment.

a total of 122 fluid cells. A typical noding of the break nozzle is shown in Fig. 46.

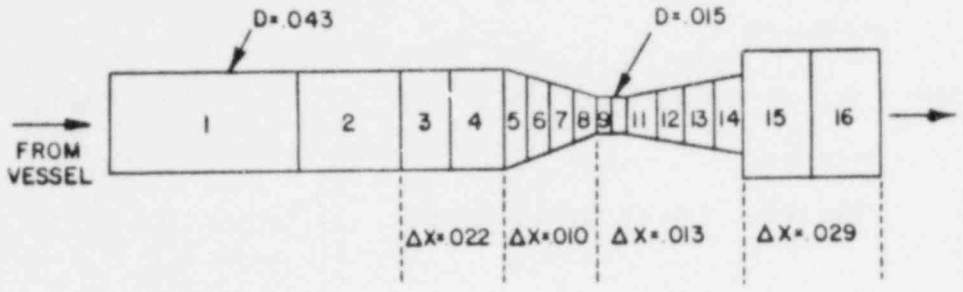

Fig. 46. Typical noding of break nozzle for Semiscale isothermal experiment.

TRAC calculations for this problem were performed in two stages. First, the initial conditions for the blowdown were obtained by performing a steady-state calculation. For this calculation, FILL modules with zero velocity are connected to the break ends of components 14 and 18 representing the initially stagnant broken loop. Starting from initial zero velocity and uniform pressure conditions for the system, and with the pressurizer partially filled with saturated liquid with the remainder being saturated vapor, the steady-state calculation is initiated by turning on the pump. The flow is accelerated to its steady-state value and the pressure distribution approaches its steady-state profile. This procedure provides self-consistent initial conditions for the blowdown transient.

The blowdown portion of the calculation is performed by restarting from the dump file obtained from the steady-state calculation and substituting BREAK modules for the FILL modules at the break end of the discharge nozzles (components 14 and 18).

3. Comparison of Best-Estimate Calculations with Experiment

Selected results of the steady-state calculation are compared with the corresponding experimentally measured values in Table III. In general the calculated steady-state results agree well with the measurements and although not identical, are acceptable for the transient initial conditions.

TABLE III

COMPARISON OF CALCULATED AND MEASURED INITIAL CONDITIONS FOR SEMISCALE TEST 1011

Quantity	Experiment	Calculated
Vessel Outlet Temperature (K)	575.9	571.4
Pressure at Vessel Outlet (Pa)	1.557×10^7	1.557×10^7
Intact Loop Volumetric Flow Rate (m^3/s)	0.0108	0.0117
Pump Differential Pressure (Pa)	2.55×10^5	2.56×10^5

Comparisons between the calculated and measured mass flows out of the blowdown-loop hot leg (component 18) and cold leg (component 14) are shown in Figs. 47 and 48, respectively. The calculated hot-leg mass flow is in excellent agreement with the measurements whereas the calculated results for the cold-leg mass flow are somewhat high.

The pressure in the vessel lower plenum is shown in Fig. 49. This pressure plot is typical of the pressure histories at all points in the vessel. Excellent agreement between calculation and measurement is obtained. The pressurizer pressure is shown in Fig. 50. The calculation overpredicts the pressure in the 3-8 s time interval but agrees well with the measurement during the remainder of the transient.

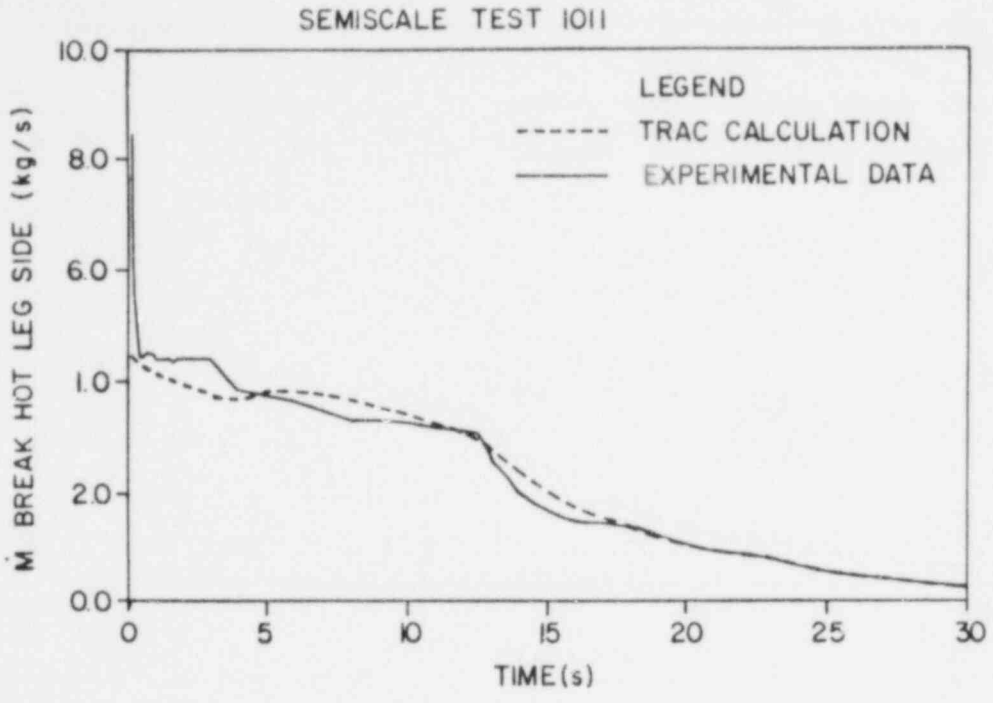

Fig. 47. Hot-leg break mass flow for Semiscale Test 1011.

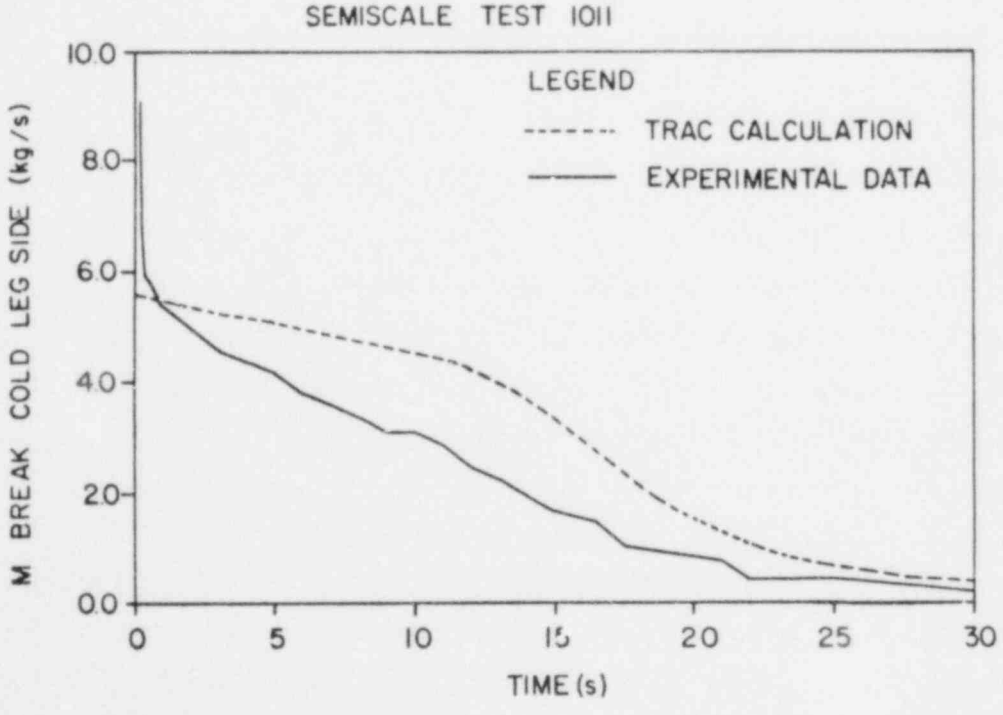

Fig. 48. Cold-leg break mass flow for Semiscale Test 1011.

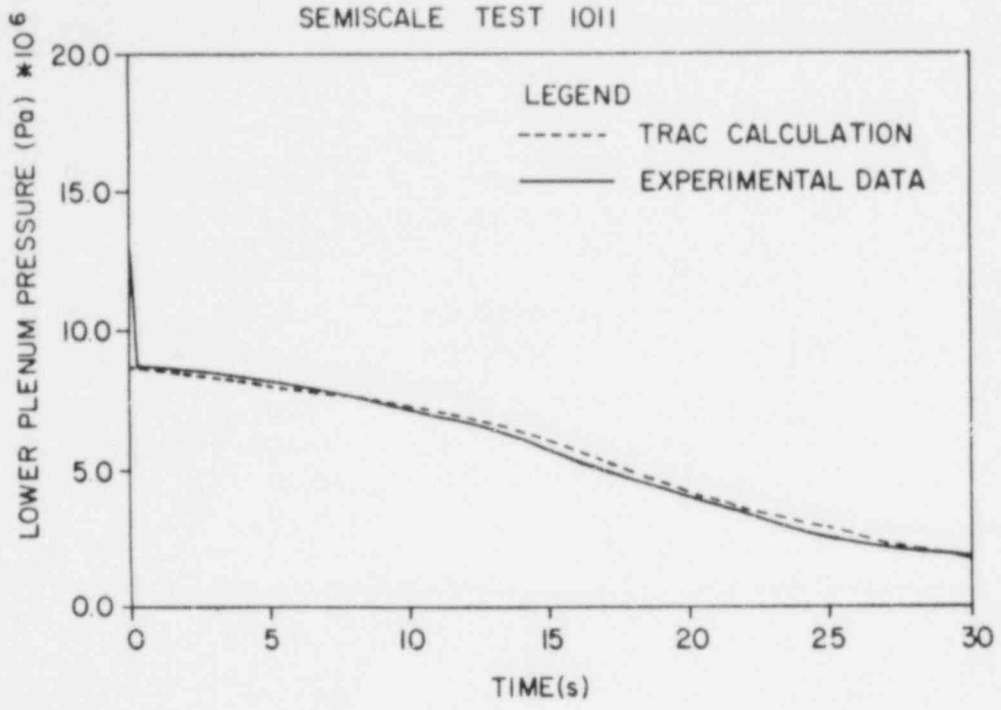

Fig. 49. Lower plenum pressure for Semiscale Test 1011.

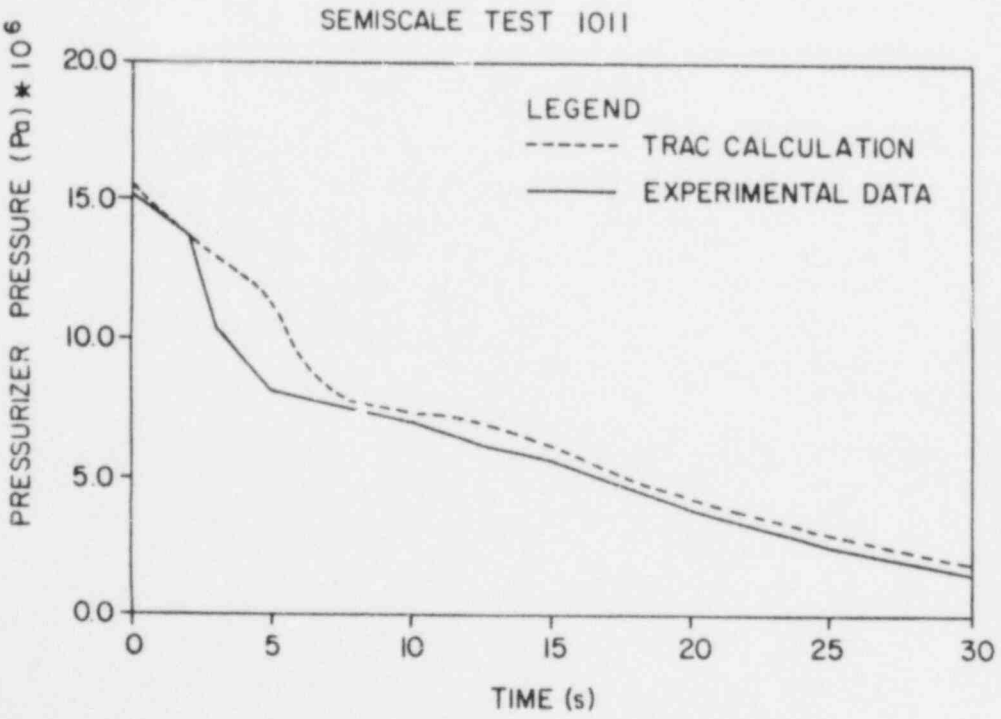

Fig. 50. Pressurizer pressure for Semiscale Test 1011.

The pump discharge density and mass flow are shown in Figs. 51 and 52, respectively. The calculations are in good agreement with the data for these quantities. The differential pressure across the pump is shown in Fig. 53. Agreement for this quantity is excellent. The fluid temperature at the pump is shown in Fig. 54; the agreement for this quantity is also excellent.

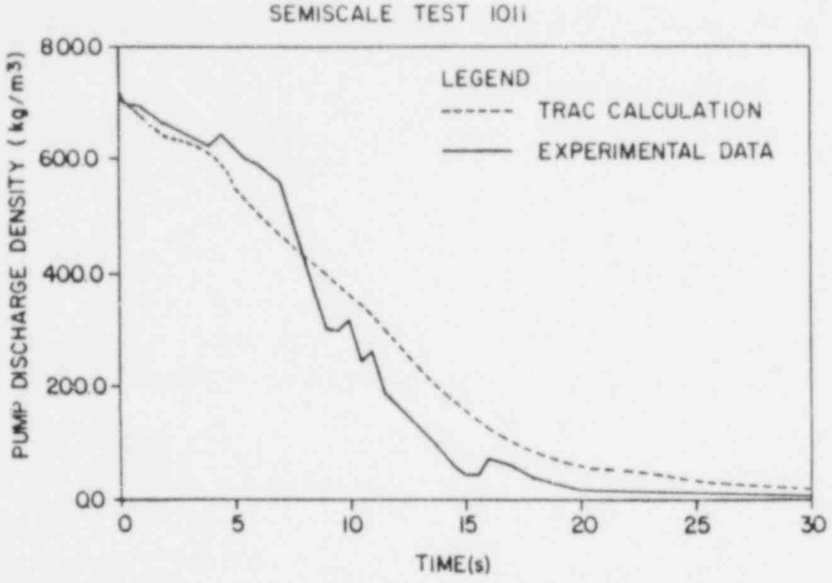

Fig. 51. Pump discharge density for Semiscale Test 1011.

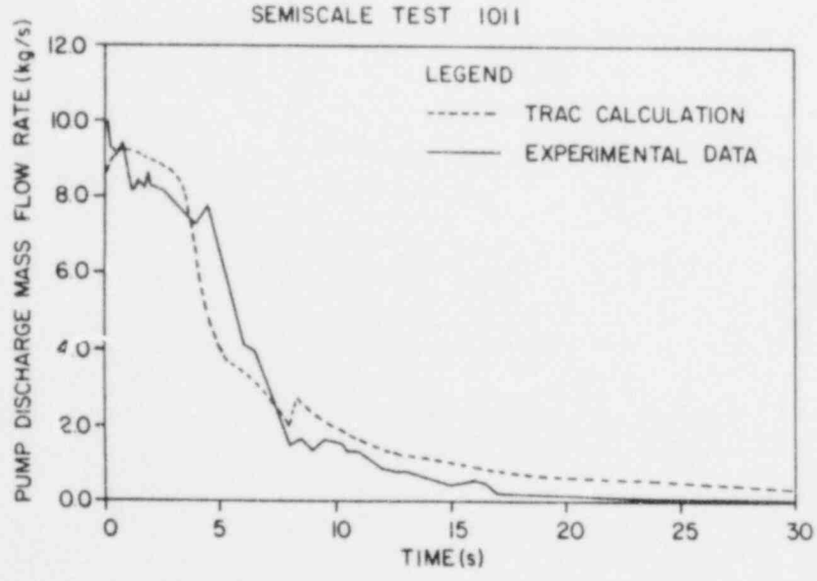

Fig. 52. Pump discharge mass flow for Semiscale Test 1011.

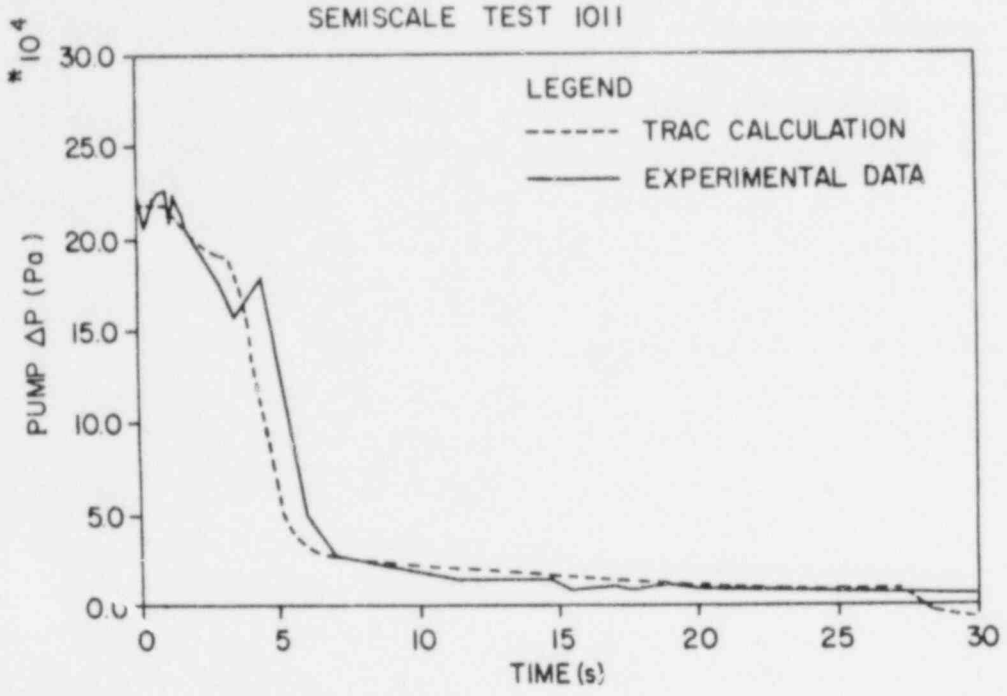

Fig. 53. Pump differential pressure for Semiscale Test 1011.

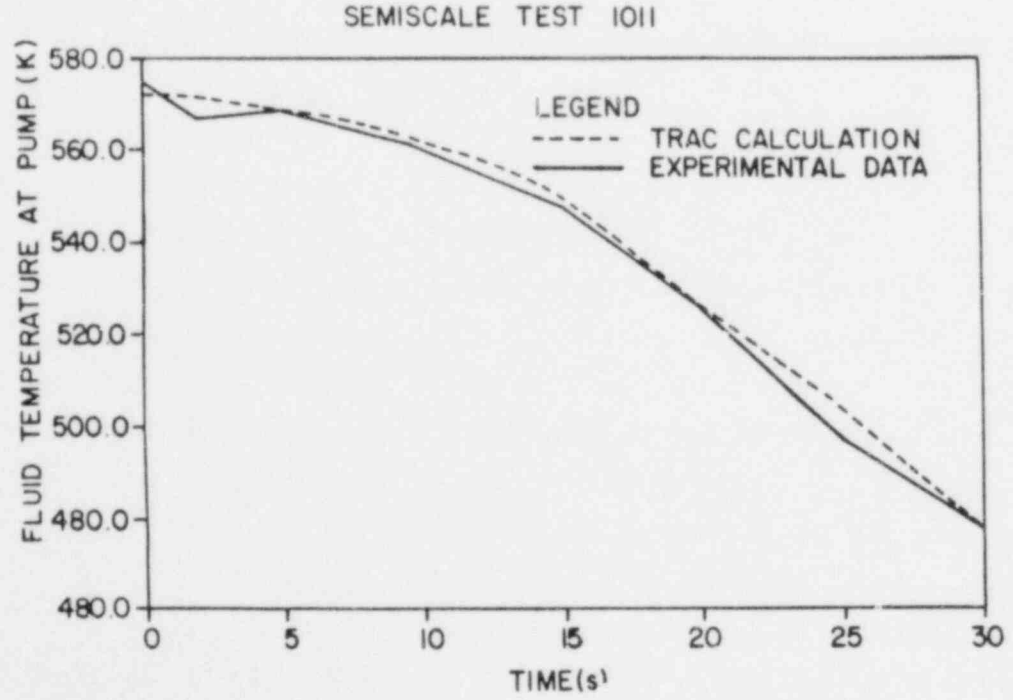

Fig. 54. Pump fluid temperature for Semiscale Test 1011.

The results shown here are typical of the agreement between calculated and measured results for other variables.

4. Parametric/Sensitivity Studies

The annular flow friction factor correlation option (NFF = 4) was specified for all components. This choice was based on a parametric study of the effects of various friction factor correlations on the results for this problem as well as others. Furthermore, this correlation was found to give the best results for the CISE pipe blowdown calculations.

The pressurizer was noded with two different volume lengths at the bottom of the pressurizer. It was found that the smaller volume gave much better calculations of pressurizer outlet density than did the larger volume. Location of this very small volume at the bottom of the pressurizer required other special noding procedures which are described in Sec. E. The time at which the pump head degrades is sensitive to the initial temperature of the fluid in the surge line which was not experimentally measured.

5. TRAC-P1A Features Tested

Semiscale Test 1011 represents the first assessment problem involving a complicated system containing a large variety of one-dimensional components interconnected in series and parallel branches. These components include a pump, steam generator (U-tube type), pressurizer, tees, pipes, breaks, and fills. In general, the results are in good agreement with the experiment data and are well within the range of calculated results obtained by others using a variety of LOCA codes.[10] Furthermore, it is encouraging that the one-dimensional model used to obtain these results is adequate since this experiment was designed to minimize multidimensional effects.

The calculated mass flow rates through the hot- and cold-leg break pipes compare favorably to predictions made by others[11] using a Moody choking model with a 0.7 multiplier. These results demonstrate the ability of TRAC to handle choking naturally without the use of a separate choking model.

The excellent agreement between the calculated and measured pump differential pressure and flow rates in the operating loop provide assurance that the one-dimensional quasistatic pump model employed in TRAC can provide good results for transient conditions even though it is based on steady-state pump data.

In summary, Semiscale Test 1011 provides a test of TRAC's ability to

handle synergistic and systems effects in coupled one-dimensional components during the blowdown stage of a LOCA. Effects associated with ECC injection and rod heat transfer during blowdown are not included in this problem.

6. Input Data Decks

A listing of the input data deck used to generate the initial conditions for the transient calculation, i.e., the data deck for the steady-state calculation, is given in Fig. 55. Several features contained in this data deck should be noted. First, the open ends of components 14 and 18 are connected to FILL components (Nos. 16 and 17) with the fill velocity specified as zero. Thus, for the steady-state calculation, there is no flow out of these pipes and stagnant fluid is present for this portion of the calculation. The lower plenum is modeled using a TEE component. A zero velocity FILL component (component No. 19) is connected to cell 9-1 of this TEE. The zero velocity boundary condition at this point represents the geometric bottom of the lower plenum.

With cell lengths of ~0.01 m in components 14 and 18, the time step size would have to be kept below ~0.1 ms for stability considerations if the partially implicit (IHYDRO = 0) hydrodynamics option were used. Therefore, the fully implicit option is specified for components 14 and 18 with the partially implicit numerical solution procedure specified for the remainder of the components.

A listing of the input data deck used for the transient blowdown calculation is shown in Fig. 56. As shown, this deck replaces the FILL components (Nos. 16 and 17) used for the steady-state calculation with BREAK components to specify the pressure boundary condition at these locations. The remainder of the initial conditions as well as the geometric data are obtained from information contained in the dump file. This file contains the results from the steady-state calculation. The transient is initiated from the information at time step number 356 of the steady-state calculation.

The computer CPU time on the CDC 7600 was 19 min for the transient calculation.

```
1                3
2 SEMISCALE TEST 1011  (STANDARD PROBLEM 2)
3 MS2S1AI
4
5
6                1              0             18             18
7          1.0 E-3        1.0 E-5        1.0 E-3
8               20            100             20
9                1              2              3              4              5
10               6              7              8              9             10
11              11             12             13             14             15
12              16             17             19
13 PIPE                        1              1
14               4              1              1              2              9
15               0              0
16    3.324800E-02  1.112520E-02                                  2.950000E+02
17    2.950000E+02
18 R 2 2.9845E-01     5.5580E-01     4.4450E-01E
19       7.7200E-04     1.0418E-03     1.9386E-03     1.5514E-03E
20 R 2 2.5650E-03R 3 3.4889E-03E
21 F     0.
22 F     0.0
23 R 2 5.7150E-02R 3 6.6650E-02E
24 F               4
25 F     0.0
26 F     0.0
27 F     0.0
28 F     5.7482E+02E
29 F     1.5513E+07E
30 F     5.7482E+02E
31 TEE                         2              2
32               2             1              9                             0
33               0             3              2              3
34    3.324800E-02  1.112520E-02                                  2.950000E+02
35    2.950000E+02
36               0             2             12
37    9.425000E-03  3.911600E-03                                  2.950000E+02
38    2.950000E+02
39 F     1.4827E-01E
40       3.7803E-01     4.4050E-01E
41 F     5.1729E-04E
42       1.0550E-04     1.2293E-04E
43 F     3.4889E-03E
44 F     2.7907E-04E
45 F     0.
46 F     0.
47 F     0.0
48       1.0000E+00R 2 0.         E
49 F     6.6650E-02E
50 F     1.8850E-02E
51 F               4
52 F               4
53 F     0.0
54 F     0.0
55 F     0.0
56 F     0.0
57 F     0.0
58 F     0.0
59 F     574.82
60 F     530.
61 F     1.551[illegible]E+07E
62 F     1.551[illegible]E+07E
63 F     574.82
```

Fig. 55. TRAC input deck for Semiscale Test 1011 steady-state calculation.

```
64 F   530.
65 PIPE                          3              3
66                11             1              3              4              9
67                 0             0
68   3.324800E-02  1.112520E-02                                                2.950000E+02
69   2.950000E+02
70     4.4480E-01    2.2380E-01    3.6225E-01    5.2735E-01R 4 6.1276E-01
71     1.9685E-01    3.8447E-01    3.4608E-01E
72     1.5514E-03    7.8080E-04    1.2633E-03    1.8394E-03R 4 2.1380E-03
73     6.8679E-04    1.3414E-03    1.4551E-03E
74 R 4 3.4889E-03    1.1009E-03R 6 3.4889E-03    8.3606E-03E
75 F   0.
76 R 2 0.            5.0000E-01R 6 1.0000E+00    5.0000E-01S
77     5.0000E-01 -0-1.0000E+00E
78 R 4 6.6650E-02    3.7440E-02R 6 6.6650E-02    1.0317E-01E
79 R 4             4             +4F            4
80 F   0.0
81 F   0.0
82 F   0.0
83 F   5.7482E+02E
84 F   1.5513E+07E
85 F   5.7482E+02E
86 PIPE                          4              4
87                3              0              4              5              9
88                0              0
89
90
91     4.4450E-01    9.4600E-01    5.1750E-01E
92     1.3300E-02    5.7000E-03    1.3910E-02E
93     8.3606E-03R 2 5.9843E-03    3.4889E-03E
94 F   0.
95 F  -1.0000E+00E
96     1.0317E-01R 2 1.3510E-02    6.6650E-02E
97 F               4
98 F   0.0
99 F   0.0
100 F  0.0
101 F  5.7482E+02E
102 F  1.5513E+07E
103 PIPE                         5              5
104               5              1              5              6              9
105               0              0
106   3.324800E-02  1.112520E-02                                                2.950000E+02
107   2.950000E+02
108     3.8450E-01    4.4480E-01    8.9850E-01    4.1470E-01    5.5280E-01
109     1.3408E-03    1.5514E-03    3.1348E-03    1.4695E-03    1.9280E-03
110     3.4889E-03    1.2426E-03R 4 3.4889E-03E
111 F   0.
112 R 3-1.0000E+00    5.0000E-01R 2 0.          E
113     6.6650E-02    3.9780E-02R 4 6.6650E-02E
114               4             +4R 4            4
115 F   0.0
116 F   0.0
117 F   0.0
118 F   5.7482E+02E
119 F   1.5513E+07E
120 F   5.7482E+02E
121 PUMP                         6              6
122               2              1              6              7              9
123               0              0              1              0              1
124
125   3.324800E-02  1.112520E-02                                                2.950000E+02
126   2.950000E+02
```

Fig. 55. (cont).

```
127   5.739000E+02  4.345000E+01  1.135500E-02  1.000000E+03  3.728000E+02
128   2.662000E+00                3.730000E+00  3.141600E+02
129                 1
130      1.1680E+00    3.8755E-01E
131      4.0776E-03    1.3520E-03E
132      3.4889E-03    7.9173E-04    3.4889E-03E
133 F  0.
134 F    0.0
135      6.6650E-02    3.1750E-02    6.6650E-02E
136                 4             +4             4
137 F    0.0
138 F    0.0
139 F    0.0
140 F    5.7482E+02E
141 F    1.5513E+07E
142 F    5.7482E+02E
143 PIPE                          7              7
144                 6             1              7              8              9
145                 1
146   3.324800E-02  1.112520E-02                 2.950000E+02
147
148      2.9210E-01    2.9880E-01    4.5150E-01    3.2100E-01S
149      2.9210E-01    2.9880E-01E
150      1.0191E-03    7.7199E-04    1.5513E-03    1.1193E-03S
151      7.4929E-04    1.0418E-03E
152      3.4889E-03    2.5652E-03    1.6989E-03    3.4889E-03S
153 R 2 2.5652E-03    3.4889E-03E
154 F    0.
155 F    0.0
156      6.6650E-02    5.7150E-02    4.6510E-02    6.6650E-02S
157 R 2 5.7150E-02    6.6650E-02E
158 R 2             4             +4F            4
159 F    0.0
160 F    0.0
161 F    0.0
162 F    5.7482E+02E
163 F    1.5513E+07E
164 F    5.7482E+02E
165 TEE                           8
166                 2             1              9
167                 0             3              8              9
168      .10795         .028575                                      295.
169       295.
170                 0             2             16
171      .033248        .0111252
172       295.
173      .1953          .53975        .53975
174 R 2 .1397
175      1.0877 E-3R 2 .012683
176 R 2 2.0194 E-4
177      3.4889 E-3    1.1401 E-3R 2  .023498
178 R 3 1.4455 E-3
179 F    0.
180 F    0.
181 R 2 0.0        R 2 -1.0
182 F    0.0
183       .06665         .03810   R 2  .085852
184 R 3  .0429
185 F               4
186 F               4
187 F     .0
188 F     .0
189 F     .0
```

Fig. 55. (cont).

```
190 F     .0
191 F     .0
192 F     .0
193 F      574.82
194 F      574.82
195 F    1.5513 E+7
196 F    1.5513 E+7
197 F      574.82
198 F      574.82
199 TEE                          9
200                 3            0              9
201                 0            4             19             10
202
203
204                 0            2              9
205
206
207 R 4 .0968375
208 R 2 .53975
209 R 4 1.9355 E-3
210 R 2 .012683
211 R 4 .019987        3.1543 E-3
212 R 3 .023498
213 F    0.
214 F    0.
215 F    1.0
216 F   -1.0
217 R 4 .1595          .063373
218 R 3 .085852
219 F               4
220 F               4
221 F    .0
222 F    .0
223 F    .0
224 F    .0
225 F    .0
226 F    .0
227 F     574.82
228 F     574.82
229 F     .5513 E+7
230 F    1.5513 E+7
231 PIPE                        10             10
232                 6            1             10             11              9
233                 0            0
234    6.110000E-02  9.525000E-03                                    2.950000E+02
235    2.950000E+02
236      1.9685E-01    2.3940E-01R 4 4.4450E-01E
237      9.6277E-04    1.5291E-03R 4 4.4266E-03E
238      3.1543E-03    3.8459E-03    3.2237E-03R 3 9.9592E-03    3.1373E-03
239 F    0.
240 F    0.
241      6.3373E-02    6.9977E-02R 5 3.6390E-02E
242 F               4
243 F    0.0
244 F    0.0
245 F    0.J
246 F    5.7482E+02E
247 F    1.5513E+07E
248 F    5.7482E+02E
249 TEE                         11             11
250                 2            1              9                              0
251                 0            3              1             14
252    3.3248C[illegible]E-02  1.112520E-02                                    2.950000E+02
```

Fig. 55. (cont).

```
253   2.950000E+02
254                0              2             11
255   1.038500E-01  2.860000E-02                                  2.950000E+02
256   2.950000E+02
257     1.9530E-01    2.0770E-01    1.9050E-01E
258 F   5.0000E-02E
259     1.0877E-03    2.7050E-02    2.7537E-04E
260 F   1.6940E-03E
261     2.5650E-03    1.1401E-03R 2 1.4455E-03E
262 R 2 3.3880E-02    3.1373E-03E
263 F   0.
264 F   0.
265 F   0.0
266 F  -1.0000E+00E
267     5.7150E-02    3.8100E-02R 2 4.2900E-02E
268 R 2 2.0770E-01    3.6390E-02E
269 F              4
270 F              4
271 F   0.0
272 F   0.0
273 F   0.0
274 F   0.0
275 F   0.0
276 F   0.0
277 F   5.7482E+02E
278 F   5.7482E+02E
279 F   1.5513E+07E
280 F   1.5513E+07E
281 F   5.7482E+02E
282 F   5.7482E+02E
283 PIPE                     12             12
284                7              1             12             13              9
285                0              0
286   9.425000E-03  3.911600E-03                                  2.950000E+02
287   2.950000E+02
288 R 3 4.4050E-01    6.3500E-01    6.5090E-01    3.5560E-01    .004
289 R 3 1.2293E-04    1.7721E-03    1.8165E-04    8.2402E-04    9.1040E-05
290 R 4 2.7907E-04R 2 5.1240E-05    3.4942E-03    2.2760E-02E
291 F   0.
292 R 3 0.         R 2 5.0000E-01R 3 1.0000E+00E
293 R 4 1.8850E-02R 2 8.0772E-03    6.6700E-02    1.7000E-01E
294 F              1
295 F   0.0
296 F   0.0
297 F   0.0
298 F   530.
299 F   1.5513 E+7
300 F   530.
301 PRIZER                   13             13
302                4             13
303           8000.    1.5513 E+7       1.0 E+5          .65
304 R 2 5.0000E-01    1.6040E-01    .004       E
305 R 2 1.1380E-02    3.6510E-03    9.1040E-05E
306 R 5 2.2760E-02E
307 F   0.
308 F  -1.0000E+00E
309 R 5 1.7000E-01E
310 F              4
311     1.0000E+00R 2 0.         E
312 F   0.0
313 F   6.1800E+02E
314 F   6.1800E+02E
315 F   1.5513E+07E
```

Fig. 55. (cont).

```
316 PIPE                          14              14
317                 1              0              16              17              9
318                 0              0
319   0.              0.              0.              0.              0.
320   0.
321      5.0000E-01
322      5.0000E-03
323 F    1.4455E-03
324 F    0.
325 F    0.
326 F    .0429
327 F              +4
328      0.
329      0.
330 F    0.
331      556.8
332      1.5513 E+7
333 PIPE                          15              15
334                 1              0              14              18              9
335                 0              0
336   0.              0.              0.              0.              0.
337   0.
338      5.0000E-01
339      5.0000E-03
340 F    1.4455E-03
341 F    0.
342 F    0.
343 F    .0429
344 F              +4
345      0.
346      0.
347 F    0.
348      556.8
349      1.5513 E+7
350 FILL                          16
351                 18             1
352      .2794          .0013316        0.0             0.0         574.82
353      1.5513 E+7
354 FILL                          17
355                 17             1
356      .2794          .0013316        0.0             0.0         574.82
357      1.5513 E+7
358 FILL                          19
359                 19             1
360      .097           1.94 E-3        0.              0.              574.82
361      1.5513 E+7
362         1.0 E-4        1.0 E-2          30.1          1000.
363              1.0            .02            2.              1.
364             -1.
```

Fig. 55. (Cont)

```
1                3
2 SEMISCALE TEST 1011
3
4
5              2424
6                 0                    1                19                19
7          1.0 E-3          1.0 E-5
8                20                  100
9                 1                    2                 3                 4                 5
10                6                    7                 8                 9                10
11               11                   12                13                14                15
12               16                   17                18                19
13 PIPE                               14                14
14               21                    1                16                17                 9
15                0                    1
16    2.145000E-02   8.737600E-03                                                  2.950000E+02
17    2.950000E+02
18       8.6360E-02      4.3180E-02R 2 2.1590E-02R 4 1.0255E-02R 2 1.2509E-02
19 R 4 1.2509E-02S
20 R 2 2.9363E-02      5.8725E-02R 4 1.3970E-01E
21       1.2483E-04      6.2415E-05     3.1207E-05     3.1207E-05     1.2539E-05
22       8.4948E-06      5.2357E-06     2.7633E-06     2.1841E-06     2.1841E-06
23       7.9516E-06      1.2746E-05     1.8672E-05     2.5727E-05R 2 6.7184E-05
24       1.3437E-04R 4 6.6583E-04E
25 R 5 1.4454E-03      1.0127E-03     6.5679E-04     3.7716E-04R 3 1.7460E-04
26       2.9908E-04      4.5685E-04S
27       6.4792E-04      8.7222E-04R 3 2.2881E-03R 4 4.7661E-03E
28 R 2 0.          R 7 .35         R 4 .35         F   0.
29 F     0.0
30 R 5 4.2900E-02      3.5909E-02     2.8918E-02     2.1914E-02R 3 1.4910E-02
31       1.9514E-02      2.4118E-02S
32       2.8722E-02      3.3325E-02R 3 5.3975E-02R 4 7.7900E-02E
33 F                 4
34 F     0.0
35 F     0.0
36 F     0.0
37 F     5.7482E+02E
38 F     1.5513E+07E
39 F     5.7482E+02E
40 PIPE                               15                15
41               19                   1                14                18                 9
42                0                   0
43    2.145000E-02   8.737600E-03                                                  2.950000E+02
44    2.950000E+02
45       2.4160E-01      4.2520E-01     1.6190E-01     3.7465E-01     5.5245E-01
46 R 2 1.03505         5.2020E-01     7.1660E-01R 2 1.03505    R 2 3.7465E-01
47       3.6200E-01      7.1025E-01     7.0390E-01     5.6420E-01     4.4450E-01
48       4.3720E-01E
49       3.4923E-04      6.1463E-04     2.3403E-04     4.3917E-03     7.9857E-04
50 R 2 1.4962 E-3       7.5195E-04     1.0358E-03R 2 1.4692 E-3      5.4156E-04
51       4.3917E-03      5.2327E-04     1.0267E-03     1.0175E-03     8.1555E-04
52       6.4252E-04      6.3197E-04E
53 R 5 1.4455E-03      5.0035E-04     1.4455E-03     5.0085E-04     1.4455E-03
54       5.0085 E-4      1.4455 E-3     5.0085 E-4R 4 1.4455 E-3     3.1066 E-4
55       1.4455 E-3      3.1066 E-4     1.43866E-3
56 R 5 .0              .01            .0             .01            .0
57       .01            .0             .01       R 4 .0             .02
58       .0             .02            .0
59 R 3 0.          R 4 1.0000E+00     9.5000E-01     9.4000E-01R 4-1.0000E+00
60       6.0000E-01      8.4000E-01     9.4000E-01     8.6000E-01     1.0000E+00
61       7.4000E-01
62 R 5 4.2900E-02      2.5253E-02     4.2900E-02     2.5253E-02     [illegible]00E-02
63       .025253        .0429          .025253   R 4 .0429          .0198882
```

Fig. 56. TRAC input deck for Semiscale Test 1011 transient calculation.

```
64      .0429           .0198882        .042799
65 F              1
66 F    0.0
67 F    0.0
68 F    0.0
69 F    5.7482E+02E
70 F    1.5513E+07E
71 F    5.7482E+02E
72 PIPE                         16              18
73              17               1              18              15              9
74               0               1
75      .02145          8.7376 E-3                                      295.
76      295.
77      .19336          .02       R 4 .0105727  R 2 .0125095  R 4 .0339725
78      .05588     R 2  .05875    R 2 .04017    E
79      2.7818 E-4      2.8773 E-5      1.3087 E-5      8.8480 E-6      5.4388 E-6
80      2.8592 E-6R 2   2.1841 E-6      7.9514 E-6      1.2745 E-5      1.8670 E-5
81      2.5726 E-5      1.2786 E-4R 2   1.3443 E-4R 2   1.9146 E-3E
82 R 3  1.4387 E-3      1.0242 E-3      6.6257 E-4      3.7935 E-4R 3   1.7460 E-4
83      2.9906 E-4      4.5682 E-4      6.4787 E-4      8.7222 E-4R 3   2.2881 E-3
84 R 2  4.7661 E-3E
85 R 2  0.          R 7 .35       R 4 .35       F   0.
86 F    0.
87 R 3  .042799         .0361125        .0290449        .0219774  R 3   .0149098
88      .0195136        .0241173        .0287210        .0333248  R 3   .053975
89 R 2  .0779
90 F              4
91 F    0.0
92 F    0.0
93 F    0.0
94 F    5.7482E+02E
95 F    1.5513E+07E
96 F    5.7482E+02E
97 BREAK                        16              16
98              15
99    .2794             1.3316 E-3  1.0             373.15          1.013250E+05
100 BREAK                       17              17
101             17
102   .2794             1.3316 E-3  1.0             373.15          1.013250E+05
103 END
104         1.0 E-4         1.0 E-2             1.
105             .20             .03             2.
106         1.0 E-4         1.0 E-2            30.
107             1.0             .09             2.
108            -1.
```

Fig. 56. (Cont.)

E. Semiscale Mod-1 Heated Loop Blowdown Test S-02-8

1. Description of Experiment

The Semiscale Mod-1 test apparatus (Ref. 12) is an improved version of the Isothermal Semiscale System which is described in Sec. D. In the Mod-1 system, nuclear heating is simulated by a core comprised of approximately 40 electrically heated rods with both the power and volume scaled to a typical PWR in a ratio of approximately 1 to 3000.

An isometric view of the test apparatus is shown in Fig. 57. It consists of a pressure vessel with simulated reactor internals; an intact loop with active steam generator, pump, and pressurizer; a broken loop with simulated steam generator, a simulated pump, and pipe rupture assemblies; and a pressure suppression system with header, auxiliary steam supply and suppression tanks. Test S-02-8 was a simulation of a double offset shear (200%) cold-leg break. It differed somewhat from other Mod-1 tests in that the resistance of the simulated pump was reduced by a factor of about 4 below the more typical value.

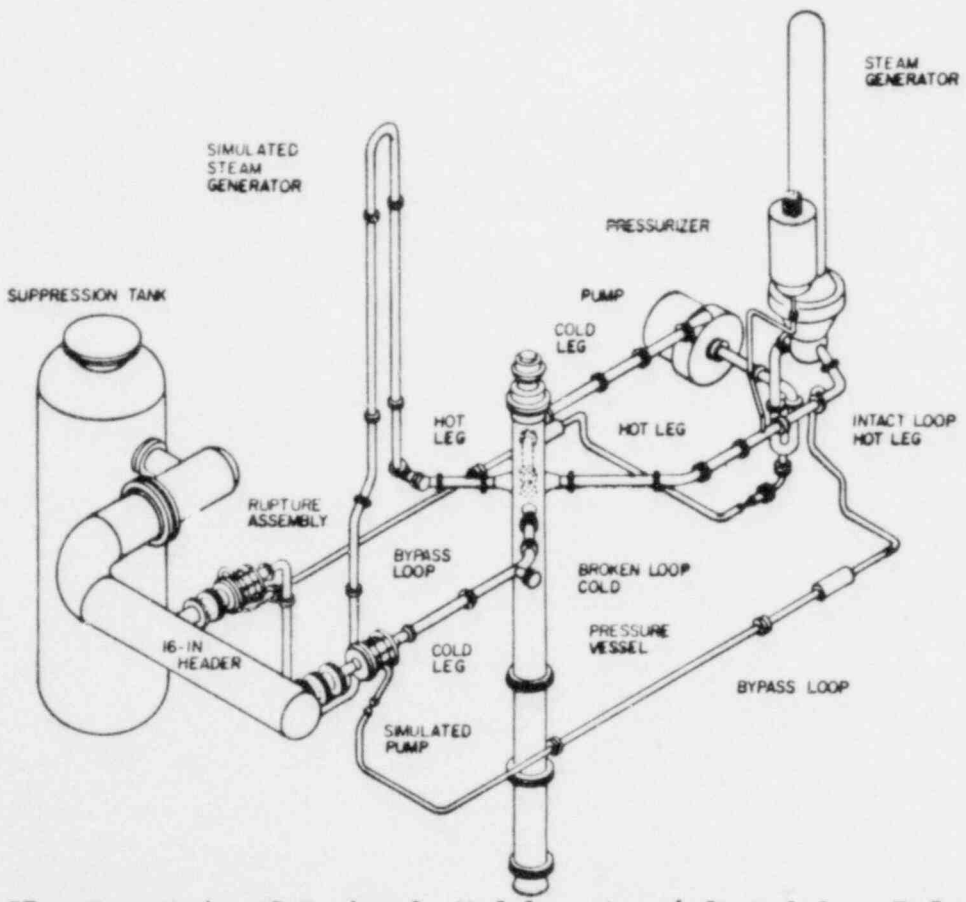

Fig. 57. Isometric of Semiscale Mod-1 system (adapted from Ref. 12).

Prior to the test the system was brought to a steady-state condition with measured parameters as given in Table IV. Blowdown was then initiated by rupturing the two rupture disks.

TABLE IV

COMPARISON OF CALCULATED AND MEASURED INITIAL CONDITIONS FOR SEMISCALE HEATED BLOWDOWN TEST S-02-8

Parameter	Units	Test Data	TRAC
Core power	MW	1.59	1.59
Intact loop cold leg fluid temperature	K	556.5	553.7
Hot to cold leg temperature differential	K	37.8	39.7
Pressurizer pressure	KPa	15600.	15596.
Pump mass flow rate	kg/s	7.35	7.38
Pump Speed	Rad/s	295.3	296.
Pump P	KPa	283.	268.

2. TRAC Best-Estimate Model

The TRAC model of the Semiscale Mod-1 Test S-02-8 is an especially good example to use in a data comparison, since it contains every component modeled by TRAC except an accumulator. As shown in Fig. 58, the system model contains a total of 111 fluid cells in one-dimensional components and 152 fluid cells in the vessel component.

A number of modeling techniques were used in the TRAC model of Semiscale Mod-1 in order to obtain a good representation of the test apparatus and at the same time minimize the computer time used for the calculations. The lower plenum was modeled using four levels in order to obtain the proper degree of mixing of the hot fluid ejected from the core into the colder fluid in the lower plenum.

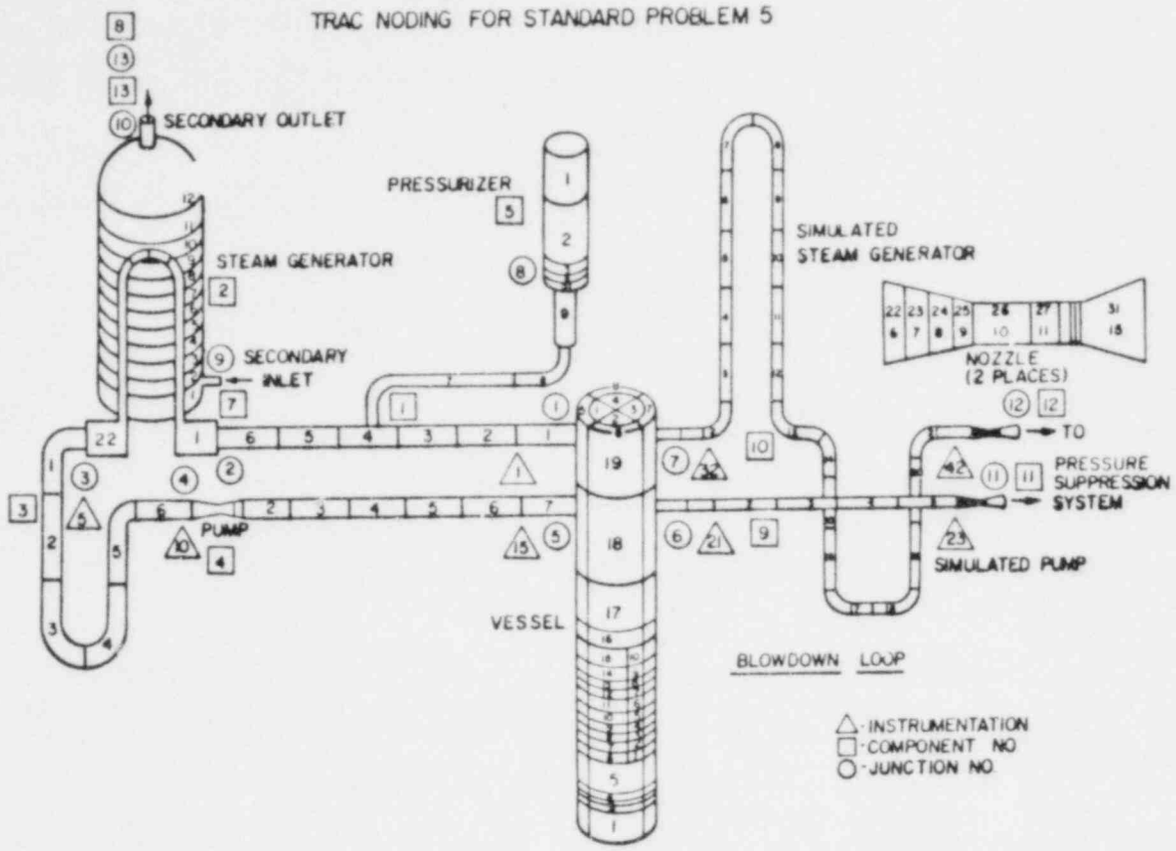

Fig. 58. TRAC noding and component schematic for Semiscale Mod-1 system.

A flow resistance was used to represent the flow distribution plates at the bottom of the core rather than a reduced flow area. In extremely long and thin fluid cells such as those needed to model the Semiscale core, the large dynamic pressure head for a greatly reduced flow area of the flow distribution plate could lead to unwanted circulation patterns being set up within the core.

In the blowdown loop a series of progressively smaller cell lengths were used approaching the expansion section of the break nozzles. Within the constant area section of the Semiscale nozzle, the flow conditions change more rapidly near the expansion section. By using progressively smaller cell lengths, the change in fluid conditions from cell to cell are more nearly equal than they would be with equal-length fluid cells.

The line leading to the pressurizer is calculated using the fully implicit scheme to minimize the effects of the high velocities within the

surge line on time step size. Since the junction between the surge line and the pressurizer was placed in the large-area part of the pressurizer and hence in a low fluid velocity region, the fluid cells at the bottom of the semi-implicit pressurizer can be very small without necessitating small time steps. This is desirable since the use of a very small fluid cell at the bottom of the pressurizer leads to a better prediction of pressurizer discharge fluid conditions.

3. Comparison of Best-Estimate Calculations with Experiment

The initial conditions calculated with TRAC for use at the start of the blowdown are compared in Table IV with the experimental data. Differences are generally due to inconsistencies in the test data. For instance the pump head, flow rate, and speed are not totally compatible with each other if the Semiscale homologous curves are correct. None of these inconsistencies are felt to seriously affect the results of the transient analysis. Therefore, further refinement of the TRAC steady-state run was not felt necessary to obtain a good TRAC calculation of the blowdown transient.

An indication of the overall performance of a LOCA analysis code is how well it predicts system pressure decay. The comparison of TRAC-predicted lower plenum pressure with Semiscale Mod-1 Test S-02-8 data[13] presented in Fig. 59 indicates that TRAC does a good job of predicting system performance. The slight underprediction of pressure beginning at 11 to 12 s is probably due to prediction of less superheat in the upper part of the core than was present in the actual test.

The most important variable which a LOCA analysis code calculates is the maximum cladding temperature. Fig. 60 presents a comparison of the TRAC predictions of this variable with a band of temperatures which includes all of the heater rod cladding thermocouples in the lower half of the highest power step in the Semiscale system. With the exception of a slightly advanced time to Departure from Nucleate Boiling (DNB) (0.2 s as opposed to 0.5 s after rupture), TRAC does an excellent job of predicting the cladding temperature response in the high power zone.

Fig. 61 compares TRAC predictions with test data for cladding temperatures at elevations in the range 0.20-0.23 m above the bottom of the heated core. This good agreement with test data is typical of all elevations in the lower half of the core. As shown in Fig. 62, however, TRAC results for the

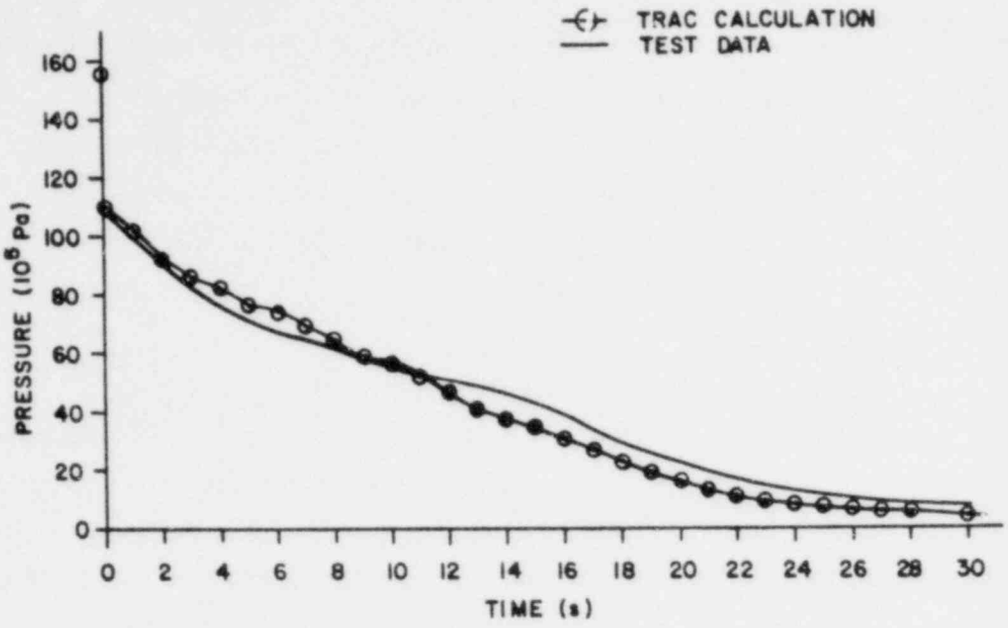

Fig. 59. Lower plenum pressure for Semiscale Test S-02-8.

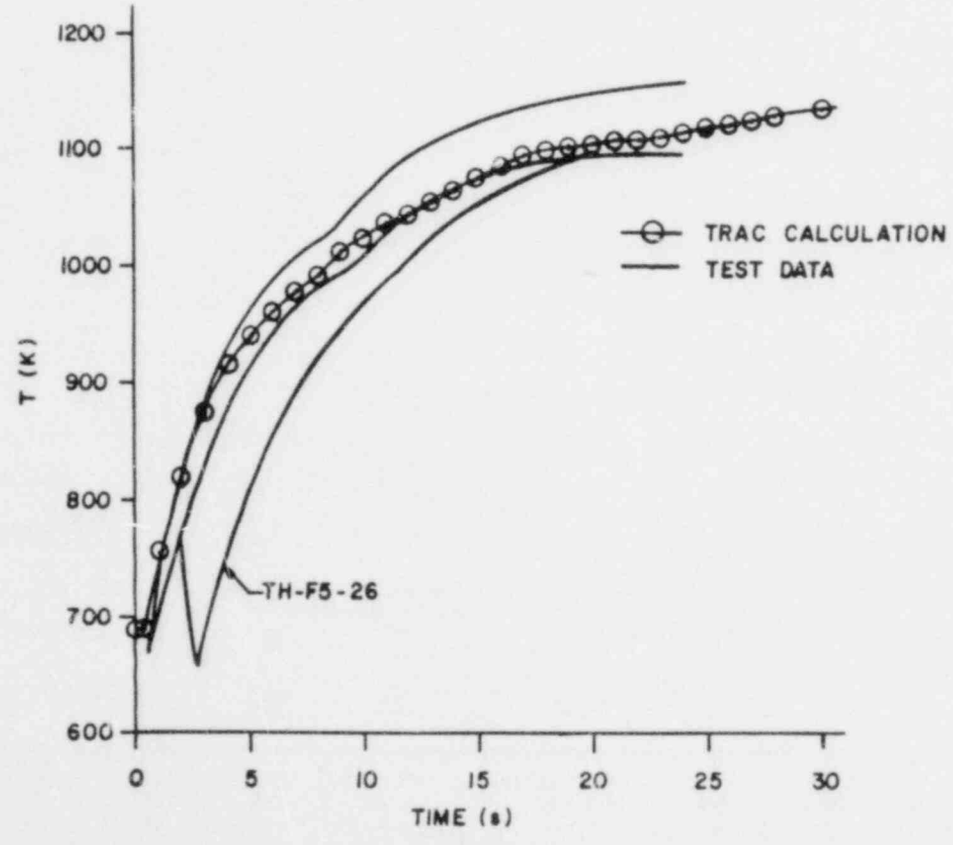

Fig. 60. Cladding temperature in high power zone for Semiscale Test S-02-8.

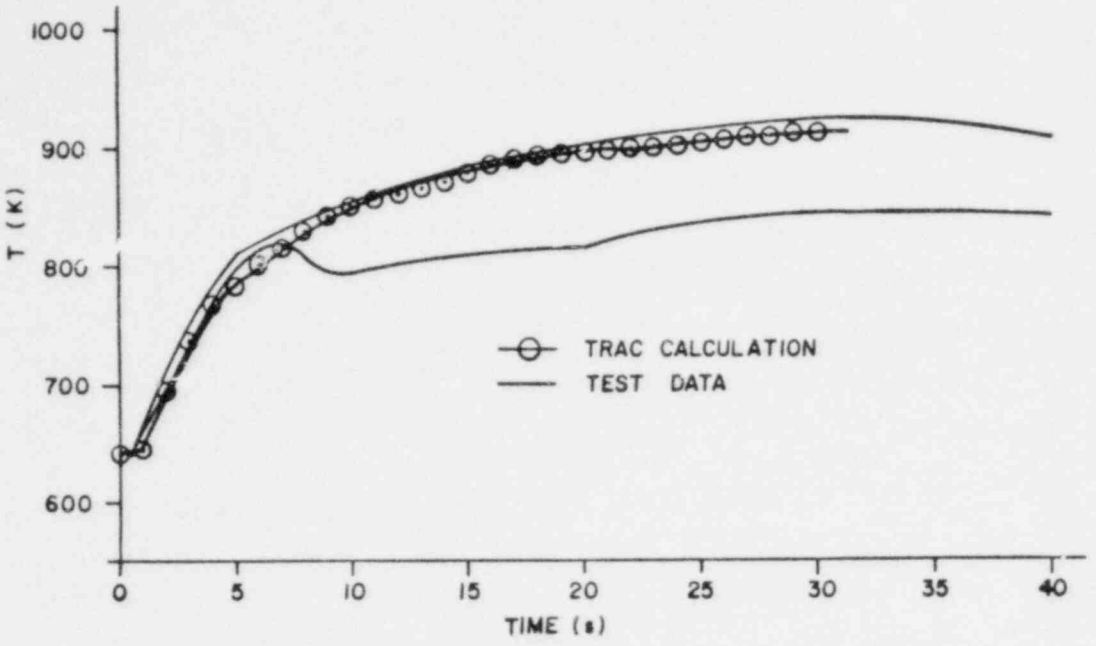

Fig. 61. Cladding temperature near bottom of core for Semiscale Test S-02-8.

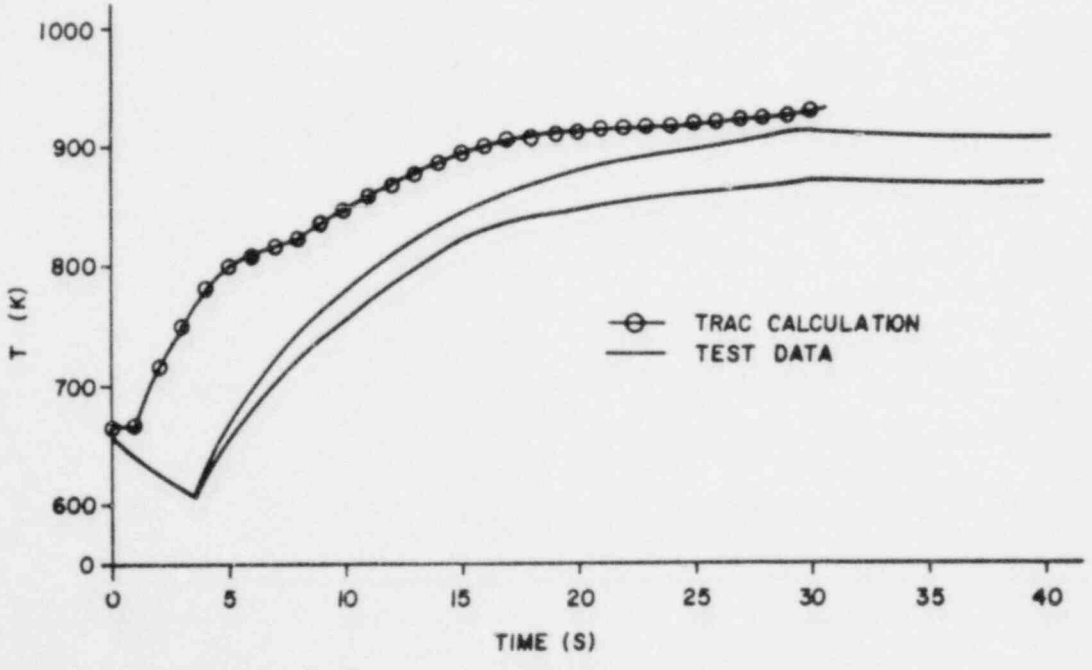

Fig. 62. Cladding temperature near top of core for Semiscale Test S-02-8.

upper half of the core have a tendency toward early DNB as opposed to the delayed DNB exhibited in the test data.

Due to the dead band in the core inlet turbine flow meter, a meaningful comparison of predicted and test-derived core inlet mass flow rate is limited to the first 6 s after rupture. This comparison is shown in Fig. 63 and indicates that TRAC predicts the magnitude of the immediate core flow reversal well but predicts the core flow to return to a positive direction about one second before the test data.

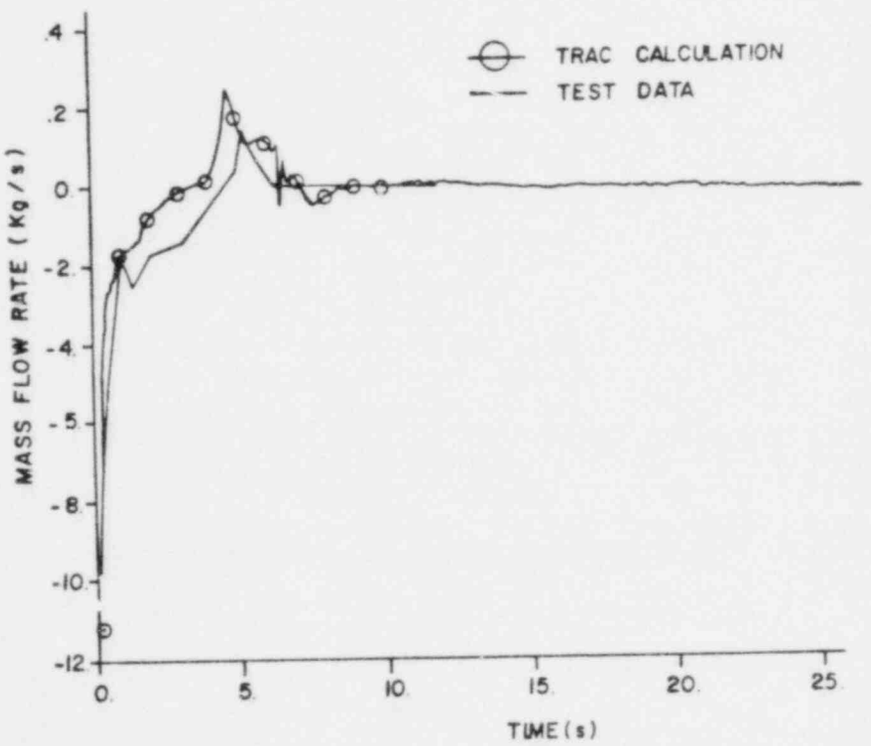

Fig. 63. Mass flow rate at core inlet for Semiscale Test S-02-8.

Fig. 64 shows that TRAC does an excellent job of predicting the hot-leg break mass flow rate. The small increase in the test data between 10 and 15 s is due to a slug of higher density fluid coming from the intact hot leg.

In Fig. 65, TRAC predictions are compared with mass flow rate measurements at the entrance and exit to the broken cold leg. Though in

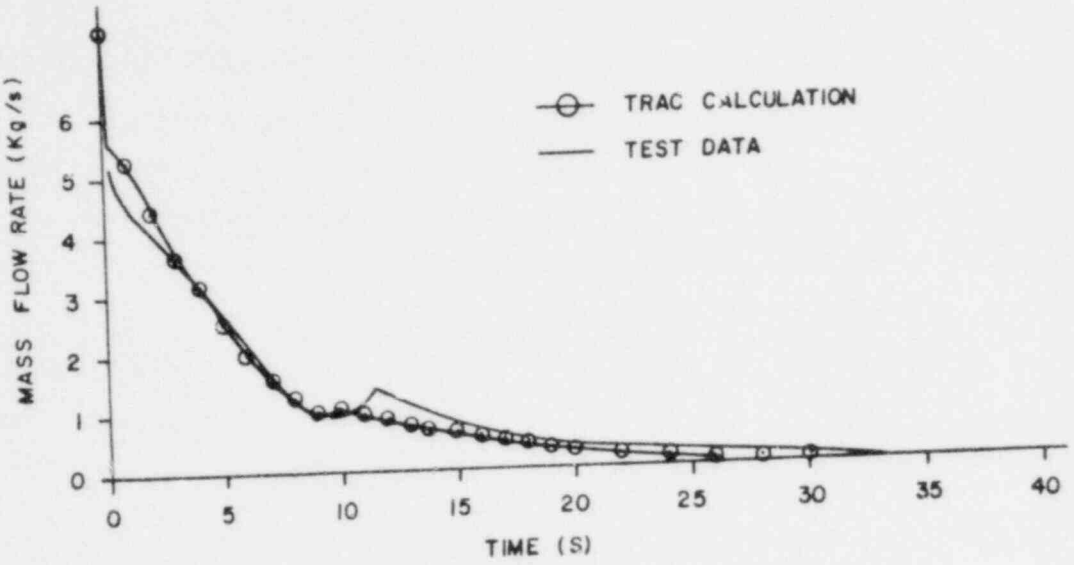

Fig. 64. Hot-leg break mass flow rate for Semiscale Test S-02-8.

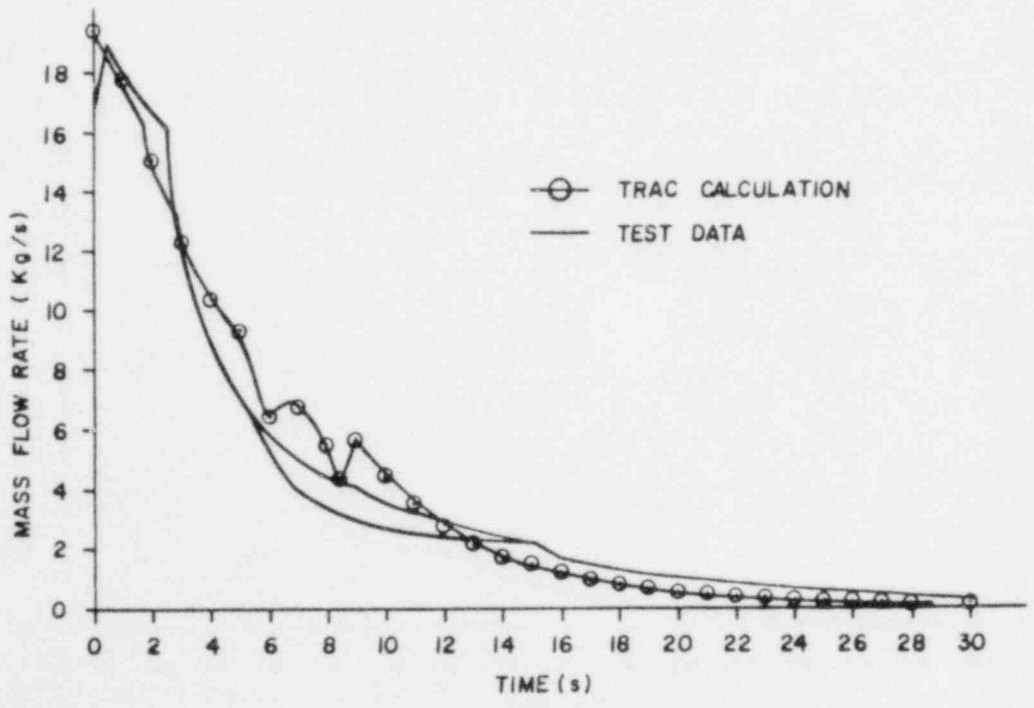

Fig. 65. Cold-leg break mass flow rate for Semiscale Test S-02-8.

general the comparison between test and calculated values is good, TRAC seems to overpredict the flow rates during the period that two-phase fluid is passing through the flow nozzle. The small underprediction of mass flow rate after 12 s is probably due to the lower calculated system pressure. TRAC calculations of pressurizer surge line flow rate agree well with test data (Fig. 66). Finally, comparisons presented in Fig. 67 of experimental and calculated pump mass flow rates demonstrate that TRAC does an excellent job of predicting intact loop fluid flow rates.

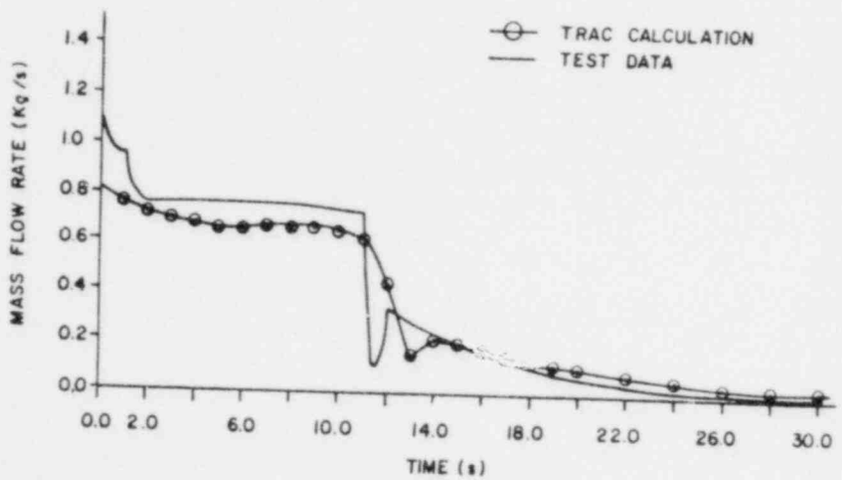

Fig. 66. Pressurizer surge line mass flow rate for Semiscale Test S-02-8.

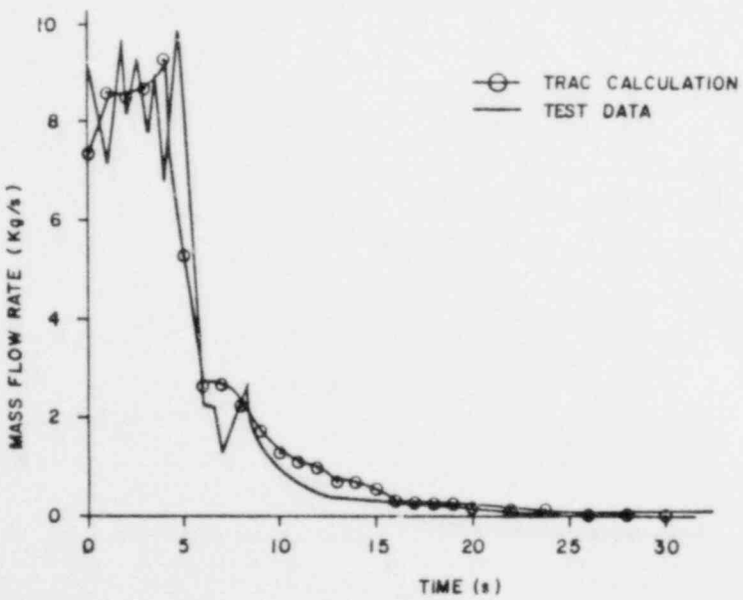

Fig. 67. Intact loop (pump inlet) mass flow rate for Semiscale Test S-02-8.

In summary, TRAC predictions of Semiscale Mod-1 Test S-02-8 (Standard Problem 5) are generally in excellent agreement with test results.

4. Parametric and Sensitivity Studies

Calculations were performed with both a two-level lower plenum and a four-level lower plenum. It was found that the four-level lower plenum gave better predictions of lower plenum temperature and early cold-leg densities than the two-level lower plenum. Some noding studies were also performed on the break nozzles. It was found that only two volumes were needed downstream of the minimum-area section of the throat to accurately calculate non-subcooled flow rates.

5. TRAC-P1A Features Tested

Semiscale Test S-02-8 provides a test of the ability of the code to accurately predict the thermal-hydraulic response of a PWR-type system during blowdown but without ECC injection. In addition to the features tested in the isothermal test (Sec. D), Test S-02-8 introduces for the first time the three-dimensional vessel component with associated rod heat transfer models. Multidimensional effects are not too significant but the test provides a good check of the rod heat transfer models during blowdown (nucleate boiling, DNB, and post-DNB regimes). With the exception of the accumulator component, all TRAC components are exercised by this problem.

6. Input Data Decks

The input data for this problem consisted of a steady-state deck and a transient deck. The steady-state deck (Fig. 68) contains all the system components except the two broken loop pipes and breaks. For the steady-state run the temperature of the fluid in the pressurizer was set to the temperature of the fluid in the intact hot leg. This maintained the fluid temperature in the pressurizer surge line at the correct temperature during the steady-state run.

The transient deck (Fig. 69) contains a description of the two broken loop lines as well as descriptions of the pressurizer and pressurizer surge line. In the transient calculation the initial temperature of the pressurizer was set to saturation conditions. The description of the pressurizer surge line was included so that the temperature of the top-most cell in the side branch could be set to saturation also.

```
1
2 HEATED CORE SEMI-SCALE PROBLEM
3 S55981  STANDARD PROBLEM 5  STEADY STATE
4
5
6                1                0               13              13
7          1.0 E-3          1.0 E-6         1.0 E-3
8               10               99              20               2
9                1                2               3               4               5
10               7                8               9              10              11
11              12               13               6
12             100                              1000.
13
14            1000                              1000.
15
16 TEE                             1
17               4                1               7
18               0                6               1               2
19   ?.335020E-02  1.112520E-02  0.              0.              295.
20     ?.
21                                 4               8
22   9             3.911600E-03  0.              0.              295.
23   2
24 F     -01
25     1.722           .72             .203            .02         E
26 F   1.7986E-03
27     7.389  E-5      3.0895 E-5      7.093  E-4      4.552  E-4E
28 F   3.4942E-03
29 R 3 4.291  E-5      3.494  E-3      2.276  E-2E
30 F   0.
31 F   .0068
32 R 6 0.               1.
33 R 5 1.0         E
34 F    6.67 E-02
35 R 3 .00739           .0667           .17
36 F             +4
37 F             +4
38 F   0.
39 F   0.
40 F   0.
41 F   0.
42 F   0.
43 F   0.
44 F   596.4
45 R 3 596.4            596.4
46 F    1.5596E+7
47 F    1.5596E+7
48 F   596.4
49 R 3 596.4            596.4
50 STGEN                           2
51               22                2               3              10
52                1                0               0               1
53   5.100000E-03  1.200000E-03
54               12                9              10
55     4.6000E-01R20 2.5680E-01     4.6000E-01E
56     9.6278 E-3R20 1.13975E-3     9.6278 E-3E
57     3.4942E-03R21 4.4000E-03     3.4942E-03
58                 R21 .093       F   0.
59 R11 1.              0.          R11-1.          E
60     6.6700E-02R21 1.0200E-02     6.6700E-02
61               +4R21           +1              +4
62     0.          R20 .444
63 F   0.
```

Fig. 68. TRAC input deck for Semiscale Test S-02-8 steady state calculation.

```
64 F    0.
65 I20   596.4          554.4
66 I20   596.4          554.4        E
67 F     1.5596E+7
68 F    2.5680E-01E
69 R10 .01121     R 2 .075
70 R11 4.3830E-02R 2 9.2000E-03E
71 F    0.          E
72 F    1.          E
73 F    1.8800E-02E
74 F              +4
75 F    5.5330E-01E
76 R 2 0.0         I 8 .303            .881
77      .005         .00524            .0055      I 8 .79              1.8
78      517.         538.2       F     544.3
79      517.         538.2       F     544.3      E
80 I10    55.7 E+5        55.6 E+5
81 F    550.
82 PIPE                          3
83                 6             1               3               4               7
84                 0             0
85    3.324800E-02  1.112520E-02  0.              0.              295.
86    295.
87 R 3 5.1000E-01R 3 4.6140E-01
88 R 3 1.7820E-03R 3 1.6122E-03
89 F    3.4942E-03
90 F    0.
91      -1.0          0.            -1.0       R 2 1.0        R 2 0.
92 F    6.6700E-02
93 F              +4
94 F    0.
95 F    0.
96 F    0.
97 F   554.4
98 F     1.5596E+7
99 F   554.4
100 PUMP                         4
101                7             1               4               5               7
102                0             0               1               0               1
103
104    3.324800E-02  1.112520E-02  0.              0.              294.5
105    295.
106    5.739000E+02  4.345000E+01  1.140000E-02    1000.           3.728000E+02
107    2.662000E+00  0.            3.730000E+00    2.960000E+02
108                1
109 R 2 5.8350E-01R 5 4.8430E-01
110 R 2 2.0388E-03R 5 1.6922E-03
111 F    3.4942E-03
112 F    0.
113 F    0.
114 F    6.6700E-02
115 F              +4
116 F    0.
117 F    0.
118 F    0.
119 F    554.4
120 F     1.5596E+7E
121 F    554.4
122 PRIZER                       5
123                4             8
124      8000.          1.5596 E07     1.0     E05     .1
125 R 2 .5              1.2840E-01     .02        E
126 R 2  1.173 E-2      3.0125 E-3     .4692  E-3E
```

Fig. 68. (cont).

```
127 R 5 2.2760 E-2E
128 R 5 0.          E
129 F  -1.0
130 R 5 .17         E
131 R 4           +4                +4
132   , 1.          R 3 0.          E
133 F   0.
134 F   596.4
135 F   596.4       E
136 F    1.5596E+7
137 VESSEL                          6
138                19               2                4                4
139                18               4                1               15                5
140                 1
141                 0               0                0
142         8026.                502.              17.3              .6        60000.
143            1.334
144                10               7                7             1000
145
146         1.59 E+6
147       .3659             .48787     S
148       .6098             .7318           1.2522           1.405            1.532        NASX
149       1.659             1.786           2.040            2.167            2.294        NASX
150       2.471             2.675           2.929            3.185            3.955
151       4.981             6.222       E
152       .0750572          .0857252
153       1.5708            3.1416          4.7124           6.2832
154                                 8                3                1
155                19               6                3                7
156                18               7                3                6
157                18               5                3                5
158                0.                              1.              1.F               0.
159 F   1.
160 F   1.
161       4.30              7.30            9.40             10.8             11.5          ZPOWR
162       10.8              9.40            7.30             4.30             1.45          ZPOWR
163       9.75              9.75            9.75             9.75         E
164                 0.          .0008001        .0018923         .0029845         .0034459  RADRD
165        .00390737            .0043688        .0043688         .0048641         .0053594  RADRD
166                   4R 2                5R 3             4                3R 2             8  MATRD
167       0.                      1.59E+6          .1              1.59E+6          .63
168        1.1022986              1.9          1.05505 E+6         8.1          .39997 E+6   PWTB
169        20.                   .0803 E+6       1000.            .0803 E+6                    PWTB
170 F                 0                                                                       NFAX
171 F   0.                                                                                    FPUO2
172 F   1.                                                                                    FTD
173 F   0.                                                                                    GMIX
174 F   0.                                                                                    GMLES
175 F   0.                                                                                    PGAPT
176 F   0.                                                                                    PLVOL
177 F   0.                                                                                    PSLEN
178 F   0.                                                                                    CLENN
179 R 4       0.0044R 4       0.0506E
180 R 4       0.1121R 4       1.3237E
181 F   .005                                                                                  LEVEL   1
182 F   .005                                                                                  LEVEL   1
183 F   .005                                                                                  LEVEL   1
184 F   .005                                                                                  LEVEL   1
185 F   .005                                                                                  LEVEL   1
186 F   .005                                                                                  LEVEL   1
187 F   1.                                                                                    LEVEL   1
188 F   1.                                                                                    LEVEL   1
189 F   1.                                                                                    LEVEL   1
```

Fig. 68. (cont).

```
190 F    1.                                                          LEVEL  1
191 R 4       0.0750R 4       0.0107E
192 R 4       0.0750R 4       0.0107E
193 R 4       0.0750R 4       0.0107E
194 F         556.4E
195 F    0.                                                          LEVEL  1
196 F    0.                                                          LEVEL  1
197 F    0.                                                          LEVEL  1
198 F    0.                                                          LEVEL  1
199 F    0.                                                          LEVEL  1
200 F    0.                                                          LEVEL  1
201 F    0.                                                          LEVEL  1
202 F    554.4                                                       LEVEL  1
203 F    554.4                                                       LEVEL  1
204 F    1.5596 E+7                                                  LEVEL  1
205 R 4          0.0R 4       0.0164E
206 R 4          0.0R 4        .4297E
207 F    .005                                                        LEVEL  2
208 F    .005                                                        LEVEL  2
209 F    .005                                                        LEVEL  2
210 F    .005                                                        LEVEL  2
211 F    .005                                                        LEVEL  2
212 F    .005                                                        LEVEL  2
213 F    1.                                                          LEVEL  2
214 F    1.                                                          LEVEL  2
215 F    .91468                                                      LEVEL  2
216 F    1.                                                          LEVEL  2
217 R 4       0.0750R 4       0.0107E
218 R 4       0.0750R 4       0.0107E
219 R 4       0.0750R 4       0.0107E
220 R 4 0.          R 4 554.4      E
221 F    0.                                                          LEVEL  2
222 F    0.                                                          LEVEL  2
223 F    0.                                                          LEVEL  2
224 F    0.                                                          LEVEL  2
225 F    0.                                                          LEVEL  2
226 F    0.                                                          LEVEL  2
227 F    0.                                                          LEVEL  2
228 F    554.4                                                       LEVEL  2
229 F    554.4                                                       LEVEL  2
230 F    1.5596 E+7                                                  LEVEL  2
231 R 4          0.0R 4       0.0164E
232 R 4          0.0R 4        .4297E
233 F    .005                                                        LEVEL  2
234 F    .005                                                        LEVEL  2
235 F    .005                                                        LEVEL  2
236 F    .005                                                        LEVEL  2
237 F    .005                                                        LEVEL  2
238 F    .005                                                        LEVEL  2
239 F    1.                                                          LEVEL  2
240 F    1.                                                          LEVEL  2
241 F    .91468                                                      LEVEL  2
242 F    1.                                                          LEVEL  2
243 R 4       0.0750R 4       0.0107E
244 R 4       0.0750R 4       0.0107E
245 R 4       0.0750R 4       0.0107E
246 R 4 0.          R 4 554.4      E
247 F    0.                                                          LEVEL  2
248 F    0.                                                          LEVEL  2
249 F    0.                                                          LEVEL  2
250 F    0.                                                          LEVEL  2
251 F    0.                                                          LEVEL  2
252 F    0.                                                          LEVEL  2
```

Fig. 68. (cont).

```
253 F    0.                                                          LEVEL  2
254 F    554.4                                                       LEVEL  2
255 F    554.4                                                       LEVEL  2
256 F    1.5596 E+7                                                  LEVEL  2
257 R 4          0.0R 4       0.0164E
258 R 4          0.0R 4        .4297E
259 F    .005                                                        LEVEL  2
260 F    .005                                                        LEVEL  2
261 F    .005                                                        LEVEL  2
262 F    .005                                                        LEVEL  2
263 F    .005                                                        LEVEL  2
264 F    .005                                                        LEVEL  2
265 F    1.                                                          LEVEL  2
266 F    1.                                                          LEVEL  2
267 F    .91468                                                      LEVEL  2
268 F    1.                                                          LEVEL  2
269 R 4      0.0750R 4       0.0107E
270 R 4      0.0750R 4       0.0107E
271 R 4      0.0750R 4       0.0107E
272 R 4 0.           R 4 554.4      E
273 F    0.                                                          LEVEL  2
274 F    0.                                                          LEVEL  2
275 F    0.                                                          LEVEL  2
276 F    0.                                                          LEVEL  2
277 F    0.                                                          LEVEL  2
278 F    0.                                                          LEVEL  2
279 F    0.                                                          LEVEL  2
280 F    554.4                                                       LEVEL  2
281 F    554.4                                                       LEVEL  2
282 F    1.5596 E+7                                                  LEVEL  2
283 R 4      0.0584R 4       0.1314E
284 R 4      1.5219R 4       3.3596E
285 F    .005                                                        LEVEL  3
286 R 4  23.         F    0.
287 F    .005
288 F    .005
289 R 4  23.         F    0.
29  F    .005                                                        LEVEL  3
29  R 4 .91468      R 4 1.0                                         LEVEL  3
29  R 4 .91468      R 4 1.0                                         LEVEL  3
293 R 4 .2758       R 4 1.                                          LEVEL  3
294 F    1.                                                          LEVEL  3
295 R 4      0.0750R 4       0.0213E
296 R 4      0.0750R 4       0.0213E
297 R 4      0.0750R 4       0.0213E
298 F         554.2E
299 F    0.                                                          LEVEL  3
300 F    0.                                                          LEVEL  3
301 F    0.                                                          LEVEL  3
302 F    0.                                                          LEVEL  3
303 F    0.                                                          LEVEL  3
304 F    0.                                                          LEVEL  3
305 F    0.                                                          LEVEL  3
306 F    554.4                                                       LEVEL  3
307 F    554.4                                                       LEVEL  3
308 F    1.5596 E+7                                                  LEVEL  3
309 R 4          0.0R 4       0.0386E
310 R 4          0.0R 4       0.9881E
311 F    .005                                                        LEVEL  4
312 F    .005                                                        LEVEL  4
313 F    .005                                                        LEVEL  4
314 F    .005                                                        LEVEL  4
315 F    .005                                                        LEVEL  4
```

Fig. 68. (cont).

```
316 F    .005                                                          LEVEL  4
317 R 4  .2758       R 4 1.                                            LEVEL  4
318 R 4  .38         R 4 1.                                            LEVEL  4
319 R 4  .2758       R 4 1.                                            LEVEL  4
320 F    0.                                                            LEVEL  4
321 R 4     .010719R 4       0.0213E
322 R 4     .010719R 4       0.0213E
323 R 4     .010719R 4       0.0213E
324 R 4 0.           R 4 554.4      E
325 F    0.                                                            LEVEL  4
326 F    0.                                                            LEVEL  4
327 F    0.                                                            LEVEL  4
328 F    0.                                                            LEVEL  4
329 F    0.                                                            LEVEL  4
330 F    0.                                                            LEVEL  4
331 F    0.                                                            LEVEL  4
332 R 4 554.4        R 4 554.4                                         LEVEL  4
333 R 4 554.4        R 4 554.4                                         LEVEL  4
334 F    1.5596 E+7                                                    LEVEL  4
335 R 4           0.0R 4       0.0321E
336 R 4           0.0R 4       0.8202E
337 F    .005                                                          LEVEL  5
338 F    .005                                                          LEVEL  5
339 F    .005                                                          LEVEL  5
340 F    .005                                                          LEVEL  5
341 F    .005                                                          LEVEL  5
342 F    .005                                                          LEVEL  5
343 R 4 .2758        R 4 1.                                            LEVEL  5
344 R 4 .38          R 4 1.                                            LEVEL  5
345 R 4 .2758        R 4 1.                                            LEVEL  5
346 F    0.                                                            LEVEL  5
347 R 4     .010719R 4       0.0213E
348 R 4     .010719R 4       0.0213E
349 R 4     .010719R 4       0.0213E
350 R 4 0.           R 4 554.4      E
351 F    0.                                                            LEVEL  5
352 F    0.                                                            LEVEL  5
353 F    0.                                                            LEVEL  5
354 F    0.                                                            LEVEL  5
355 F    0.                                                            LEVEL  5
356 F    0.                                                            LEVEL  5
357 F    0.                                                            LEVEL  5
358 R 4 554.4        R 4 554.4                                         LEVEL  5
359 R 4 554.4        R 4 554.4                                         LEVEL  5
360 F    1.5596 E+7                                                    LEVEL  5
361 R 4           0.0R 4       0.0321E
362 R 4           0.0R 4       0.8202E
363 F    .005                                                          LEVEL  6
364 F    .005                                                          LEVEL  6
365 F    .005                                                          LEVEL  6
366 F    .005                                                          LEVEL  6
367 F    .005                                                          LEVEL  6
368 F    .005                                                          LEVEL  6
369 R 4 .2758        R 4 1.                                            LEVEL  6
370 R 4 .38          R 4 1.                                            LEVEL  6
371 R 4 .2758        R 4 1.                                            LEVEL  6
372 F    0.                                                            LEVEL  6
373 R 4     .010719R 4       0.0213E
374 R 4     .010719R 4       0.0213E
375 R 4     .010719R 4       0.0213E
376 R 4 0.           R 4 554.4      E
377 F    0.                                                            LEVEL  6
378 F    0.                                                            LEVEL  6
```

Fig. 68. (cont).

```
379 F    0.                                                    LEVEL  6
380 F    0.                                                    LEVEL  6
381 F    0.                                                    LEVEL  6
382 F    0.                                                    LEVEL  6
383 F    0.                                                    LEVEL  6
384 R 4 554.4      R 4 554.4                                   LEVEL  6
385 R 4 554.4      R 4 554.4                                   LEVEL  6
386 F   1.5596 E+7                                             LEVEL  6
387 R 4          0.0R 4      0.0321E
388 R 4          0.0R 4      0.8202E
389 F    .005                                                  LEVEL  7
390 F    .005                                                  LEVEL  7
391 F    .005                                                  LEVEL  7
392 F    .005                                                  LEVEL  7
393 F    .005                                                  LEVEL  7
394 F    .005                                                  LEVEL  7
395 R 4 .2758      R 4 1.                                      LEVEL  7
396 R 4 .38        R 4 1.                                      LEVEL  7
397 R 4 .2758      R 4 1.                                      LEVEL  7
398 F    0.                                                    LEVEL  7
399 R 4     .010719R 4      0.0213E
400 R 4     .010719R 4      0.0213E
401 R 4     .010719R 4      0.0213E
402 R 4 0.         R 4 554.4      E
403 F    0.                                                    LEVEL  7
404 F    0.                                                    LEVEL  7
405 F    0.                                                    LEVEL  7
406 F    0.                                                    LEVEL  7
407 F    0.                                                    LEVEL  7
408 F    0.                                                    LEVEL  7
409 F    0.                                                    LEVEL  7
410 R 4 554.4      R 4 554.4                                   LEVEL  7
411 R 4 554.4      R 4 554.4                                   LEVEL  7
412 F   1.5596 E+7                                             LEVEL  7
413 R 4          0.0R 4      0.0642E
414 R 4          0.0R 4      1.6404E
415 F    .005                                                  LEVEL  8
416 F    .005                                                  LEVEL  8
417 F    .005                                                  LEVEL  8
418 F    .005                                                  LEVEL  8
419 F    .005                                                  LEVEL  8
420 F    .005                                                  LEVEL  8
421 R 4 .2758      R 4 1.                                      LEVEL  8
422 R 4 .38        R 4 1.                                      LEVEL  8
423 R 4 .2758      R 4 1.                                      LEVEL  8
424 F    0.                                                    LEVEL  8
425 R 4     .010719R 4      0.0213E
426 R 4     .010719R 4      0.0213E
427 R 4     .010719R 4      0.0213E
428 R 4 0.         R 4 554.4      E
429 F    0.                                                    LEVEL  8
430 F    0.                                                    LEVEL  8
431 F    0.                                                    LEVEL  8
432 F    0.                                                    LEVEL  8
433 F    0.                                                    LEVEL  8
434 F    0.                                                    LEVEL  8
435 F    0.                                                    LEVEL  8
436 R 4 554.4      R 4 554.4                                   LEVEL  8
437 R 4 554.4      R 4 554.4                                   LEVEL  8
438 F   1.5596 E+7                                             LEVEL  8
439 R 4          0.0R 4      0.0321E
440 R 4          0.0R 4      0.8202E
441 F    .005                                                  LEVEL  9
```

Fig. 68. (cont).

```
442 F    .005                                                    LEVEL  9
443 F    .005                                                    LEVEL  9
444 F    .005                                                    LEVEL  9
445 F    .005                                                    LEVEL  9
446 F    .005                                                    LEVEL  9
447 R 4 .2758      R 4 1.                                        LEVEL  9
448 R 4 .38        R 4 1.                                        LEVEL  9
449 R 4 .2758      R 4 1.                                        LEVEL  9
450 F   0.                                                       LEVEL  9
451 R 4     .010719R 4      0.0213E
452 R 4     .010719R 4      0.0213E
453 R 4     .010719R 4      0.0213E
454 R 4 0.          R 4 554.4      E
455 F   0.                                                       LEVEL  9
456 F   0.                                                       LEVEL  9
457 F   0.                                                       LEVEL  9
458 F   0.                                                       LEVEL  9
459 F   0.                                                       LEVEL  9
460 F   0.                                                       LEVEL  9
461 F   0.                                                       LEVEL  9
462 R 4 554.4      R 4 554.4                                     LEVEL  9
463 R 4 554.4      R 4 554.4                                     LEVEL  9
464 F   1.5596 E+7                                               LEVEL  9
465 R 4          0.0R 4      0.0321E
466 R 4          0.0R 4      0.8202E
467 F    .005                                                    LEVEL 10
468 F    .005                                                    LEVEL 10
469 F    .005                                                    LEVEL 10
470 F    .005                                                    LEVEL 10
471 F    .005                                                    LEVEL 10
472 F    .005                                                    LEVEL 10
473 R 4 .2758      R 4 1.                                        LEVEL 10
474 R 4 .38        R 4 1.                                        LEVEL 10
475 R 4 .2758      R 4 1.                                        LEVEL 10
476 F   0.                                                       LEVEL 10
477 R 4     .010719R 4      0.0213E
478 R 4     .010719R 4      0.0213E
479 R 4     .010719R 4      0.0213E
480 R 4 0.          R 4 554.4      E
481 F   0.                                                       LEVEL 10
482 F   0.                                                       LEVEL 10
483 F   0.                                                       LEVEL 10
484 F   0.                                                       LEVEL 10
485 F   0.                                                       LEVEL 10
486 F   0.                                                       LEVEL 10
487 F   0.                                                       LEVEL 10
488 R 4 554.4      R 4 554.4                                     LEVEL 10
489 R 4 554.4      R 4 554.4                                     LEVEL 10
490 F   1.5596 E+7                                               LEVEL 10
491 R 4          0.0R 4      0.0447E
492 R 4          0.0R 4      1.1431E
493 F    .005                                                    LEVEL 11
494 F    .005                                                    LEVEL 11
495 F    .005                                                    LEVEL 11
496 F    .005                                                    LEVEL 11
497 F    .005                                                    LEVEL 11
498 F    .005                                                    LEVEL 11
499 R 4 .2758      R 4 1.                                        LEVEL 11
500 R 4 .38        R 4 1.                                        LEVEL 11
501 R 4 .2758      R 4 1.                                        LEVEL 11
502 F   0.                                                       LEVEL 11
503 R 4     .010719R 4      0.0213E
504 R 4     .010719R 4      0.0213E
```

Fig. 68. (cont).

```
505 R 4     .010719R 4      0.0213E
506 R 4 0.          R 4 554.4      E
507 F    0.                                                    LEVEL 11
508 F    0.                                                    LEVEL 11
509 F    0.                                                    LEVEL 11
510 F    0.                                                    LEVEL 11
511 F    0.                                                    LEVEL 11
512 F    0.                                                    LEVEL 11
513 F    0.                                                    LEVEL 11
514 R 4 554.4       R 4 554.4                                  LEVEL 11
515 R 4 554.4       R 4 554.4                                  LEVEL 11
516 F    1.5596 E+7                                            LEVEL 11
517 R 4          0.0R 4      0.0516E
518 R 4          0.0R 4      1.3175E
519 F    .005                                                  LEVEL 12
520 F    .005                                                  LEVEL 12
521 F    .005                                                  LEVEL 12
522 F    .005                                                  LEVEL 12
523 F    .005                                                  LEVEL 12
524 F    .005                                                  LEVEL 12
525 R 4 .2758       R 4 1.                                     LEVEL 12
526 R 4 .38         R 4 1.                                     LEVEL 12
527 R 4 .2758       R 4 1.                                     LEVEL 12
528 F    0.                                                    LEVEL 12
529 R 4     .010719R 4      0.0213E
530 R 4     .010719R 4      0.0213E
531 R 4     .010719R 4      0.0213E
532 R 4 0.          R 4 554.4      E
533 F    0.                                                    LEVEL 12
534 F    0.                                                    LEVEL 12
535 F    0.                                                    LEVEL 12
536 F    0.                                                    LEVEL 12
537 F    0.                                                    LEVEL 12
538 F    0.                                                    LEVEL 12
539 F    0.                                                    LEVEL 12
540 R 4 554.4       R 4 554.4                                  LEVEL 14
541 R 4 554.4       R 4 554.4                                  LEVEL 14
542 F    1.5596 E+7                                            LEVEL 12
543 R 4          0.0R 4      0.0642E
544 R 4          0.0R 4      1.6404E
545 F    .005                                                  LEVEL 13
546 F    .005                                                  LEVEL 13
547 F    .005                                                  LEVEL 13
548 F    .005                                                  LEVEL 13
549 F    .005                                                  LEVEL 13
550 F    .005                                                  LEVEL 13
551 R 4 .2758       R 4 1.                                     LEVEL 13
552 R 4 .38         R 4 1.                                     LEVEL 13
553 R 4 .2758       R 4 1.                                     LEVEL 13
554 F    0.                                                    LEVEL 13
555 R 4     .010719R 4      0.0213E
556 R 4     .010719R 4      0.0213E
557 R 4     .010719R 4      0.0213E
558 R 4 0.          R 4 554.4      E
559 F    0.                                                    LEVEL 13
560 F    0.                                                    LEVEL 13
561 F    0.                                                    LEVEL 13
562 F    0.                                                    LEVEL 13
563 F    0.                                                    LEVEL 13
564 F    0.                                                    LEVEL 13
565 F    0.                                                    LEVEL 13
566 R 4 554.4       R 4 554.4                                  LEVEL 13
567 R 4 554.4       R 4 554.4                                  LEVEL 13
```

Fig. 68. (cont).

```
568 F   1.5596 E+7                                                    LEVEL 13
569 R 4     0.0289R 4      0.0648E
570 R 4      .7504R 4      1.6570E
571 F   .005                                                          LEVEL 14
572 F   .005                                                          LEVEL 14
573 F   .005                                                          LEVEL 14
574 F   .005                                                          LEVEL 14
575 F   .005                                                          LEVEL 14
576 F   .005                                                          LEVEL 14
577 R 4 .2758      R 4 1.                                             LEVEL 14
578 R 4 .38        R 4 1.                                             LEVEL 14
579 R 4 .2758      R 4 1.                                             LEVEL 14
580 F   0.                                                            LEVEL 14
581 R 4     0.1576R 4      0.0213E
582 R 4     0.1576R 4      0.0213E
583 R 4     0.1576R 4      0.0213E
584 R 4 596.4      R 4 555.4      E
585 F   0.                                                            LEVEL 14
586 F   0.                                                            LEVEL 14
587 F   0.                                                            LEVEL 14
588 F   0.                                                            LEVEL 14
589 F   0.                                                            LEVEL 14
590 F   0.                                                            LEVEL 14
591 F   0.                                                            LEVEL 14
592 F   596.4                                                         LEVEL 14
593 F   596.4                                                         LEVEL 14
594 F   1.5596 E+7                                                    LEVEL 14
595 R 4     0.0864R 4      0.1945E
596 R 4     2.2510R 4      4.9697E
597 F   .005                                                          LEVEL 14
598 F   .005                                                          LEVEL 14
599 F   .005                                                          LEVEL 14
600 F   .005                                                          LEVEL 14
601 F   .005                                                          LEVEL 14
602 F   .005                                                          LEVEL 14
603 R 4 .2758      R 4 1.                                             LEVEL 14
604 R 4 .38        R 4 1.                                             LEVEL 14
605 R 4 .2758      R 4 1.                                             LEVEL 14
606 F   0.                                                            LEVEL 14
607 R 4     0.1576R 4      0.0213E
608 R 4     0.1576R 4      0.0213E
609 R 4     0.1576R 4      0.0213E
610 R 4 596.4      R 4 555.4      E
611 F   0.                                                            LEVEL 14
612 F   0.                                                            LEVEL 14
613 F   0.                                                            LEVEL 14
614 F   0.                                                            LEVEL 14
615 F   0.                                                            LEVEL 14
616 F   0.                                                            LEVEL 14
617 F   0.                                                            LEVEL 14
618 F   596.4                                                         LEVEL 14
619 F   596.4                                                         LEVEL 14
620 F   1.5596 E+7                                                    LEVEL 14
621 R 4     0.1152         0.2531         0.2593         0.2531         0.2593E
622 R 4     3.0017         6.4670         6.6262         6.4670         6.6262E
623 F   .005                                                          LEVEL 15
624 F   .005                                                          LEVEL 15
625 F   .005                                                          LEVEL 15
626 F   .005                                                          LEVEL 15
627 F   .005                                                          LEVEL 15
628 F   .005                                                          LEVEL 15
629 R 4 .2758      R 4 1.719                                          LEVEL 15
630 R 4 .38        R 4 1.                                             LEVEL 15
```

Fig. 68. (cont).

```
631 R 4 .2758      R 4 1.                                                  LEVEL 15
632 F   0.                                                                 LEVEL 15
633 R 4      0.1576R 4      0.0213E
634 R 4      0.1576R 4      0.0213E
635 R 4      0.1576R 4      0.0213E
636 R 4 596.4      R 4 555.4      E
637 F   0.                                                                 LEVEL 15
638 F   0.                                                                 LEVEL 15
639 F   0.                                                                 LEVEL 15
640 F   0.                                                                 LEVEL 15
641 F   0.                                                                 LEVEL 15
642 F   0.                                                                 LEVEL 15
643 F   0.                                                                 LEVEL 15
644 F   596.4                                                              LEVEL 15
645 F   596.4                                                              LEVEL 15
646 F   1.5596 E+7                                                         LEVEL 15
647 R 4      0.0044          0.3152          0.3090          0.3152          0.3090E
648 R 4      0.1121          8.0494          7.8902          8.0494          7.8902E
649 F   .005                                                              LEVEL 16
650 F   .005                                                              LEVEL 16
651 F   .005                                                              LEVEL 16
652 F   .005                                                               EVEL 16
653 F   .005                                                              LEVEL 16
654 F   .005                                                              LEVEL 16
655 F   '.56451                                                           LEVEL 16
656 R 4 .47        R 4 1.                                                 LEVEL 16
657 F   0.                                                                 LEVEL 16
658 F   1.                                                                 LEVEL 16
659 R 4      0.0750R 4      0.0107E
660 R 4      0.0750R 4      0.0107E
661 R 4      0.0750R 4      0.0107E
662 F         596.4E
663 F   0.                                                                 LEVEL 16
664 F   0.                                                                 LEVEL 16
665 F   0.                                                                 LEVEL 16
666 F   0.                                                                 LEVEL 16
667 F   0.                                                                 LEVEL 16
668 F   0.                                                                 LEVEL 16
669 F   0.                                                                 LEVEL 16
670 F   596.4                                                              LEVEL 16
671 F   596.4                                                              LEVEL 16
672 F   1.5596 E+7                                                         LEVEL 16
673 F   0.                                                                 ROD DATA
674      680.9          680.9          672.5          651.3          637.9  ROD DATA
675      626.1          615.7          607.0          594.0          582.1  ROD DATA
676      766.4          766.4          752.2          716.7          693.8  ROD DATA
677      673.8          656.1          641.3          619.6          599.7  ROD DATA
678      827.3          827.3          809.2          763.9          734.3  ROD DATA
679      708.4          685.5          666.5          639.0          613.7  ROD DATA
680      866.1          866.1          845.5          793.6          759.5  ROD DATA
681      729.8          703.4          681.7          650.4          621.6  ROD DATA
682      885.2          885.2          863.3          808.3          771.9  ROD DATA
683      740.2          712.1          689.0          655.8          625.2  ROD DATA
684      869.7          869.7          849.1          797.4          763.2  ROD DATA
685      733.5          707.1          685.4          654.2          625.4  ROD DATA
686      837.7          837.7          819.7          774.4          744.8  ROD DATA
687      718.9          696.0          677.1          649.8          624.8  ROD DATA
688      788.9          788.9          774.8          739.4          716.5  ROD DATA
689      696.4          678.7          664.0          642.6          623.1  ROD DATA
690      715.3          715.3          706.9          685.9          672.4  ROD DATA
691      660.6          650.2          641.5          628.8          617.1  ROD DATA
692      637.6          637.6          634.7          627.5          623.0  ROD DATA
693      619.1          615.5          612.6          608.2          604.2  ROD DATA
```

Fig. 68. (cont).

694 F	0.					ROD DATA
695	680.9	680.9	672.5	651.3	637.9	ROD DATA
696	626.1	615.7	607.0	594.0	582.1	ROD DATA
697	766.4	766.4	752.2	716.7	693.8	ROD DATA
698	673.8	656.1	641.3	619.6	599.7	ROD DATA
699	827.3	827.3	809.2	763.9	734.3	ROD DATA
700	708.4	685.5	666.5	639.0	613.7	ROD DATA
701	866.1	866.1	845.5	793.6	759.5	ROD DATA
702	729.8	703.4	681.7	650.4	621.6	ROD DATA
703	885.2	885.2	863.3	808.3	771.9	ROD DATA
704	740.2	712.1	689.0	655.8	625.2	ROD DATA
705	869.7	869.7	849.1	797.4	763.2	ROD DATA
706	733.5	707.1	685.4	654.2	625.4	ROD DATA
707	837.7	837.7	819.7	774.4	744.8	ROD DATA
708	718.9	696.0	677.1	649.8	624.8	ROD DATA
709	788.9	788.9	774.8	739.4	716.5	ROD DATA
710	696.4	678.7	664.0	642.6	623.1	ROD DATA
711	715.3	715.3	706.9	685.9	672.4	ROD DATA
712	660.6	650.2	641.5	628.8	617.1	ROD DATA
713	637.6	637.6	634.7	627.5	623.0	ROD DATA
714	619.1	615.5	612.6	608.2	604.2	ROD DATA
715 F	0.					ROD DATA
716	680.9	680.9	672.5	651.3	637.9	ROD DATA
717	626.1	615.7	607.0	594.0	582.1	ROD DATA
718	766.4	766.4	752.2	716.7	693.8	ROD DATA
719	673.8	656.1	641.3	619.6	599.7	ROD DATA
720	827.3	827.3	809.2	763.9	734.3	ROD DATA
721	708.4	685.5	666.5	639.0	613.7	ROD DATA
722	866.1	866.1	845.5	793.6	759.5	ROD DATA
723	729.8	703.4	681.7	650.4	621.6	ROD DATA
724	885.2	885.2	863.3	808.3	771.9	ROD DATA
725	740.2	712.1	689.0	655.8	625.2	ROD DATA
726	869.7	869.7	849.1	797.4	763.2	ROD DATA
727	733.5	707.1	685.4	654.2	625.4	ROD DATA
728	837.7	837.7	819.7	774.4	744.8	ROD DATA
729	718.9	696.0	677.1	649.8	624.8	ROD DATA
730	788.9	788.9	774.8	739.4	716.5	ROD DATA
731	696.4	678.7	664.0	642.6	623.1	ROD DATA
732	715.3	715.3	706.9	685.9	672.4	ROD DATA
733	660.6	650.2	641.5	628.8	617.1	ROD DATA
734	637.6	637.6	634.7	627.5	623.0	ROD DATA
735	619.1	615.5	612.6	608.2	604.2	ROD DATA
736 F	0.					ROD DATA
737	680.9	680.9	672.5	651.3	637.9	ROD DATA
738	626.1	615.7	607.0	594.0	582.1	ROD DATA
739	766.4	766.4	752.2	716.7	693.8	ROD DATA
740	673.8	656.1	641.3	619.6	599.7	ROD DATA
741	827.3	827.3	809.2	763.9	734.3	ROD DATA
742	708.4	685.5	666.5	639.0	613.7	ROD DATA
743	866.1	866.1	845.5	793.6	759.5	ROD DATA
744	729.8	703.4	681.7	650.4	621.6	ROD DATA
745	885.2	885.2	863.3	808.3	771.9	ROD DATA
746	740.2	712.1	689.0	655.8	625.2	ROD DATA
747	869.7	869.7	849.1	797.4	763.2	ROD DATA
748	733.5	707.1	685.4	654.2	625.4	ROD DATA
749	837.7	837.7	819.7	774.4	744.8	ROD DATA
750	718.9	696.0	677.1	649.8	624.8	ROD DATA
751	788.9	788.9	774.8	739.4	716.5	ROD DATA
752	696.4	678.7	664.0	642.6	623.1	ROD DATA
753	715.3	715.3	706.9	685.9	672.4	ROD DATA
754	660.6	650.2	641.5	628.8	617.1	ROD DATA
755	637.6	637.6	634.7	627.5	623.0	ROD DATA
756	619.1	615.5	612.6	608.2	604.2	ROD DATA

Fig. 68. (cont).

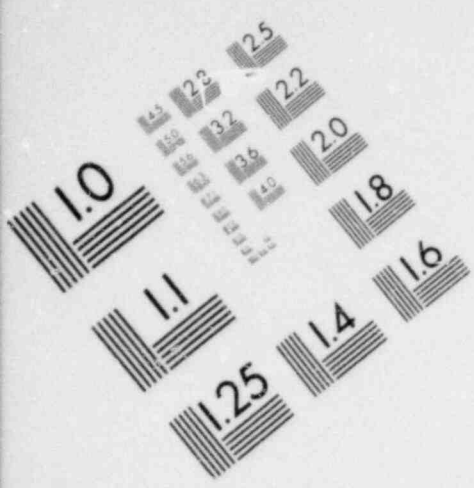

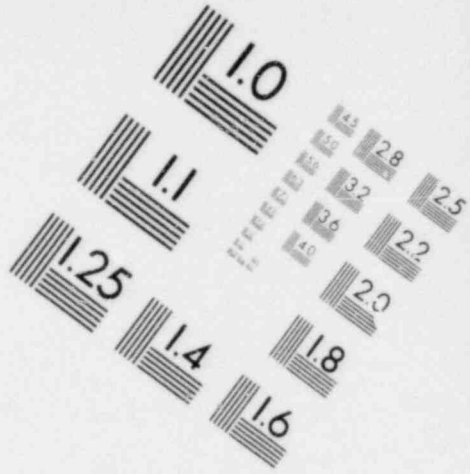

IMAGE EVALUATION
TEST TARGET (MT-3)

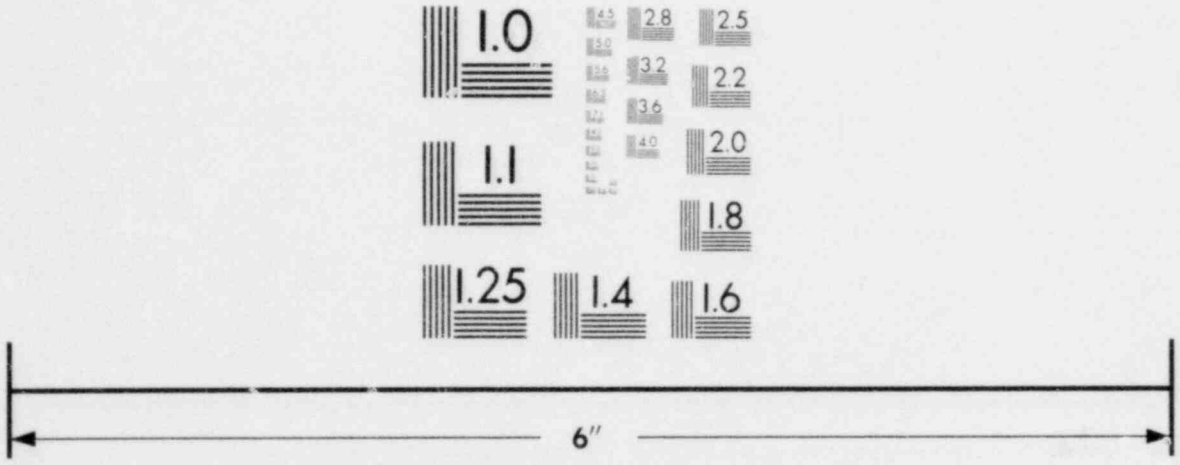

MICROCOPY RESOLUTION TEST CHART

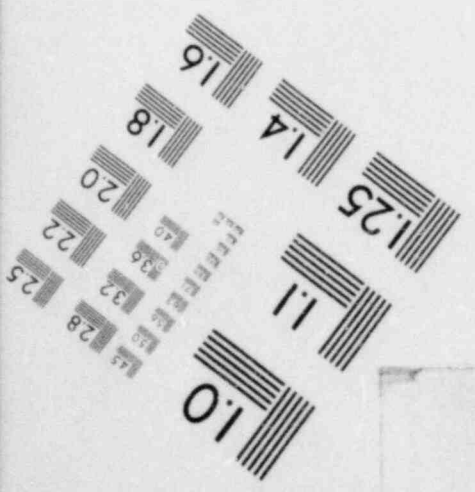

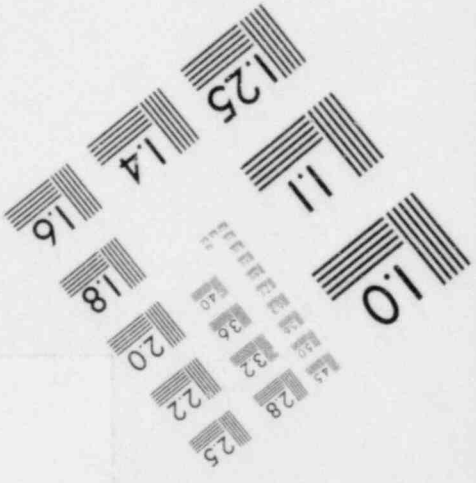

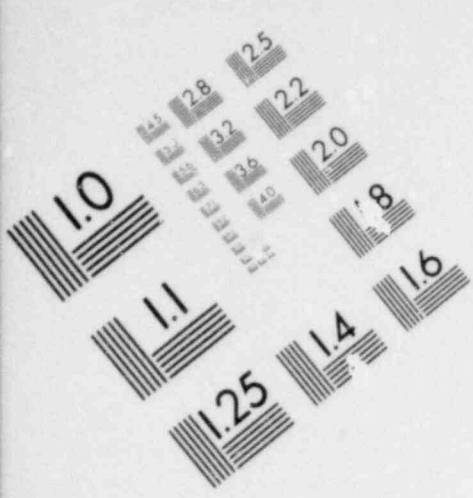

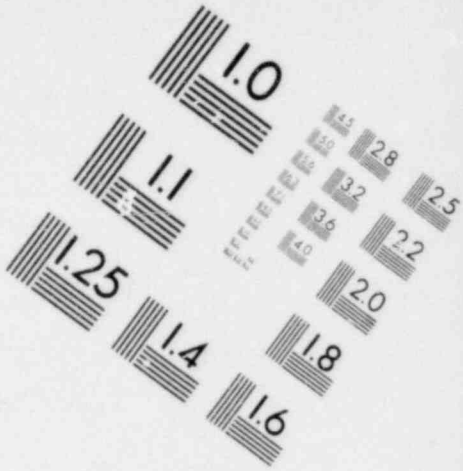

IMAGE EVALUATION
TEST TARGET (MT-3)

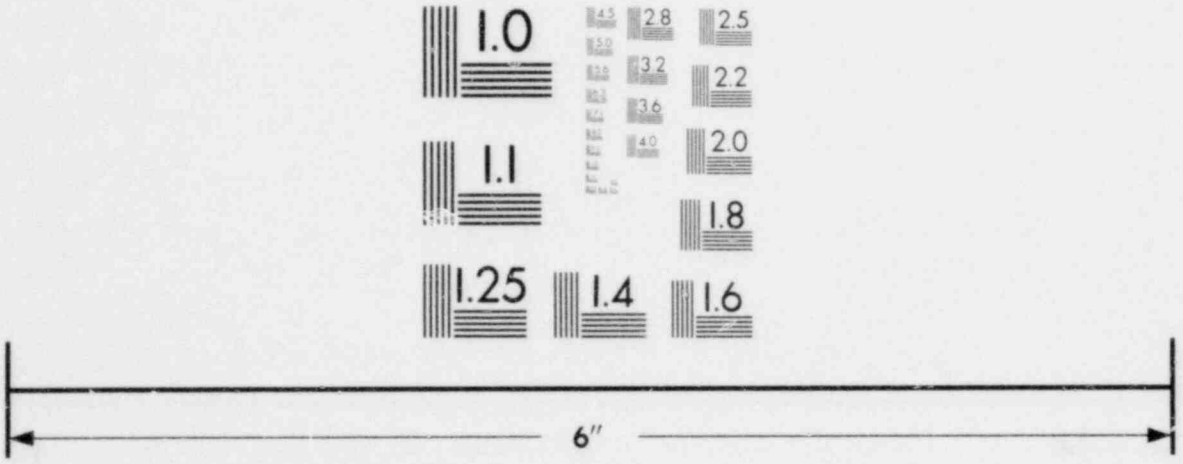

MICROCOPY RESOLUTION TEST CHART

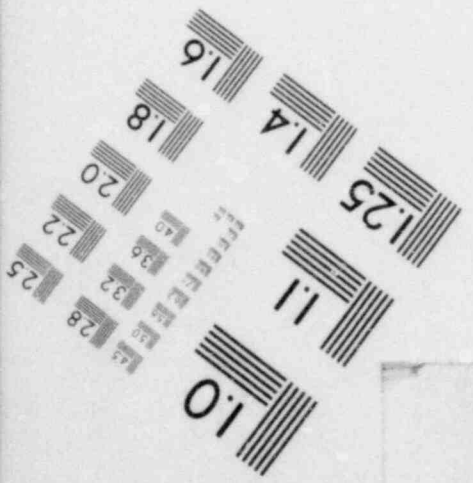

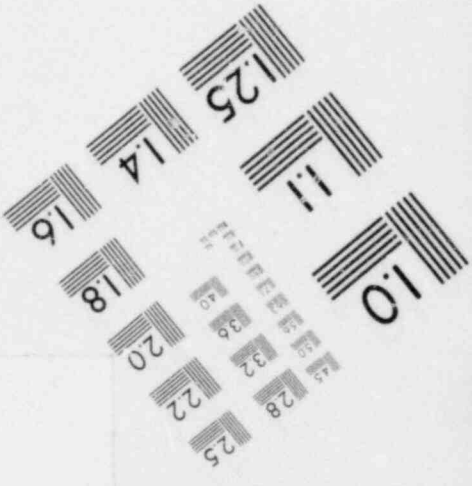

```
FILL                       7
               9           4           100          3
    .26          .01         0.          .05           490.5
     55.7 E+5
    0.           .05         .1          0.            1000.
    0.
BREAK                      8
              13
    .26            2.0 E-3    .93          543.8         55.6 E+5
PIPE                       9
               1           0           6            11          7
               0           0
   0.          0.          0.          0.          0.
   0.
      5.0000E-01
      5.0000E-03
F     1.0000E-03
F     0.
F     0.
F     3.6000E-02
F             +4
      0.
      0.
F     0.
      554.4
        1.5596E+7
PIPE                      10
               1           0           7            12          7
               0           0
   0.          0.          0.          0.          0.
   0.
      5.0000E-01
      5.0000E-03
F     1.0000E-03
F     0.
F     0.
F     3.6000E-02
F             +4
      0.
      0.
F     0.
      554.4
        1.5596E+7
FILL                      11
              11           1
   .1          .001        0.          0.          554.4
        1.5596E+7
FILL                      12
              12           1
   .1          .001        0.          0.          596.4
        1.5596E+7
VALVE                     13
               2           0          10           13



               3         100           3                        2
          9.2 E-3    1.88 E-2
F     .5
F         4.6 E-3
F         9.2 E-3
F     0.
F     0.
```

Fig. 68. (cont).

```
820 F       1.38E-2
821                 4              4              4
822 F   0.
823     0.              1.              .1             0.              1000.
824     0.
825 F   .881
826 F   1.8
827 F   544.3
828 F     55.6 E+5
829          1.0E-4          .005        80.01             1.
830              4.0          .10             4.0             1.
831              -1.
```

Fig. 68. (Cont)

```
1                3
2 S5T9HI  TIGHTER CONV CRITERIA
3 SEMISCALE TRANSIENT
4 USE WITH RESTART S5S98CR
5              3201     0.0
6                0               1              13              13
7           1.0E-4          1.0E-5
8               20             100                              2
9                1               2               3               4               5
10               6               7               8               9              10
11              11              12              13
12             100                              1.
13
14            1000
15
16 PIPE                          9
17               15              1               6              11               7
18                0              1
19    3.335000E-02  1.112520E-02                                          2.930000E+02
20    2.930000E+02
21      5.3486E-01R 2 4.0399E-01R 2 4.0747E-01R 4 .0105727  R 1  .0125095
22      .0062547       .0031274  R 2 .0015637       .13589    E
23      1.8689E-03R 2 1.4116E-03R 2 7.099  E-4    1.25103 E-5    8.91850 E-6
24     5.93451 E-6    3.55829 E-6R 1 3.04406E-6    .152203 E-5S
25      .751101E-6R 2 .375551E-6     7.13999E-5E
26      3.4942E-03R 2 3.4942E-03R 2 1.4455E-03    1.37228 E-3    1.00382 E-3
27     6.92839 E-4    4.39347 E-4R 62.43340 E-4    8.72228 E-4
28 R 6 0.          R10 .0073
29 F    0.0
30      4.8260E-02R 2 6.6700E-02R 2 4.2900E-02     .0418          .0357505
31      .0297010       .0236515  R 6 .0176020       .0333250
32 F             4
33 F
34 F
35 F
36 I 3 555.3           553.2      F   553.2
37 F    1.5596 E+7
38 I 3 555.3           553.2      F   553.2
39 PIPE                         10
40               31              1               7              12               7
41                0              1
42    3.335000E-02  1.112520E-02                                          2.930000E+02
43    2.930000E+02
44      5.1690E-01     3.8570E-01R10 5.1530E-01R 2 6.4260E-01     4.5840E-01
45 R 2 4.0640E-01R 2 5.2780E-01R 2 [illegible]E-01R 4 .0105727  R 1  .0125095
46      .0062547       .0031274  R 2 .0015637       .13589    E
47      1.8066E-03     1.3479E-03R10 1.[illegible]43E-03R 2 9.2880E-04     6.6261E-04
48 R 2 7.4050E-04R 2 6.0175E-04R 2 4.9514 E-4    1.25103 E-5    8.91850 E-6
49     5.93451 E-6    3.55829 E-6R 1 3.04406E-6    .152203 E-5S
50      .751101E-6R 2 .375551E-6     7.13999E-5E
51      3.4942E-03R 2 3.4949E-03R 9 3.7378E-03R 3 1.4455E-03R 3 2.4475E-04
52 R 4 1.1401 E-3    1.00382 E-3    6.92839 E-4    4.39347 E-4R 62.43340 E-4
53     8.72228 E-4
54 R 2 11.         R11 1.25           1.3        R 6 .0113      R 2 0.
55 R10 .0073
56                      5.0000E-01R 5 1.0000E+00R 4-1.0000E+00 -0-5.0000E-01
57 R 2  -1.0      R 2 0.          R 3  1.0       F  0.0
58      4.8260E-02R 2 6.6700E-02R 9 6.8990E-02R 3 4.2900E-02R 3 1.7650E-02
59 R 4 .0381          .0357505         .0297010       .0236515  R 6 .0176020
60      .0333250
61 F             4
62 F
63 F
```

Fig. 69. TRAC input deck for Semiscale Test S-02-8 transient calculation.

```
64 F
65 I19 592.          585.9      F   585.9
66 F   1.5596 E+7
67 I19 592.          585.9      F   585.9
68 BREAK                       11
69             11
70          .13589   7.13949 E-5  1.000000E+00    396.7          2.206 E+05
71 BREAK                       12
72             12
73          .13589   7.13949 E-5  1.000000E+00    396.7          2.206 E+05
74 TEE                         1                 0
75                4            1                 7  0.                      0
76                0            6                 1            2             0
77   3.335020E-02  1.11252CE-02  0.                0.                2.950000E+02
78   2.950000E+02
79                1            4                 8
80   9.425000E-03  3.911600E-03  0.                0.                2.950000E+02
81   2.950000E+02
82 F   5.1430E-01E
83      1.7220E+00    7.2000E-01    2.0300E-01    2.0000E-02E
84 F   1.7986E-03E
85      7.3890E-05    3.0895E-05    7.0930E-04    4.5520E-04E
86 F   3.4942E-03E
87 R 3 4.2910E-05R 1 3.4940E-03R 1 2.2760E-02E
88 F   0.          E
89 F   6.8000E-03E
90 R 6 0.          R 1 1.0000E+00E
91 F   1.0000E+00E
92 F   6.6700E-02E
93 R 3 7.3900E-03R 1 6.6700E-02R 1 1.7000E-01E
94 F              4E
95 F              4E
96 F   0.          E
97 F   0.          E
98      7.8194E-14    7.9334E-14    7.9321E-14    7.8141E-14    7.7606E-14
99      7.7240E-14E
100     1.8901E-16    1.7093E-16    1.6150E-16    2.4436E-18E
101     3.1344E+00    3.1344E+00    3.1345E+00    3.1345E+00    3.1623E+00
102     3.1624E+00    3.1624E+00E
103 R 3-2.2555E+00R 1-2.7700E-02R 1-4.2524E-03E
104 R 3 5.9334E+02R 3 5.9339E+02E
105 R 3 5.9640E+02    618.4      E
106     1.5591E+07    1.5591E+07    1.5591E+07    1.5590E+07    1.5590E+07
107     1.5590E+07E
108     1.5592E+07    1.5594E+07    1.5597E+07    1.5596E+07E
109     5.9343E+02    5.9344E+02    5.9345E+02    5.9349E+02    5.9350E+02
110     5.9351E+02E
111 R 3 5.9640E+02    618.4      E
112 PRIZER                     5                 0
113               4            8
114   8.000000E+03  1.559600E+07  1.000000E+05  1.000000E-01
115 R 2 5.0000E-01R 1 1.2840E-01R 1 2.0000E-02E
116 R 2 1.1730E-02R 1 3.0125E-03R 1 4.6920E-04E
117 F   2.2760E-02E
118 F   0.          E
119 F  -1.0000E+00E
120 F   1.7000E-01E
121 F              4E
122 R 1 1.0000E+00R 3 0.          E
123 R 4 0.          R 1 4.2524E-03E
124 F   6.1840E+02E
125 F   6.1840E+02E
126 F   1.5596E+07E
127 END
128          1.0E-5         2.0E-2           1.0           1.0
129          1.0            2.0E-2            2.
130          1.0E-5         2.0E-2           30.1           1.0
131          1.0            1.0E-1            2.
132    -1.
```

Fig. 69. (cont).

Running times for the steady-state and blowdown calculations were 51 and 126 min, respectively, on the CDC 7600 computer. These running times are reasonable considering the complexity of the model used in the calculations.

F. Creare Countercurrent Flow Experiments

1. Description of Experiments

The Creare countercurrent flow experiments investigated the effects on ECC penetration to the lower plenum of countercurrent steam flow rate, downcomer wall superheat, and ECC subcooling. The basic component of the Creare test facility is a 1/15-scale (linear dimension), multiloop, cylindrical model of a PWR downcomer region. A detailed description of this facility and its operation is given by Creare, Inc., Hanover, New Hampshire in Ref. 14. The Creare vessel can be arranged in at least six different geometrical configurations. The configuration used in the tests analyzed is the so-called "base-line" configuration having a 0.0127 m (0.5-in.) downcomer gap and a "deep plenum" geometry.

The vessel has four cold legs oriented 90° to each other. Three of the cold legs are assumed to be "intact" and are connected to ECC injection lines. A single "broken" cold leg connects to the pressure suppression tank. There are also four hot legs; however in the tests presently being considered, hot and cold legs alternate and the hot legs are closed off.

The test procedures for the countercurrent flow tests are as follows. A constant steam flow rate through the vessel is established and the vessel is purged of air. The steam enters at the top of the vessel, flows down the center of the vessel into the lower plenum, up the downcomer, and out the broken cold leg. After reaching the steady steam flow rate, water is then injected simultaneously into the three intact cold legs at a constant preset flow rate with equal flows into each intact cold leg. After a short transient period, the plenum normally begins to fill. The test is run until the lower plenum is full or until the filling rate can be determined from strip chart records. A complete penetration curve is composed of a set of tests at a given liquid injection rate and liquid temperature with the steam flow rate varied over a range such that water delivery ranges from complete delivery to complete bypass.

2. TRAC Best-Estimate Model

The TRAC model of the Creare vessel is shown in Fig. 70. The vessel was modeled using 7 axial levels with each level subdivided into 2 radial and 8 azimuthal zones for a total of 112 mesh cells. The 4 sources (pipes) at level 6 led to the selection of 8 rather than 4 azimuthal zones which would have placed an ECC source into each cell at this level. One radial segment in the downcomer was chosen because this is typical for our full-scale PWR model.

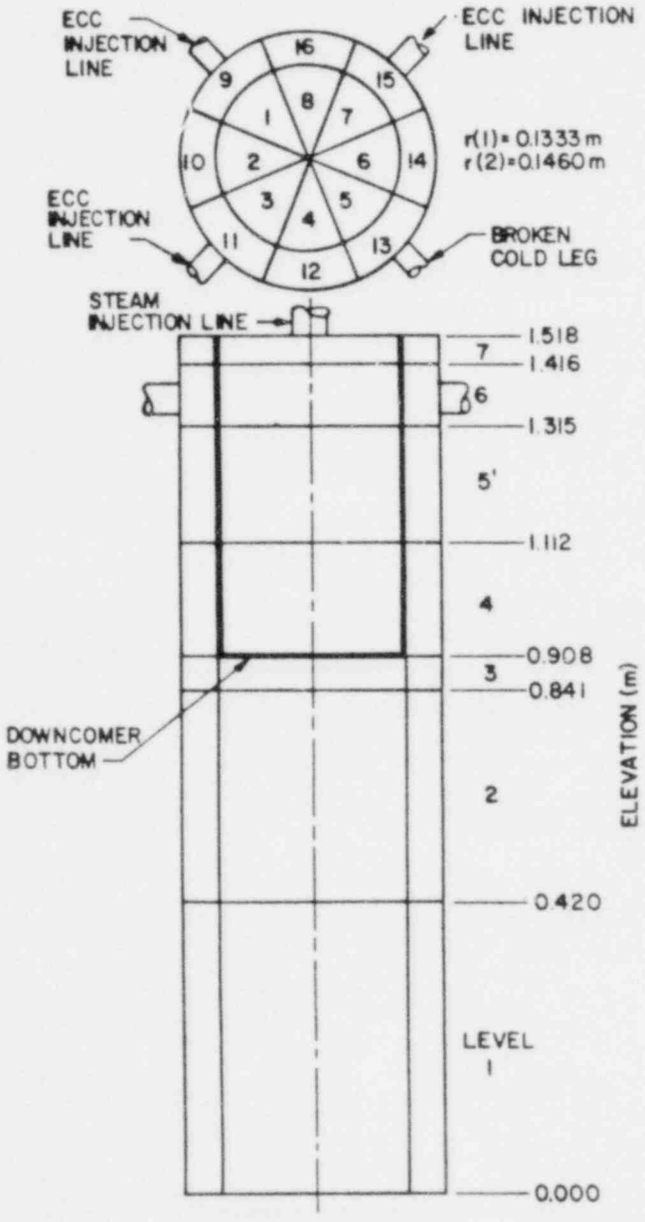

Fig. 70. TRAC noding for Creare 1/15-scale vessel.

The rationale for axial level dimensions are as follows. Levels 1 and 2 allow for pooling of the liquid in the lower plenum and the results are not sensitive to the relative height of each cell. Level 3 allows for flow resolution near the bottom of the downcomer. Levels 4, 5, and 6 allow for resolution of flows in the downcomer region, while level 7 can resolve any liquid "stored" in the upper part of the downcomer.

The calculational procedure parallels that of the Creare experimental procedure. A steady-state calculation is performed to establish a constant reverse steam flow and lower plenum pressure. The steam is injected into 8 PIPES connected at cell numbers 1 through 8 at level 7 using FILL modules. The "intact" cold legs are isolated with zero velocity FILL modules. The "broken" cold leg is connected to a BREAK module with the pressure selected to give the correct lower plenum pressure. This assures the correct liquid subcooling when the ECC is injected. This steady-state calculation is run until J^*_{gc} (dimensionless reverse core steam flow rate, see Ref. 14) reaches a constant value, which normally takes about 3 s of simulation time. The transient calculaton is started from the steady-state dump with the FILL velocities on the three intact cold legs replaced so as to give the correct ECC injection flow and temperature.

For these Creare calculations only, additional editing and graphics information was incorporated into the code. Specifically, the instantaneous values of J^*_{gc} and J^*_{fd} (dimensionless water flow rate delivered to the lower plenum) are calculated at the bottom of the downcomer and the collapsed liquid level in the lower plenum is calculated based on the volume of liquid in Levels 1, 2, and 3. Also calculated is the liquid mass "stored" in the downcomer; plotting of this variable reveals any storage and dumping of liquid in the downcomer region. The plotted values of J^*_{gc} and J^*_{fd} for each calculation are determined as follows. The value of J^*_{gc} is the initial steady-state value. This variable undergoes an initial transient following ECC injection and may not return to the full value due to steam condensation. The calculated value of J^*_{fd} is determined from the average lower plenum filling rate as is the case with the experimental results.

3. Comparison of Best-Estimate Calculations with Experiments

The Creare countercurrent flow experiments covered a wide range of ECC flow rates and subcoolings. Four TRAC calculations were made to generate two

complete penetration curves. These two curves are: (a) 1.86 x 10^{-3} m^3/s and 373 K (30 gpm and 212°F) and (b) 3.78 x 10^{-3} m^3/s flow rate and 339 K (60 gpm at 150°F) . The reactor scale injection flow rate is 3.78 x 10^{-3} m^3/s (60 gpm).

The basis for selecting these two penetration curves is to separate the basic phenomena determining whether ECC bypass or delivery will occur. These phenomena are interfacial momentum and energy exchange between the liquid and the steam. The first case has very low subcooling since the system pressure ranged from 1-3 atmospheres. Thus, the only effect that can produce bypass is the interfacial drag between the steam and the liquid. The calculated penetration curve for this case gives an appraisal of the constitutive relationship describing interfacial momentum exchange. Moreover, since the calculations cover the range of complete bypass to complete dumping, different flow regimes exist in the downcomer at the bypass point than at the complete delivery point.

Figure 71 compares the results of the low subcooling case. Near the complete dumping location at J^*_{gc} = 0.043, the calculated J^*_{fd} is equal to 0.047 which is in excellent agreement with the measured value of 0.051. At a high steam flow rate, J^*_{gc} = 0.14, there is almost complete bypass of the injected liquid. At this steam flow rate, TRAC also predicts nearly complete bypass. The calculated J^*_{fd} is equal to 0.005 while the measured value is 0.004.

The tests with ECC injected at 60 gpm and 150°F have significant subcooling since the system pressure varies from 1-2.5 atmospheres. Thus, interfacial heat transfer now becomes significant in determining the quantity of liquid delivered. Moreover, the penetration curves become much flatter as the ECC subcooling is raised (see Ref. 14). This means that the system "wants to operate" in either a complete bypass or complete delivery mode. Operation in the intermediate delivery/bypass range is thus experimentally difficult to achieve as the change in steam flow rate required to cause a transition from complete delivery to complete bypass is very small.

Figure 72 compares the results for the high subcooling case. The complete dumping location at J^*_{gc} = 0.10 is again in excellent agreement. The calculation shows that almost all of the injected liquid is delivered to the

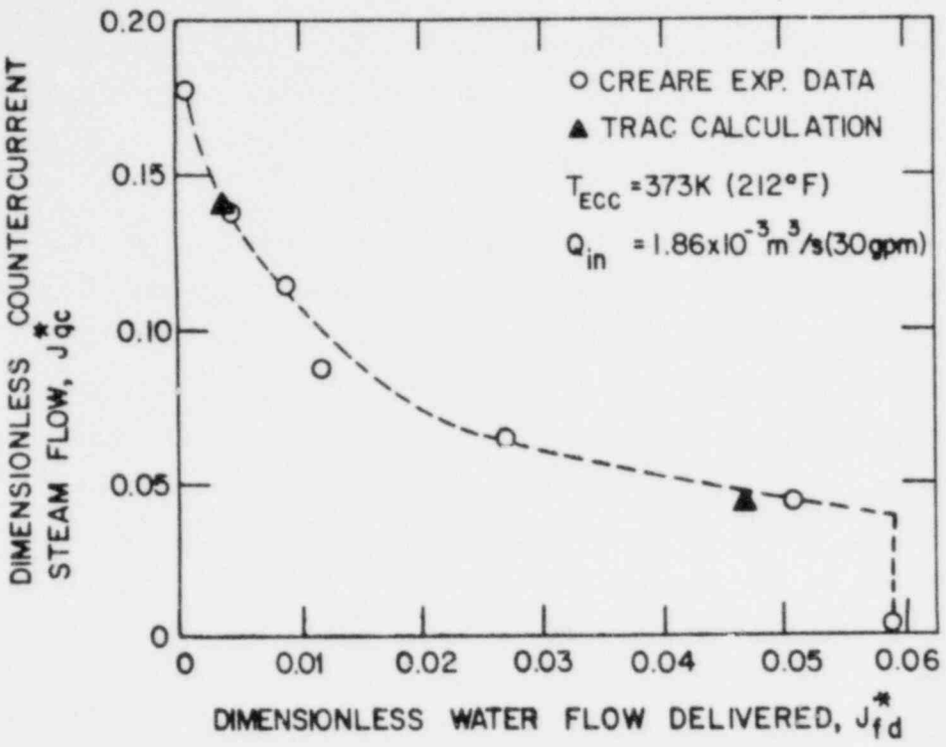

Fig. 71. Comparison of calculated and measured flooding curves for Creare low subcooling tests.

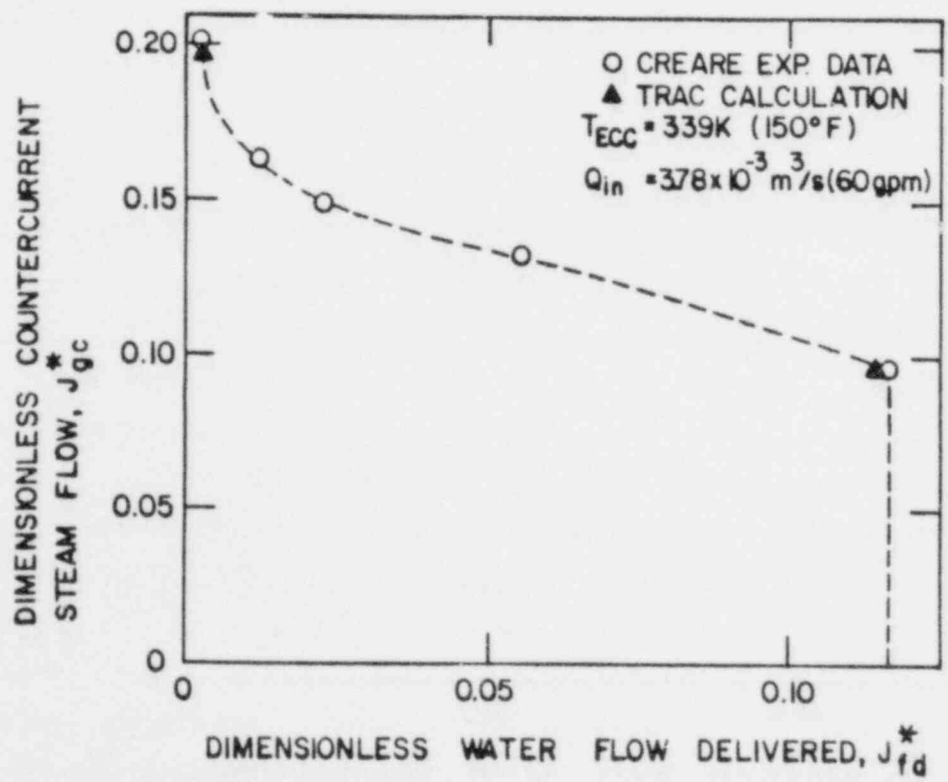

Fig. 72. Comparison of calculated and measured flooding curves for Creare high subcooling tests.

lower plenum. At a steam flow rate of $J^*_{gc} = 0.20$, essentially all of the liquid is bypassed in both the experiment and in the TRAC calculation. Thus, the critical end points for this relatively high subcooling penetration case are predicted quite well.

The calculated values for the dimensionless steam flow (J^*_{gc}) and liquid flow (J^*_{gd}) may be very oscillatory during the transient. The calculated value of J^*_{gc} for the case having high subcooling and nearly complete bypass is shown in Fig. 73. It is seen that J^*_{gc} is reduced from its initial steady-state value of 0.20 shortly after ECC enters the downcomer. The reason for this is that part of the steam flow is condensed by the cold ECC fluid. The resulting water flow rate to the downcomer bottom (Fig. 74) is also quite oscillatory. However, the time integrated value of this curve is the quantity of liquid delivered to the lower plenum and is shown to be quite smooth in Fig. 75. Thus, even though the instantaneous liquid delivery to the lower plenum is erratic, the resulting collapsed water level in the lower plenum is a smooth function.

4. Parametric Study

An investigation was made to identify the effect of mesh size on these results. A VESSEL module containing 480 cells (base model was 112) was used. This model has 15 axial levels, 8 azimuthal segments, and 4 radial zones. Only the low subcooling penetration curve was regenerated. Although the results were in agreement to within approximately $\pm$ 10%, it is felt that further noding sensitivity studies are needed.

5. TRAC-P1A Features Tested

These calculations serve as "code-testing" for the interfacial momentum and heat transfer constitutive relationships in the three-dimensional VESSEL module. The comparisons between experimental data and TRAC calculations were in very good overall agreement. This indicates that TRAC is capable of satisfactorily predicting the bypass and penetration of ECC in annular downcomer geometries at this scale of experiment. Results of LOFT Test L1-4 (see Sec. H) indicate that TRAC also accurately predicts bypass on a larger scale facility; however, further comparisons at even larger scale are needed.

6. Input Data Decks

A listing of a typical data deck used to generate the steady-state steam flow is given in Fig. 76. FILL component numbers 11 - 18 are used to specify

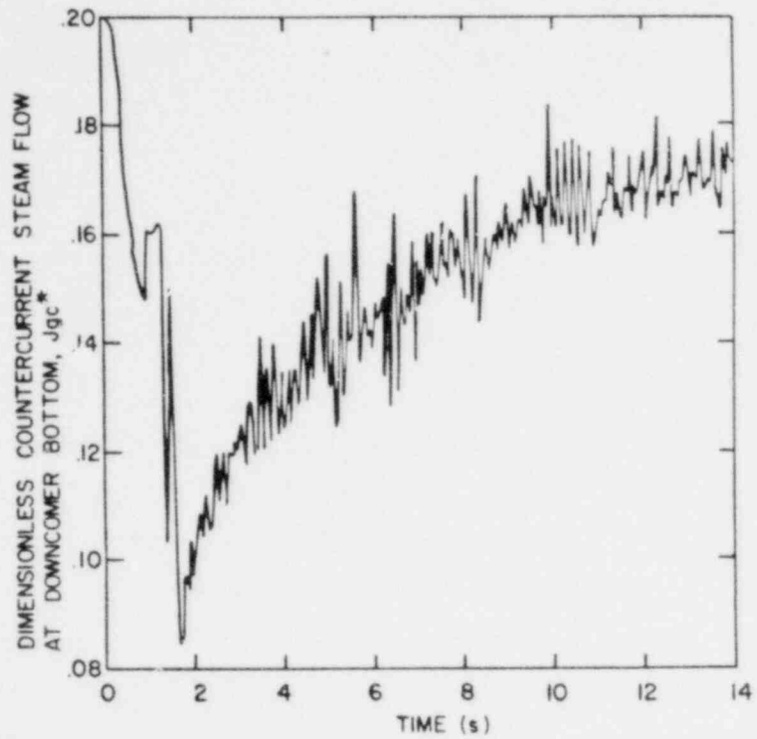

Fig. 73. Dimensionless steam flow for high subcooling and nearly complete bypass Creare test.

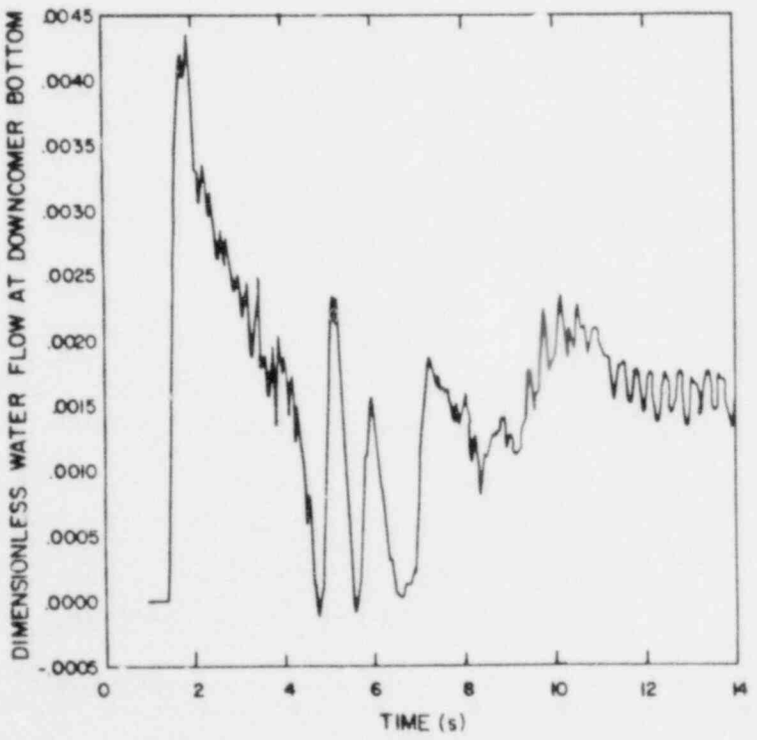

Fig. 74. Dimensionless water flow for high subcooling and nearly complete bypass Creare test.

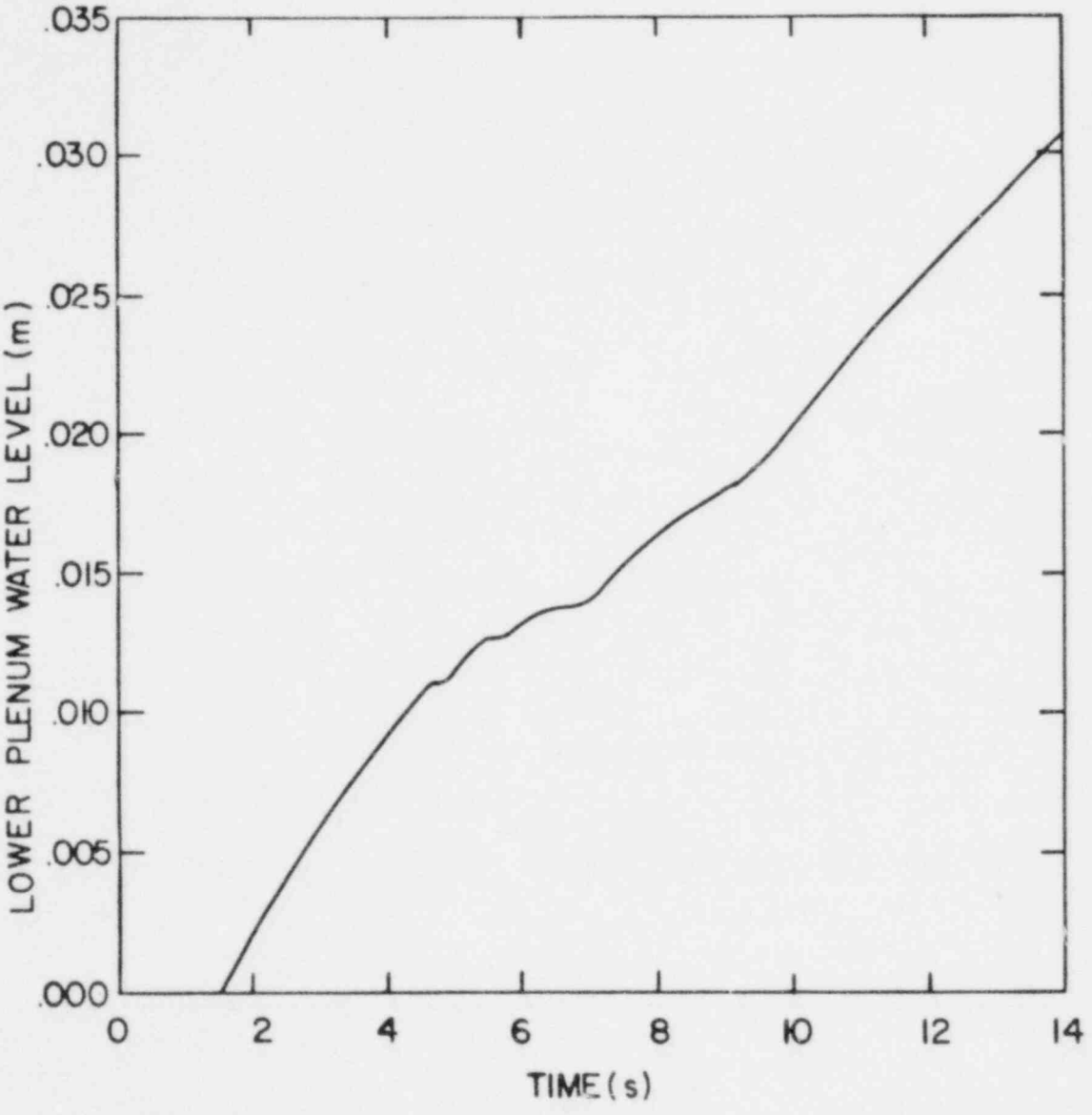

Fig. 75. Lower plenum water level for high subcooling and nearby complete bypass Creare test.

```
              1
CASE 8 JG*= 0.14 P=1.74BAR
                              1             25            24            1
      1.0E-3             2.E-6          1.0E-3
          10                20                             1
          11                 2             3               4            5
           6                 7             8               9           10
          12                13            14              15           16
          17                18            19              20           21
          22                23            24              25            1
        2000                 0          -1.0             0.0

VESSEL                       1             1
           7                 2             8              12
           7                 3             1


      8026.0             502.0          17.3             0.6          1.0
         1.0



       0.420             0.841         0.908           1.112        1.315
       1.416             1.518
      0.1333            0.1460
      0.7854            1.5710        2.3500          3.1420        3.927
       4.712            5.4980        6.2830
           6                 9             3               1
           6                11             3               2
           6                13             3               3
           6                15             3               4
           7                 5             2               9
           7                 1             2              60
           7                 2             2              61
           7                 3             2              62
           7                 4             2              63
           7                 6             2              64
           7                 7             2              65
           7                 8             2              66
F        0.0E
F        0.0E
F        0.0E
F        0.0E
F        0.0E
F        0.0E
F        0.0E
F        0.0E
F        1.0E
F        1.0E
F        1.0E
F        1.0E
F       0.01E
F       0.01E
F       0.01E
F      395.0E
F        1.0E
F        0.0E
F        0.0E
F        0.0E
F        0.0E
F        0.0E
F        0.0E
```

Fig. 76. TRAC input deck to generate initial conditions for a typical Creare test.

```
F          395.0E
F          395.0E
F         1.1E05E
F            0.0E
F            0.0E
F            0.0E
F            0.0E
F            0.0E
F            0.0E
F            0.0E
F            0.0E
F            1.0E
F            1.0E
F            1.0E
F            1.0E
F           0.01E
F           0.01E
F           0.01E
F          395.0E
F            1.0E
F            0.0E
F            0.0E
F            0.0E
F            0.0E
F            0.0E
F            0.0E
F          395.0E
F          395.0E
F         1.1E05E
F            0.0 E
F            0.0 E
F            0.0E
F            0.0E
F            0.0E
F            0.0E
F            0.0E
F            0.0E
F            1.0E
F            1.0E
F            1.0E
F            1.0E
F           0.01E
F           0.01E
F           0.01E
F          395.0E
F            1.0E
F            0.0E
F            0.0E
F            0.0E
F            0.0E
F            0.0E
F            0.0E
F          395.0E
F          395.0E
F         1.1E05E
F            0.0 E
F            0.0 E
F            0.0E
F            0.0E
F            0.0E
F            0.0E
F            0.0E
```

Fig. 76 (Cont.)

```
R 8        1.00R 8        1.0E
F           1.0E
F           1.0E
F           1.0E
F          0.01E
F          0.01E
F          0.01E
F         395.0E
F           1.0E
F           0.0E
F           0.0E
F           0.0E
F           0.0E
F           0.0E
F           0.0E
F          395.0E
F          395.0E
F         1.1E05E
F           0.0 E
F           0.0 E
F           0.0E
F           0.0E
F           0.0E
F           0.0E
F           0.0E
F           0.0E
R 8        1.00R 8        1.0E
F           1.0E
F           1.0E
F           1.0E
F          0.01E
F          0.01E
F          0.01E
F         395.0E
F           1.0E
F           0.0E
F           0.0E
F           0.0E
F           0.0E
F           0.0E
F           0.0E
F           0.0E
F          395.0E
F          395.0E
F         1.1E05E
F         0.0    E
F         0.0    E
F           0.0E
F           0.0E
F           0.0E
F           0.0E
F           0.0E
F           0.0E
R 8         1.00          1.0          0.59          1.0          0.59
             1.0         0.59           1.0         0.59E
R 8         1.0           1.0          0.25          1.0          0.25
             1.0         0.25           1.0         0.25E
R 8         1.0           1.0          0.31          1.0          0.31
             1.0          0.3           1.0         0.31E
F           1.0E
F          0.01E
F          0.01E
F          0.01E
F         395.0E
```

Fig. 76 (Cont.)

```
F           1.0E
F           0.0E
F           0.0E
F           0.0E
F           0.0E
F           0.0E
F           0.0E
F         395.0E
F         395.0E
F        1.1E05E
F          0.0 E
F          0.0 E
F           0.0E
F           0.0E
F           0.0E
F           0.0F
F           0.0E
F           0.0E
R 8         1.00R 8          1.0E
F           1.0E
F           1.0E
F           1.0E
F          0.01E
F          0.01E
F          0.01E
F         395.0E
F           1.0E
F           0.0E
F           0.0E
F           0.0E
F           0.0E
F           0.0E
F           0.0E
F         395.0E
F         395.0E
F        1.1E05E
PIPE                          10              10
                1             0               9              10
                0             1

F           2.0E
F       2.40E-2E
F       2.53E-4E
F           0.1E
F           0.0E
F           0.1E
F             0E
F           0.0E
F           1.0E
F          0.00E
F         395.0E
F       1.05E05E
PIPE                          19              19
                1             0              50              60
                0             1

F           2.0E
F       2.40E-2E
F       2.53E-4E
F           0.1E
F           0.0E
```

Fig. 76 (Cont.)

```
F           0.1E
F             0E
F           0.0E
F           1.0E
F          0.00E
F         395.0E
F       1.05E05E
PIPE                      20              20
                1          0              51              61
                0          1

F           2.0E
F       2.40E-2E
F       2.53E-4E
F           0.1E
F           0.0E
F           0.1E
F             0E
F           0.0E
F           1.0E
F          0.00E
F         395.0E
F       1.05E05E
PIPE                      21              21
                1          0              52              62
                0          1

F           2.0E
F       2.40E-2E
F       2.53E-4E
F           0.1E
F           0.0E
F           0.1E
F             0E
F           0.0E
F           1.0E
F          0.00E
F         395.0E
F       1.05E05E
PIPE                      22              22
                1          0              53              63
                0          1

F           2.0E
F       2.40E-2E
F       2.53E-4E
F           0.1E
F           0.0E
F           0.1E
F             0E
F           0.0E
F           1.0E
F          0.00E
F         395.0E
F       1.05E05E
PIPE                      23              23
                1          0              54              64
                0          1
```

Fig. 76 (Cont.)

```
F          2.0E
F       2.40E-2E
F       2.53E-4E
F          0.1E
F          0.0E
F          0.1E
F            0E
F          0.0E
F          1.0E
F         0.00E
F        395.0E
F       1.05E05E
PIPE                        24              24
                1           0              55              65
                0           1

F          2.0E
F       2.40E-2E
F       2.53E-4E
F          0.1E
F          0.0E
F          0.1E
F            0E
F          0.0E
F          1.0E
F         0.00E
F        395.0E
F       1.05E05E
PIPE                        25              25
                1           0              56              66
                0           1

F          2.0E
F       2.40E-2E
F       2.53E-4E
F          0.1E
F          0.0E
F          0.1E
F            0E
F          0.0E
F          1.0E
F         0.00E
F        395.0E
F       1.05E05E
FILL                        11              11
               10
              0.1           0.1             1.0            68.0           395.0
         1.85E05
FILL                        12              12
               50
              0.1           0.1             1.0            68.0           395.0
         1.85E05
FILL                        13              13
               51
              0.1           0.1             1.0            68.0           395.0
         1.85E05
FILL                        14              14
               52
              0.1           0.1             1.0            68.0           395.0
         1.85E05
FILL                        15              15
```

Fig. 76 (Cont.)

```
          53
          0.1          0.1          1.0          68.0         395.0
       1.85E05
FILL                    16           16
          54
          0.1          0.1          1.0          68.0         395.0
       1.85E05
FILL                    17           17
          55
          0.1          0.1          1.0          68.0         395.0
       1.85E05
FILL                    18           18
          56
          0.1          0.1          1.0          68.0         395.0
       1.85E05
PIPE                     2            2
            1            0            1            5            1
            0            0

F           0.1E
F       1.78E-4E
F       1.78E-3E
F           0.1E
F           0.0E
F       4.76E-2E
F             0E
F           0.0E
F           1.0E
F           0.0E
F         395.0E
F        1.12E5E
PIPE                     3            3
            1            0            2            6            1
            0            0

F           0.1E
F       1.78E-4E
F       1.78E-3E
F           0.1E
F           0.0E
F       4.76E-2E
F             0E
F           0.0E
F           1.0E
F           0.0E
F         395.0E
F        1.12E5E
PIPE                     4            4
            1            0            3            7            1
            0            0

F           1.6E
F       2.84E-3E
F       1.78E-3E
F         0.001E
F           0.0E
F       4.76E-2E
F             0E
F           0.0E
F           1.0E
```

Fig. 76 (Cont.)

```
F          0.0E
F        395.0E
F      1.12E5E
PIPE                        5              5
             1              0              4              8              1
             0              0

F          0.1E
F       1.78E-4E
F       1.78E-3E
F          0.1E
F          0.0E
F       4.76E-2E
F            0E
F          0.0E
F          1.0E
F          0.0E
F        395.0E
F      1.12E5E
FILL                        6              6
             5
            .1             0.1            0.0            0.0           395.0
       1.05E05
FILL                        7              7
             6
            .1             0.1            0.0            0.0           395.0
       1.05E05
FILL                        9              9
             8
            .1             0.1            0.0            0.0           395.0
       1.05E05
BREAK                       8              8
             7                                            3
           0.1             0.1            1.0          395.0         1.74E05
         0.1E-4            0.1           50.0
           3.00            0.10           0.5
-1.0
```

Fig. 76 (Cont.)

```
CREARE PROBLEM 2
JG* = 0.14 Q=30 GPM  TECC=212 F
             -1        0.0
                         1             25             24              1
        1.0E-3       5.0E-6         1.0E-3
             10           20                            1
             11            2              3              4              5
              6            7              8              9             10
             12           13             14             15             16
             17           18             19             20             21
             22           23             24             25              1
           2000            0           -1.0            0.0
FILL                        6              6
             5
            .1             0.1            0.0          0.3545         374.0
       1.12E5
FILL                        7              7
             5
            .1             0.1            0.0          0.3545         374.0
       1.12E5
FILL                        9              9
             8
            .1             0.1            0.0          0.3545         374.0
       1.12E5
END
         0.1E-4            0.1           50.0
           0.50            0.05           0.5
-1.0
```

Fig. 77. TRAC restart deck for a typical Creare ECC injection calculation.

the inlet steam conditions. BREAK component number 8 specifies the boundary pressure needed at the broken cold leg to produce the correct lower plenum pressure. The restart input deck for the ECC injection calculation is given in Fig. 77. Note that the only components replaced are FILLs 6 - 8 which are connected to the three intact cold legs. These new FILLs specify the ECC liquid injection conditions.

The CPU time for the steady-state (initial condition) runs varied from 5 min to 30 min depending on steam velocity. The CPU time for transient (ECC injection) calculations varied from 20 min to 60 min depending on steam flow rate and ECC liquid temperature.

G. FLECHT Forced Flooding Tests

1. Description of Experiments

The FLECHT (Full Length Emergency Cooling Heat Transfer) program is a series of reflood heat transfer simulation experiments designed to yield separate effects experimental data for use in evaluating heat transfer performance of emergency core cooling systems in pressurized water reactors. The FLECHT tests to date can be separated into four categories: the early, high flooding rate tests,[15,16] systems effects tests (FLECHT-SET),[17-19] low flooding rate tests,[20-22] and skewed power profile tests.[23,24] The high and low flooding rate tests are of particular interest since these were performed with forced flooding injection, which minimized system effects, and are the simplest to evaluate for code model testing.

Except for the more recent skewed power tests, the experiments were performed with 100 full-scale, electrically heated, nuclear fuel-rod simulators in a square duct housing. Figure 78 illustrates a cross section of the rod bundle, indicating local power factors and instrumentation locations. It should be noted that changes in instrumentation were made as the test series progressed. The rod bundle illustrated is from the FLECHT-SET series and was chosen to show the housing and dimensions. A nuclear fuel rod simulator is illustrated in Fig. 79. The axial power profile of a nuclear rod was approximated by a step-wise variation in the number of heater wire coils per unit length. The total power during the experiment was programmed to follow the ANS power decay curve, plus 20 percent, normalized to an assumed delay time until the start of reflood (usually 30 s).

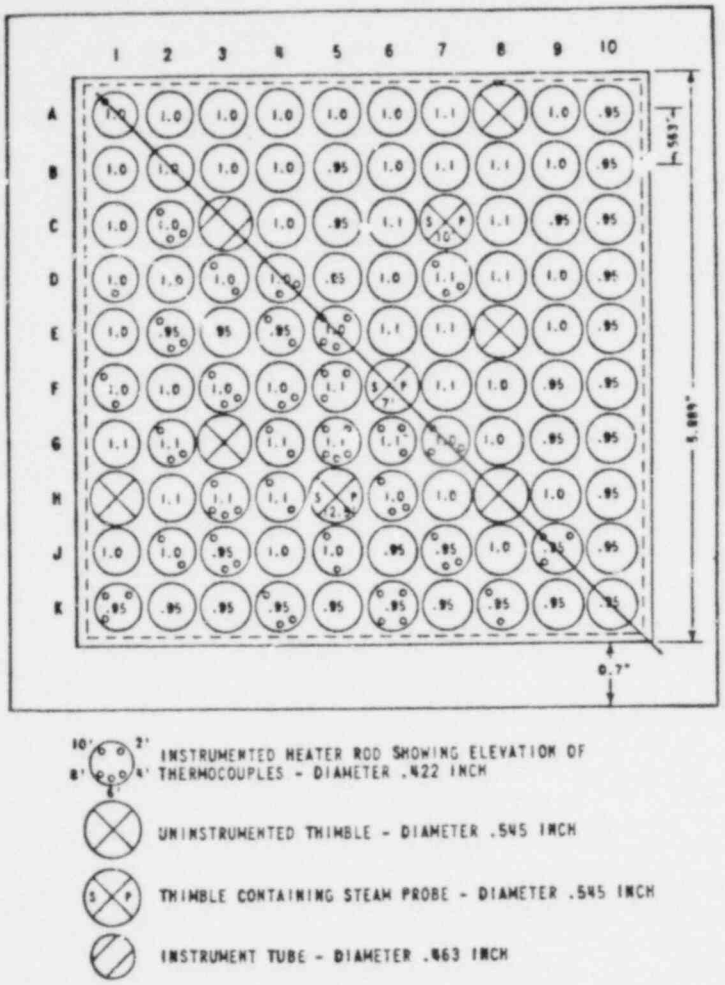

Fig. 78. Cross section of FLECHT test bundle (adapted from Ref. 17).

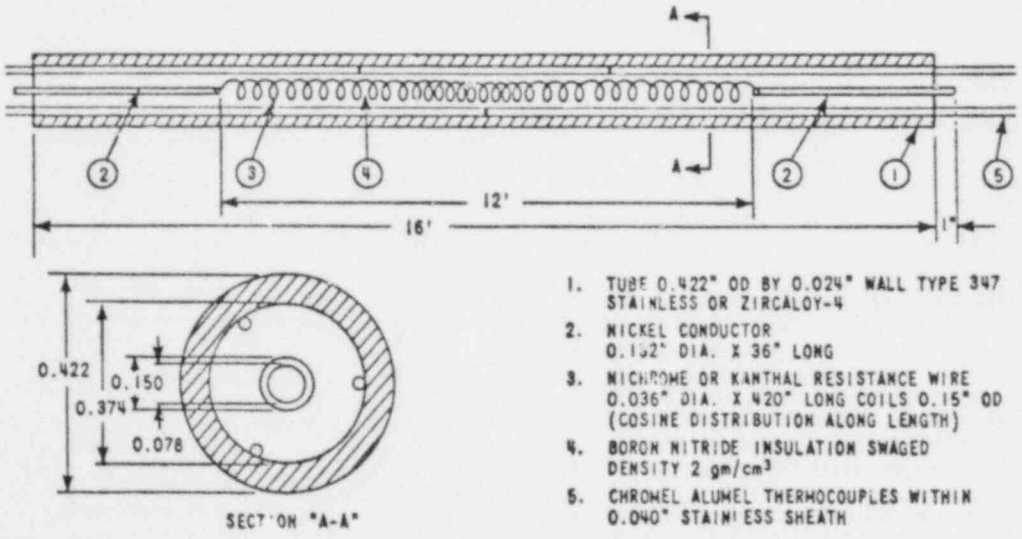

Fig. 79. FLECHT heater rod cross section (adapted from Ref. 17).

The test procedure was as follows. The lower section of the flow housing was filled with water to the bottom of the heated rod length. Power to the rods and housing was applied and maintained until the desired initial rod cladding temperatures were attained (see the FLECHT-SET Phase A report[17] for the housing initial temperatures criteria). Flooding at the specified rate (based on cold condition rates) was then initiated and simultaneously the power was ramped on the desired decay curve. Temperatures and related fluid conditions were recorded until the bundle was completely quenched.

2. TRAC-P1A Best-Estimate Model

The TRAC noding simulation of the FLECHT forced-flooding system is illustrated in Fig. 80. The slab vessel option was used to model the test section

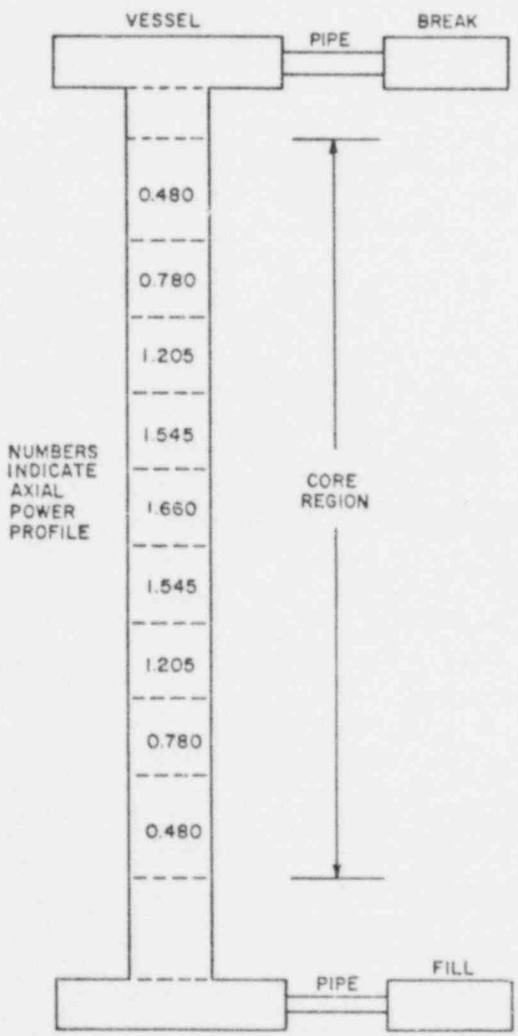

Fig. 80. TRAC noding schematic for FLECHT forced flooding experiments.

housing and pipe components were used to simulate the fill and exhaust connections. No attempt was made to model the separation of liquid and vapor in the upper plenum; hence, the drain connection was deleted. For future systems-effects test predictions, more accurate plena geometric input descriptions should be made. Since model assessment normally used for typical PWR nodings was desired, the TRAC noding (9 core levels) required averaging of the FLECHT power profile. Figure 81 illustrates the actual FLECHT power profile and the power shape used. The fuel rod simulators were modeled with 8 radial nodes at each core level. The power decay factors for the early FLECHT tests and the ANS based factors used in subsequent tests are tabulated in Table V.

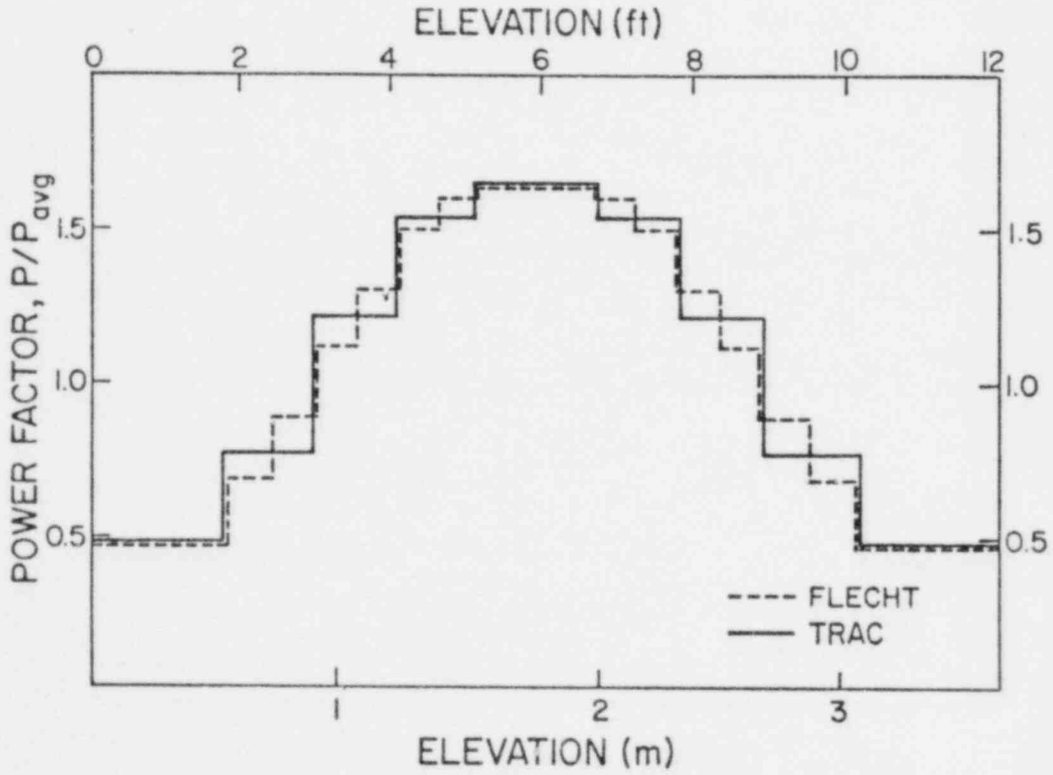

Fig. 81. Axial power profile for FLECHT forced flooding experiments.

TABLE V

FLECHT POWER DECAY FACTORS

Curve B[25] (normalized to 20 s)		ANS Curve[17] (normalized to 30 s)	
Time (s)	PF	Time (s)	PF
0	1.0	0	1.0
6	0.896	10	0.953
12	0.828	20	0.917
18	0.782	30	0.840
24	0.744	40	0.867
30	0.715	50	0.848
42	0.672	100	0.782
54	0.634	150	0.740
66	0.608	200	0.695
78	0.591	250	0.661
90	0.576	300	0.634
102	0.566	350	0.611
120	0.553	400	0.593
150	0.534	450	0.576
180	0.516	500	0.562
210	0.502	600	0.538
240	0.487	700	0.519
270	0.474	800	0.502
300	0.464	900	0.488
390	0.438	1000	0.476

Initial conditions were set at measured input values for rod, housing wall, and fluid temperatures. Since sufficient experimental detail is not available to determine all necessary input values precisely, some interpolation or estimation of initial temperatures was performed. The initial and boundary conditions of the FLECHT tests selected for simulation by TRAC are presented in Table VI.

TABLE VI

FLECHT EXPERIMENTAL TEST CONDITIONS FOR TRAC SIMULATIONS

Test Number	Pressure (MPa)	Inlet Fluid Temp. (K)	Flooding Rate (m/s)	Peak Power (kW/m)
03541	0.39	337.6	0.25	4.07
04831	0.28	324.8	0.04	3.12
02414	0.28	327.1	0.02	2.76

3. Comparison of Best-Estimate Calculations with Experiment

The comparisons of the TRAC calculations and the measured data of clad temperature and quench front propagation histories are shown in Figs. 82-87. The important results taken at the six-foot elevation are summarized in Table VII. TRAC predicted the maximum temperature and therefore the temperature rise quite well for all the tests. Also for Test 03541, the turnaround and quench times compared very well with the data. A single temperature profile comparison is shown (Fig. 82) for Test 03541 as this is the only data presented in the FLECHT Data Report (see Ref. 15) for this test. The quench front propogation predicted for Test 03541 also compared very well with experimental data as shown in Fig. 85.

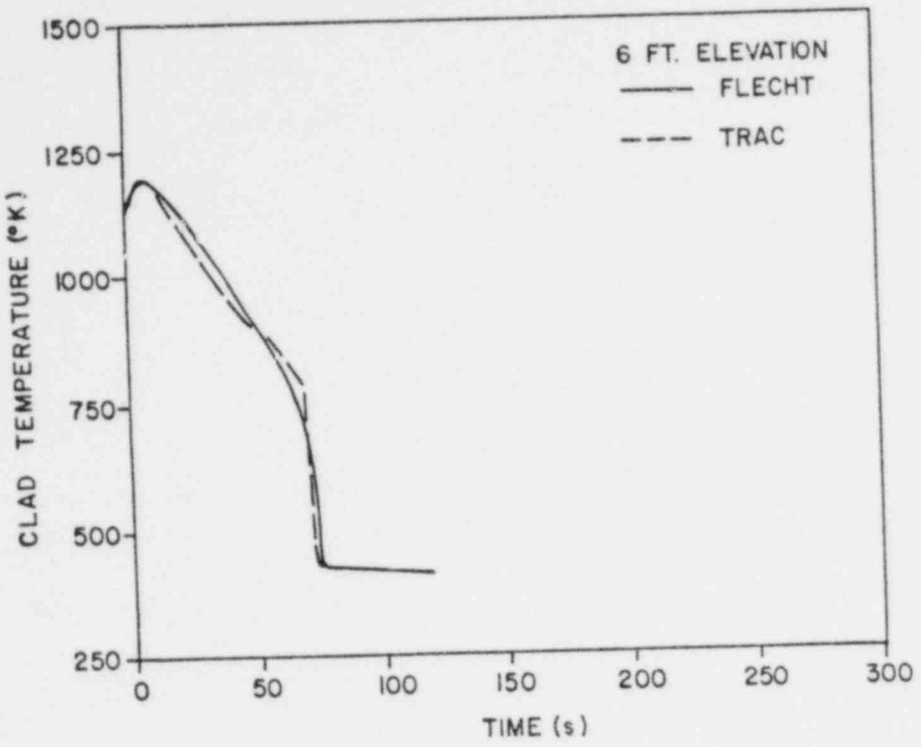

Fig. 82. Cladding temperature response at bundle midheight for FLECHT Test 03541.

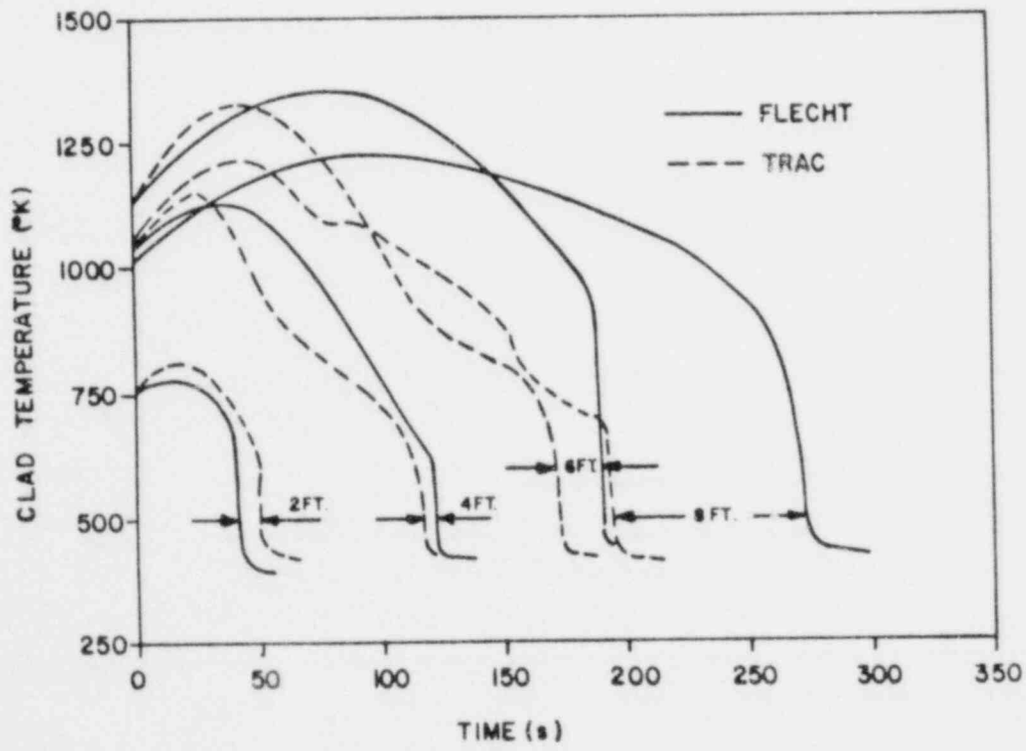

Fig. 83. Cladding temperature response for FLECHT Test 04831.

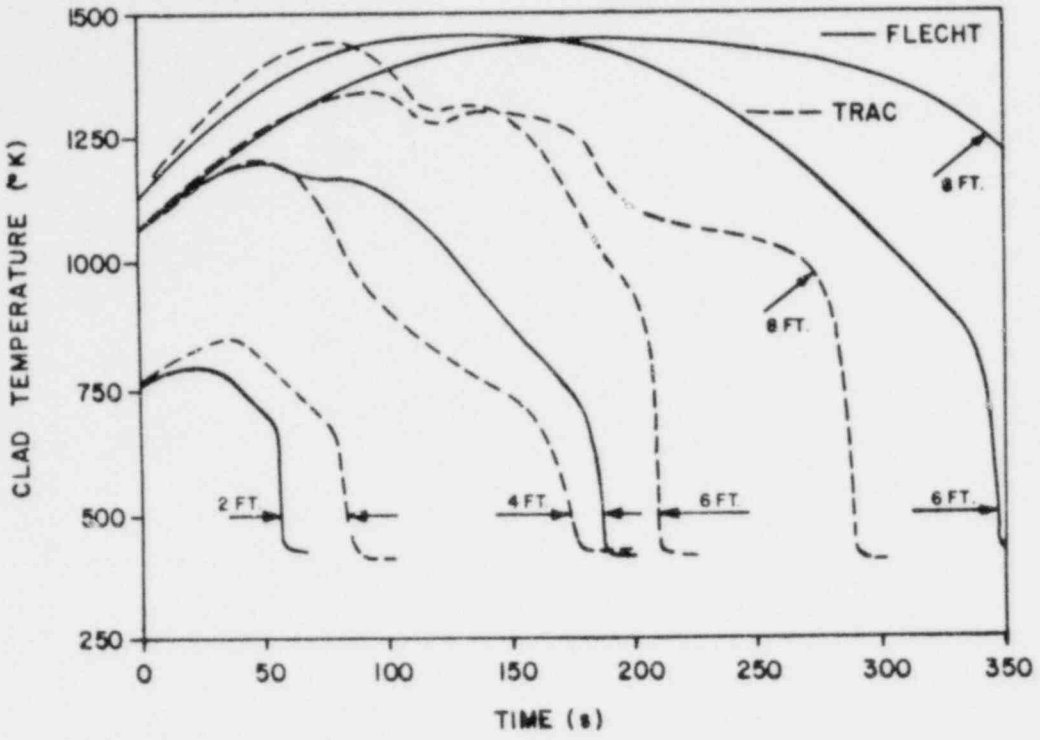

Fig. 84. Cladding temperature response for FLECHT Test 02414.

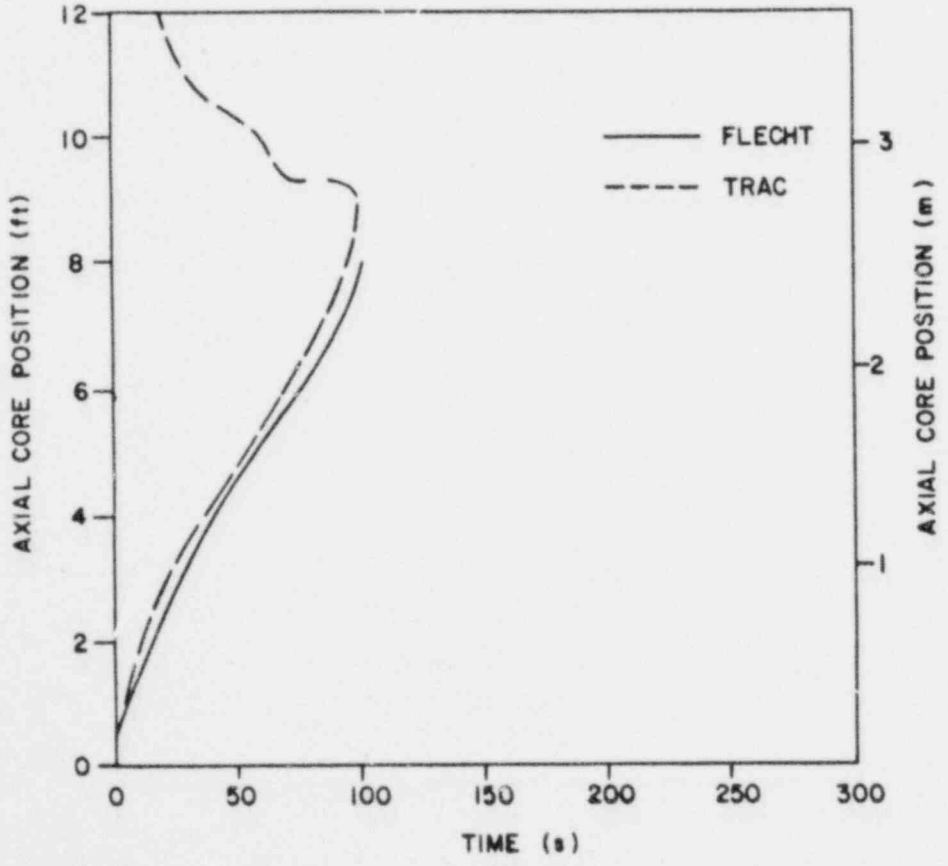

Fig. 85. Quench front history for FLECHT Test 03541.

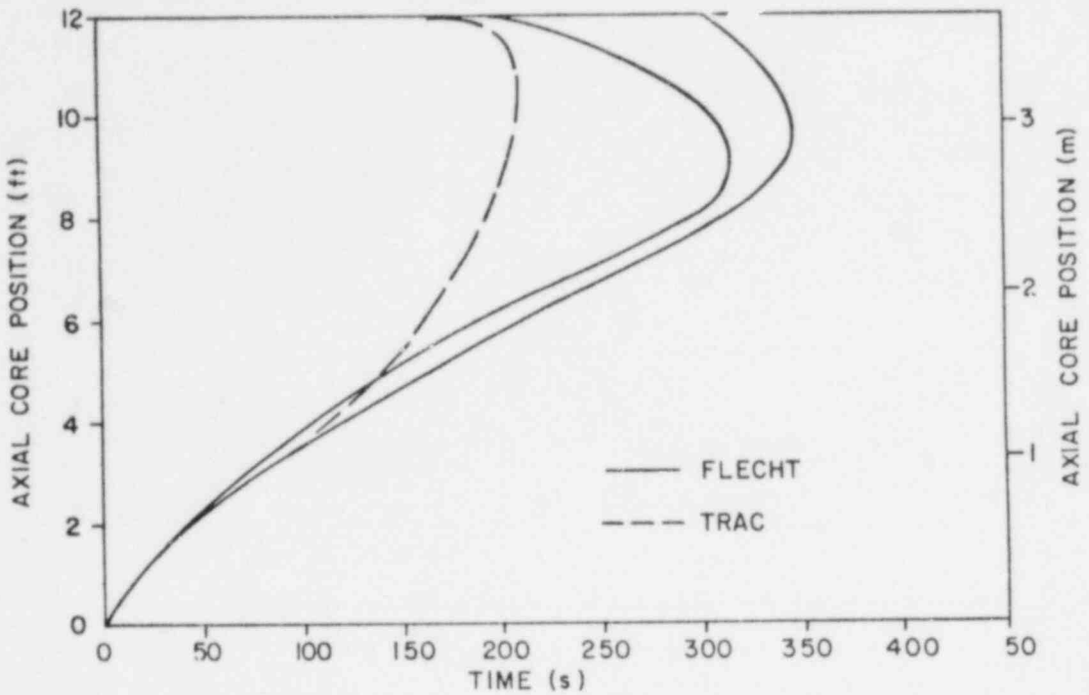

Fig. 86. Quench front history for FLECHT Test 04831.

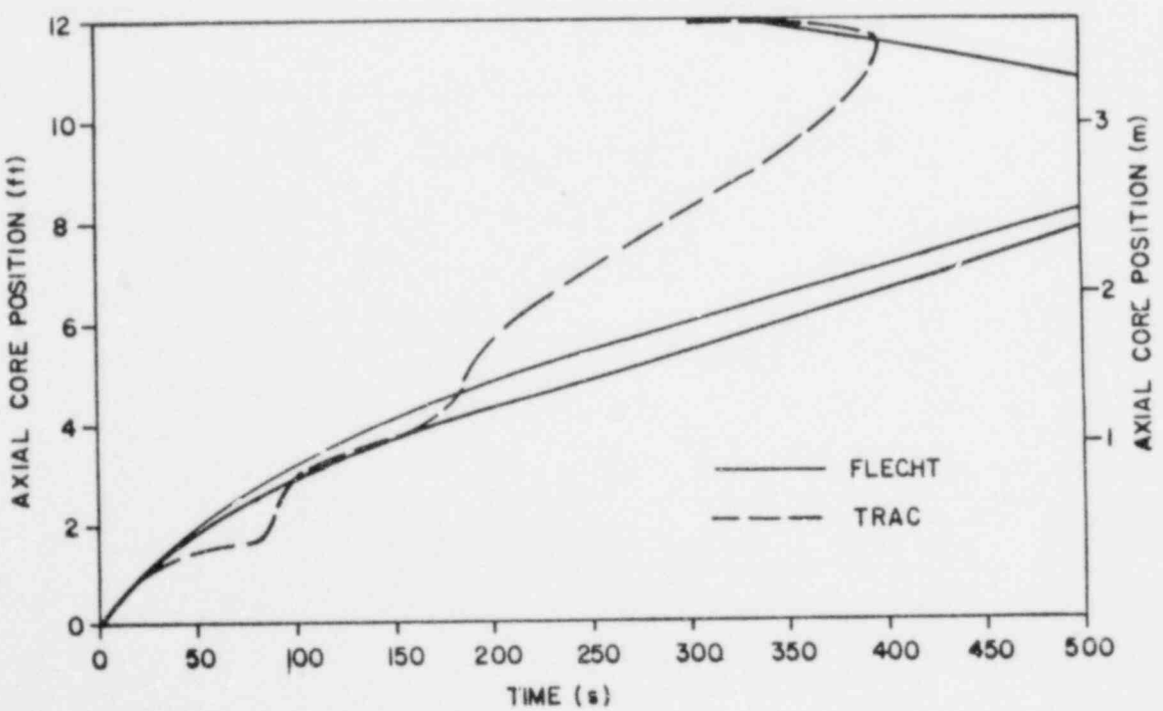

Fig. 87. Quench front history for FLECHT Test 02414.

TABLE VII

SUMMARY OF CALCULATED AND MEASURED FLECHT RESULTS
AT THE BUNDLE MIDHEIGHT

Test Number	03541		04831		02414	
	Exp	TRAC	Exp	TRAC	Exp	TRAC
Initial Temp. (K)	1143.0	1144.0	1144.3	1144.0	1144.3	1144.0
Maximum Temp. (K)	1193.0	1190.0	1333.2	1333.0	1452.7	1449.0
Temp. Rise (K)	50.0	46.0	188.9	189.0	308.4	305.0
Turnaround Time (s)	8.0	6.0	74.4	40.0	96.4	80.0
Quench Time (S)	71.0	72.0	219.0	170.0	344.8	210.0

The TRAC calculations of the clad temperatures for the lower flooding rate tests shown in Figs. 83 and 84 do not compare very well with the experimental data. The important phenomena such as turnaround time, quench time, and quench temperatures for the upper regions of the rod bundle show that TRAC predicts a much earlier turnaround time which in turn results in lower quench temperatures and earlier quench times.

The early turnaround times are probably a result of excess vapor generation calculated in the lower region of the rod bundle. Underprediction of carryover rates results in a rapid refill of the core region and accounts for early quenching.

TRAC tends to overpredict the heat transfer coefficient for the upper regions of the rod bundle from the turnaround point to the quench time. This

resulted in wall temperatures that were lower than the experimental data. Consequently, the quench temperatures were also low as compared to the data.

The phenomena of early turnaround time and large heat transfer predictions are also illustrated in Figs. 86 and 87. The quench front histories of the tests show that a falling film contributed to the early quenching of the upper portion of the heater rods.

4. Sensitivity Studies

Several sensitivity studies were performed with an early version of the TRAC due prior to the release of TRAC-P1A. These studies were used to investigate the effects of varying the heat transfer and hydrodynamic mesh spacings on the code predictions. This study consisted of varying the noding of the rod bundle for Test 03541. Several noding selections of the hydrodynamic and heat transfer mesh cells were chosen based on a range of mesh spacings normally used for TRAC assessment calculations.

The results of this study showed that the peak clad temperature and the quench times were not sisgnificantly affected by the variations in the mesh spacings. Slight differences in peak clad temperatures were observed which can be attributed to the interpolation method used to initialize the fine-mesh temperature field. These diffferences converged as the noding was increased. Also the predictions of the time to reach peak clad temperature were affected by the variations in the vessel noding. The time to peak clad temperature tended to increase as the noding was refined until convergence was attained.

For noding selections that are less than a one-to-one correspondence to the FLECHT stepped axial power profile, the averaging of the power shape results in additional discrepancies. The variation in results as a function of the hydrodynamic mesh cell length is due mainly to the axial void fraction profile used in the heat transfer coefficient calculation in the post-CHF regimes. The conclusion drawn from this exercise is that in the range of nodings expected for TRAC applications, the reflood methodolgy is not a strong function of noding size.

5. TRAC-P1A Features Tested

The comparisons of the TRAC predictions and the FLECHT reflood data were used to evaluate the two-phase flow and reflood heat transfer models in the vessel component. It is apparent that the reflood heat transfer models are currently less than satisfactory for predicting the low reflood rate phenomena

observed in the FLECHT forced flooding experiments. Specifically, the quench front propagation, liquid entrainment, and transition and film boiling heat transfer models are items requiring further development. Based on these forced flooding experiments alone, no assessment can be made of the models under gravity-flow and systems-response conditions.

6. Input Data Decks

A listing of a TRAC input data deck used to simulate a typical FLECHT reflood test is shown in Fig. 88. The average ratio of CPU to transient time for the FLECHT simulations was 25:1.

H. LOFT Nonnuclear Test L1-4

1. Description of Experiment

The Loss of Fluid Test Facility (LOFT)[26] is a scale model of a large pressurized water reactor (LPWR). The volume scaling ratio between the LOFT system and the LPWR is approximately 1:60; flow and break areas are also scaled using the same ratio. The LOFT L1-4 system consists of a pressure vessel; an intact loop with a pressurizer, steam generator, and two pumps; a blowdown loop with a simulated steam generator, a simulated pump, and two quick-opening valves (full opening time of 17.5 ms); and a pressure suppression system. Major components of LOFT are shown in Fig. 89.

The pressure vessel contains a hydraulic core simulator, upper and lower plena, a downcomer, and a core support barrel. The blowdown loop is a volume-scaled representation of one loop of a four-loop LPWR. The simulated steam generator and pump consist of piping containing many orifice plates to achieve the desired hydraulic resistance. The intact loop has a volume approximately three times larger than the blowdown loop, and represents three intact loops of a four-loop LPWR. This loop has a U-tube steam generator, two centrifugal pumps, and a pressurizer. The pressure suppression system simulates the large containment volume and back pressure of the LPWR, and contains the blowdown effluent.

Test L1-4 is the fourth in a series of five nonnuclear isothermal blowdown tests performed as part of the LOFT integral test program. Test L1-4 is U.S. Standard Problem 7. The purposes of Test L1-4 are to provide information on delayed HPIS (High Pressure Injection System) and LPIS (Low Pressure Injection

```
1                    1
2  FLECHT FLOODING RATE TEST NO. 04831
3                    0              0.0
4                    0                1                5                4                1
5            1.0E-03          1.0E-06          1.0E-03
6                   10              100               10                1                0
7                    1                2                3                4               5E
8                 1001                0          1.0E-05            0.0
9                    5               13               -1               -4
10 FILL                               1                1
11                   1                4             1001                3
12         3.048E-01      6.1778E-04              0.0              0.0          3.25E02
13             3.2E05
14                0.0              0.0          1.0E-05      2.4076E-01          1.0E+03
15       2.4076E-01E
16 PIPE                               2                2
17                   1                0                1                2                6
18                   0                0
19          2.54E-02          5.0E-03              0.0              0.0          3.0E02
20            3.0E02
21 F       3.048E-01E
22 F      6.1778E-04E
23 F      2.0268E-03E
24 F         5.0E-03E
25 F              0.0E
26 F        5.08E-02E
27 F                0E
28 F             0.0E
29 F             0.0E
30 F             0.0E
31 F         3.25E02E
32 F      2.75800E05E
33 PIPE                               3                3
34                   1                0                3                4                6
35                   0                0
36          2.54E-02          5.0E-03              0.0              0.0          3.0E02
37            3.0E02
38 F       3.048E-01E
39 F       2.471E-03E
40 F       8.107E-03E
41 F         5.0E-03E
42 F              0.0E
43 F       1.016E-01E
44 F                0E
45 F             0.0E
46 F             1.0E
47 F             0.0E
48 F          4.04E02E
49 F      2.75800E05E
50 BREAK                              4                4
51                   4
52         3.048E-01        2.471E-03              1.0          4.04E02      2.75800E05
53 VESSEL                             5                5
54                  13                1                1                2
55                   0                0                0               11                2
56                   1
57                   0                0                0
58        7.8488E+03       4.663E+02        4.33E+01              0.8          6.0E+04
59         1.3341E00
60                   8               12                7             1001
```

Fig. 88. TRAC input deck for a typical FLECHT reflood test.

61		1001	0	0	0	45
62		6,297E+25	0,0	0,0		
63		1,5240E-01	4,5720E-01	1,00584E00	1,37160E00	1,73736E00
64		2,10312E00	2,46888E00	2,83464E00	3,20040E00	3,56616E00
65		4,11480E00	4,26720E00	4,52120E00E		
66		1,4958E-01E				
67		1,4958E-01E				
68		1	1	3	2	
69		13	1	3	3	
70		0,0	1,0	0,0	0,0	0,0
71		0,0	0,0E			
72	F	1,0E				
73	F	1,0E				
74		2,892E-01	4,699E-01	7,259E-01	9,307E-01	1,0
75		9,307E-01	7,259E-01	4,699E-01	2,892E-01E	
76		90,E				
77		0,0	9,9060E-04	1,9050E-03	3,3274E-03	4,7498E-03
78		4,7498E-03	5,0546E-03	5,3594E-03E		
79		4	5	4	4	3
80		8	8E			
81		0,0	6,297E+05	10,0	6,001E+05	20,0
82		5,774E+05	30,0	5,604E+05	50,0	5,340E+05
83		70,0	5,145E+05	100,0	4,924E+05	150,0
84		4,660E+05	200,0	4,376E+05	300,0	3,992E+05
85		500,0	3,539E+05	1000,0	2,997E+05E	
86	F	5E				
87	F	0,0E				
88	F	0,0E				
89	F	0,0E				
90	F	0,0E				
91	F	0,0E				
92	F	0,0E				
93	F	0,0E				
94	F	0,0E				
95	F	0,0E				
96	F	0,0E				
97	F	5,0E-03E				
98	F	5,0E-03E				
99	F	5,0E-03E				
100	F	5,0E-03E				
101	F	5,0E-03E				
102	F	5,0E-03E				
103	F	5,725E-01E				
104	F	0,0E				
105	F	5,725E-01E				
106	F	0,0E				
107	F	1,270E-02E				
108	F	1,270E-02E				
109	F	1,270E-02E				
110	F	0,0E				
111	F	0,0E				
112	F	0,0E				
113	F	0,0E				
114	F	0,0E				
115	F	0,0E				
116	F	0,0E				
117	F	0,0E				
118	F	4,04E02E				
119	F	3,25E02E				
120	F	2,75800E05E				

Fig. 88. (cont).

```
121 F      0,18236E
122 F       28,476E
123 F      5,0E-03E
124 F      5,0E-03E
125 F      5,0E-03E
126 F      5,0E-03E
127 F      5,0E-03E
128 F      5,0E-03E
129 F    5,725E-01E
130 F          0,0E
131 F    5,725E-01E
132 F          0,0E
133 F    1,270E-02E
134 F    1,270E-02E
135 F    1,270E-02E
136 F      4,00E02E
137 F          0,0E
138 F          0,0E
139 F          0,0E
140 F          0,0E
141 F          0,0E
142 F          0,0E
143 F          0,0E
144 F      4,04E02E
145 F      4,00E02E
146 F  2,75800E05E
147 F      0,32826E
148 F       51,256E
149 F      5,0E-03E
150 F      5,0E-03E
151 F      5,0E-03E
152 F      5,0E-03E
153 F      5,0E-03E
154 F      5,0E-03E
155 F    5,725E-01E
156 F          0,0E
157 F    5,725E-01E
158 F          0,0E
159 F    1,270E-02E
160 F    1,270E-02E
161 F    1,270E-02E
162 F      4,75E02E
163 F          1,0E
164 F          0,0E
165 F          0,0E
166 F          0,0E
167 F          0,0E
168 F          0,0E
169 F          0,0E
170 F      4,75E02E
171 F      4,04E02E
172 F  2,75800E05E
173 F      0,21884E
174 F       34,171E
175 F      5,0E-03E
176 F      5,0E-03E
177 F      5,0E-03E
178 F      5,0E-03E
179 F      5,0E-03E
180 F      5,0E-03E
181 F    5,725E-01E
182 F          0,0E
183 F    5,725E-01E
184 F          0,0E
185 F    1,270E-02E
186 F    1,270E-02E
187 F    1,270E-02E
188 F      5,00E02E
189 F          1,0E
190 F          0,0E
191 F          0,0E
192 F          0,0E
193 F          0,0E
194 F          0,0E
195 F          0,0E
196 F      5,00E02E
197 F      4,04E02E
198 F  2,75800E05E
199 F      0,21884E
200 F       34,171E
201 F      5,0E-03E
202 F      5,0E-03E
203 F      5,0E-03E
204 F      5,0E-03E
205 F      5,0E-03E
206 F      5,0E-03E
207 F    5,725E-01E
208 F          0,0E
209 F    5,725E-01E
210 F          0,0E
211 F    1,270E-02E
212 F    1,270E-02E
213 F    1,270E-02E
214 F      5,50E02E
215 F          1,0E
216 F          0,0E
217 F          0,0E
218 F          0,0E
219 F          0,0E
220 F          0,0E
221 F          0,0E
222 F      5,50E02E
223 F      4,04E02E
224 F  2,75800E05E
225 F      0,21884E
226 F       34,171E
227 F      5,0E-03E
228 F      5,0E-03E
229 F      5,0E-03E
230 F      5,0E-03E
231 F      5,0E-03E
232 F      5,0E-03E
233 F    5,725E-01E
234 F          0,0E
235 F    5,725E-01E
236 F          0,0E
237 F    1,270E-02E
238 F    1,270E-02E
239 F    1,270E-02E
240 F      6,00E02E
241 F          1,0E
242 F          0,0E
243 F          0,0E
244 F          0,0E
245 F          0,0E
246 F          0,0E
247 F          0,0E
248 F      6,00E02E
249 F      4,04E02E
250 F  2,75800E05E
251 F      0,21884E
252 F       34,171E
253 F      5,0E-03E
254 F      5,0E-03E
255 F      5,0E-03E
256 F      5,0E-03E
257 F      5,0E-03E
258 F      5,0E-03E
259 F    5,725E-01E
260 F          0,0E
261 F    5,725E-01E
262 F          0,0E
263 F    1,270E-02E
264 F    1,270E-02E
265 F    1,270E-02E
266 F      6,25E02E
267 F          1,0E
268 F          0,0E
269 F          0,0E
270 F          0,0E
271 F          0,0E
272 F          0,0E
273 F          0,0E
274 F      6,25E02E
275 F      4,04E02E
276 F  2,75800E05E
277 F      0,21884E
278 F       34,171E
279 F      5,0E-03E
280 F      5,0E-03E
281 F      5,0E-03E
282 F      5,0E-03E
283 F      5,0E-03E
284 F      5,0E-03E
285 F    5,725E-01E
286 F          0,0E
287 F    5,725E-01E
288 F          0,0E
289 F    1,270E-02E
290 F    1,270E-02E
291 F    1,270E-02E
292 F      6,00E02E
293 F          1,0E
294 F          0,0E
295 F          0,0E
296 F          0,0E
297 F          0,0E
298 F          0,0E
299 F          0,0E
300 F      6,00E02E
```

Fig. 88. (Cont.)

```
301 F       4.04E02E
302 F   2.75800E05E
303 F      0.21884E
304 F       34.171E
305 F       5.0E-03E
306 F       5.0E-03E
307 F       5.0E-03E
308 F       5.0E-03E
309 F       5.0E-03E
310 F       5.0E-03E
311 F     5.725E-01E
312 F           0.0E
313 F     5.725E-01E
314 F           0.0E
315 F     1.270E-02E
316 F     1.270E-02E
317 F     1.270E-02E
318 F       5.50E02E
319 F           1.0E
320 F           0.0E
321 F           0.0E
322 F           0.0E
323 F           0.0E
324 F           0.0E
325 F           0.0E
326 F       5.50E02E
327 F       4.04E02E
328 F   2.75800E05E
329 F      0.21884E
330 F       34.171E
331 F       5.0E-03E
332 F       5.0E-03E
333 F       5.0E-03E
334 F       5.0E-03E
335 F       5.0E-03E
336 F       5.0E-03E
337 F     5.725E-01E
338 F           0.0E
339 F     5.725E-01E
340 F           0.0E
341 F     1.270E-02E
342 F     1.270E-02E
343 F     1.270E-02E
344 F       5.00E02E
345 F           1.0E
346 F           0.0E
347 F           0.0E
348 F           0.0E
349 F           0.0E
350 F           0.0E
351 F           0.0E
352 F       5.00E02E
353 F       4.04E02E
354 F   2.75800E05E
355 F      0.32026E
356 F       51.256E
357 F       5.0E-03E
358 F       5.0E-03E
359 F       5.0E-03E
360 F       5.0E-03E

361 F       5.0E-03E
362 F       5.0E-03E
363 F     5.725E-01E
364 F           0.0E
365 F     5.725E-01E
366 F           0.0E
367 F     1.270E-02E
368 F     1.270E-02E
369 F     1.270E-02E
370 F       4.75E02E
371 F           1.0E
372 F           0.0E
373 F           0.0E
374 F           0.0E
375 F           0.0E
376 F           0.0E
377 F           0.0E
378 F       4.75E02E
379 F       4.04E02E
380 F   2.75800E05E
381 F      0.09118E
382 F       14.238E
383 F       5.0E-03E
384 F       5.0E-03E
385 F       5.0E-03E
386 F       5.0E-03E
387 F       5.0E-03E
388 F       5.0E-03E
389 F     5.725E-01E
390 F           0.0E
391 F     5.725E-01E
392 F           0.0E
393 F     1.270E-02E
394 F     1.270E-02E
395 F     1.270E-02E
396 F       4.50E02E
397 F           1.0E
398 F           0.0E
399 F           0.0E
400 F           0.0E
401 F           0.0E
402 F           0.0E
403 F           0.0E
404 F       4.50E02E
405 F       4.04E02E
406 F   2.75800E05E
407 F           0.0E
408 F           0.0E
409 F       5.0E-03E
410 F       5.0E-03E
411 F       5.0E-03E
412 F       5.0E-03E
413 F       5.0E-03E
414 F       5.0E-03E
415 F     5.725E-01E
416 F           0.0E
417 F     5.725E-01E
418 F           0.0E
419 F     1.270E-02E
420 F     1.270E-02E
```

Fig. 88 (cont)

```
421 F     1.270E-02E
422 F           0.0E
423 F           1.0E
424 F           0.0E
425 F           0.0E
426 F           0.0E
427 F           0.0E
428 F           0.0E
429 F           0.0E
430 F       4.04E02E
431 F       4.04E02E
432 F    2.75800E05E
433 F           0.0E
434 R 0    6.00E02R 0    0.50E02R 0    1.020E03R 0    1.090E03R 0    1.140E03
435 R 0   1.090E03R 0   1.020E03R 0    0.50E02R 0     6.00E02E
436         1.0E-04       1.0E-02       4.0E+02
437         5.0E+00       1.0E-01       5.0E+00
438           -1.0
```

Fig. 88. (cont)

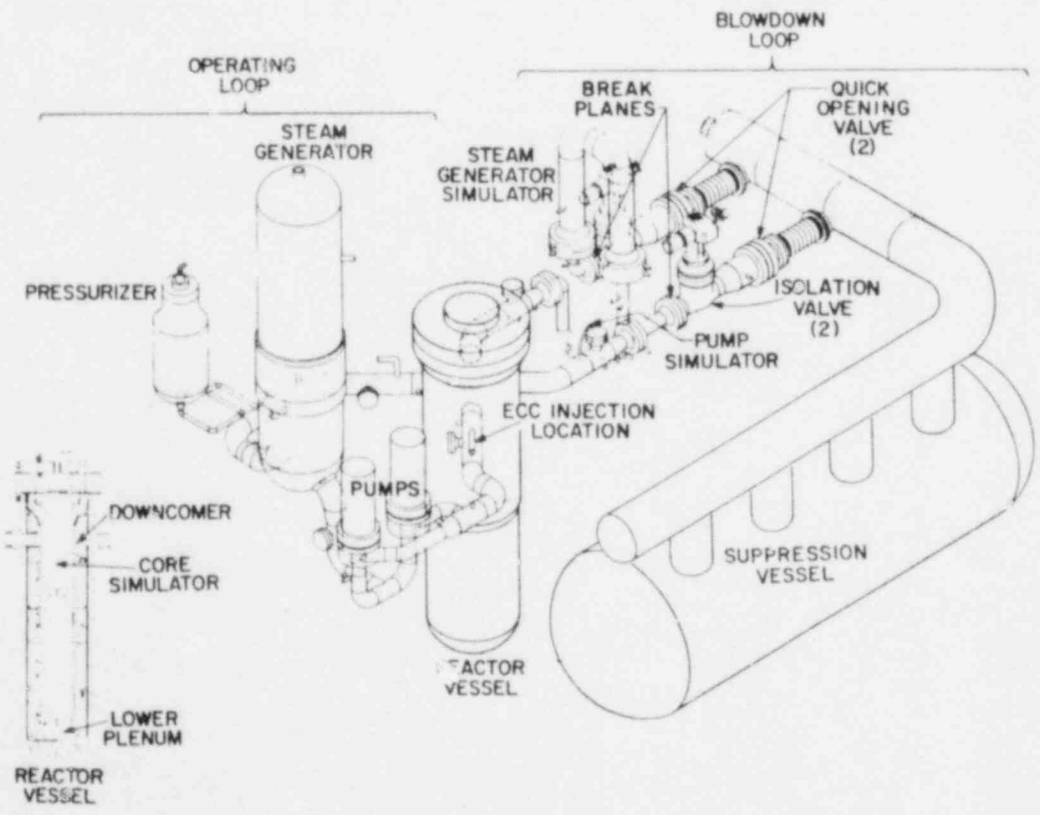

Fig. 89. LOFT major components.

System) cold leg injection, obtain data for evaluating downcomer bypass and mixing of the ECC with the primary coolant, and provide thermal-hydraulic data for comparison with test predictions and other experimental data for code assessment purposes.

Prior to the blowdown test, the primary system was brought to its initial temperature, pressure, and flow rate of 552 K, 15.75 MPa, and 268.4 kg/s, respectively, using the work energy addition of the primary coolant pumps. Isothermal conditions were obtained in the nonflowing blowdown loop by means of recirculation lines connected to the intact loop. Before the system temperature exceeded 366.3 K, the secondary side of the steam generator was drained to the 0% power water level (2.59 m from the top of the tube sheet).

Immediately prior to blowdown, the pressurizer heaters were de-energized and the blowdown was initiated by opening the two quick-opening valves. Their full-opening area simulates a 200% (i.e., 100% break area in each leg) double-ended offset shear break in the cold leg. Electrical power to the primary system motor generator was terminated within 1 s after blowdown initiation which allowed the pumps to coast down under the influence of the flywheels and the fluid dynamic forces on the pumps.

ECC injection was directed to the intact cold leg during blowdown. Injection from an accumulator is initiated at a system low pressure trip of 4.24 MPa (absolute pressure). The HPIS pump is preset to inject at 1.085×10^{-3} m^3/s and to initiate at 22 s after blowdown. The LPIS pump is adjusted to initiate no sooner than 35.5 s after the initiation of blowdown, and its flow rate varies from zero to 0.01 m^3/s depending on a LOFT system pressure.

The TRAC calculation consists of predicting the system thermal-hydraulic response for 60 s following the blowdown initiation.

2. TRAC-P1A Best-Estimate Model

As shown in Fig. 89, the LOFT system contains a variety of components interconnected in series and parallel branches. Furthermore, this system is complicated by area changes and orifice plates. TRAC models the blowdown and intact loops with one-dimensional components; the reactor vessel component is modeled with the three-dimensional VESSEL module (see Fig. 90).

The TRAC model uses 26 components with 27 junctions for a total of 215 fluid cells. The reactor vessel component is divided into 9 axial, 2 radial and 4 azimuthal segments for a total of 72 fluid cells. The upper and lower

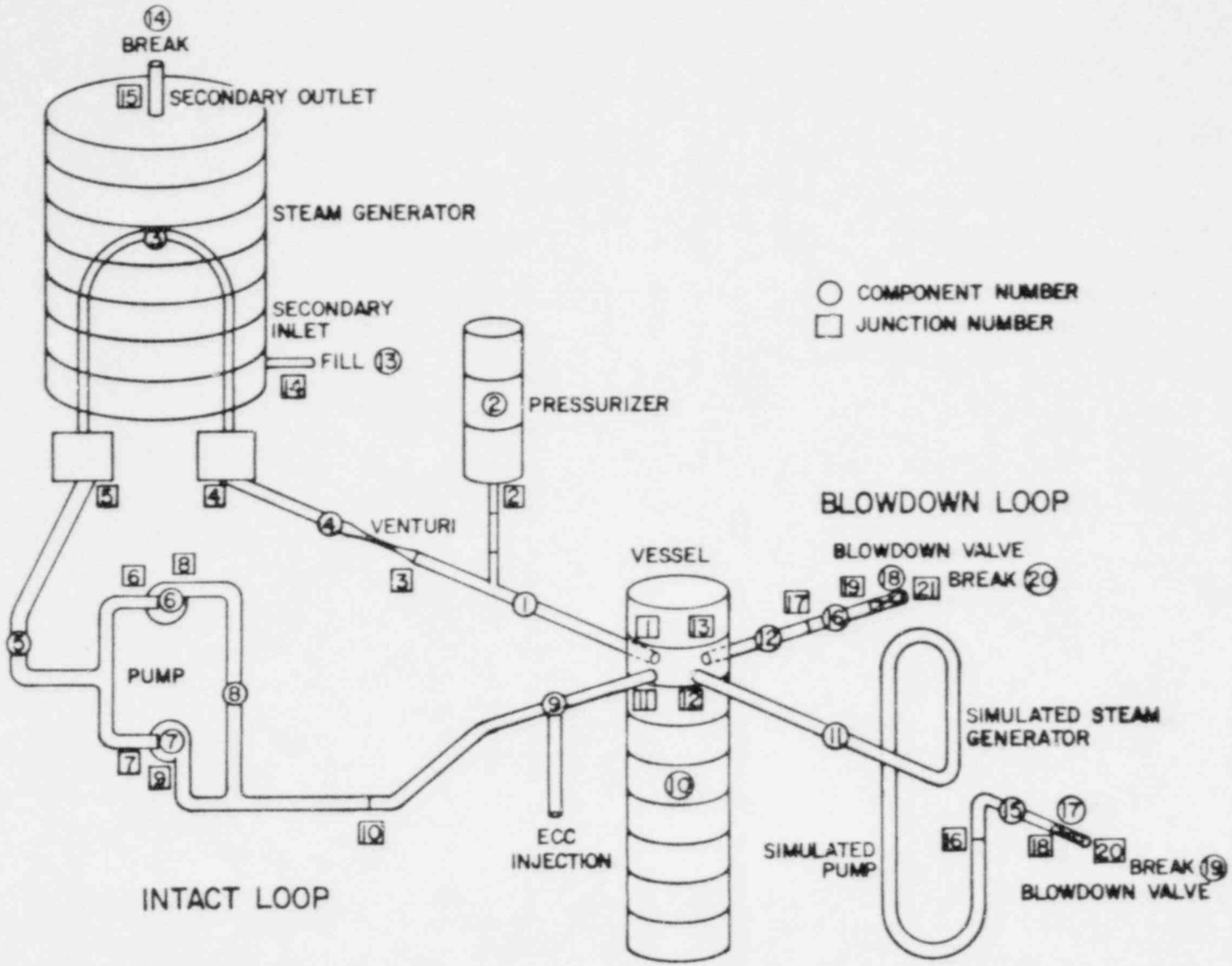

Fig. 90. TRAC component schematic for LOFT Test L1-4.

plena contain 4 and 8 fluid cells, respectively. Typical cell dimensions are approximately 0.2 - 2.0 m, except near breaks. The cell length near the breaks varies from 0.0127 to 0.1 m. The semi-implicit option was used for all components except for the broken pipes where the fully implicit option was employed. The TRAC representation of the ECC system consists of an accumulator connected to a series of two tees. These tees are connected to two FILL modules specifying the HPIS and LPIS flows (see Fig. 90).

The TRAC calculation for this problem was performed in two stages. First, steady-state conditions were obtained by running a transient calculation (i.e., use of the transient option in TRAC) starting from an initial zero flow rate, a uniform pressure and temperature, and with the two quick-opening valves closed. Startup of the two pumps at time zero causes the system flow rate, pressure, and temperature to quickly approach their steady-state values after one loop cycle time (3 to 4 s). As shown in Table VIII, all of the calculated steady-state parameters are within 3 per cent of the measured values. The blowdown portion of the calculation is performed by restarting from the dump file obtained from the steady-state calculation, and activating the two quick-opening valves.

TABLE VIII

COMPARISON OF CALCULATED AND MEASURED INITIAL CONDITIONS FOR LOFT TEST L1-4

Parameters	Calculated	Measured
Loop Mass Flow Rate (kg/s)	261.60	268.40
Pressurizer Pressure (MPa)	15.7	15.75
Pressurizer Water Mass (kg)	419.15	418.80
Pressurizer Water Level (m)	1.17	1.16
Steam Generator Primary Side Pressure (MPa)	15.70	15.75
Steam Generator Primary Side Inlet/Outlet Temperature (K)	552.30/553.00	554.00/552.00
Steam Generator Secondary Side Temperature (K)	55[illegible]	552.00
Steam Generator Secondary Side Pressure (MPa)	6.66	6.65
Core Inlet/Outlet Temperature (K)	552.70/552.6	552.00/554.00
Total System Water Volume at 552 K and 15.75 MPa (m^3)	7.72	7.73
Differential Pressure in Intact Loop Across Primary Pumps 1 and 2 (MPa)	0.139	0.140

3. Comparison of Best-Estimate Calculation with Experiment.

Typical comparisons of the calculated results with experimental data[27] are shown in Figs 91 through 109. Error bands for these experimental data are not available at this time. Experimental data for mass flow rate obtained from different instrumentation at the same location are shown when these data differ appreciably.

Figures 91 and 92 compare mass flow rates per system volume from the blowdown legs. The measured mass flow rate from the simulated pump side of

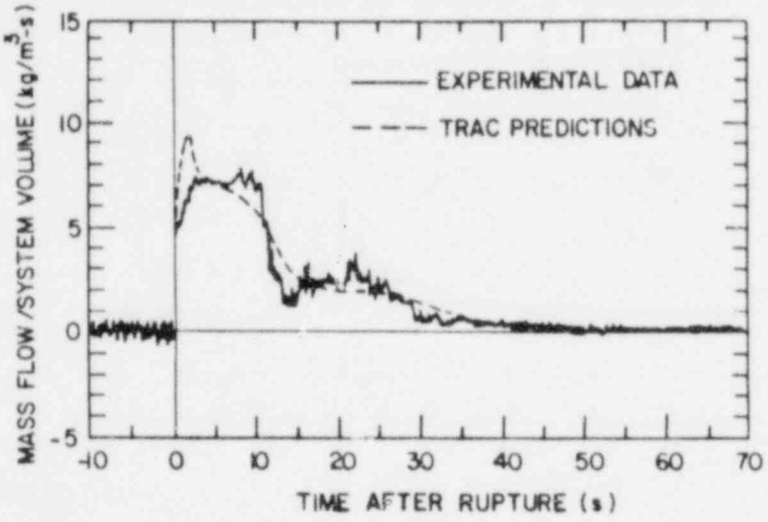

Fig. 91. Mass flow rate in broken hot leg for LOFT Test L1-4.

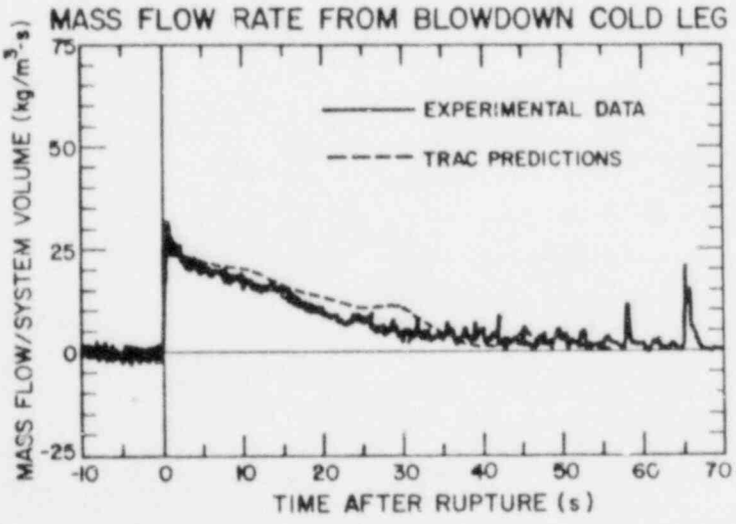

Fig. 92. Mass flow rate in broken cold leg for LOFT Test L1-4.

the break (Fig. 91) is approximately constant in the interval 3-10 s. This is probably because the pressure losses associated with the many orifice plates in the simulated steam generator and pump result in an approximately constant upstream choking pressure. No attempt was made to model in detail these numerous orifice plates.

The mass flow rate from the vessel side of the break (Fig. 92) decreases monotonically because the pressure losses in this leg are not sufficient to maintain a choking upstream pressure. Oscillations in the measured mass flow rate beginning at approximately 25 s are due to ECC bypass; TRAC predicts these oscillations in mass flow rate and fluid density very well. It should be noted that TRAC does not use any choking models or break flow multipliers to calculate the critical flow from these blowdown loops; rather, fine meshing is used at choking locations to resolve the steep pressure gradients at these points.

Figure 93 compares the flow rate per system volume in the intact cold leg. The sharp initial increase and decrease in this variable at early times is due to the initial reactor vessel decompression. Oscillations in the measured flow rate at the intact cold leg beginning at approximately 23 s are due to the ECC injection. TRAC predicts very well the initial sudden increase and decrease as well as the later oscillations in the flow rate.

A comparison of the measured intact hot leg mass flow rate per system volume with the TRAC result is made in Fig. 94. Experimental measurements indicate an initial sudden flow direction reversal in the interval 0-2 s, and then a more or less constant flow rate during the period of 2-5 s. Although TRAC predicts an initial sudden decrease, it does not calculate flow reversal in the interval 0-2 s. A more or less constant flow rate during the period 2-5 s is calculated but this value is half as large as the measurement.

These discrepancies are thought to be a result of a calculated shorter pressurizer emptying time (Fig. 108). Since the pressurizer was emptied more quickly, and at the same time the two pumps in the intact loop were running almost at full speed, the added inertia generated by additional liquid from the pressurizer prevents a flow direction reversal. This effect also acts to maintain a higher flow rate in the interval of 0-2 s which results in a lower flow rate in the interval 2-5 s. It should be pointed out that the measured

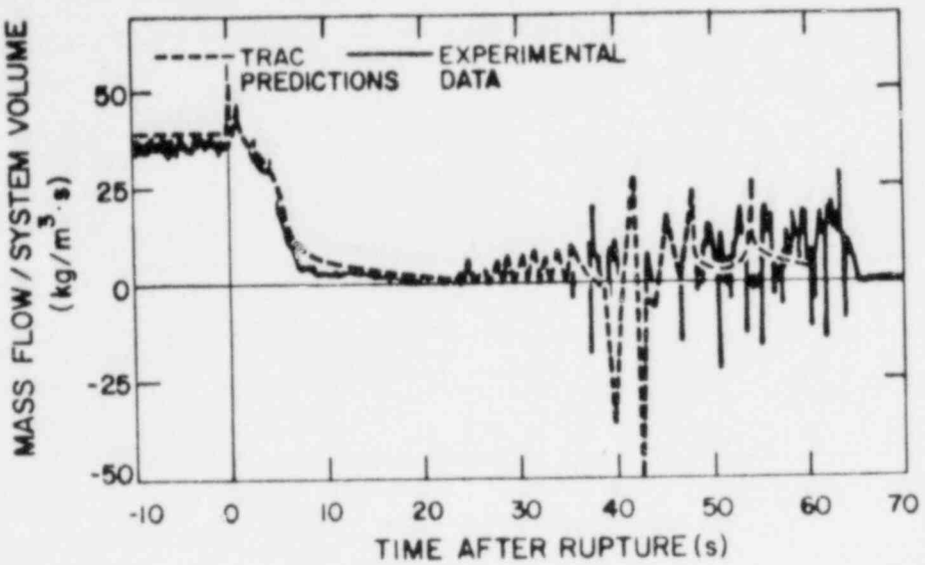

Fig. 93. Mass flow rate in intact cold leg for LOFT Test L1-4.

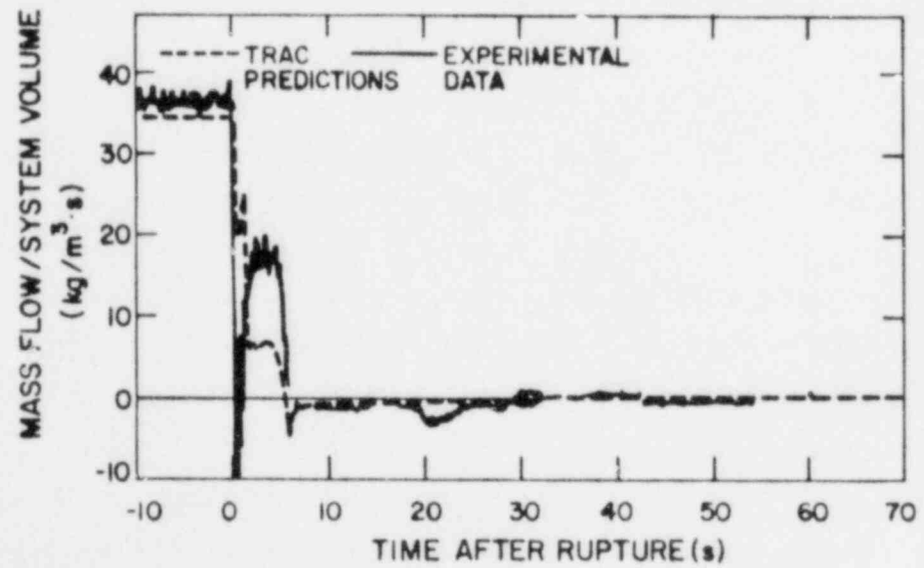

Fig. 94. Mass flow rate in intact hot leg for LOFT Test L1-4.

steady-state mass flow rate in the intact cold leg is not equal to that in the intact hot leg (Figs 93 and 94). This is presumably due to instrumentation error.

Figure 95 compares the mass flow rate per system volume from the intact loop steam generator outlet. TRAC predicts the mass flow rate very well including an initial increase in the mass flow rate. Figure 96 compares the two-phase mixture density in the intact cold leg. Oscillations in the two-phase mixture density beginning at approximately 27 s are due to the cold ECC injection. TRAC predicts these oscillations very well.

The two-phase mixture density in the intact hot leg is shown in Fig. 97. TRAC predicts the two-phase mixture density very well including the increase at approximately 13 s. The increase detected by two of the instruments at about 22 s was not observed in the TRAC calculation. Experimental and calculated densities at the intact steam generator outlet are shown in Fig. 98. TRAC predicts the overall trend adequately but the experimental results decrease more rapidly.

Calculated and experimental densities in the blowdown cold and hot legs are compared in Figs. 99 and 100. Calculated oscillations in the two-phase mixture density at the blowdown cold leg beginning at 27 s, as well as the increase in the two-phase mixture density during the period 26-37 s, are due to bypass of the cold ECC. Except for the magnitude of the oscillations, TRAC predicts the cold leg two-phase mixture density very well. The calculated hot leg mixture density is within the spread of the exerimental results.

The differential pressure across the two primary pumps in the intact loop is shown in Fig. 101. TRAC predicts this quantity very well except that the negative spikes measured after about 30 s are not seen in the calculation. Pressures in the intact loop, blowdown loop, and reactor vessel core simulator are shown in Figs. 102, 103, and 104, respectively. TRAC results for these pressures are in excellent agreement with the measurements.

Figure 105 compares the downcomer fluid temperature directly below the intact cold leg. Accumulator ECC injection was initiated at approximately 23 s in the calculation. The effects of the cold (303 K) ECC water on the downcomer fluid temperature were seen after a delay of about 10 s. The measured fluctuations in this fluid temperature probably occur whenever the

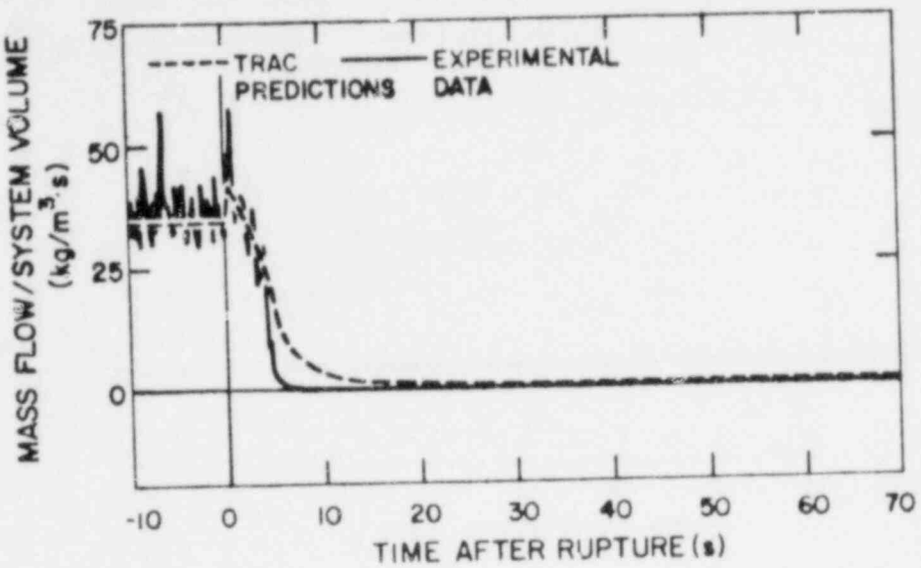

Fig. 95. Mass flow rate at steam generator outlet for LOFT Test L1-4.

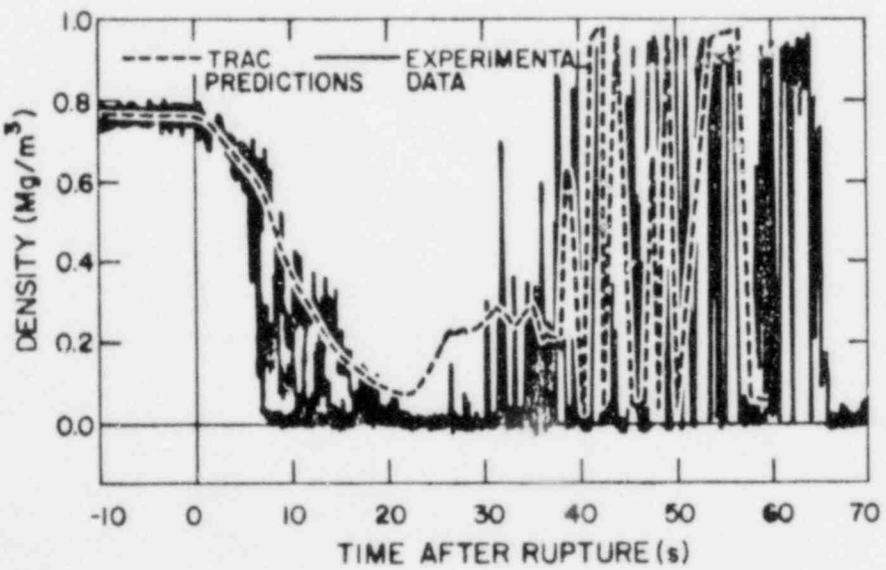

Fig. 96. Mixture density in the intact cold leg for LOFT Test L1-4.

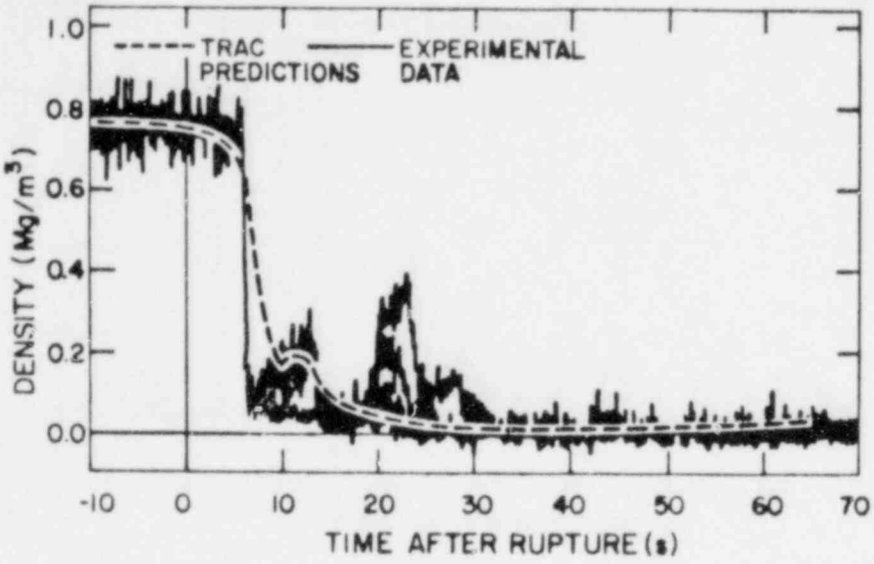

Fig. 97. Mixture density in the intact hot leg for LOFT Test L1-4.

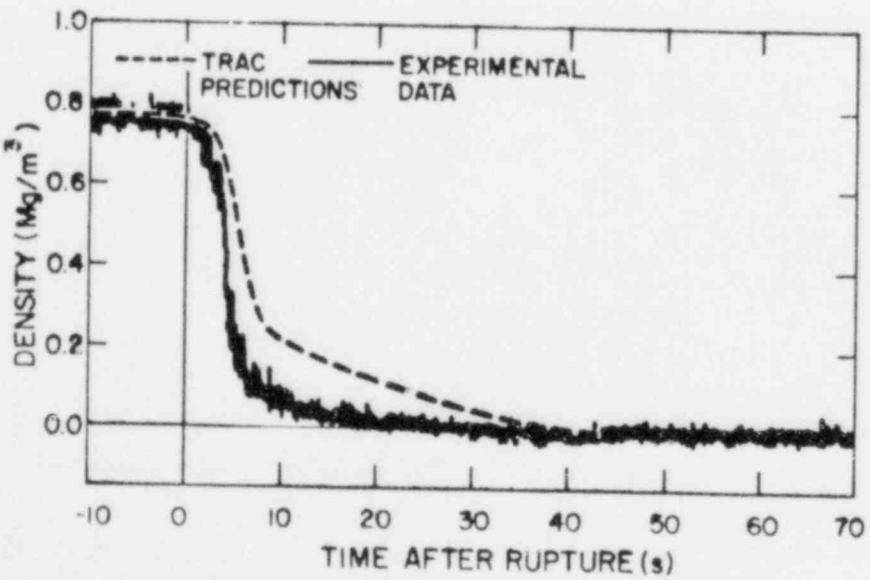

Fig. 98. Mixture density at the steam generator outlet for LOFT Test L1-4.

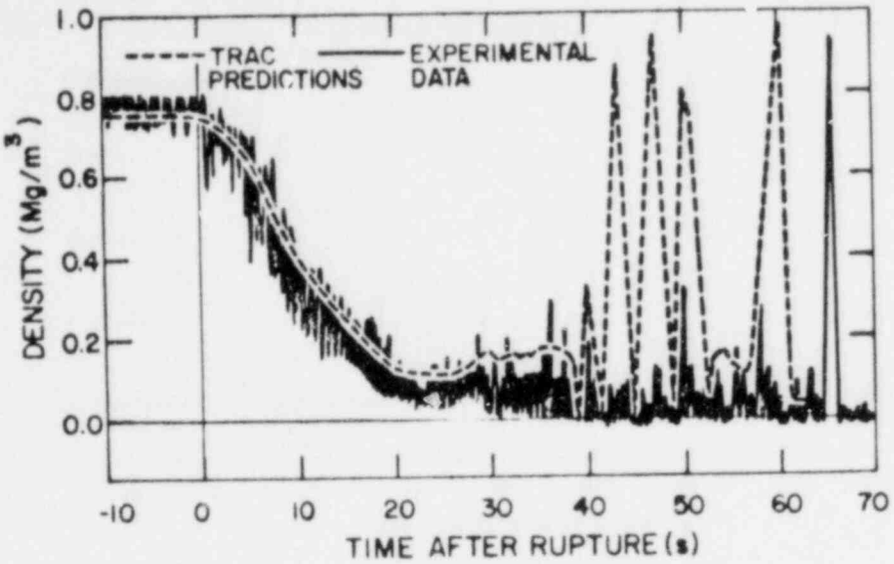

Fig. 99. Mixture density in broken cold leg for LOFT Test L1-4.

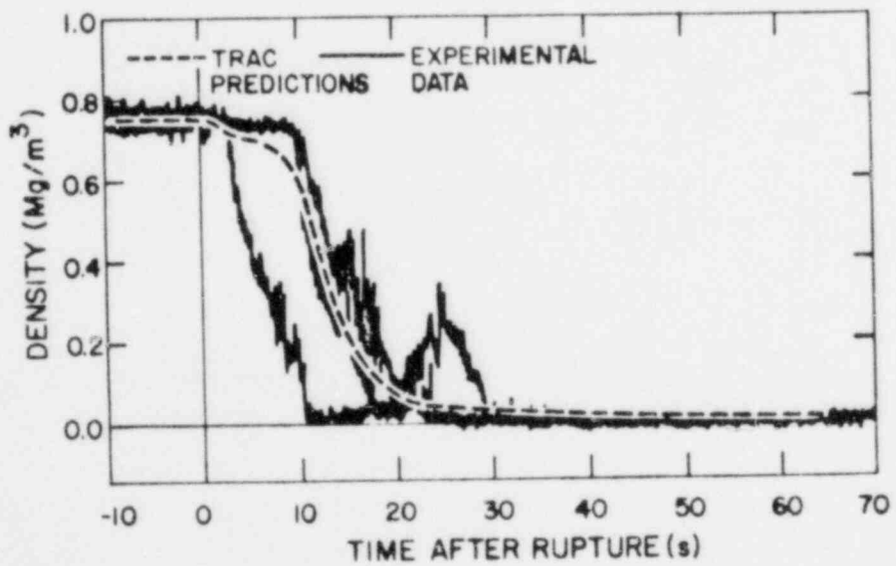

Fig. 100. Mixture density in broken hot leg for LOFT Test L1-4.

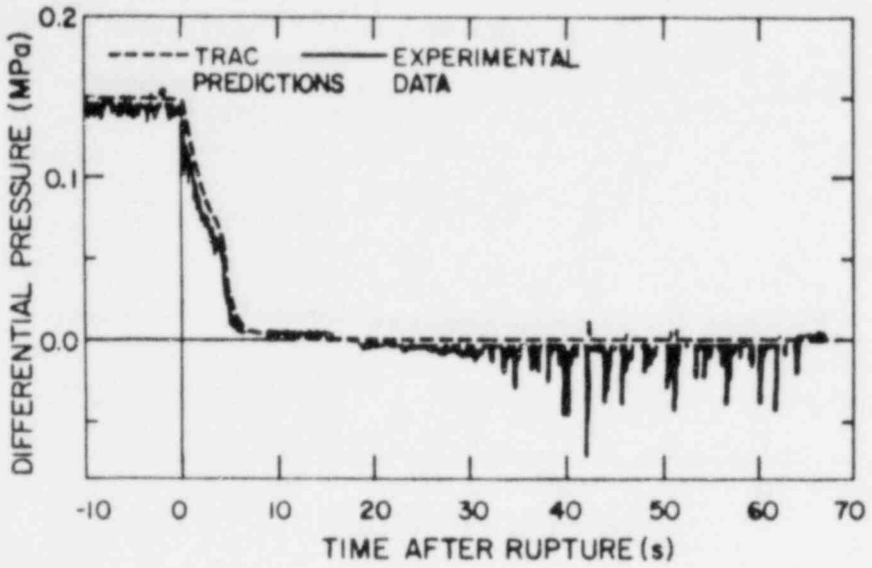

Fig. 101. Differential pressure across primary coolant pumps for LOFT Test L1-4.

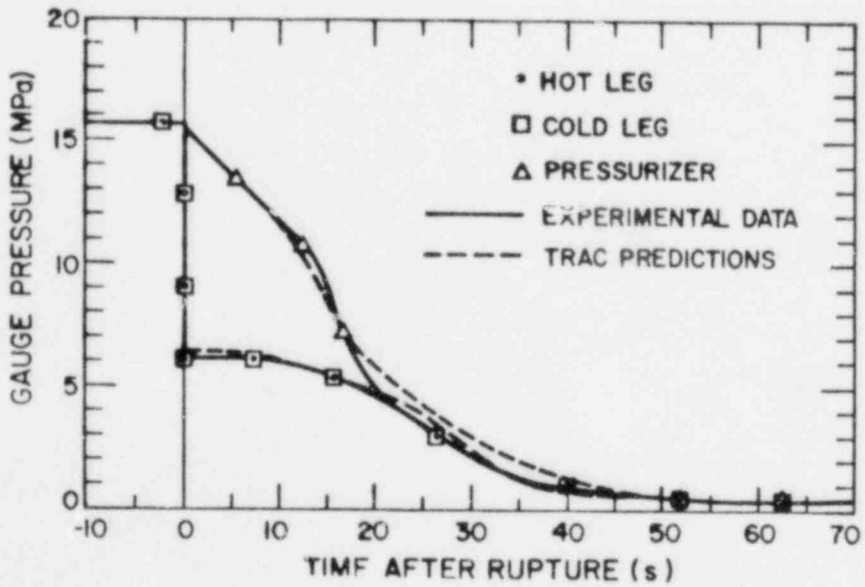

Fig. 102. Intact loop pressures for LOFT Test L1-4.

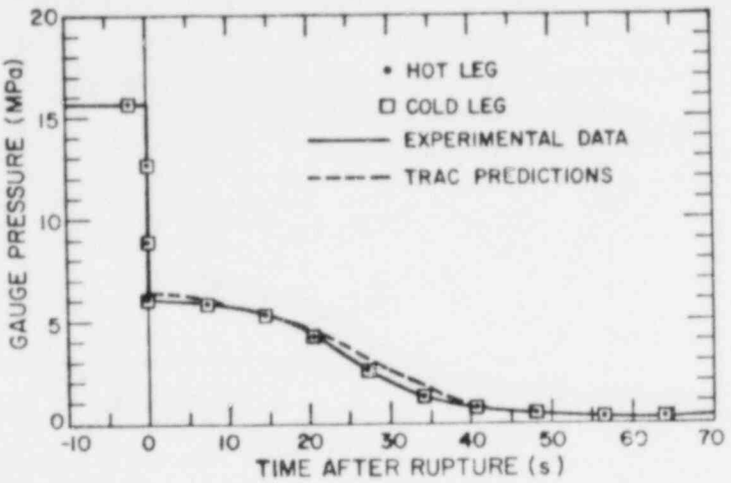

Fig. 103. Broken loop pressures for LOFT Test L1-4.

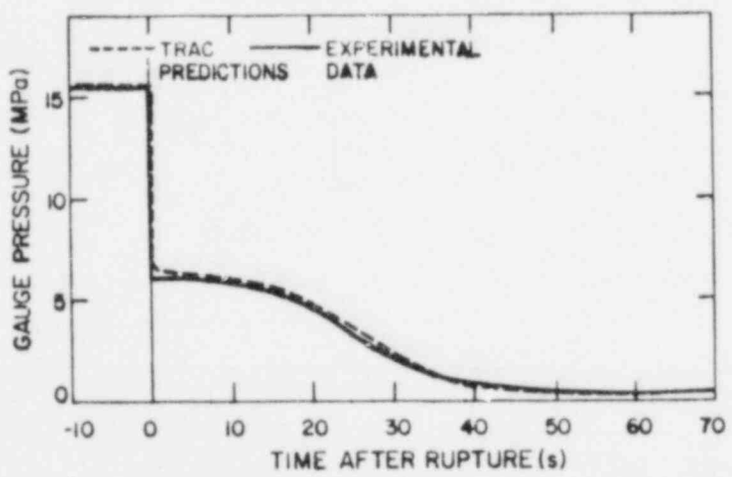

Fig. 104. Vessel pressure for LOFT Test L1-4.

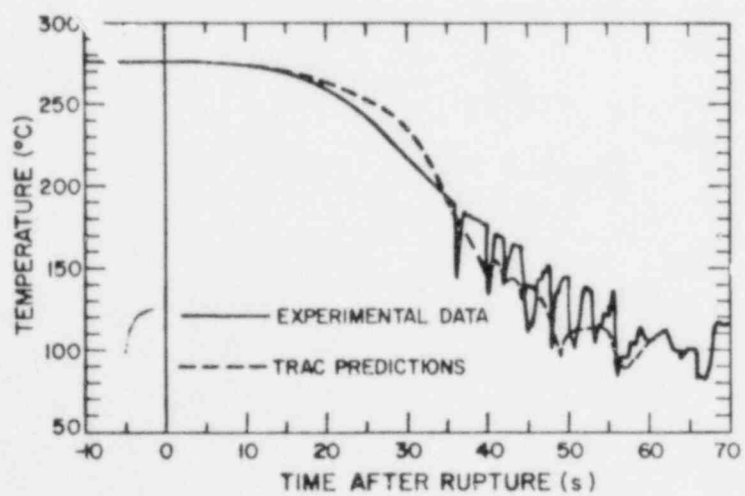

Fig. 105. Downcomer fluid temperature for LOFT Test L1-4.

thermocouple is wetted by the colder ECC water. Since the TRAC fluid temperature is representative of a much larger fluid volume, it predicts an average temperature fluctuation that falls within these larger fluctuations.

Figure 106 shows a comparison of the measured and calculated fluid temperature in the blowdown cold leg. The TRAC results agree with the experimental data very well up to 35 s. After that time TRAC predicts oscillations in the fluid temperature, whereas the measured fluid temperature decreases more or less monotonically.

Oscillation in the blowdown cold leg fluid temperature calculated by TRAC is due to ECC bypass. The experimental data in the fluid temperature do not show any ECC bypass effects. However, a detailed examination of these experimental data raise questions as to the accuracy of the measurement after 40 s. First, the measured as well as the calculated two-phase mixture density in the blowdown cold leg clearly show the ECC bypass effects (see Fig. 99). Second, the measured fluid temperature after about 40 s is superheated by 10-40 K based on the pressure measurements (see Fig. 103). However, other isothermal blowdown test results[28,29] show that the system pressure and fluid temperature follow the saturation line after the first few seconds even in the case of a subcooled water blowdown. A possible explanation for the measured superheated fluid temperature is instrumentation error; the thermocouple may have been overheated by a surrounding hot wall.

Figure 107 compares the measured and calculated fluid temperature in the reactor vessel core simulator. The TRAC predictions agree with experimental data very well up to 35 s. During the period 35-60 s, TRAC predicts oscillations in the fluid temperature, whereas the measured fluid temperature decreases monotonically . Oscillations in the fluid temperature predicted by TRAC are due to the cold ECC injection water. However, the experimental data does not show any effects of the ECC injection water. The measured fluid temperature is again superheated by 10-40 K based on the measured pressure (see Fig. 104). Based on previous arguments this is a questionable result. It should be noted that there were only two "qualified engineering units data" measurements among 29 reactor fluid temperature measurements; the remaining 27 data measurements are either "restrained" or "channel failed" data.[27]

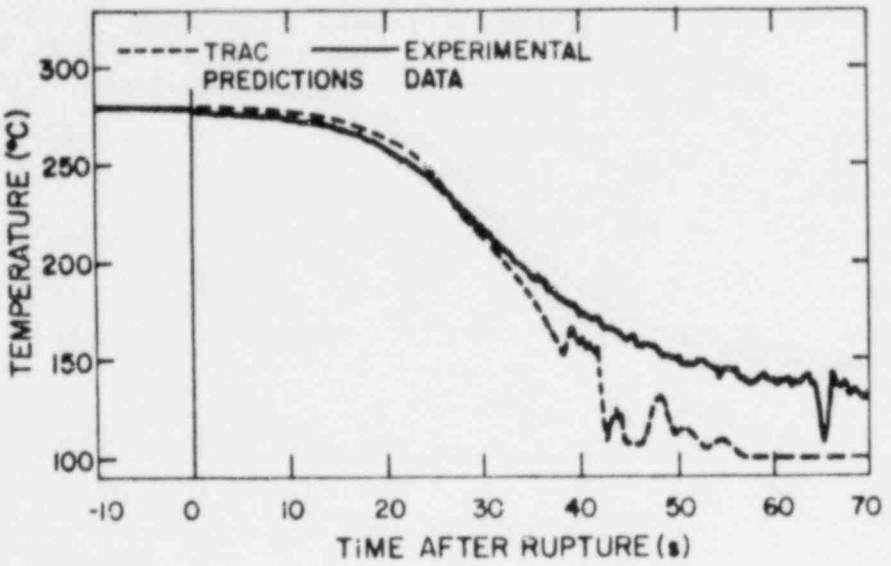

Fig. 106. Broken cold leg fluid temperature for LOFT Test L1-4.

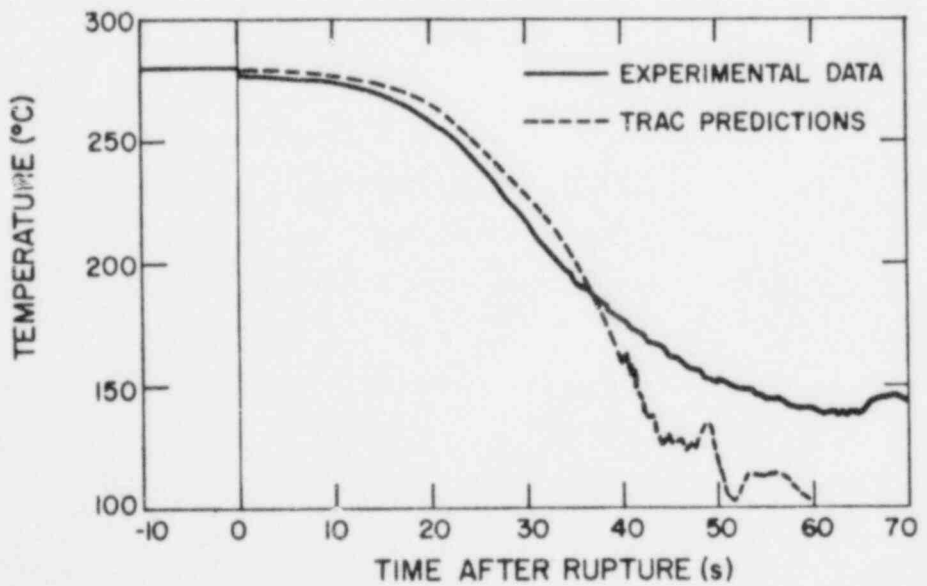

Fig. 107. Fluid temperature in reactor vessel core simulator for LOFT Test L1-4.

Figure 108 compares calculated and measured liquid levels in the pressurizer. The TRAC calculation underpredicts the liquid level in the pressurizer (i.e., the pressurizer empties too rapidly). This is probably due to insufficient friction losses in the pressurizer surge line.

A comparison of the measured and calculated reactor vessel liquid mass is made in Fig. 109. TRAC predicts the reactor vessel liquid mass very well including the time to refill and the subsequent oscillations in the reactor vessel liquid mass due to slugging ECC delivery. The early time (0-20 s) rapid depletion of mass in the data is thought to be due to the lack of water level instrumentation within the core. Thus, the core water level is assumed to be equal to the water level measured by the two downcomer instrument stalks.

4. Parametric Studies

A parametric study was performed to optimize the fluid cell length near breaks. The results concluded that the longer the fluid cell length is, the higher the mass flow rate from the breaks. A fluid cell length of approximately 0.027 m was chosen for the best-estimate calculation, since further reduction of the mesh size does not result in any significant change in the calculated mass flow rate (e.g., less than 0.1%). The time-step size is severely limited if the semi-implicit option is used with this small cell length. Therefore, the fully implicit option was used near the breaks and the semi-implicit option was employed for the remainder of the one-dimensional components.

5. TRAC-P1A Features Tested

LOFT Test L1-4 provided the first opportunity to test the ability of TRAC to predict integral effects during the blowdown and refill stages of a LOCA. With the exception that the core simulator did not contain any heat generating rods, all the TRAC components needed to analyze a full-scale LWR LOCA were exercised in this problem.

The good agreement obtained between calculated and measured results indicates that TRAC-P1A provides a good representation of integral effects during blowdown and refill for a facility whose scale is intermediate between Semi-scale and a full-scale PWR. In particular, these results indicate that the effects resulting from cold ECC injection and bypass are properly represented by the physical models and correlations in TRAC.

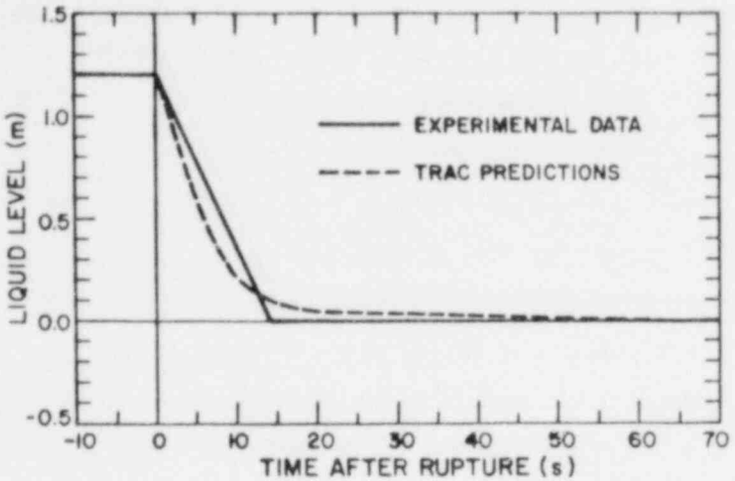

Fig. 108. Pressurizer liquid level for LOFT Test L1-4.

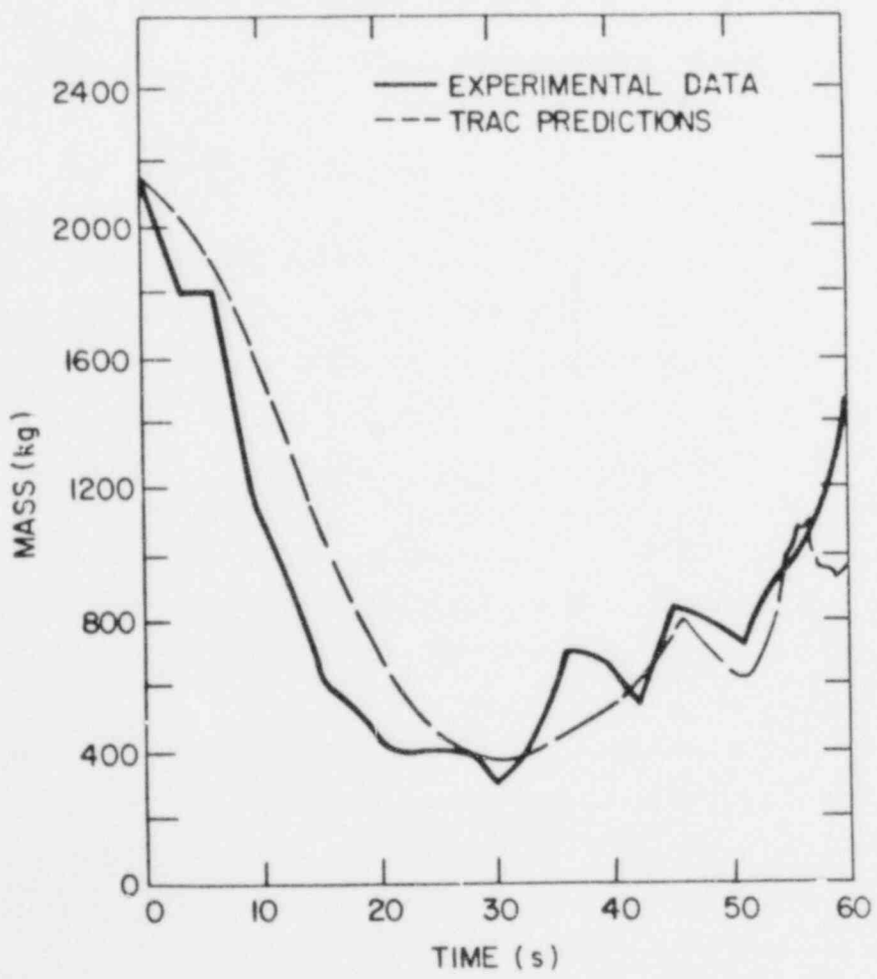

Fig. 109. Reactor vessel liquid mass for LOFT Test L1-4.

6. Input Data Decks

Figure 110 is a listing of the input data deck for calculating the initial steady-state conditions for Test L1-4. Note that the initial flow rates in all components are set to zero including the fill flow rates in components 14 and 22. In addition, the quick-opening valves in components 17 and 18 are closed during this calculation. Detailed pump input data is supplied because the built-in pump data for Semiscale is not appropriate for the LOFT pumps.

A listing of the input data deck for the blowdown/refill transient is shown in Fig. 111. The two quick-opening valves begin to open at time zero and the two pumps trip at 1 s. In addition the pressurizer heater is de-energized at time zero. Components 11, 12, 15, and 16 are included in the input deck so that their friction factors can be respecified. These friction factors were obtained by matching the broken loop mass flow rates at approximately 10 s into the transient. The remaining initial conditions, as well as the geometric data, are obtained from the information contained in the dump file from the steady-state calculation.

The computer CPU times on the CDC 7600 were 40 s for the steady-state calculation 40 min for the transient calculation.

III. SUMMARY AND CONCLUSIONS

The set of problems analyzed in this document have served a dual purpose in the development of TRAC-P1A. First, they constitute a minimal set of calculations that can serve as code assessment problems in that they cover the range of separate effects for the blowdown, refill, and reflood phases as well as system integral effects. Secondly, this set of problems has served in the quality assurance effort during the developmental phase from version P1 to P1A. That is, each time a change was made to the intermediate developmental versions, these test problems were reanalyzed and the effects of these changes evaluated. This procedure was followed both for model changes as well as for programming changes. This procedure has proven to be extremely valuable in identifying any errors or model inaccuracies before they become embedded in the code. However, the calculational costs must be kept affordable which implies that the problem set be kept to a minimum that includes the important phenomenological effects.

```
                1
LOFT TEST L1-4  1   STEADY STATE
               -1            0,0
                0              1                21              22               1
    0,010000E0     0,000050E0     0,001000E0
               10             30               20               2
                1              2                3               4               5
                6              7                8               9              11
               12             13               14              15              16
               17             18               19              20              21
               10
                1              0        100,0

                2              0        100,0

TEE                            1
                4              1                7           0,0                 0
                0              4                1             3
  1,420000E-01  3,650000E-02            0,0           0,0   2,950000E02
    2,950000E2
                0              3                2
  2,330050E-02  8,696800E-03            0,0           0,0   2,950000E02
    2,950000E2
R 2 666,75E-03     41,91E-02      66,01E-02E
    2149,85E-3    2642,77E-03     2221,69E-3E
R 24233,39E-05     266,18E-04    4190,92E-05E
    3114,87E-6     3695,37E-6     5705,88E-6E
F  6342,53E-05E
R 3 1449,29E-6     5732,12E-6E
F          0,0E
    1652,98E-4     5503,15E-6     4668,77E-6
F          0,0E
         1,00E0R 2         0,0         1,00E0E
F       2,84E-1E
R 3 4295,68E-5     8543,04E-5E
F           +4E
R 2          +4R 2          +4E
F          0,0E
F          0,0E
F          0,0E
F          0,0E
F   0,
F          0,0E
F      5,52E+02E
F      5,52E+02E
F     15,75E+06E
F     15,75E+06E
F      5,52E+02E
F      5,52E+02E
PIPE                           4
                4              1                3               4               7
                0              0
  1,505690E-01  3,761400E-02            0,0           0,0   2,950000E02
  2,950000E+02
    1,16E-01      73,66E-02     35,56 E-02      53,34E-02E
   4955,48E-05    4672,31E-05    2605,16E-05    433,26E-004E
R 36342,53E-05R 28319,46E-05E
F          0,0E
R 4         0,0    7071,07E-04
R 3    2,84E-01R 23254,64E-04E
```

Fig. 110. TRAC input data deck for calculation of initial conditions for LOFT Test L1-4.

```
R 2          +4R 2          +4             +4E
F           0,0E
F           0,0E
F           0,0E
F      5,54E+02E
F     15,75E+06E
F      5,54E+02E
PRIZER                      2
                3           2
  0,048000E-06  1,565000E+07  1,378020E+05   1,167600E00
   5307,32E-04R 2   58,38E-02E
       0,30E00R 2     0,33E00E
R 35652,63E-04    5732,12E-06E
R 3          0,0     4668,77E-6E
F     -1,00E00E
R 3  848,36E-03    8543,04E-05E
R 3           4             +4E
       1,00E00R 2          0,0E
F           0,0E
F      6,19E+02E
F      6,19E+02E
F     15,75E+06E
STGEN                       3
              10            3              4              5             10
               1            0              0              1
  5,105400E-03  1,244600E-03
               7           14             15
         1,0000R 86419,85E-04         1,0000E
    3354,06E-04R 89698,57E-05    3354,06E-04E
    8319,46E-05R 91511,71E-04    8319,46E-05E
     ,00       R 9 0,0168          ,00       E
    7071,07E-04R 4     1,00E00          0,0R 4   -1,00E00   -7071,07E-4E
    3254,64E-04R 91021,08E-05    3254,64E-04E
               4           +1R 7          1            +1             4E
             0,0   17,60000000R 6 3802,86E-2   17,60000000          0,0E
F           0,0E
F           0,0E
R 5    5,54E+02R 5    5,52E+02E
R 5    5,54E+02R 5    5,52E+02E
F     15,75E+06E
R 46419,85E-04R 31170,23E-03E
    4008,61E-04R 37355,19E-04R 31157,07E-03E
     8107,32E-6R 6     1,15E00    1824,15E-5E
F           0,0E
F       1,00E00E
       10,16E-2R 6 1210,06E-3       15,24E-2E
              +4R 6           4            +4E
         22,000R 3 4729,93E-2R 3          0,0E
R 4          0,0    2631,54E-4R 2          1,0E
F           0,0E
F        5,52E2E
F        5,52E2E
F       66,50E5E
F        5,52E2E
TEF                         5
               2            1              7           0,0             0
               0            3              6             7
   1,420870E-1   3,572600E-2            0,0           0,0   2,950000E+2
   2,950000E+2
               0            2              5
```

Fig. 110. (cont).

```
   1.420870E-1   3.572600E-2          0.0          0.0   2.950000E+2
   2.950000E+2
       6.35E-1     167.64E-2       6.35E-1E
     131.4i E-2     124.46E-2E
     2746.75E-5    1124.88E-4    2746.75E-5'
      834.66E-4    9004.81E-5E
     3661.31E-5R 2 6342.49E-5    3.66131E-2
R 2 6342.49E-5     8319.46E-5E
F          0.0E
F          0.0F
R 2     -1.00E0R 2      1.00E0E
           0.0          1.00E0    7071.07E-4E
      215.91E-3R 2 2841.74E-4     215.91E-3E
R 2 2841.74E-4     3254.64E-4E
F           +4E
F           +4E
F          0.0E
F          0.0E
F          0.0E
F          0.0E
F          0.0E
F          0.0E
F        5.52E2E
F        5.52E2E
F       15.75E6E
F       15.75E6E
F        5.52E2E
F        5.52E2E
PUMP                      6
               2          1          6          8          7
               3          0          1          1          1
               1          9
   1.079550E-1   2.835930E-2          0.0          0.0   2.950000E2
   2.950000E2
    914.00       6.30449ØE2   3.2ØØØØØE-1   6.2Ø6980E2   3.696610E2
    3.174380E2   3.68125000    2.311875E2   1.884960E2
               0
               7         10         11         11         13
              10         14          6         12          8
               4          6          2          2          2
               2         11          7
        -1.00E0       2.44E0     -0.80E0       2.03E0     -0.40E0
         1.60E0      -0.20E0       1.47E0          0.0       1.40E0
         0.40E0       1.30E0       1.00E0     1.00E0E
        -1.00E0      -1.00E0      -0.40E0      -0.94E0      -0.30E0
        -0.83E0          0.0      -0.68E0       0.20E0      -0.51E0
         0.40E0      -0.28E0       0.60E0          0.0       0.70E0
         0.18E0       0.80E0       0.40E0       1.00E0       1.00E0E
        -1.00E0       2.44E0      -0.83E0       2.00E0      -0.70E0
         1.70E0      -0.65E0       1.60E0      -2.45E0       1.32E0
        -0.17E0       1.10E0          0.0       0.93E0       0.50E0
         0.83E0       0.78E0       0.83E0       0.95E0       0.93E0
         1.00E0       1.00E0E
        -1.00E0      -1.00E0      -0.80E0      -0.60E0      -0.60E0
        -0.30E0      -0.44E0      -0.10E0      -0.23E0       0.10E0
        -0.05E0       0.23E0       3.99E-1       0.33E0       0.40E0
         0.27E0       0.62E0       0.48E00       0.90E0       0.83E0
         1.00E0       1.00E0E
        -1.00E0       3.61E0      -0.90E00       3.49E0      -0.80E0
         3.83E0      -0.60E0       4.62E00      -0.50E0       4.63E0
```

Fig. 110. (cont).

```
-0,40F0          4,27E0          -0,20E00         2,82E0           0,0
 1,45F0          0,12E0           0,55E00         0,20E0          0,26E0
 0,40F0          0,25E0           0,90E00         0,22E0          1,00E0
    0,0E
    0.0          -0,68E0          0,10E0         -0,58E0          0,20E0
-0,51F0          0,30E0          -0,49E0          0,40E0         -0,48E0
 0,60F0         -0,43E0          0,70E0         -0,37E0          0,80E0
-0,26F0          0,90E0          -0,07E0          1,00E0             0,0E
-1,00E0          3,61E0          -0,83E0          2,60E0         -0,70E0
 2,03F0         -0,65E0           1,85E0         -0,45E0          1,37E0
-0,17F0          1,05E0              0,0          0,83E0          0,20E0
 0,76E0          0,40E0           0,73E0          0,50E0          0,76E0
 0,60E0          0,88E0           0,76E0          1,31E0          0,95E0
 2,08E0          1,00E0           2,46E0E
    0.0          0,24E0          3,99E-1          0,82E0          0,40E0
 0,77F0          0,62E0           1,58E0          0,90E0          2,16E0
 1,00E0          2,46E0E
-1,00E0          2,00E0          -0,80E0          1,40E0         -0,70E0
 1,20E0         -0,60E0           1,03E0         -0,40E0          0,80E0
-0,20E0          0,66E0          -0,10E0          0,61E0             0,0
 0,60E0          0,10E0           0,61E0          0,20E0          0,63E0
 0,60E0          0,83F0           1,00E0          1,00E0E
-1,00E0         -1,00E0          -0,30E0         -0,90E0         -0,20E0
-0,87E0         -0,10E0          -0,81E0             0,0         -0,68E0
 0,40E0         -0,27E0           0,50E0          0,50E0          1,00E0
 1,00F0E
-1,00E0          2,00E0          -0,10E0          1,35E0          0,50E0
 0,83E0          1,00E0           0,34E0E
-1,00E0         -1,00E0          -0,30E0         -0,90E0         -0,10E0
-0,52F0          0,40E0          -0,27E0          0,50E0             0,0
 1,00F0          0,34E0E
-1,00E0             0,0           1,00E0             0,0E
-1,00E0             0,0           1,00E0             0,0E
-1,00E0             0,0           1,00E0             0,0E
-1,00F0             0,0           1,00E0             0,0E
    0.0             0,0           0,10E0             0,0
 0,05F0          0,24E0           0,80E0          0,30E0          0,15E0
 0,40F0          0,98E0           0,60E0          0,97E0          0,96E0
 0,90E0          0,90E0           0,80E0          0,96E0          0,80E0
 1,00E0             0,0E                                         0,50E0
0,                0,                .1              0,                .15
    0,48E-1         0,22E0           5,64E-1            0,80E0          5,64E-1
     0,96F0       4,54E-1            1,00E0         0,76E-1E
    0,0          188,496             4,00          157,08
 131,95           19,00             94,25           29,00             9,00
   31,50           63,36             46,50           78,54            68,07
 62,83            69,00               48.17 E                          64,00
F   1352.13E-3E
F   4955.48E-5E
F   3661.31E-5E
F         0.0E
F       +1,00F0E
F    215.91E-3E
F            4E
F          0,0E
F          0.0E
F          0.0E
F       5.53E2E
F      15.75E6E
F       5.53E2E
```

Fig. 110. (cont.)

```
PUMP                    7
          2             1             7             9             7
          0             0             1             1             1
          1             8
1,079550E-1   2,835930E-2           0,0           0,0    2,950000E2
 2,950000E2
 914,00        6,304490E2   3,200000E-1   6,206980E2    3,696610E2
317,438         3,68125       231,186       170,693
          0
          7            10            11            11            13
         10            14             6            12             8
          4             6             2             2             2
          2            11             7
     -1,00F0       2,44E0       -0,80E0       2,03E0       -0,40E0
      1,60E0       -0,20E0       1,47E0          0,0       1,40E0
      0,40F0       1,30E0        1,00E0       1,00E0E
     -1,00F0       -1,00E0       -0,40E0       -0,94E0       -0,30E0
     -0,83E0          0,0        -0,68E0       0,20E0        -0,51E0
      0,40E0       -0,28E0       0,60E0          0,0        0,70E0
      0,18F0       0,80E0        0,40E0        1,00E0       1,00E0E
     -1,00E0       2,44E0        -0,83E0       2,00E0        -0,70E0
      1,70F0       -0,65E0       1,60E0        -0,45E0       1,32E0
     -0,17E0       1,10E0           0,0        0,93E0        0,50E0
      0,83E0       0,78E0        0,83E0        0,95E0        0,93E0
      1,00F0       1,00E0E
     -1,00F0       -1,00E0       -0,80E0       -0,60E0       -0,60E0
     -0,30E0       -0,44E0       -0,10E0       -0,23E0        0,10E0
     -0,05E0        0,23E0       3,99E-1       0,33E0        0,40E0
      0,27E0       0,62E0        0,48E00       0,90E0        0,83E0
      1,00E0       1,00E0E
     -1,00E0       3,61E0        -0,90E00      3,49E0        -0,80E0
      3,83E0       -0,60E0       4,62E00       -0,50E0       4,63E0
     -0,40E0       4,27E0        -0,20E00      2,82E0           0,0
      1,45E0       0,12E0        0,55E00       0,20E0        -0,26E0
      0,40E0       0,25E0        0,90E00       0,22E0        1,00E0
         0,0E
         0,0       -0,68E0         0,10E0       -0,58E0        0,20E0
     -0,51E0        0,30E0       -0,49E0        0,40E0       -0,48E0
      0,60E0       -0,43E0        0,70E0       -0,37E0        0,80E0
     -0,26E0        0,90E0       -0,07E0        1,00E0           0,0E
     -1,00E0        3,61E0       -0,83E0        2,60E0        -0,70E0
      2,03E0       -0,65E0        1,85E0       -0,45E0        1,37E0
     -0,17E0        1,05E0           0,0        0,83E0        0,20E0
      0,76E0        0,40E0        0,73E0        0,50E0        0,76E0
      0,60E0        0,88E0        0,78E0        1,31E0        0,95E0
      2,08E0        1,00E0        2,46E0E
         0,0        0,24E0        3,99E-1       0,82E0        0,40E0
      0,77E0        0,62E0        1,58E0        0,90E0        2,18E0
      1,00E0        2,46E0E
     -1,00F0        2,00E0       -0,80E0        1,40E0       -0,70E0
      1,20E0       -0,60E0        1,03E0       -0,40E0        0,80E0
     -0,20E0        0,66E0       -0,10E0        0,61E0           0,0
      0,60E0        0,10E0        0,61E0        0,20E0        0,63E0
      0,60E0        0,83E0        1,00E0        1,00E0E
     -1,00E0       -1,00E0       -0,30E0       -0,90E0       -0,20E0
     -0,87E0       -0,10E0       -0,81E0          0,0        -0,68E0
      0,40E0       -0,27E0        0,50E0        0,15E0        1,00E0
      1,00F0E
     -1,00E0        2,00E0       -0,10E0        1,35E0        0,50E0
      0,83E0        1,00E0        0,34E0E
```

Fig. 110. (cont).

```
        -1,00F0          -1,00E0        -0,30E0         -0,90E0          -0,10E0
        -0,52E0           0,40E0        -0,27E0          0,50E0              0,0
         1,00F0           0,34E0E
        -1,00F0              0,0         1,00E0              0,0E
        -1,00E0              0,0         1,00E0              0,0E
        -1,00F0              0,0         1,00E0              0,0E
        -1,00F0              0,0         1,00E0              0,0E
            0,0              0,0         0,10E0              0,0         0,15E0
         0,05F0           0,24E0         0,80E0          0,30E0          0,96E0
         0,40F0           0,98E0         0,60E0          0,97E0          0,80E0
         0,90F0           0,90E0         0,80E0          0,96E0          0,50E0
         1,00E0              0,0E
    0,              0,              ,1              ,15
        0,48E-1           0,22E0         5,64E-1         0,80E0          5,64E-1
         0,96E0          4,54E-1         1,00E0          0,76E-1E
    0,0            1706,93E-01           4,00E0        142,42E0          9,00E0
     118,33           19,00          78,54             28,00           54,45
      46,50           78,54          64,00             62,83           69,00
          40,32 F
F    1352,13E-3E
F    4955,48E-5E
F    3661,31E-5E
F           0,0F
F       1,00E0E
F      215,91-3E
F             4E
F           0,0E
F           0,0E
F           0,0E
F        5,53F2E
F       15,75F6E
F        5,53E2E
TEF
                                8
              2                 1               7            0,0               0
              0                 2               9             10
   1,079550E-1    2,835930E-2                 0,0            0,0     2,950000E2
    2,950000E2
              0                 1
                                                8
   1,079550E-1    2,835930E-2                 0,0            0,0     2,950000E2
    2,950000E2
     130,81E-2       111,76E-2E
     542,92E-3E
    4785,57E-5      6630,76E-5E
    2543,94E-5E
R 2  3661,31E-5     6342,49E-5E
F    3661,31E-5E
F           0,0E
F           0,0E
F           0,0E
F           0,0E
R 2   215,91E-3      ,284174
F     215,91E-3E
F            +4E
F             4E
F           0,0E
F           0,0E
F           0,0E
F           0,0E
F           0,0E
F           0,0E
```

Fig. 110. (cont).

```
F        5,53E2E
F        5,53E2E
F       15,75E6E
F       15,75E6E
F        5,53E2E
F        5,53E2E
TEE                          9
                2            1             7          0,0              0
                0            3            10           11
   1,420870E-1   3,572600E-2          0,0          0,0      295,0
       295,00
                0            1            22
   4,366260E-2   1,348740E-2          0,0          0,0      295,0
    295,0
     116,84E-2R 2 7087,35E-4E
          1,500E
     7419,05E-5R 2 4474,09E-5E
     8983,31E-6E
F     6342,4E-5E
F     598,92E-5E
F         0,000E
F           0,0E
F           0,0E
F           0,0E
F    2841,74E-4E
F    8732,52E-5E
F              4E
F              4E
F           0,0E
F           0,0E
F           0,0E
F           0,0E
F           0,0E
F           0,0E
F      552,5    E
F      552,5    E
F       15,79E6E
F       15,79E6E
F        552,00E
F        552,00E
VESSEL                      10
               9             2            4            4
               9             2            1            0            0
               0
               0             0            0
     0,007800E6    0,557668E3    0,016206E3    0,600000E0           0,0
     1,500000E0
               0             2            6
               0             0            0            0            0
             0,0           0,0          0,0
          0,38E0        0,76E0       1,52E0       2,28E0       3,04E0
          3,80E0        4,56E0       5,32E0      59,02E-1E
        35,56E-2      46,99E-2E
      1570,80E-3    3141,59E-3   4712,39E-3   6283,19E-3E
               8             5            3           11
               0             2            3           12
               8             7            3           13
               8             4            3            1
             0,0           0,0       1,00E4          0,0
 R 4 1987,58E-4R 4 4941,45E-4E
```

Fig. 110. (cont).

```
R 4    334.39E0R 4   1143.35E0E
F           0.0E
F           0.0E
F           0.0E
F           0.0E
F           0.0E
F           0.0E
R 4 9735.62E-4R 4        0.577E
F        1.00E0E
F        1.00E0E
R 4      1.00E0R 4          0.0E
R 4 3673.95E-4R 4  1757.43E-4E
R 4 3128.57E-4R 4   194.34E-3E
R 4    45.23E-2R 4          0.0E
F    555.       E
F           0.0E
F           0.0E
F           0.0E
F           0.0E
F           0.0E
F           0.0E
F           0.0E
F        5.55E2E
F        5.55E2E
F       15.75E6E
R 4 1987.58E-4R 4  4941.45E-4E
R 4    334.39E0R 4   1143.35E0E
F           0.0E
F           0.0E
F           0.0E
F           0.0E
F           0.0E
F           0.0E
R 4 9735.62E-4R 4        0.577E
F        1.00E0E
R 4     0.25   R 4         1.00E
R 4      1.00E0R 4          0.0E
R 4 3673.95E-4R 4  1757.43E-4E
R 4 3128.57E-4R 4   194.34E-3E
R 4    45.23E-2R 4          0.0E
F    555.       E
F           0.0E
F           0.0E
F           0.0E
F           0.0E
F           0.0E
F           0.0E
F           0.0E
F        5.55E2E
F        5.55E2E
F       15.75E6E
R 4 3975.16E-4R 4   988.29E-3E
R 4    668.78E0R 4  2286.70E0E
F           0.0E
F           0.0E
F           0.0E
F           0.0E
F           0.0E
F           0.0E
R 4 9735.62E-4R 4        0.577E
```

Fig. 110. (cont).

```
R 4 7775.16E-4R 4      0.50E0E
R 4         1.0R 4     0.57700E
F           0.0E
R 4 2087.61E-4R 4 1063.06E-4E
R 4 1353.69E-4R 4 4574.89E-5E
F           0.0E
F   552.       E
F           0.0E
F           0.0E
F           0.0E
F           0.0E
F           0.0E
F           0.0E
F           0.0E
F       5.52E2E
F       5.52E2E
F      15.75E6E
R 4 3975.16E-4R 4  988.29E-3E
R 4   668.78E0R 4  2286.70E0E
F           0.0E
F           0.0E
F           0.0E
F           0.0E
F           0.0E
F           0.0E
R 4 9735.62E-4R 4       0.577E
R 4      1.00E0R 4      0.50E0E
R 4      1.00E0R 4     0.577E0E
F           0.0E
R 4 4845.03E-4R 4 1063.06E-4E
R 4 3128.57E-4R 4 4574 89E-5E
F           0.0E
F   552.       E
F           0.0E
F           0.0E
F           0.0E
F           0.0E
F           0.0E
F           0.0E
F           0.0E
F       5.52F2E
F       5.52E2E
F      15.75E6E
R 4 3975.16E-4R 4  98H.29E-3E
R 4   668.78E0R 4  2286.70E0E
F           0.0E
F           0.0E
F           0.0E
F           0.0E
F           0.0E
F           0.0E
R 4 9735.62E-4R 4       0.577E
R 4      1.00E0R 4      0.50E0E
R 4      1.00E0R 4     0.577E0E
F           0.0E
R 4 4845.03E-4R 4 1063.06E-4E
R 4 3128.57E-4R 4 4574.89E-5E
F           0.0E
F   332.       E
F           0.0E
```

Fig. 110. (cont).

```
F           0.0E
F           0.0E
F           0.0E
F           0.0E
F           0.0E
F           0.0E
F        5.52E2E
F        5.52E2E
F       15.75E6E
R 4 3975.16E-4R 4   988.29E-3E
R 4   668.78E0R 4  2286.70E0E
F           0.0E
F           0.0E
F           0.0E
F           0.0E
F           0.0E
F           0.0E
R 4 9735.62E-4R 4       0.577E
R 4     1.00E0R 4      0.50E0E
R 4    0.1840R 4     0.57700E
F           0.0E
R 4 4845.03E-4R 4 1063.06E-4E
R 4 3128.57E-4R 4 4574.89E-5E
F           0.0E
F    552.     E
F           0.0E
F           0.0E
F           0.0E
F           0.0E
F           0.0E
F           0.0E
F           0.0E
F        5.52E2E
F        5.52E2E
F       15.75E6E
R 4 3975.16E-4R 4   988.29E-3E
R 4   668.78E0R 4  2286.70E0E
F           0.0E
F           0.0E
F          0.00E
F           0.0E
F          0.00E
F          0.00E
R 4 9735.62E-4R 4       0.577E
R 4     1.00E0R 4      0.50E0E
R 4    0.1038R 4     0.57700E
F           0.0E
R 4 4845.03E-4R 4 1063.06E-4E
R 4   30.48E-2R 4 4574.89E-5E
F           0.0E
R 4 552.      R 4      5.55E2E
F           0.0E
F           0.0E
F           0.0E
F           0.0E
F           0.0E
F           0.0E
F           0.0E
R 4     5.52E2R 4      5.55E2E
R 4     5.52E2R 4      5.55E2E
```

Fig. 110. (cont).

```
F       15,75E6E
R 4 3975,16E-4R 4   988,29E-3E
R 4   668,78E0R 4  2286,70E0E
F           0,0E
F           0,0E
F           0,0E
F           0,0E
F           0,0E
F           0,0E
R 4 9735,62E-4R 4       0,577E
R 4     1,00E0R 4      0,50E0E
R 4       1,00R 4       0,577E
            0,0    1494,06E-4              0,0    1494,06E-4     1130,64E-4
            0,0    1130,64E-4              0,0E
R 4 4845,03E-4R 4 1063,06E-4E
R 4 8669,01E-5R 4 4574,89E-5E
            0,0       2,84E-1              0,0        2,84E-1        2,84E-1
            0,0       2,84E-1              0,0E
R 4 555,      R 4     5,55E02E
F           0,0E
F           0,0E
F           0,0E
F           0,0E
F           0,0E
F           0,0E
F           0,0E
R 4     5,52E2R 4      5,55E2E
R 4     5,52E2R 4      5,55E2E
F      15,75E6E
R 4 3044,14E-4R 4 7568,22E-4E
R 4 5121,44E-1R 4  1751,13E0E
F           0,0E
F           0,0E
F           0,0E
F           0,0E
F           0,0E
F           0,0E
R 4 9735,62E-4R 4       0,577E
R 4     1,00E0R 4      0,50E0E
F           0,0E
F           0,0E
R 4 4845,03E-4R 4 1063,06E-4E
F           0,0E
F           0,0E
R 4 552,      R 4   552,0   E
F           0,0E
F           0,0E
F           0,0E
F           0,0E
F           0,0E
F           0,0E
F           0,0E
R 4     5,52E2R 4      5,55E2E
R 4     5,52E2R 4      5,55E2E
F      15,75E6E
FILL                    13
          14
        1,00E0         1,00E0          0,0           0,0        5,53E2
       15,75E6
BREAK                   14
```

Fig. 110. (cont).

```
               15                0
           1.00E0           1.00E0           1.00E0           5.53E2          66.50E5
PIPE                            11
               16                1               12               16                7
                0                0
       0.144514E0     0.758863E-1              0.0              0.0       2.950000E2
       2.950000E2
R 3 5583.76E-4         525.78E-3       4674.87E-4        558.61E-3       1987.49E-3
R 2 1077.21E-3        1987.49E-3       5102.86E-4       5462.91E-4       4862.83E-4
          2.54E-1      171.45E-3       1746.25E-4E
R 3   35.44E-3        4728.01E-6       3757.89E-6       4660.33E-6       1968.55E-4
R 2 1138.34E-4        1968.55E-4       4072.76E-6       4063.49E-6        317.15E-5
       1611.49E-5     7091.63E-6       1107.57E-5E
R 3 6342.33E-5         139.13E-4R 2 8364.71E-6       1914.12E-5R 2 1056.26E-4
       1914.12E-5     1056.26E-4R 2 8364.71E-6       6342.53E-5R 2 9462.37E-6
       6342.53E-5E
              0.0     2671.39E-5R 3        0.0       2614.89E-5              0.0
        111.08E-2     3234.17E-5       2273.55E-5        111.08E-2R 3           0.0
       1302.49E-4     6805.72E-3             0.0E
R 5         0.0R 3       1.00E0              0.0R 5    -1.00E0R 3           0.0E
R 3       2.84E-1     1330.96E-4R 2     10.32E-2       1756.41E-5R 2 3667.25E-4
       1756.41E-5R 3    10.32E-2          2.84E-1R 2 1197.61E-5          2.84E-1E
F              4E
F            0.0E
F            0.0E
F            0.0E
F         5.54E2E
F        15.75E6E
F         5.54E2E
PIPE                            15
               25                1               16               18                7
                0                1
       8331.79E-5      164.79E-3              0.0              0.0           2.95E2
           2.95E2
        27.94E-2R 2 2118.36E-4R 4 1871.66E-4R 2 1496.06E-4           8413.75E-5
       5609.17E-5     2804.58E-5R 6      1.27E-2       2716.39E-5       5432.78E-5
R 2 8149.17E-5R 3       19.05E-2E
       6860.64E-6R 2 1766.69E-6R 4 1567.35E-6R 2 1245.95E-6            703.79E-6
       4691.93E-7     2345.97E-7R 6 1062.32E-7       1411.33E-6       2822.65E-6
R 2 4233.99E-6R 3 9897.61E-6E
       6342.53E-5R18 8364.71E-6R 7 5195.56E-5E
R 3           0.0     4396.98E-5R 5          0.0     4396.98E-5R16          0.0E
R 3         0.0R 5       1.00E0       7071.07E-4R17         0.0E
        2.84E-01R18     10.32E-2R 7     25.72E-2E
F              4E
F            0.0E
F            0.0E
F            0.0E
F         5.45E2E
F        15.75E6E
F         5.45E2E
VALVE                           17
                2                1               18               20                7
                0                0
       0.128600E0     0.277813E-1              0.0              0.0       2.950000E2
       2.950000E2
                4                2                2                                 2
       0.05272920       0.09525000
            1.500         2.0000E
       3252.71E-5     6058.79E-5E
```

Fig. 110. (cont).

```
    5195,56E-5     5272,92E-5     5855,64E-5E
F         0,0E
F         0,0E
     25,72E-2     9524,99E-5     273,05E-3E
F           4E
F         0,0E
          0,0      0,000001       1,75E-2        1,00E0E
          0,0        1,00E0E
F         0,0E
     545,0          374,0     E
       15,75E6        1,01E5E
     545,0          374,0     E
BREAK                    19
            20            0
    0,822325E0   0,605879E-1         1,00E0         3,73E2       101,33E3
PIPE                     12
             3             1             13             17              7
             0             0
    0,142000E0   3,571240E-2            0,0            0,0    2,950000E2
    2,950000E2
F   5583,76E-4E
F     35,44E-3E
R 3 6342,53E-5     1387,58E-5E
          0,0      2673,86E-3R 2   44,38E-5E
F         0,0E
R 3    2,84E-1     1329,18E-4E
F           4E
F         0,0E
F         0,0E
F         0,0E
F       5,52E2E
F      15,75E6E
F       5,52E2E
PIPE                     16
            25             1             17             19              7
             0             1
   0,958804E-1    0,159919E0            0,0            0,0    2,950000E2
    2,950000E2
       1,27E-1     9925,54E-5     7444,15E-5R 2 4962,77E-5R 2 2481,39E-5
R 6    1,27E-2R 2 2579,69E-5     5159,38E-5     7739,06E-5     1183,93E-4
    1851,91E-4R 3 2160,57E-4     2063,75E-4     3460,75E-4       46,99E-2E
    1479,66E-6     9355,59E-7      701,67E-6R 2  467,78E-6R 2  233,89E-6
R 6 1062,32E-7R 2 6067,41E-7     1213,48E-6     1820,22E-6     2284,08E-6
    4355,69E-6R 3 5081,64E-6     4853,93E-6     1798,07E-5     2441,41E-5E
    1387,58E-5R 6 9425,75E-6R 6 8364,71E-6R10 2351,98E-5R 3 5195,56E-5E
      44,38E-5         8,8E-4R24         0,0E
F         0,0E
    1329,18E-4R 6  109,55E-3R 6   10,32E-2R10  173,05E-3R 3   25,72E-2E
F           4E
F         0,0E
F         0,0E
F         0,0E
F       5,45E2E
F      15,75E6E
F       5,45E2E
VALVE                    18
             2             1             19             21              7
             0             0
    0,128600E0   0,277813E-1            0,0            0,0    2,950000E2
    2,950000E2
```

Fig. 110. (cont)

```
                4              2               2                              2
        5,273E-2       9,525E-2
           1.5E0       2,00E0E
       3282,71E-5    6058,79E-5E
       5195,56E-5    5272,92E-5    5855,64E-5E
F          0,0E
F          0.0E
        25,72E-2     9524,99E-5     273,05E-3E
F            4E
F          0,0E
           0.0        0,00001        1.75E-2        1,00E0E
           0.0       1,00E0E
F          0,0E
          545.0         373.0E
        15,75E6        1,01E5E
          545.0         373,0E
BREAK                      20
             21             0
             .2           ,06            1,0          373,0          1,01E5
FILL                       21
             22             2                             22
            1.5  8,9830000E-3            0,0            0,0           305,0
       15,79E06
            0.0           0,0        23,00E0            0.0         24,00E0
     4598,44E-3         25,0      4842,05E-3        30,0000      7245,71E-3
        35,0000    8159,19E-3        39,0000     7994,39E-3         40,0000
     8405,13E-3       45,0000     8668,94E-3         55,000       8,3300000
         58,000    8287,92E-3          60,00    1104,04E-02    63,0
     4337,64E-3        65,000     3485,94E-3          59,00      5969,41E-3
         70,000     540,74E-2          80,00     3481,93E-3          90,000
     2888,37E-3       100,000     2596,84E-3       120,0000        2484,1E-3
       180,0000    2343,22E-3       200,0000    2343,22E-3E
        1,0E-4            0.1           99,0            1,0
            1.0          5,00            5,0            1,0
-1.
```

Fig. 110. (cont).

```
                1
LOFT TEST L1-4  1 BLOWDOWN
              145          0.0
                0            1              26              27               1
          2.0E-3       2.0E-6       1.0E-2
               20           50              20               3
                1            2               3               4               5
                6            7               8               9              11
               12           13              14              15              16
               17           18              19              20              21
               22           23              24              25              27
               10
                1            0          1.0

                2            0          0.0

                3           -1       424.01E4            0.0
               27            0               1               0
PIPE                        12
                3            1              13              17               7
                0            0
     0.142000E0   3.571240E-2            0.0             0.0    2.950000E2
     2.950000E2
F    5583.76E-4E
F      35.44E-3E
R 3 6342.53E-5     1387.58E-5E
           0.0     2671.89E-3       44.38E-3            0.0E
F          0.0E
R 3    2.84E-1     1329.18E-4E
F             4E
F          0.0E
F          0.0E
F          0.0E
F       5.52E2E
F      15.75E6E
F       5.52E2E
PIPE                        16
               25            1              17              19               7
                0            1
    0.958804E-1     0.159919E0             0.0             0.0    2.950000E2
     2.950000E2
        1.27E-1     9925.54E-5     7444.15E-5R 2 4962.77E-5R 2 2481.39E-5
R 6     1.27E-2R 2 2579.69E-5     5159.38E-5     7739.06E-5     1183.93E-4
     1851.91E-4R 3 2160.57E-4     2063.75E-4     3460.75E-4       46.99E-2E
     1479.66E-6     9355.59E-7      701.67E-6R 2  467.78E-6R 2  233.89E-6
R 6 1062.32E-7R 2 6067.41E-7     1213.48E-6     1820.22E-6     2284.08E-6
     4355.69E-6R 3 5081.64E-6     4853.93E-6     1798.07E-5     2441.41E-5E
     1387.58E-5R 6 9425.75E-6R 6 8364.71E-6R10 2351.98E-5R 3 5195.56E-5E
R 7          0.0R 7         1.6R 8         0.0R 4        0.20E
F            0.0E
     1329.18E-4R 6  109.55E-3R 6   10.32E-2R10  173.05E-3R 3   25.72E-2E
F             4E
F          0.0E
F          0.0E
F          0.0E
F       5.45F2E
F      15.75E6E
F       5.45F2E
PIPE                        11
               16            1              12              16               7
```

Fig. 111. TRAC input data deck for calculation of the LOFT Test L1-4 transient.

```
                 0              0
      0,144514F0   0,758863E-1           0,0          0,0     2,950000E2
      2,950000F2
R 3 5583,76E-4      525,7AE-3      4674,87E-4     558,61E-3     1987,49E-3
R 2 1077,21E-3     1987,49E-3      5102,86E-4    5462,91E-4     4862,83E-4
       2,54E-1      171,45E-3      1746,25E-4E
R 3   35,44E-3     4728,01E-6      3757,89E-6    4660,33E-6     1968,55E-4
R 2 1138,34E-4     1968,55E-4      4072,76E-6    4063,49E-6      317,15E-5
    1611,49E-5     7091,63E-6      1107,57E-5E
R 3 6342,53E-5      139,13E-4R 2 8364,71E-6      1914,12E-5R 2 1056,26E-4
    1914,12E-5     1056,26E-4R 2 8364,71E-6      6342,53E-5R 2 9462,37E-6
    6342,53E-5F
           0.0     2671,89E-3R 3         0,0     2614,89E-5            0,0
      111,08E-2    3234,17E-5      2273,55E-5     111,08E-2R 3         0,0
    1302,49E-4     1700,00E-3            0,0E
R 5        0.0R 3     1,00E0             0,0R 5   -1,00E0R 3           0,0E
R 3    2.84E-1     1330,96E-4R 2    10,32E-2     1756,41E-5R 2 3667,25E-4
    1756,41E-5R 3   10,32E-2          2,84E-1R 2 1197,61E-5        2,84E-1E
F               4E
F            0,0E
F            0,0E
F            0.0E
F         5,54F2E
F        15,75F6E
F         5,54E2E
PIPE                           15
                25              1             16           18              7
                 0              1
    8331,79E-5      164,79E-3            0,0          0,0          2,95E2
        2,95E2
      27,94E-2R 2 2118,36E-4R 4 1871,66E-4R 2 1496,06E-4      8413,75E-5
    5609,17E-5     2804,58E-5R 6      1,27E-2    2716,39E-5      5432,78E-5
R 2 8149,17E-5R 3   19,05E-2E
    6860,64E-6R 2 1766,69E-6R 4 1567,35E-6R 2 1245,95E-6       703,79E-6
    4691,93E-7     2345,97E-7R 6 1062,32E-7      1411,33E-6      2822,65E-6
R 2 4233,99E-6R 3 9897,61E-6E
    6342,53E-5R18 8364,71E-6R 7 5195,56E-5E
R 3        0,0     4396,98E-5R 5         0,0   4396,98E-5R16           0,0E
R 3        0.0R 5     1,00E0     7071,07E-4R17        0,0E
      2,84E-01R18   10,32E-2R 7    25,72E-2E
F               4E
F            0.0E
F            0.0E
F            0.0E
F         5,45E2E
F        15,75F6E
F         5,45E2E
PRIZER                          2
                 3              2
              0.00  1,565000E+07   1.378020E+05   1,167600E00
   5307,32E-04R 2   58,38E-02E
       0,30E00R 2    0,33E00E
R 35652,63E-04    5732,12E-06E
R 3        0.0    4668,77E-6E
F      -1.00E00E
R 3 848,36E-03    8543,04E-05E
R 3          4            +4E
       1.00E00R 2          0,0E
F            0,0E
F       6,19E+02E
```

Fig. 111. (cont).

```
F      6,19E+02E
F     15,75E+06E
VALVE                    18
                2                1              19              21               7
                0                0
     0,128600E0    0,277813E-1            0,0             0,0     2,950000E2
     2,950000E2
                4                2               2                               2
       5,273E-2       9,525E-2
            1,5E0          2,00E0E
     3282,71E-5     6058,79E-5E
     5195,56E-5     5272,92E-5     5855,64E-5E
            1,0            1,0           1,0E
F           0,0E
       25,72E-2     9524,99E-5      273,05E-3E
F              4E
F           0,0E
            0,0        0,00001        1,75E-2         1,00E0E
            0,0          1,00E0E
F           0,0E
          545,0          373,0
         59,00E5         1,01E5
          545,0          373,0
VALVE                    17
                2                1              18              20               7
                0                0
     0,128600E0    0,277813E-1            0,0             0,0     2,950000E2
     2,950000E2
                4                2               2                               2
     0,05272920     0,09525000
            1,500        2,00000E
     3282,71E-5     6058,79E-5E
     5195,56E-5     5272,92E-5     5855,64E-5E
F           1,0E
F           0,0E
       25,72E-2     9524,99E-5      273,05E-3E
F              4E
F           0,0E
            0,0        0,000001        1,75E-2         1,00E0E
            0,0          1,00E0E
F           0,0E
       545,0          374,0    E
         15,75E6         1,01E5E
       545,0          374,0    E
TEE                      21
                1                0               7            0,0               0
                0                2              23            22
    4,366260E-2    0,348740E-2            0,0           ,0          295,0
          295,0
                0                2              27
    1,699260E-2    7,137400E-3            0,0           0,0        295,0
          295,0
F     218,44E-2E
F     218,44E-2E
F    5233,12E-5E
F    5233,12E-5E
R 2 2395,68E-5      598,92E-5E
R 2 2395,68E-5      598,92E-5E
F          00,0E
F        0,4500E
```

Fig. 111. (cont).

```
F           0,0E
F           0,0E
R 2 1746,50E-4     8732,52E-5E
H 2 1746,50E-4     8732,52E-5E
F             4F
F             4E
F           0,0E
F           0,0E
F           0,0E
F           0,0E
F           0,0E
F           0,0E
F      552,50E0E
F      552,50E0E
F       15,75E6E
F       15,75E6E
TEE                    22
              1              0             7          0,0              0
              0              4            24           26
   6,590000E-2   1,823720E-2          0,0          0,0      295,0
     295,0
              0              5            25
   4,366260E-2   0,348740E-2          0,0          0,0       295,0
     295,0
R 1    45,72E-1      421,64E-2E
F        1,50F0E
R 3 2495,10E-4     1385,18E-4E
    8983,81E-5     2046,50E-5     8983,81E-5     5233,31E-5     8983,81E-5E
    2395,68E-5S
R 3 5457,32E-5     3285,22E-5E
     598,92E-5     1364,33E-5      598,92E-5     3488,87E-6R 2  598,92E-5E
F        0,5500E
F           0,0E
F           0,0E
F           0,0E
    1746,50E-4S
R 3   26,36E-2      204,52E-3E
    8732,52E-5       13,18E-2     8732,52E-5     6664,96E-5R 2 8732,52E-5E
F             4E
F             4E
F           0,0E
F           0,0E
F           0,0E
F           0,0E
F           0,0E
F           0,0E
F     305,67E00E
F      297,44E0E
F        4,24E6E
F        4,24E6E
ACCUM                  23
              3            26
    8863,34E-4     1288,58E-3        2,25E-2E
    1104,36E-3     1605,57E-3     2803,48E-5E
R 3 1245,99E-3     3285,22E-5E
F       0,5500E
F         -1,0E
H 3 1259,54E-3      204,52E-3E
F             4E
            1,0R 2         0,0E
```

Fig. 111. (cont).

```
F          0.0E
F     290,63F0E
F     290,63F0E
F       4,24E6E
FILL                        24
             23              3                          10
           1.50   8,983810E-3           0,0    0,421345E0    0,297440E3
         4,24E6
     2757,89E+1    1580,04E-3    2757,89E+2    1474,71E-3    5929,47E+2
     1264,04E-3    8273,68E+2     109,55E-2    1103,16E+3    8426,90E-4
     1351,37E+3    5477,49E-4    1434,10E+3    4213,45E-4    1516,84E+3
     2106,73E-4    1558,21E+3      1,00E-10      17,00E+8      1,00E-10E
FILL                        25
             25              2                           4
           2,50   0,226783E-2           0,0           0,0    0,297440E3
         4,24E6
            0.0           0.0          22,0          0,0S
        22,10E0    1196,09E-3        1,00E3   1196,08E-3E
VALVE                       27
              2              0           27            24             7
              0              0
    4,366260E-2   0,348740E-2           0,0           0,0         295,0
          295.0
              2              3                                        2
      598,92E-5    8732,52E-5
F     109,22E-2E
F    2616,56E-5E
      598,92E-5R 2 2395,68E-5E
F       0,4500E
F          0,0E
     8732,52E-5R 2 1746,50E-4E
F            4E
F          0,0E
F          0,0E
F          0,0E
       552,5 E0      305,67E0E
        15,75E6        4,24E6E
END
        1,0E-4           0,1          60,0
           1,0          0,05           5,0
-1.
```

Fig. 111. (cont).

The conclusion that can be drawn from the results of these calculations is that TRAC-P1A is capable of representing a wide range of phenomena in experimental facilities of considerably different geometrical sizes and arrangements. Moreover, the experimental conditions that existed during these tests encompassed the spectrum of expected fluid thermodynamic conditions and flow topologies for a loss-of-coolant accident. These test problems have exercised the hydrodynamics and associated constitutive packages of both the one-dimensional drift-flux routines and the three-dimensional two-fluid routines. The heat transfer phenomena in these problems have covered essentially the entire boiling map for wall heat transfer in pipes, slabs, and steam generators and for the rods during the reflood phase.

In general, the calculated results agree very well with the blowdown data from the Edwards, CISE, Marviken, Semiscale, and LOFT tests. As mentioned in the individual discussion for these calculations, the critical flow was in all cases computed by use of the implicit hydrodynamics with fine noding. This procedure eliminates user selection of a critical flow (break) model and discharge coefficients. The procedure yielded very good results in all the problems for subcooled, saturated, and superheated fluids. The only disadvantage to this approach is the extra computing costs incurred in having to use many nodes. This is particularly a problem in analyzing small break experiments which typically have long transient times necessitating the use of few mesh cells in the calculation. This motivates the inclusion of a break flow model into TRAC for use in small break calculations. The selection of the break model and any associated user input could be determined by first performing sensitivity calculations that used the normal TRAC procedure of numerically calculating the critical flow.

For the Creare downcomer calculations of the refill/bypass phase the results are excellent. TRAC-P1A generated two separate flooding curves, complete bypass to complete delivery, for a wide range of ECC water subcoolings and injection flow rates. Although not reported here, similar agreement was obtained for the larger Battelle 2/15-scale vessel. The LOFT L1-4 test furnished integral system data on the downcomer behavior of subcooled water injected into the intact cold leg. TRAC-P1A did an excellent job of predicting the time and magnitude at which lower plenum refill began. Moreover, the measured density "slugging" in the broken cold leg due to ECC

bypass was in qualitative agreement with the data. Subsequent calculation of LOFT test L1-5 have shown similar agreement with downcomer data. Although none of the problems in this volume have addressed the calculation of refill/bypass with the one-dimensional drift-flux package, other calculations have shown that the results are generally poor except in the highly dispersed flow regime. Model changes to improve these results have not been investigated since the next TRAC version is expected to use a two-fluid formulation for the one-dimensional hydrodynamics. This will allow for a more natural calculation of the flooding process.

For the reflood phase, the single experimental facility discussed in this volume is the FLECHT forced flooding tests. These calculations show that TRAC-P1A does a satisfactory job for the high flooding rate cases in which the core region is filled before the progression of the quench front. For the low flooding rate cases, in which the progress of the quench front is largely determined by precooling, TRAC-P1A does not satisfactorily represent the observed phenomena. Model development utilizing a completely different approach to treat reflood is currently underway and the results appear very encouraging.

It should be noted that the initial conditions used for the FLECHT tests are based entirely on what previous computer codes showed to be the expected core conditions at the beginning of reflood in a full-scale reactor, e.g. rod temperatures of 1140 K. However, the recent experimental data from the LOFT nuclear Tests L2-2 and L2-3 have shown that the nuclear core experiences considerable cooling during blowdown and refill resulting in clad temperatures at the beginning of reflood of 600 K to 800 K. These lower temperatures resulted in considerably faster than expected reflooding of the core. Therefore the use of lower initial rod temperatures for reflood experiments should be considered. This would be expected to make calculation of the reflood process somewhat simpler.

As mentioned in the introduction, code assessment is a two step process. The results reported herein are part of the developmental code assessment effort. The independent code assessment effort is now formally established and chartered with assessing the current frozen, release version of TRAC. This effort has already provided pretest and posttest predictions for tests in a number of facilities including nuclear LOFT, Semiscale Mod-3, PKL, LOBI, and

the Japanese Cylindrical Core Test Facility. TRAC-P1A is being used to investigate hypothetical accidents in full-scale PWRs as well as to simulate the Three-Mile Island accident. The developmental assessment effort is investigating recent code improvements through reanalysis of the test problems in this volume as well as through analysis of the above mentioned facilities. These two code assessment efforts will continue to expand to allow for a more comprehensive assessment of the TRAC code and to reflect the latest priorities of the Nuclear Regulatory Commission.

REFERENCES

1. "TRAC-P1: An Advanced Best Estimate Computer Program for PWR LOCA Analysis, Vol. I: Methods, Models, User Information, and Programming Details," Los Alamos Scientific Laboratory report LA-7279-MS, Vol. I (NUREG/CR-0063) (June 1978).

2. "TRAC-P1A: An Advanced Best-Estimate Computer Program for PWR LOCA Analysis," Los Alamos Scientific Labortory report LA-7777-MS (NUREG/CR-0665) (May 1979).

3. A. R. Edwards and T. P. O'Brien, "Studies of Phenomena Connected with the Depressurization of Water Reactors," J. of British Nucl. Energy Society 9, 125-135 (April 1970).

4. R. W. Garner, "Comparative Analyses of Standard Problems - Standard Problem One (Straight Pipe Depressurization Experiments)," Aerojet Nuclear Company report I-212-74-5.1 (October 1973).

5. A. Premoli and W. T. Hancox, "An Experimental Investigation of Subcooled Blowdown with Heat Addition," Submission to Committee on the Safety of Nuclear Installations Specialists Meeting on Transient Two-Phase Flow, Toronto, Ontario (August 1976).

6. W. T. Hancox and A. Premoli, "Standard Problem 3: Subcooled Blowdown with Heat Addition," Submission to CSNI Ad Hoc Group on Emergency Core Cooling, Bethesda, Maryland (Revised March 1976).

7. W. T. Hancox to L. Shotkin, personal communication (August 31, 1976).

8. L. Ericson, L. Gros d'Aillon, D. Hall, J. Ravnsborg, O. Sandervag, and H. Akesson, "The Marviken Full-Scale Critical Flow Test Interim Report, Results from Test 4," Marviken report MX3-40 (May 1978).

9. S. A. Naff and P. A. Pinson, "1-1/2 Loop Semiscale Isothermal Test Program and System Description in Support of Experiment Data Reports," Aerojet Nuclear Company report ANCR-1143 (February 1974).

10. D. J. Barnum, "Comparative Analysis of Standard Problems - Standard Problem 2," Aerojet Nuclear Company report NUREG-75-0361, Rev. (June 1975).

11. C. E. Cartmill, "Thermal-Hydraulic Response of the Semiscale MOD-1 System - Isothermal Test Series," Aerojet Nuclear Company report ANCR-1228 (October 1975).

12. L. J. Ball, D. J. Hanson, K. A. Dietz, and D. J. Olson, "Semiscale Program Description," Idaho National Engineering Laoratory report TREE-NUREG-1210 (May 1978).

13. H. S. Crapo and K. E. Sackett, "Experimental Data Report for Semiscale Mod-1 Test S-02-8 (Blowdown Heat Transfer Test)," Aerojet Nuclear Company report ANCR-NUREG-1238 (August 1976).

14. C. J. Crowley, J. A. Block, and C. N. Cary, "Downcomer Effects in a 1/15-Scale PWR Geometry - Experimental Data Report," Creare, Inc. report NUREG-0281 (May 1977).

15. J. O. Cermak, et. al., "PWR Full Length Emergency Cooling Heat Transfer (FLECHT) Group I Test Report," Westinghouse Electric Corp. report WCAP-7435 (1970).

16. F. F. Cadek, T. P. Dominicis, and R. H. Leyse, "PWR FLECHT Group II Test Report," Westinghouse Electric Corp. report WCAP-7544 (1970).

17. J. A. Blaisdell, L. E. Hochreiter, and J. P. Waring, "PWR FLECHT-SET Phase A Report," Westinghouse Electric Corp. report WCAP-8238 (1973).

18. J. P. Waring, E. R. Rosal, and L. E. Hochreiter, "PWR FLECHT-SET Phase B1 Data Report," Westinghouse Electric Corp. report WCAP-8431 (1974).

19. J. P. Waring and L. E. Hochreiter, "PWR FLECHT-SET Phase B1 Evaluation Report," Westinghouse Electric Corp. report WCAP-8583 (1975).

20. F. F. Cadek, et. al., "PWR FLECHT Final Report Supplement," Westinghouse Electric Corp. report WCAP-7931 (1972).

21. E. R. Rosal, et. al., "FLECHT Low Flooding Rate Cosine Test Series Data Report," Westinghouse Electric Corp. report WCAP-8651 (1975).

22. G. P. Lilly, et. al., "PWR FLECHT Cosine Low Flooding Rate Test Series Evaluation Report," Westinghouse Electric Corp. report WCAP-8838 (1977).

23. E. R. Rosal, C. E. Conway, and M. C. Krepinevich, "FLECHT Low Flooding Rate Skewed Test Series Data Report," Westinghouse Electric Corp. report WCAP-9108 (1977).

24. G. P. Lilly, et. al., "PWR FLECHT Skewed Profile Low Flooding Rate Test Series Evaluation Report," Westinghouse Electric Corp. report WCAP-9183 (1977).

25. W. L. Kirchner, "Reflood Heat Transfer In a Light Water Reactor," U.S. Nuclear Regulatory Commission report NUREG-0106 (1976).

26. H. C. Robinson, "LOFT Systems and Test Description (Loss-of-Coolant Experiments Using a Core Simulator)," Idaho National Engineering Laboratory report TREE-NUREG-1019 (November 1976).

27. D. L. Batt, "Experimental Data Report for LOFT Nonnuclear Test L1-4," Idaho National Engineering Laboratory report TREE-NUREG-1084 (July 1977).

28. R. T. Alleman, et al., "Coolant Blowdown Studies of a Reactor Simulator Containing a Perforated Sieve Plate Separator," Battelle Northwest Laboratory report BNWL-1463 (February 1971).

29. B. C. Slifer, "Loss-of-Coolant Accident and Emergency Core Cooling Models for General Electric Boiling Water Reactors," General Electric Topical report NEDO-10329 (April 1971).

DISTRIBUTION

	Copies
Nuclear Regulatory Commission, R4	328
Technical Information Center, Oak Ridge, Tennessee	2
Los Alamos Scientific Laboratory	115
	445

☆U.S. Government Printing Office: 1979 — 677-115/195